INFORMATION TO USERS

This manuscript has been reproduced from the microfilm master. UMI films the text directly from the original or copy submitted. Thus, some thesis and dissertation copies are in typewriter face, while others may be from any type of computer printer.

The quality of this reproduction is dependent upon the quality of the copy submitted. Broken or indistinct print, colored or poor quality illustrations and photographs, print bleedthrough, substandard margins, and improper alignment can adversely affect reproduction.

In the unlikely event that the author did not send UMI a complete manuscript and there are missing pages, these will be noted. Also, if unauthorized copyright material had to be removed, a note will indicate the deletion.

Oversize materials (e.g., maps, drawings, charts) are reproduced by sectioning the original, beginning at the upper left-hand corner and continuing from left to right in equal sections with small overlaps.

ProQuest Information and Learning
300 North Zeeb Road, Ann Arbor, MI 48106-1346 USA
800-521-0600

Université d'Ottawa · University of Ottawa

Live Hard Die Young. Insight into the Short Life Time of Highly Active Vanadium(III) Catalysts: the James Dean of α-Olefin Polymerization Catalysts

A Thesis Submitted to the

School of Graduate Studies and Research

In Partial Fulfillment of the Requirements

for the Degree of

Doctor of Philosophy

In the Ottawa-Carleton Chemistry Institute

Department of Chemistry

University of Ottawa

Ottawa, Ontario

Candidate

Damien Francis Reardon

Supervisor

Professor Sandro Gambarotta

Abstract

The reaction schemes described above outline the different steps, which lead to the polymerization of α-olefins. These mechanistic pathways are generally accepted by the scientific community for group IV catalysts and have been established for some time now. More recent studies have been focused on investigating catalysts that are not supported by a group IV metal centre and not supported by cyclopentadienyl ligands. Another field of research is geared toward the understanding of the catalyst/co-catalyst interaction in order to optimize activity and selectivity of the catalyst. The three main features that are believed to lead to successful polymerisation catalysts are, 1) *electron deficiency*; a fourteen electron configuration seems to be the winning recipe for obtaining highly active species; 2) the possibility to *vacate a coordination site* adjacent to the propagating polymer chain, 3) the active catalyst should preferentially bear a *positively charged metal* centre which increases the electrophilic properties important for enhancing the coordination of the α-olefin. Some neutral alkyl-metal complexes have been reported to polymerize α-olefins[1] however the catalytic activities were typically low.

The catalytic performances are mainly induced by the supporting ligand for many reasons, which determine selectivity, activity and polymer structure. Firstly, the ligand gives control over the coordination geometry and the number of occupied sites around the metal centre. Secondly, the ligand controls and stabilizes the active oxidation state, which in turn is of the utmost importance to the high performance of the catalyst. Finally, the ligand will also play a central role in the steric protection of the active site and will have a

great influence over the stereochemical properties of the transition state, which are eventually translated to the polymer structure.[2]

The effects of different donor atoms of the supporting ligands (i.e. oxygen and nitrogen donor ligands) are at the root of this study as well as an attempt to improve our understanding of the catalyst/co-catalyst interaction. The oxygen and nitrogen donor-based ligand systems were chosen for several reasons. These ligand systems are easily accessible, inexpensive and present a wide range of possibilities from an electronic point of view since they can be considered as either two or four electron donors. Furthermore, the steric properties of the ligand system can also be tuned quite easily via relatively simple organic procedures. In view of these observations, nitrogen and oxygen donor ligands are great candidates to "overthrow" the currently ruling cyclopentadienyl ligands, which have dominated the field of Ziegler-Natta group IV catalysts for α-olefin polymerization in the past 30 years.

As mentioned above, relatively little is known about group (V)[3] transition metals complexes polymerizing α-olefins where information is mainly available for Ta(V) and Nb(V). Vanadium catalytic systems in α-olefin polymerization remain relatively underdeveloped mainly due to the fact that four of the five-oxidation states display paramagnetism properties. However, great efforts to surmount these obstacles have lead to the development of a handful of vanadium-based catalytic systems.[4] Although the drawbacks of vanadium-based catalysts such as air-sensitivity and deactivation to lower oxidation states remain rather severe, industry maintains great interest in vanadium catalysts since specific polymer properties remain unique to vanadium catalytic systems. Vanadium catalysts produce random and amorphous ethylene/propylene co-polymers

with low crystallinity and furthermore they can be used in making more elaborate ter-polymers with a third monomer such as norbornylene. Studies by Ziegler's group have emphasized through theoretical calculations the high potential of the d^2 electronic configuration of vanadium(III) towards polymerization due to a low α-olefin insertion energy barrier and a high chain termination energy barrier[5].

Simply based on the lack of knowledge in the area of vanadium polymerization mechanism our group has set out to investigate possible activation pathways through a series of alkylation reactions to assess the vanadium-carbon bond stability by using a variety of oxygen and nitrogen donor-based supporting ligands. Upon using alkylating agents such as the alkylaluminium co-catalysts, attempts to trap and crystallize the active intermediate were attempted only to elucidate the deactivation process.

In order to assess and to picture more clearly the effectiveness of the α-olefin polymerization activities of the vanadium organometallic complexes synthesized in this thesis, a table rating the catalysts has been drawn using numbers obtained from a recent review article from Gibson's group.[2] (see Table 1.1)

Table 1.1 Quantifying Catalytic Activity for α-Olefin Polymerization

Rating	**Activity [g $mmol^{-1}$ h^{-1} atm^{-1}]**
Very low	< 1
Low	1-10
Moderate	10-100
High	100-1000
Very high	> 1000

In contrast to group IV polymerization catalysts, the vanadium-based catalysts are capable of high activities and rapid (almost suicidal) deactivation through reduction of the metal centre in close parallel to the lifestyle of the great American actor James Dean. Insight into the activation and deactivation pathways of vanadium-based catalysts and a few other metal congeners such as zirconium, chromium, and manganese will be investigated in the following thesis.

The second chapter will cover insight into the activation and deactivation pathways of the industrially used tris(acetylacetonato) vanadium complex in the co-polymerization of ethylene and propylene forming a polymer used in the production of synthetic rubber. The treatment of V(*acac*)$_3$ with the co-catalyst to be deactivated through "leaching" of the *acac* ligand to the aluminium metal centre.

In order to remedy the ligand migration to the co-catalyst a vanadium (III) complex supported by a nitrogen donor based ligand such as a bis(imino)pyridine ligand. Supporting the metal centre with a nitrogen donor based ligand system has proven to be quite successful with respects to the ligand leaching problem, increasing considerably the activity of the catalyst and inducing structure into the polymer. The bis(imino)pyridyl ligand has also opened the door to stabilizing low-valent transition metal complexes bearing alkyl groups. These results will be discussed in more depth in chapter 3 and chapter 4.

In attempt to combine the migratory properties of the oxygen donor based ligands and the stabilization properties nitrogen donor based ligands, the reactivity of the acetylpyrrolide ligand system was investigated with V(III). Two novel organometallic complexes were synthesized where, in one case, vanadium(III) mediated an aldolic

condensation of the acetylpyrrolide ligand and in a second case a vanadium(II) metal centre promoted a pinacolic coupling of the ligand. (Chapter 5)

Chapter 6 in mainly focused on the vanadium/aluminium interaction and the role of the co-catalyst in the activation and deactivation of the vanadium metal centre. In this case the vanadium centre is supported by a the bulky N,N,N, *tris*-trimethylsilyl diethylenediamidoamino ligand. Formation of novel vanadium/aluminium clusters were synthesized and have given great insight into the vanadium/aluminium interaction and has demonstrated involvement of the ligand as seen previously in the case of the bis(imino)pyridyl ligand system.

Preliminary reactivity of the *meso*-diphenyldipyrrolemethane ligand was investigated with Zr(IV), V(III), Cr(III), Cr(II) in Chapter 7. These reactions revealed the possible bonding modes of the pyrrolide moiety with the metal centre. Treatment of the V(III) *meso*-diphenyldipyrrolidemethane complex with a sterically demanding aryloxide lead to an interesting deoxygenation reaction of the aryloxide to form an oxygen bridged vanadium dimer which exerted high polymerization activities upon activation with dimethylaluminiumchloride.

To Diane, Frank and Joël

Acknowledgements

My ethereal journey through the world of chemistry could not have been possible without a truly great guide, my supervisor Sandro Gambarotta. He has fulfilled his role of university professor to the extreme in many ways. Firstly, he was able to transmit his knowledge and chemical intuition in a clear and concise manner to stimulate the thinking process and to realise those ideas in the lab. Secondly, he has given me the possibility to share the fruit of my labours with the scientific community by giving me the opportunity to attend and present my work in local, national and international chemistry conferences. Lastly, I would like to acknowledge Sandro's sense of humour, which has kept me smiling on the edge of my seat during group meetings.

To the lab colleagues I have had the pleasure to work with from the four corners of the world who have shared their scientific and cultural experiences in many a discussion in the lab. You have strengthened my desire to travel and discover the beauty of your countries of origin.

I would also like to acknowledge Dr. Hoch (Bayer AG) and Dr. Zahalka (Bayer) for the industrial internship at Bayer AG in Dormagen, Germany.

Special thanks to Dr. Wilson at Dow Chemicals and Dr. Wang at Nova Chemicals who have done the testing and the high temperature GPC polymer characterization of the good and not so good catalysts we have synthesized in our labs.

Thanks to Glenn Yap for all the X-ray structures he solved and teaching me how to develop my ability to pick single opaque dark brown crystals suitable for analysis.

To my mother Diane, who has never understood why I chose to study chemistry of all the possible subjects and who has taught to smile and not take life so seriously. To my father Frank, who listened to the frustrations of my chemistry and discuss the new advancements in my research project. To my brother, Joël who has taught me to lighten-up from time to time and who has exposed me to the phatest and funky beats on this earth.

To Sylvie, who has supported me in the writing process and with whom those warm summer nights have been filled with passionate discussions. (K)

Many thanks to all my friends who have in their own way influenced me to become a more complete, well-rounded person.

List of Publcations

Reardon, D.; Kovacs, I.; Ruppa, K. B. P.; Feghali, K.; Gambarotta, S.; Petersen, J.; Reactivity of Coordinatively Unsaturated Trivalent Chromium Complexes with Sulfur: Preparation of Novel Sulfide-Bridged Dinuclear Cr^{IV} Derivatives; *Chem. Eur. J.*, **1997**, *3*, 1482.

Ma, Y.; Reardon, D.; Gambarotta, S.; Yap, G. P. A.; Zahalka, H.; Lemay, C.; Vanadium-Catalyzed Ethylene-Propylene Co-polymerization: The Question of the Metal Oxidation State in Ziegler-Natta Polymerization Promoted by V(β-diketonate)$_3$; *Organometallics*, **1999**, *18*, 2773.

Reardon, D.; Conan, F.; Gambarotta, S.; Yap, G. P. A.; Wang, Q.; Life and Death of an Active Ethylene Polymerization Catalyst. Ligand Involvement in Catalyst Activation and Deactivation. Isolation and Characterization of Two Unprecedented Neutral and Anionic Vanadium(I) Alkyls; *J. Am. Chem. Soc.*, **1999**, *121*, 9318.

Feghali, K.; Harding, D. J.; Reardon, D.; Gambarotta, S.; Yap, G. P. A.; Wang, Q.; Stability of Metal-Carbon Bond *versus* Metal Reduction During Ethylene Polymerization Promoted by a Vanadium Complex: the Role of the Aluminium Co-Catalyst; **2001** submitted.

Reardon, D.; Harding, D. J.; Guan, J. W.; Gambarotta, S.; Yap, G. P. A.; Wilson, D. R.; Vanadium-Promoted Aldol Condensation and Pinacolic Coupling of Acetylpyrrole: Formation of Two New Potent Catalysts for Olefin Co-Polymerization; **2001**, submitted.

Reardon, D.; Harding, D. J.; Gambarotta, S.; Yap, G. P. A.; Wilson; Mono and Zero Valent Mn Complexes Supported by the α,α-Diiminato Pyridine Ligand: Aborted Catalysts for α-Olefin Polymerization, **2001**, submitted.

List of Abbreviations

acac	acetylacetonato
Å	angström
Anal.	Analysis
atm	atmosphere
BM	Bohr magneton
br	broad
°C	degrees Celsius
Calcd.	calculated
cat.	catalyst
cm^{-1}	wave number
Cp	cyclopentadienyl
Cy	cyclohexyl
Cy-acac	2-acetyl-cyclohexanone
δ	chemical shift
D_{calcd}	calculated density
DEAC	diethylaluminiumchloride
DMAC	dimethylaluminiumchloride
DME	dimethylethyleneglycol
DSC	density scanning calorimetry
EASC	ethylaluminiumsesquichloride
ETA	ethyl-1,1,1-trichloroacetate
Et	ethyl
EP	ethylene propylene elastomers
EPDM	ethylene propylene diene elastomers
F_{000}	electronic density
FTIR	Fourier transform infrared spectroscopy
F.W.	Formula weight
F-acac	1,1,1,5,5,5-hexafluoropentadione
g	grams
G.o.F.	goodness of fit
GPC	gel permeation chromatography
h	hour
i-Pr	isopropyl
i-Bu	isobutyl
INDO	incomplete neglect of differential overlap
K	Kelvin
kg	kilogram
L	ligand
LLDPE	linear low-density polyethylene
m	medium
μ_{calcd}	absorption coefficient
μ_{eff}	effective magnetic moment in Bohr magnetons
μmol	micromole
M	molar

MAO	methylalumoxane
mM	millimolar
Me	methyl
Mes	mesitylene
MHz	megahertz
min	minute
ml	millilitre
mmol	millimole
m.p.	melting point
NMR	nuclear magnetic resonance
ORTEP	Oak Ridge thermal ellipsoid program
PD	polydispersity (M_w/M_n)
Ph	phenyl
PMAO	polymethylalumoxane
ppm	parts per million
psig	pounds per square inch of gas
psi	pounds per square inch
Py	pyridine
R	alkyl group (found in reaction schemes)
R	reliability factor (crystallographic tables)
s	strong
sccm	square cubic centimetre
sh	sharp
T	temperature
t-Bu	tertiary butyl
t-Bu acac	2,2,6,6-tetramethylheptadi-3,5-one
THF	tetrahydrofuran
THF-d_8	deuterated THF
TMA	trimethylaluminium
TMEDA	N, N, N', N'-tetramethylethylenediamine
TMS	trimethylsilane
UV-vis	ultra-violet visible
V	volume
w	weak
X	halogen
XRF	X-ray fluorescence
XRD	X-ray diffraction
ZINDO	Zerner incomplete neglect of differential overlap

Table of Contents

References

1.(a) Kreuder, C.; Jordan, R. F.; Zhang, H.; *Organometallics*, **1995**, *14*, 2993-3001.

b) Wang, C.; Friedrich, S.; Younkin, T. R.; Li, R. T.; Grubbs, R. H.; Bansleben, D. A.; Day, M. W.; *Organometallics*; **1998**, *17 (15)*, 3149-3151.

(c) Crowther, D. J.; Baenzinger, N. C.; Jordan, R. F.; *J. Am. Chem. Soc.*, **1991**, *113*, 1455-1457.

(d) Jiménez Pindado, G.; Thornton-Pett, M.; Bochmann, M.; *J. Chem. Soc.Dalton Trans.*, **1997**, 3115-3127.

(e) Hessen, B.; van der Heijden, H.; *J. Am Chem. Soc.*, **1996**, *118*, 11670-11671.

(f) Rodriguez, G.; Bazan, G. C.; *J. Am. Chem. Soc.*, **1997**, *119*, 343-352.

(g) Rodriguez, G.; Bazan, G. C.; *J. Am. Chem. Soc.*, **1995**, *117*, 10155-10156.

(h) Pastor, A.; Kiely, A. F.; Henling, L. M.; Day, M. W.; Bercaw, J. E.; *J. Organomet. Chem.*, **1997**, *528*, 65-75.

2. Britovsek, G. J. P.; Gibson, V. C.; Wass, D. F.; *Angew. Chem. Int. Ed.*, **1999**, *38*, 428-447.

3.(a) Bazan, G. C.; Donnely, S. J.; Rodriguez, G.; *J. Am. Chem. Soc.*; **1995**, *117*, 2671-2672.

(b) Gibson ,V. C.; *J. Chem. Soc. Dalton Trans.*, **1994**, 1607.

(c) Antonelli, D. M.; Leins, A.; Stryker, J. M.; *Organometallics*, **1997**, *16*, 2500-2502.

(d) Mashima, K.; Fujikawa, S.; Tanaka, Y.; Urata, H.; Tanaka, E.; Nakamura, A.; *J. Chem. Soc. Chem. Comm.*, **1994**, 1623.

(e) Mashima, K.; Fujikawa, S.; Tanaka, Y.; Urata, H.; Oshiki, T.; Tanaka, E.; Nakamura, A.; *Organometallics*, **1995**, *14*, 2633-2640.

(f) Mashima, K.; Tanaka, Y.; Kaidzu, M.; Nakamura, A.; *Organometallics*, **1996**, *15*, 2431-2433.

(g) Hakala, K.; Lofgren, *Macromol. Chem. Rapid Commun.*, **1997**, *18*, 635-638.

4.(a) Coles, M. P.; Gibson, V. C.; *Polym. Bull.*, **1994**, *33*, 529-533.

(b) Scheuer, S.; Fischer, J.; Kress, J.; *Organometallics*, **1995**, *14*, 2627-2629.

(c) Doi, Y., Suzuki, S.; Soga, K. *Macromolecules*, **1986**, *19*, 2896.

(d) Ouumi, T.; Soga, K. *Makromol. Chem.*, **1992**, *193*, 823.

(e) Gumbolt, A.; Helberg, J.; Schleitzer, G. *Makromol. Chem.*, **1967**, *101*, 229.

(f) Adisson, E. *J. Polym. Sci., Part A: Polym. Chem.*, **1994**, *32*, 1033.

(g) Davis, S. C.: von Hellens, W.; Zahalka, H. *Polymer Material Encyclopedia Vol. 3*: Salamone, J. C., Ed.; CRC Press Inc.; Boca Raton, FL, **1996**.

(h) Sinn, H.; Kaminski, W. *Adv. Organomet. Chem.*; Stone, F.G.A.; West R. Eds.; Academic Press: New York, **1980.**

(i) Doi, Y.; Tokuhiro, N.; Nunomura, M.; Miyake, H.; Suuki, S.; Soga, K. *Transition Metals and Organometallics as Catalysts for Olefin Polymerization*; Kaminsky, W.; Sinn H. Eds.; Springer-Verlag: Berlin, **1988.**

(j) Carrick, W. L. *J. Am. Chem. Soc.* **1958**, *80*, 6455.

(k) Christman, D. L. *J. Polymer Sci.* **1972**, *A-1*, 471.

(l) Pasquon, I. G.; Giannini, U. *Catalysis*; Anderson, J. R.; Boudart, M. Eds.; Springer-Verlag: Berlin, **1984**

(m) Carrick, W. L.; Kluiber, R. W.; Bonner, E. F.; Wartman, L. H.; Rugg, F. M.; Smith J. J. *J. Am. Chem. Soc.* **1960**, *82*, 3883.

(n) Lehr, M. H. *Macromolecules* **1968**, *1*, 178.

(o) Christman, D. L.; Keim, G. I. *Macromolecules* **1968**, *1*, 358.

(p) Lehr, M. H.; Carmen, C. J. *Macromolecules* **1969**, *2*, 217.

(q) Duck, E. W.; Grant, D.; Horder, J. R.; Jenkins, D. K.; Marlow A. E.; Wallis, S. R.; Doughty, A. G.; Maradon, J. M.; Skinner, G. A. *European Polymer J.* **1974**, *10*, 481.

(r) Schuere, S. ; Fisher, J.; Kress, J. *Organometallics* **1995**, *14*, 2627.

(s) Feher, F. J.; Blanski, R. L. *J. Am. Chem. Soc.* **1992**, *114*, 5886.

(t) Feher, F. J.; Walzer, J. F.; Blanski, R. L. *J. Am. Chem. Soc.* **1991**, *113*, 3618.

(u) Feher, F. J.; Blanski, R. L. *Organometallics* **1993**, *12*, 958.

(v) Cucinella, S.; Mazzei A. U.S. Patent 3,711,455, CI. 260-85.3 **1973.**

(w) Boor Jr., J.; Youngman, E. A. *J. Polymer Sci* **A-1**, **1966**, *4*, 1861.

(x) Zambelli, A.; Proto, A.; Longo, P. *Ziegler Natta Catalysis*; Fink, G.; Mulhaupt, R.; Brintzinger, H. H. Eds., Springer-Verlag Berlin, **1995.**

5. Schmid, R.; Ziegler, T.; *Organometallics*, **2000**, *19*, 2756-2765

Introduction

Introduction

1.1 Characteristics of Transition Metal Complex Catalysts

In the early development of the science of microbiology researchers came to the realization that many specific cellular functions are regulated by enzymatic reactions, which could be described as Mother Nature's own catalysts. Many of these enzymes were revealed to be dependent on transition metals to render the high efficiency and the high selectivity of the thousands of reactions that occur daily, under mild conditions, in living organisms. These catalytic reactions span a wide range of uses, from the most spectacular transformation of solar energy into chemical energy as in the photosynthetic systems found in the plant kingdom mediated by manganese porphyrin complexes, to the transformation of atmospheric dinitrogen into ammonia by a complex series of reactions mediated by iron/sulphur and molybdenum/sulphur cluster-based enzymes and co-enzymes found in certain types of bacteria[1].

These naturally occurring catalysts have inspired the industrial use of catalysts to accelerate industrial processes to catalyze a wide variety of chemical reactions. In this context, the catalyst can be more specifically defined as a substance in which a transition metal complex serves as an active site that will influence the rate of the reaction and reduce the activation energy barrier without itself being used up in the reaction. The catalyst can therefore also be considered as a reactant and a product in the reaction. Ideally speaking the catalyst concentration is very small and stays constant throughout the reaction assuming pristine catalytic conditions and in the absence of catalyst poisons

to ultimately obtain a "living polymerization" catalyst in standard temperature and pressure conditions.

Catalysts are classified in two major categories namely, homogeneous or heterogeneous catalytic systems. Transition metal complexes are, in the greater scheme of things, classified as homogeneous catalysts, and have certain advantages over heterogeneous catalysts such as metals and metal oxides. The heterogeneous catalysts usually activate the substrate via high surface reactivity that in turn allows specific reactions to occur even in the absence of solvent. One of the many advantages of the heterogeneous catalysts lies simply in the fact that they are relatively easy to prepare and inexpensive. Another advantage is the fact that these catalysts are thermally robust and less sensitive to "poisoning" or to decomposition when compared to homogeneous early transition metal complex catalysts. However, the fact that heterogeneous catalysts in nature are reactively dependent on the physical and chemical structure of the surface, makes the study of catalytic reactions difficult to characterize.

The homogeneous catalytic systems on the other hand have the great advantage in this respect since discrete molecular systems can be monitored and characterized in the dynamic catalytic process. In order to characterize the molecular active species, a wide variety of spectroscopic methods have been developed to describe the structure and nature of transition metal complexes. Major advances in the field of organometallic chemistry have come about since the advent of single crystal X-ray structural analysis, which plays an important role in revealing the "true face" of transition metal complexes. The elucidated structures obtained from the X-ray studies enable organometallic chemists

to determine transition metal complex geometries including bond distances and bond angles yielding important structural information on the influence of the ligand in the catalytic process. Furthermore, in the case of paramagnetic complexes where nuclear magnetic resonance spectroscopy is still an ambiguous inconclusive experimental technique, single crystal X-ray structure analysis is considered to be virtually the only characterization method. By isolating and defining the structure of the initial complex, the activated intermediate and the deactivated organometallic product, allowed us to propose a plausible reaction mechanism describing the catalytic steps, a method which gives more insight into the molecular structure than paramagnetic nuclear magnetic resonance spectroscopy which in many cases presents broad resonance peaks that are relatively hard to assign concisely. The catalytic process targeted by this thesis work is the polymerization of α-olefins mediated for the most part by vanadium organometallic complexes supported by oxygen and nitrogen donor based ligand systems.

Homogeneous catalysis opens the doors to endless synthetic possibilities to tune and induce selectivity by choosing the right metal in the right oxidation state and to tailor suitable supporting ligand systems, a feature which is less accessible despite recent advances in surface organometallic chemistry in developing well defined heterogeneous catalysts. A good example of the tunable selectivity of homogeneous catalysts can be demonstrated by the kinetic resolution of racemic 3-substituted α-olefins with zirconocene catalysts developed by the group of Bercaw.[2] (Scheme 1.1)

Scheme 1.1 Example of the Tunable Selectivity of a Homogeneous Catalyst

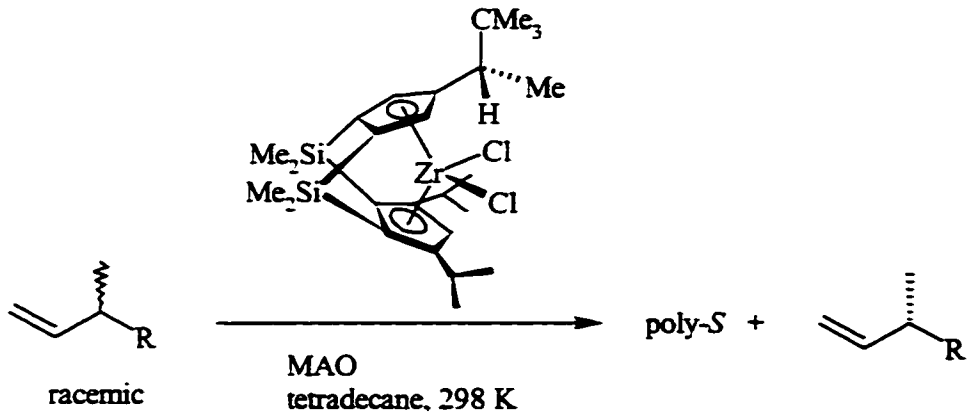

1.2 Ziegler-Natta Polymerization Catalysts

The discovery by Ziegler and Natta in the '50s concerning the ability of a catalytic mixture of $MCl_x/AlEt_3$ (M = Ti, Zr, V; x = 3, 4) to form relatively large amounts of high value polymers from inexpensive α-olefins have an enormous impact on our modern lifestyle. Since then, this great catalytic process has been the target of a tremendous amount of research. Today the worldwide production of polyethylene, polypropylene and EPDM elastomers is estimated at about 79.6 x 10^6 tons per year.[3f] Earlier developments in this field include the synthesis of stabilized group IV metallocenes in high oxidation states developed for polymerization in the late 1970's and the well-known constrained geometry catalysts.[3] In combination with the development of novel co-catalysts such as methylalumoxane[4] and "cationizing" reagents such as $Na[B\{3,5\text{-}(CF_3)_2C_6H_3\}_4]$ or $[Ph_3C][B(C_6F_5)_4]$[5] a phenomenal increase of activity, extended catalyst life, control over polymer molecular weight distributions have been obtained.

Research in the development of this field has grown towards synthesizing catalysts that can tailor polymer properties. Competing with other methods of polymerization such as ring opening olefin metathesis (ROMP) based on the molybdenum (VI) Schrock type catalysts[6] or the ruthenium (IV) Grubbs type catalysts (figure 1.1),[7] the field of cationic Ziegler-Natta polymerization catalyst design is today gearing towards the synthesis of new organometallic complexes having the capacity of inserting functionalised monomers in order to synthesize novel polymers tailored to specific industrial needs.

Figure 1.1 ROMP Catalysts

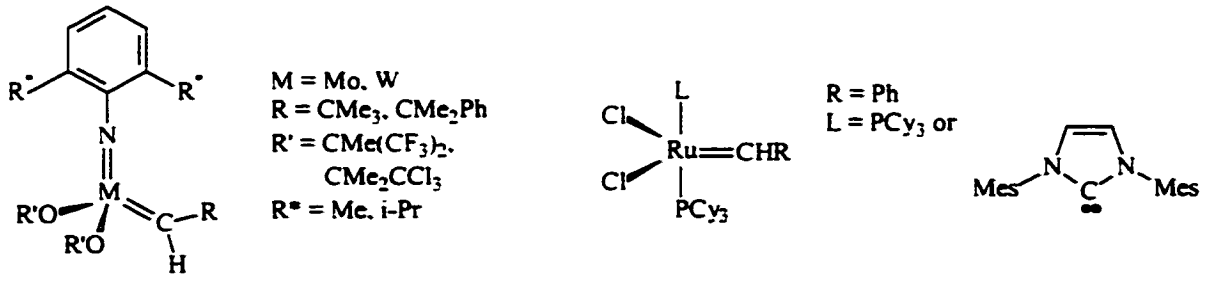

Schrock-type Catalyst **Grubbs-type Catalyst**

Conventional cationic Ziegler-Natta polymerization systems are based on electron-deficient group IV metals such as Ti(IV) and Zr(IV). Organometallic complexes synthesized for polymerization have strong Lewis acid properties and require a co-catalyst for two purposes. The first is to alkylate the metal centre in the case where the complex does not bear any alkyls to initiate chain growth (Scheme 1.2).

Scheme 1.2 Alkylation of the Catalyst by the Co-catalyst

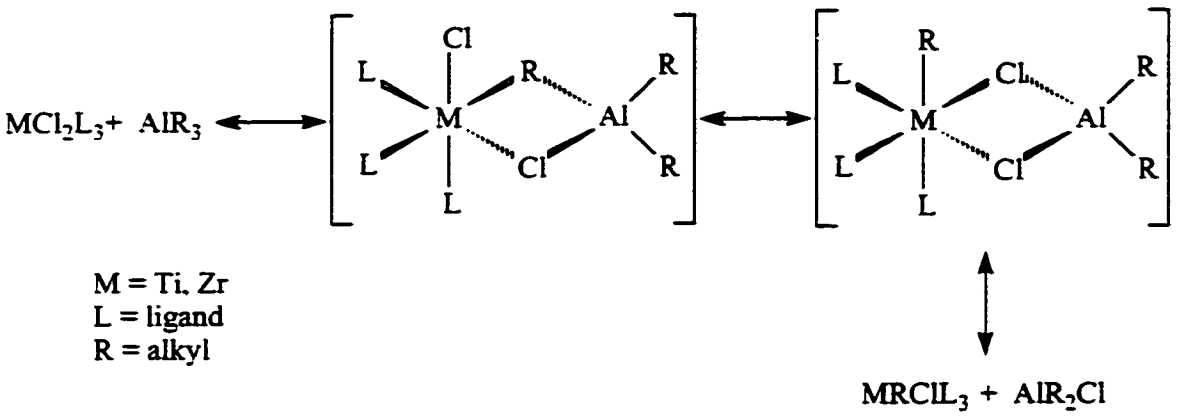

The second is to cationize the metal centre to coordinate α-olefins, an important intermediate step discovered by Jordan in the mid '80s and improved by other groups (Scheme 1.3). More recent findings by Erker's group[5] have demonstrated that the formation of the cation can not only be conducted by the use of an aluminium–based co-catalyst but also by using a borane based reagent, to form an analogous species in solution.

Scheme 1.3 Formation of the Cationic Catalytic Species

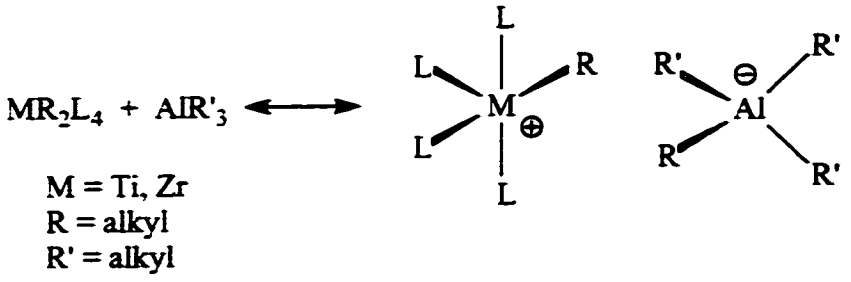

Initial insertion of the α-olefin into the metal-carbon is generally agreed upon to happen through coordination of the olefin in the empty coordination site of the organometallic complex followed by migration of the alkyl to the olefin forming in the process an alkyl chain augmented by a minimum of two carbons depending on which α-olefin is inserted (Scheme 1.4). Subsequent insertions of the olefin into the growing alkyl chain are observed. The propagation of the alkyl chain will continue (Scheme 1.4) until chain termination steps occur through processes such as β-H elimination chain transfer.

Scheme 1.4 Initial Olefin Insertion into the Metal-Carbon Bond

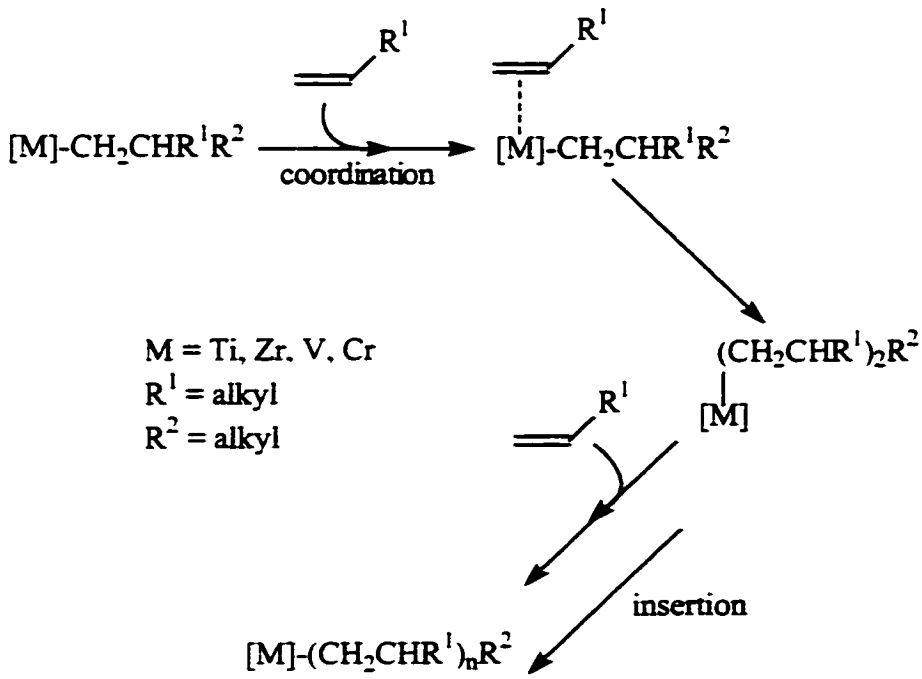

The key to high chain propagation and therefore to high molecular weight fractions lies in the stability of the metal-carbon bond and how susceptible the complex is to β-H elimination of the growing alkyl chain. Once the alkyl chain has undergone β-H

elimination, olefin insertion can continue via insertion into the metal-hydrogen bond as described in Scheme 1.5 until catalyst is deactivated or chain termination occurs once again.

Given the tremendous activity of Cp-based group IV catalysts towards α-olefin polymerization, development of novel supporting ligand systems is a current and growing field of research. Good alternatives to the cyclopentadienyl ligand system were discovered to be the oxygen and nitrogen donor based ligands, which can be designed to be isolobal to the Cp ligand systems and have demonstrated to possess activities that are quite comparable to the activities expressed by metallocenes.

Scheme 1.5 Chain Termination through β-H Elimination

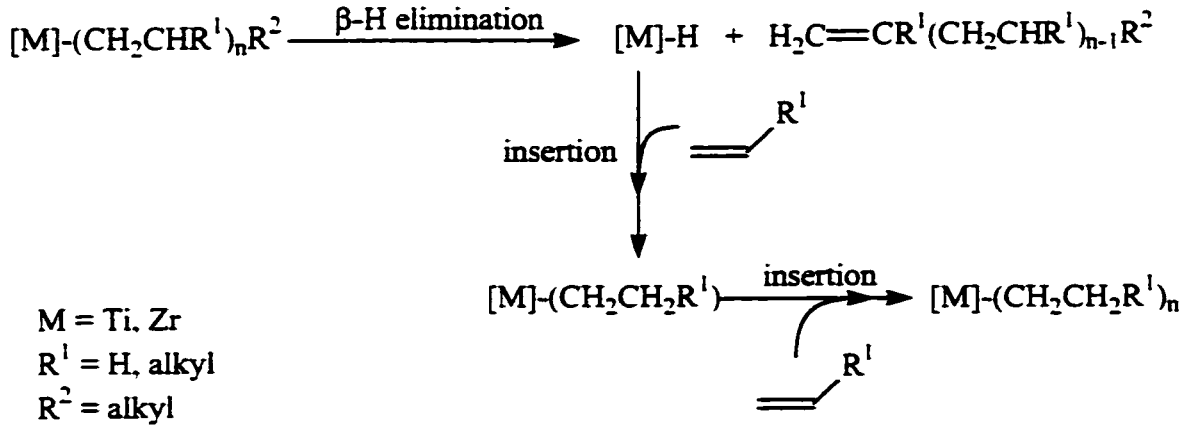

Examples of successful group IV transition metal catalysts supported by oxygen/nitrogen ligand systems are described in Figure 1.2[8].

Figure 1.2 Alternative Group IV Catalysts to the Conventional Metallocenes

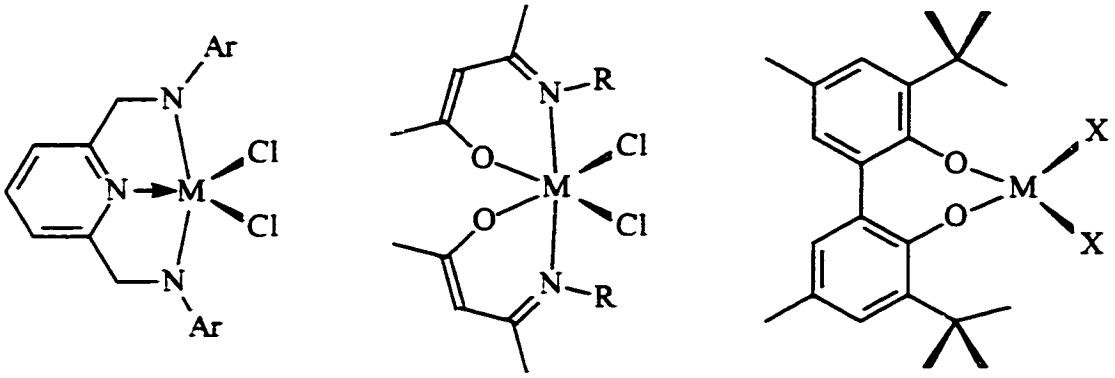

M = Ti, Zr, Hf

The success of the group IV catalysts in polymerization of α-olefins has prompted research in the synthesis of novel organometallic complexes concentrating on different metals such as group V, group VI and even more recently in the development of late-transition metal polymerization catalysts[12].

A literature search of vanadium α-olefin polymerization determined that this field of research is underdeveloped with respect to the mechanistic aspects of the polymerization and limits itself to the synthesis of a few organometallic complexes, which have demonstrated catalytic activity (figure 1.3)[9, 14c]. Yet, industrial use of vanadium-based catalysts is dominant in the production of elastomers, the crude material used to produce synthetic rubber. Furthermore, the chemistry of group V transition metals differs from the chemistry of group IV elements simply due to the wide range oxidation states available to the metal centre. The mechanism of activation and deactivation of the vanadium catalytic species brought forward in the following thesis may somewhat differ from the proposed reaction schemes for group IV catalytic systems since vanadium has

the possibility to exist in six oxidation states (-1, 0, +1, +2, +3, +4, +5). Only the higher oxidation states (+3, +4 and +5) are believed to be catalytically active towards α-olefin polymerization. The main drawback of vanadium catalysts has lies in the fact that the vanadium based complexes synthesized to date have a tendency to be reduced to lower oxidation states which are inactive towards polymerization. Industrial processes therefore have recourse to "reactivating" substances (such as ethyl-1,1,1-trichloroacetate) that reoxidize the vanadium centre back to its original active oxidation state. The mechanism of "reactivation" remains quite obscure and will be treated more extensively in this thesis.

Figure 1.3 Examples of Vanadium Catalysts with Different Oxidation States[10, 14c]

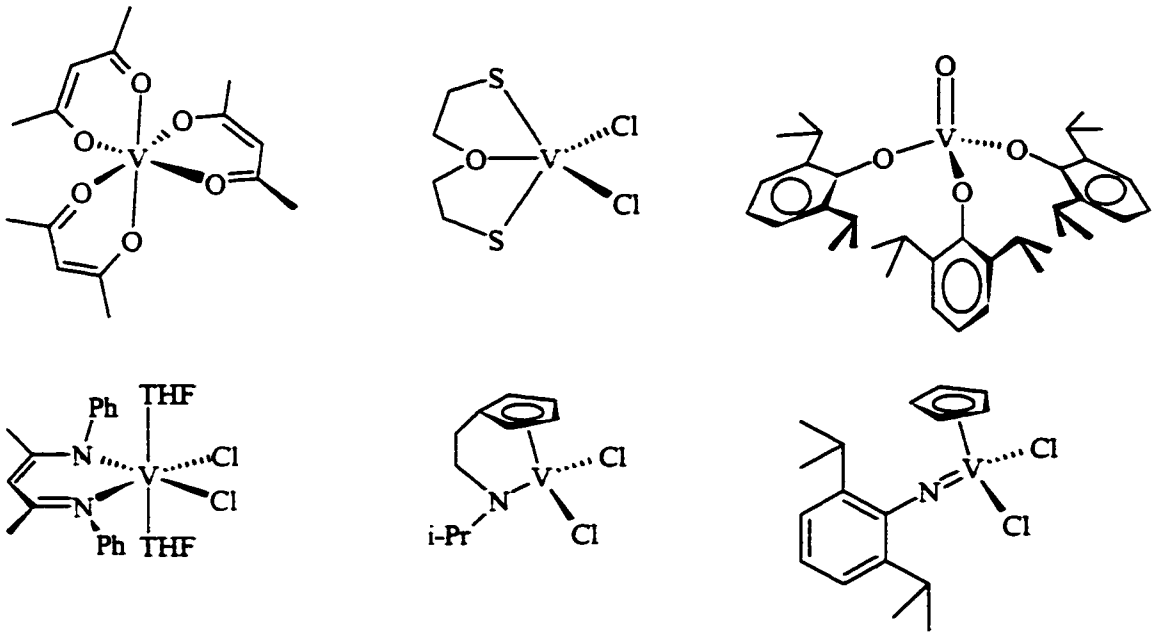

1.3 References

1. Georgiadis, M. M.; Komiya, H.; Chakrabarti, P.; Woo, D.; Kornuc, J. J.; Rees, D. C., *Science*, **1992**, *257*, 1653.

2.(a) Herzog, T. A.; Zubris, D. L.; Bercaw, J. E.; *J. Am. Chem. Soc.*, **1996**, *118*, 11988.

(b) Veghini, D.; Henling, L. M.; Burkhardt, T. J.; Bercaw, J. E.; *J. Am. Chem. Soc.*, **1999**, *121*, 564.

3.(a) Bochman, M.; *J. Chem. Soc. Dalton Trans.*, **1996**, 255.

(b) Brintzinger, H. H.; Fischer, D.; Mülhaupt, R.; Rieger, B.; Waymouth, R. M.; *Angew. Chem.*, **1995**, *107*, 1255.

(c) Brintzinger, H. H.; Fischer, D.; Mülhaupt, R.; Rieger, B.; Waymouth, R. M.; *Angew. Chem. Int. Ed. Engl.*; **1995**, *34*, 1143.

(d) Möhring, P. C.; Coville, N. J.; *J. Organomet. Chem.*, **1994**, *479*, 1.

(e) Gupta, V. K.; Satish, S.; Bhardwaj, I. S.; *Rev. Macromol. Mol. Chem. Phys. C*, **1994**, *34*, 439.

(h) Kaminsky, W.; *J. Chem. Soc. Dalton Trans.*, **1998**, 1413.

(i) Soga, K.; Shiono, T.; *Prog. Polym. Sci.*; **1997**, *22*, 1503.

(j) Jordan, R. F.; *Adv. Organomet. Chem.*, **1991**, *32*, 325.

4. Brookhart, M.; Grant, B.; Volpe, A. F.; *Organometallics*, **1992**, *11*, 3920.

5.(a) Temme, B.; Erker, G.; Karl, J.; Luftmann, H.; Fröhlich, R.; Kotila, S.; *Angew. Chem.*, **1995**, *107*, 1867.

(b) Temme, B.; Erker, G.; Karl, J.; Luftmann, H.; Fröhlich, R.; Kotila, S.; *Angew. Chem. Int. Ed. Engl.*, **1995**, *34*, 1755.

(c) Temme, B.; Karl, J.; Erker, G.; *Chem. Eur. J.*, **1996**, *2*, 919.

(d) Karl, J.; Erker, G.; *Chem Ber.*, **1997**, *130*, 1261.

6.(a) Hoveyda, A. H.; Schrock, R. R.; *Chem. Eur. J.*, **2001**, *7*, 945.

(b) Feldman, J.; Davis, W. M.; Schrock, R. R.; *J. Am. Chem. Soc.*, **1986**, *108*, 2771

(c) Boyd, T. J.; Schrock, R. R.; *Macromolecules*, **1990**, *23*, 2819.

7.(a) Pederson, R. L.; Grubbs, R. H.; US Patent 6,215,019 B1

(b) Pederson, R. L.; Grubbs, R. H.; US Patent 5,916,983

(c) Schwab, P.; Grubbs, R.; Ziller, J., *J. Am. Chem. Soc.*; **1996**, 100-110

(d) Nguyen, S.; Grubbs, R.; *J. Am. Chem. Soc.*, **1993**, *115*, 9858.

8.(a) Schaverien, C. J.; *J. Mol. Catal.*; **1994**, *90*, 177-183.

(b) *Chem. Eng. News*, **1978**, *56(31)*, 24.

(c) Pelletier, J. F.; Mortreux, A.; Petit, F.; Olonde, X.; Bujadoux, K.; *Stud. Surf. Sci. Catal.*, **1994**, *89*, 249.

9.(a) Henderson, R. A.; Hughes, D. L.; Janas, Z.; Richards, R.; Sobota, P.; Szafert, S.; *J. Organomet. Chem.*, **1998**, *554*, 195-201.

(b) Chan, M. C. W.; Cole, J. M.; Gibson, V. C.; *Chem. Comm.*; **1997**, 2345.

(c) Janas, Z.; Jerzykiewicz, L. B.; Przybylak, S.; Richards, R. L.; Sobota, P.; *Organometallics*, **2000**, *19*, 4252.

(d) Woo-Kyn, K.; Fevola, M. J.; Liable-Sands, L. M.; Rheingold, A. L.; Theopold, K. H.; *Organometallics*, **1998**, *17*, 4541.

(e) Witte, P.T.; Meetsma, A.; Hessen, B.; *Organometallics*, **1999**, *18*, 2944.

Chapter 2

Vanadium-Catalyzed Ethylene-Propylene Co-polymerization: The Question of the Metal Oxidation State in Ziegler-Natta Polymerization Promoted by V(ß-diketonate)$_3$.

Abstract

Chapter 2 *presents four different V(β-diketonate)$_3$ complexes [β-diketonate = 2,4-pentanedione (acac), 2-acetylcyclohexanone (Cy-acac), 2,2,6,6-tetramethyl-3,5-heptanedione (t-Bu-acac), and 1,1,1,5,5,5-hexafluoro-2,4-pentanedione (F-acac)] that have been prepared and tested as catalysts for propylene-ethylene co-polymerization with the aim of gaining insights into the structure of the active species. Data on polymer composition and catalyst activity indicate that one of the roles of the Al co-catalyst is to trigger a major ligand scrambling around the transition metal. Attempts to isolate the catalytically active species afforded a compound formulated as {[(β-diketonate)AlCl$_2$][VCl$_2$][(β-diketonate)$_2$AlCl]}. This species, which displayed only a minor catalytic activity, arises from a parasite process (catalyst deactivation). The formulation was supported by chemical degradation experiments with THF, which afforded a mixture of [V$_2$Cl$_3$(THF)$_6$][AlCl$_4$] and [(acac)$_2$Al(THF)$_2$][AlCl$_4$]* ***(2.5)****. Two unprecedented V(II) complexes (R-acac)$_2$V(TMEDA) [R = H(****2.7a****), Cy(****2.7b****), t-Bu (****2.7c****)] have been prepared and reacted with halocarbons to model the reactivation process. The results indicated that the primary role of reactivating substances, commonly employed in the industrial processes, is to reoxidize V(II) to the trivalent state. The reaction formed the catalyst precursor (R-acac)$_2$VCl(TMEDA), which was characterized on the basis of analytical and spectroscopic data. In agreement with this proposal, a trapping experiment carried out with ZnCl$_2$ or oxidation with CuCl allowed the isolation and characterization of (t-Bu-acac)$_2$V(TMEDA)][X] [X = ZnCl$_4^-$ (****2.8****), CuCl$_2^-$ (****2.9****)]. The structures of* ***2.5****,* ***2.7a****,* ***2.8****, and* ***2.9*** *have been elucidated by X-ray diffraction.*

2.1 Introduction

The Ziegler-Natta olefin polymerisation certainly is among the most famous catalytic processes discovered in this century. It is used worldwide for the large-scale production of polymers important to modern society. The process is very efficient, and a

remarkable wealth of technology has been developed to improve even further its efficiency and stereoselectivity.[12] However, despite the enormous commercial interest involved in this science, the understanding of the mechanism remains limited. Major breakthroughs in this direction were obtained with the discovery of the cationic Ziegler-Natta catalysts[3] and more recently, with the discovery that a cationic aluminium alkyl derivative may catalyse olefin polymerisation in the absence of transition metals.[4] Today it is well established that an enhanced Lewis acidity and the employment of a large excess of Al-based co-catalyst are the recipe of a successful and efficient catalytic system. However, the recent discovery that some electron-rich late transition metal complexes may also act as powerful Ziegler-Natta catalysts[5] has rejuvenated the academic and industrial interest for a better understanding of these remarkable systems.

The main stream of research in this field has relatively ignored group V metals, and information remained mainly limited to the patent literature[6] until recently, when the appearance of a few reports[7] indicated a revival of interest for vanadium-based Ziegler-Natta catalysis.[8] In fact, the current paucity of this literature is in striking contrast with the fact that vanadium catalysts are widely used for the industrial production of ethylene-propylene-diene elastomers (EPDM).[9] The most surprising peculiarity of this vanadium-based catalytic system consists of the employment of a coordinatively saturated V(β-diketonate)$_3$ complex containing vanadium in the trivalent oxidation state. Given its d^2 electronic configuration and the medium oxidation state, this species certainly cannot be considered as an "acidic" complex and somewhat deviates from the usual Ziegler-Natta paradigm. Therefore, the excellent activity of this particular catalytic system poses some fascinating mechanistic questions. The fact that the catalyst is coordinatively saturated

implies that one of the functions of the Al co-catalyst is to trigger a major molecular reorganisation around the transition metal. It is reasonable to assume that at least one of the *acac* ligands is abstracted by the Al co-catalyst to form a coordinatively unsaturated vanadium alkyl. On the other hand, it is well established that the chlorine content of the co-catalyst is a determining factor for the activity of the catalyst.[8] Thus; other questions arise about the structure of the catalyst and the role of the halogen. Is the active complex ionic with a positive charge on the transition metal or is it instead a species containing both vanadium and aluminium in the same molecular aggregate?[10]

The second point of interest concerns the oxidation state of the vanadium centre during the catalytic cycle. The +3 oxidation state of vanadium is a fairly stable one, and scarce are the examples of stable homoleptic alkyl derivatives that have been reported in the literature.[11] On the other hand, the aluminium alkyl co-catalyst certainly has the sufficient reducing strength to lower the oxidation state of vanadium to the +2 state.[12] In agreement with this idea, a recent report has suggested the possibility that an in situ generated V(II) alkyl complex might work as a catalyst precursor.[11b] In addition, some V(II) salts have been reported to be active ethylene polymerisation catalysts.[11c] Conversely, ESR experiments have indicated that the oxidation state +2 might be inert toward polymerisation, in agreement with the observation that vanadium catalysts typically die over the course of few minutes after displaying initially high polymerisation rates.[13] Thus, the possible reduction of the V(β-diketonate)$_3$ catalyst is commonly regarded as a deactivating process.[11d] This idea is further supported by the fact that the employment of mild oxidising agents (chlorinated esters or halocarbons) as catalyst reactivators is critical for the optimisation of the catalytic cycle. Literature proposes certain mechanisms of

reactivation through chlorination of the vanadium(II) metal centre upon deactivation[14]. The complete series of organic complexes formed in solution still remains speculative although it has been agreed that reductive coupling of the halogenated substrates by vanadium(II) does occur through the following mechanism where R-Cl is a perchlorinated organic substrate (Scheme 2.1).

Scheme 2.1 Reactivation of the Vanadium Catalyst Using a Perchlorinated Organic Reagent.

$V(III) \rightarrow V(II)$ *via aluminium alkyls radical coupling*

$V(II) + R\text{-}Cl \rightarrow V(III)^{+\cdot} + RCl^{\cdot -}$ *single electron transfer*

$V(III)^{+\cdot} + R\text{-}Cl^{\cdot -} \rightarrow V(III)Cl + R\cdot$

$R\text{-}Cl^{\cdot -} \rightarrow$ *further reaction products via aluminium alkyls*

$2\ R\cdot \rightarrow R\text{-}R$ *alkyl radical reductive coupling.*

The role of these substances is debated since in addition to reoxidising the metal centre to a higher oxidation state (+3 or +4) that is able to restart the cycle, they also react in a destructive manner with the co-catalyst. Since the catalyst oxidation state and the role of the reactivators remain speculative, we have carried out the present study with the aim to gain some insight into both the catalyst structure and the metal oxidation state of the catalytically active species. In this chapter we describe our findings.

2.2 Experimental Section

All operations were performed under inert atmosphere with the use of standard Schlenk techniques or in a nitrogen-filled drybox. $VCl_2(TMEDA)_2$,[15] $VCl_3(THF)_3$,[16] $V(acac)_3$ **(2.1)**,[17] and $[V_2Cl_3(THF)_6][AlCl_4]$[18] were prepared according to published procedures. Solvents were dried by following standard procedures. NMR spectra were recorded on a Bruker AMX-500 spectrometer by using vacuum-sealed samples prepared in a drybox. Ethyl trichloroacetate, 1,1,2-trichloroethane, 2,4-pentanedione (*acac*), 2-acetylcyclohexanone (*Cy-acac*), 2,2,6,6-tetramethyl-3,5-heptanedione (*t-Bu-acac*), and 1,1,1,5,5,5-hexafluoro-2,4-pentanedione (*F-acac*) were purchased from Aldrich and dried using activated molecular sieves. Infrared spectra were recorded on Mattson 3000 FTIR spectrometer. Nujol mulls were prepared in the drybox. $Et_3Al_2Cl_3$, Et_2AlCl (DEAC), MeLi, and *i*-BuLi (Aldrich) were used as received. Magnetic measurements were carried out with a Gouy balance (Johnson Matthey) at room temperature. The magnetic moments were calculated by standard methods,[19] and corrections for underlying diamagnetism were applied to the data.[20]

Synthesis of V(*Cy-acac*)$_3$ (2.2)

In a modification of a previously reported preparation[21] an ether solution of MeLi (7.8 ml, 1.4 M) was added dropwise and under vigorous stirring at -78 °C to a solution of 2-acetylcyclohexanone (1.54 g, 11.0 mmol) in THF (100 ml). Stirring was continued for 1 h. After warming the reaction mixture to room temperature, the addition of $VCl_3(THF)_3$ (1.37 g, 3.7 mmol) resulted in a dark brown colour. The reaction mixture was stirred overnight. The solvent was evaporated in vacuo, and the residual brown solid was

resuspended in hexane (350 ml). After filtration of LiCl and partial removal of the solvent, the resulting solution was allowed to stand at -30 °C for 2 days, upon which brown micro-crystals of **2.2** (1.0 g, 2.2 mmol, 59%) separated. Anal. Calcd (Found) for $VC_{24}H_{33}O_6$: C 61.53 (61.12), H 7.10 (7.33). IR (Nujol mull, cm^{-1}) : 1568(br, s), 1460(br, s), 1375(sh), 1261(m), 1166(m), 994(m), 962(m), 825(w), 711(w). $\mu_{eff} = 2.89\ \mu_{BM}$.

Synthesis of V(*t-Bu-acac*)$_3$ (2.3)

Using *t-Bu-acacH* (1.3 ml, 6.2 mmol) in THF (150 ml) and MeLi (4.5 ml, 1.4 M) an identical procedure was followed as for the preparation of **2.2**. (Yield: 0.70 g, 1.2 mmol, 57%). Anal. Calcd (Found) for $VC_{33}H_{57}O_6$: C 65.98 (65.17), H 9.56 (9.13). IR (Nujol mull, cm^{-1}): 1539(s), 1501(s), 1462(s), 1382(s), 1357(s), 1224(m), 1175(m), 1144(m), 1021(m), 873(m), 795 (m), 761(w), 740(w), 628(m). $\mu_{eff} = 2.86\ \mu_{BM}$.

Synthesis of V(*F-acac*)$_3$ (2.4)

An identical procedure as for **2.2** was followed by using *F-acacH* (0.9 ml, 6 mmol) in THF (150 ml) and MeLi (4.3 ml, 1.4 M) at -78 °C. Yield: 0.55 g, 0.82 mmol, 41%). Anal. Calcd (Found) for $VC_{15}H_3F_{21}O_6$: C 24.71 (25.08), H 0.41 (0.42). IR (Nujol mull, cm^{-1}) : 1596(s), 1524(s), 1456(s), 1419(s), 1381(s), 1358(s), 1275(m), 1190(w), 1163(m), 1020(m), 962(m), 825 (m), 711(m), 667(s). $\mu_{eff} = 2.90\ \mu_{BM}$.

Reaction of V(*acac*)$_3$ with $AlCl_3$. Preparation of [Al(acac)$_2$(THF)$_2$][$AlCl_4$] (2.5)

Solid V(*acac*)$_3$ (0.97 g, 2.8 mmol) was dissolved in THF (150 ml) and treated with $AlCl_3$ (0.75 g, 5.6 mmol). The resulting solution slowly changed colour from reddish brown to

light yellow. After concentration to a small volume, the resulting solution was allowed to stand at -78 °C for 2 days, upon which colourless crystals of $[Al(acac)_2(THF)_2][AlCl_4]$ separated (0.40 g, 0.74 mmol, yield 28%). Anal. Calcd (Found) for $Al_2C_{18}H_{30}O_6Cl_4$: C 40.17 (39.66), H 5.62 (5.67). IR (Nujol mull, cm^{-1}): 1574(s), 1538(s), 1459(s), 1399(s), 1377(s), 1345(m), 1295(m), 1198(w), 1021(s), 953(m), 872(s), 808(s), 702(m), 660(m), 620(m). ^1H NMR (THF-d_8, 500 MHz, ppm) : 5.78 (2H, CH *acac*), 3.58 (CH_2 THF), 2.03 (12H, CH_3 *acac*), 1.74 (CH_2, THF). ^{13}C NMR (THF-d_8, 125.7 MHz, ppm) : 195.22 (C=O, *acac*), 103.92 (CH, *acac*), 68.598 (CH_2, THF), 26.855 (CH_3, *acac*), 26.351 (CH_2, THF). ^{27}Al NMR (THF-d_8, 130.3 MHz, ppm) : 102.57 (sharp s, $[Al(acac)_2(THF)_2]^+$), 3.01 (very broad, $[AlCl_4]^-$).

Reaction of V(*acac*)$_3$ with EtAlCl$_2$.

The addition of a hexane solution of $EtAlCl_2$ (18 ml 1.0 M) to a solution of V(*acac*)$_3$ (2.1 g, 6.0 mmol) in toluene (150 ml) at room temperature changed instantaneously the colour from reddish brown to brown. An insoluble light brown precipitate appeared almost immediately (2.6 g, 4.7 mmol, 78%) and was filtered after the mixture was stirred for 2 h. Dissolution the solid in THF (100 ml) turned the colour light green. After filtration and concentration to small volume, the resulting solution was allowed to stand at -78 °C for 2 days, upon which a mixture of colourless crystals of $[Al(acac)_2(THF)_2][AlCl_4]$ (**2.5**) and light green crystals of $[V_2Cl_3(THF)_6][AlCl_4]$ (**2.6**) separated. The large size of the crystals allowed physical separation under the microscope, and analytically pure samples of **2.5** (0.5 g, 0.93 mmol, yield 10%) and **2.6** (0.7 g, 0.88 mmol, yield 29%) were obtained. Both compounds were identified by comparison of their spectroscopic data, crystallographic

cell parameters, and combustion analysis data with those of analytically pure samples prepared according to literature procedures.[4]

Synthesis of $[V_2Cl_3(THF)_6][AlCl_4]$ (2.6)

Method A: see above description.

Method B: To a solution of $VCl_3(THF)_3$ (3.3g, 8.8 mmol) in THF (150 ml) the 18 ml of Et_3Al (1.0 M solution in hexane) was added at room temperature. The mixture was stirred for 2 hours upon which the colour changed from purple/pink to light green, and then allowed to stand at –30°C for 48 hours, eventually yielding a small crop of light green crystals of $[V_2Cl_3(THF)_6][AlCl_4]$ (1.4 g, 1.7 mmol, 39%).

Synthesis of V(*acac*)$_2$(TMEDA) (2.7a).

A solution of *acacH* (0.58 ml, 5.7 mmol) in THF (150 ml) was treated with a solution of MeLi in ether (4.1 ml, 5.7 mmol, 1.4 M) at -78 °C. Gas evolution took place, and the mixture was maintained under vigorous stirring for 1 h while warming to room temperature. $VCl_2(TMEDA)_2$ (0.88 g, 2.8 mmol) was added to the mixture. The resulting dark violet-blue solution was stirred for several hours. The solution was evaporated to dryness and the residual solid redissolved in hexane (50 ml). A small amount of insoluble and colourless material was eliminated by filtration, and the filtrate was allowed to stand at -30 °C for 2 days. Dark violet-blue crystals of **2.7a** separated (0.51 g, 1.4 mmol, yield 50%). Anal. Calcd (Found) for $VC_{16}H_{30}N_2O_4$: C 52.60 (52. 68), H 8.28 (8.33), N 7.67 (7.34). IR (Nujol mull, cm^{-1}) : 1576(s), 1522(s), 1457(s), 1376(s), 1283(s), 1190(s), 1124(m), 1017(s), 953(s), 924(s), 796(s), 756(s), 654(s). $\mu_{eff} = 3.58\ \mu_{BM}$.

Synthesis of V(*Cy-acac*)$_2$(TMEDA) (2.7b).

Using freshly distilled *Cy-acacH* (1.47 ml, 11.3 mmol) and NaH (0.27 g, 11.3 mmol), an identical procedure as for the synthesis of **2.7a** in THF (100 ml) at room temperature was followed (1.49 g, 3.34 mmol, yield 59%). Anal. Calcd (Found) for $VC_{20}H_{38}N_2O_4$: C 57.00 (56.86), H 9.09 (9.01), N 6.65 (6.65). IR (Nujol mull, cm^{-1}): 1571(s), 1510(m), 1462(m), 1411(s), 1378(s), 1327(m), 1285(m), 1256(m), 1167(m), 1078(m), 1027(m), 1005(w), 993(w), 920(m), 853(m), 722(w), 652(m), 566(w). $\mu_{eff} = 3.79\ \mu_{BM}$.

Synthesis of V(*t-Bu-acac*)$_2$(TMEDA) (2.7c).

An identical procedure to the synthesis of **2.7a** was followed by using freshly distilled *t-Bu-acacH* (2.36 ml, 11.3 mmol) in THF (100 ml) and NaH (0.27 g, 11.3 mmol) at room temperature. (1.69 g, 3.16 mmol, yield: 56%). Anal. Calcd (Found) for $VC_{28}H_{52}N_2O_4$: C 63.02 (62.99), H 10.20 (10.14), N 5.25 (5.17). IR (Nujol mull, cm^{-1}): 1559(s), 1510(s), 1456(m), 1398(s), 1376(s), 1285(m), 1256(m), 1188(m), 1125(m), 1099(m), 1058(m), 1005(s), 955(m), 920(m), 797(m), 755(m), 722(w), 652(m), 566(w). $\mu_{eff} = 3.82\ \mu_{BM}$.

Reaction of V(*acac*)$_2$(TMEDA) with 1,1,2-trichloroethane.

A solution of V(*Cy-acac*)$_2$(TMEDA) (2.0 g, 4.5 mmol) in toluene (100 ml) was treated with 1 equiv. of 1,1,2-trichloroethane (0.42 ml, 4.5 mmol). The colour of the solution immediately changed from dark blue to reddish brown. After stirring the mixture overnight, the solvent was evaporated in vacuo, affording a green precipitate of V(*Cy-acac*)Cl_2(TMEDA) (0.77 g, 2.0 mmol, yield 45%). Anal. Calcd (Found) for $VC_{14}H_{27}O_2N_2Cl_2$: C, 44.58 (44.63); H, 7.21 (7.19); N, 7.43 (7.38). IR (Nujol mull, cm^{-1}):

1572 (s), 1463.7 (s), 1414 (s), 1378 (s), 1365(s), 1352(s), 1322(s), 1279(s), 1251(s), 1172(s), 1135(m), 1121(w), 1101(w), 1074(w), 1061(w), 1043(m), 1031(m), 1018(s), 997(s), 963(s), 952(s), 928(m), 901(w), 887(m), 859(m), 817(m), 803, 765(w), 722(m), 709(s), 657(m), 636(w), 591(w), 570(w). $\mu_{eff} = 2.77\ \mu_{BM}$.

The mother liquor was evaporated to dryness under reduced pressure and the residual solid redissolved in freshly distilled ether (100 ml). V(*Cy-acac*)$_3$ precipitated after concentration of the solution and cooling to -20 °C (0.8 g, 1.7 mmol, yield 38%). The compound was identified by comparison of the analytical and spectroscopic properties with those of an analytically pure sample.

Synthesis of [V(*t-Bu-acac*)$_2$(TMEDA)]$_2$[ZnCl$_4$] (2.8).

A mixture of [V(*t-Bu-acac*)$_2$(TMEDA)] (1 g, 1.8 mmol) with excess $ZnCl_2(THF)_2$ was added to a dry toluene solution (100 ml) containing 3 equiv. of ethyl trichloroacetate (0.75 ml, 5.4 mmol). Stirring for 12 h resulted in a drastic colour change from dark blue to a reddish brown. After partial removal of the solvent in vacuo, the solution separated as red cubic crystals of **2.7** (0.22 g, 0.17 mmol, yield 19%) upon standing at room temperature for a few hours. Anal. Calcd (Found) for $V_2C_{56}H_{108}O_8N_4ZnCl_4$: C, 52.77 (52.82); H, 8.54 (8.55); N, 4.40 (4.41). IR (Nujol mull, cm^{-1}): 1561(s), 1510(s), 1456(m), 1376(s), 1286(m), 1186(m), 1125(m), 1098(m), 1057(m), 1003(s), 953 (m), 920(m), 798(m), 755(m), 722(w), 654(m), 566(w); $\mu_{eff} = 2.82\mu_{BM}$.

Synthesis of [V(*t-Bu-acac*)$_2$(TMEDA)][CuCl$_2$] (2.9).

A crystalline sample of **2.6c** (2.00 g, 3.3 mmol) was dissolved in toluene (100 ml). Upon addition of excess anhydrous CuCl (0.49 g, 4.9 mmol), there was no immediate colour change. The mixture was stirred and heated at 110°C for 12 h, upon which a dark burgundy red solution was formed. The solution was filtered to eliminate some colloidal copper and excess CuCl. The solution was concentrated in vacuo and allowed to stand overnight at room temperature. Burgundy red crystals of [V(*t-Bu-acac*)$_2$ (TMEDA)]$^+$[CuCl$_2$]$^-$ separated (0.80 g, 1.2 mmol, yield 36%). Anal. Calcd (Found) for $VC_{28}H_{54}N_2O_4CuCl_2$: C 50.33 (50.21), H 8.15 (8.09), N 4.19 (4.13). IR (Nujol mull, cm^{-1}): 1582(s), 1531(s), 1456(s), 1376(s), 1327(m), 1286(m), 1172(m), 1036(s), 921(m), 853(s), 722(m), 668(m). $\mu_{eff} = 3.92\ \mu_{BM}$.

2.3 General Polymerisation Procedure

Catalysts were evaluated by co-polymerising ethene-propene in cyclohexane solutions at 2 bar total pressure and 22 °C. Experiments were carried out in 200 ml of cyclohexane in magnetically agitated glass reactors using a continuous flow of 1000 sccm ethene and 1000 sccm propene. After equilibration of the cyclohexane with the EP feed, 0.2 mmol of co-catalyst were added followed by 5 μmol of V(β-diketonate)$_3$ containing a chlorinated ester such as ethyl trichloroacetate. The total amount of reactivating substance that was added to the reaction mixture was 20 μmol. Polymerisation reactions were carried out for 30 min followed by addition of 5 ml of ethanol and depressurisation. The EP rubber was recovered by solvent evaporation and dried in a vacuum oven at 60°C. The polymer composition was determined by FTIR using the ratio of peak heights

of the bands at 1155 cm^{-1} and 720 cm^{-1} after calibration with standard samples. The molecular weights were determined by GPC at 140 °C by using trichlorobenzene as a solvent. The molecular weights are reported as polystyrene equivalents.

2.4 X-ray Diffraction Structural Studies.

Suitable crystals were mounted with cooled, viscous oil on thin, glass fibres. Data were collected on a Bruker SMART 1k CCD diffractometer using 0.3° ω-scans at 0°, 90°, and 180° in ϕ. Cell constants were calculated from reflection data obtained from 60 data frames collected at different parts of the Ewald sphere. No absorption corrections were required. The reflection data for **2.9** were uniquely consistent for the reported space group. No symmetry higher than triclinic was observed for complexes **2.7a** and **2.5**. The reflection data for **2.5** were consistent for *Cc* and *C2/c*. For **2.7a**, **2.5**, and **2.8**, solutions in the centric option yielded chemically reasonable and computationally stable results of refinement. The structures were solved by direct methods, completed with subsequent Fourier synthesis, and refined with full-matrix least squares procedures based on F^2.
The copper atom of **2.9** and the zinc atom of **2.8** are located on 2-fold axes of symmetry. Two, symmetry-unique, half-molecules of the cation in **2.5** are each located on an inversion centre. One of the two half-cations has a co-ordinated molecule of THF that is disordered in two contributing conformational forms with a 60/40-site occupancy distribution. All non-hydrogen atoms were refined with anisotropic displacement parameters. Hydrogen atoms were assigned with idealised geometry and constrained with an isotropic riding model. Crystallographic details are presented in Appendix 1. All

scattering factors are contained in the SHELXTL 5.03 program library (Sheldrick, 1997, WI).

Complex of V(*t-Bu-acac*)$_3$ (2.3) and V(*F-acac*)$_3$ (2.4)

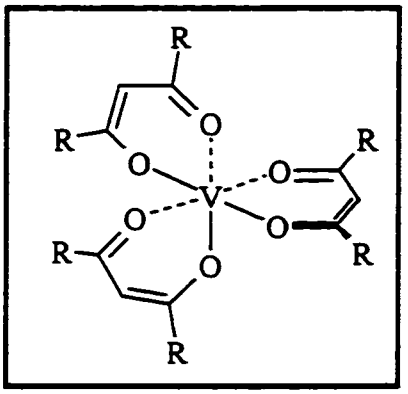

Complexes **2.3** (figure 2.1) and **2.4** (figure 2.2) are identical to the structure of V(*acac*)$_3$ reported by Morosin[16]. The octahedral vanadium centres are encompassed by three ligands which are slightly distorted in both complex **2.3** [O(2A)-V(1)-O(2) = 176.2(3)°, O(2A)-V(1)-O(3) = 90.3(2)°, O(3)-V(1)-O(2) = 92.4(2)°, O(3)-V(1)-O(3A) = 87.7(3)°, O(2)-V(1)-O(1) = 85.7(2)°] and complex **2.4** [O(3)-V-O(5) = 88.62(11)°, O(3)-V-O(6) = 91.15(11)°, O(6)-V-O(5) = 87.81(11)°, O(3)-V-O(1) = 178.29(12)°]. The O-V-O interring angles are different from those of V(*acac*)$_3$ [O(1)-V-O(6) = 91.7(2)°, O(1)-V-O(5) = 89.8(2)°, O(5)-V-O(6) = 88.86(14)°]. The average bond V-O bond distances of 1.97Å reported for the V(*acac*)$_3$ complex are, as expected, quite similar to those found in complex **2.3** and **2.4** that have average V-O bond lengths of 1.98Å.

Figure 2.1 ORTEP of V(*t-Bu-acac*)$_3$ (2.3)

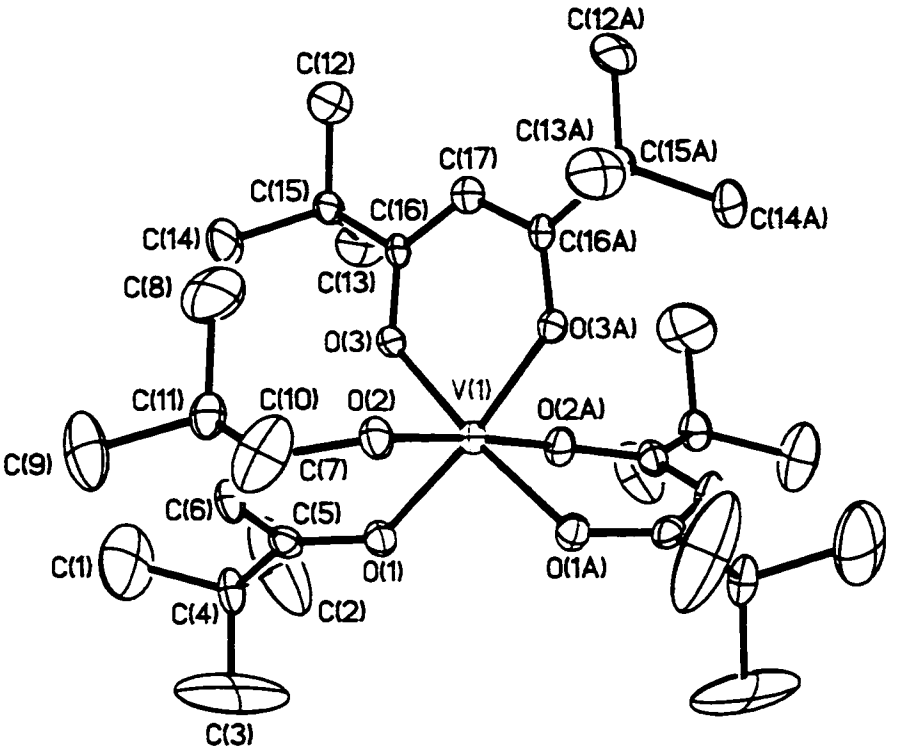

Selected Bond Distances (Å) and Angles (°) for Complex 2.3

Distances	Angles
V(1)-O(2) = 1.962(5)	O(2A)-V(1)-O(2) = 176.2(3)
V(1)-O(1) = 2.013(5)	O(2A)-V(1)-O(3) = 90.3(2)
V(1)-O(3) = 1.970(5)	O(3)-V(1)-O(2) = 92.4(2)
V(1)-O(2A) = 1.962(5)	O(3)-V(1)-O(3A) = 87.7(3)
V(1)-O(1A) = 2.013(5)	O(2)-V(1)-O(1) = 85.7(2)
V(1)-O(3A) = 1.970(5)	

Figure 2.2 ORTEP of V(*F-acac*)$_3$ (2.4)

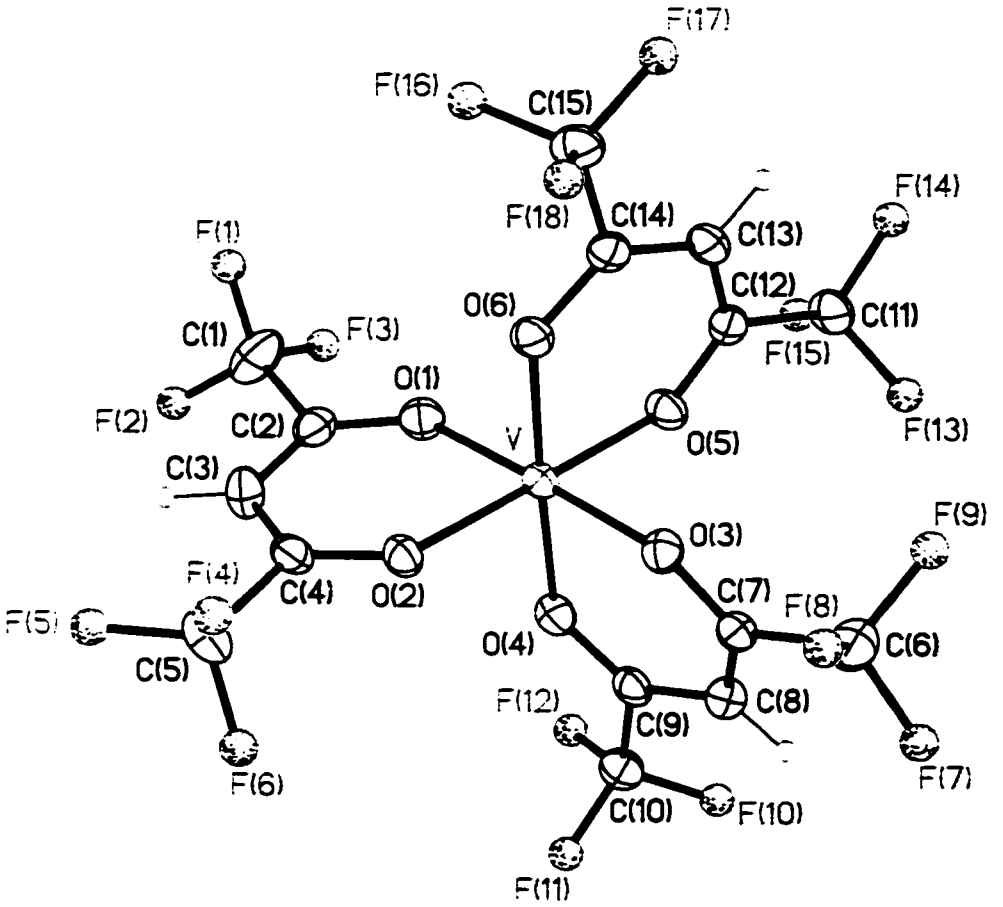

Selected Bond Distances (Å) and Angles (°) for Complex 2.4

Distances	Angles
V-O(1) = 1.986(3)	O(3)-V-O(5) = 88.62(11)
V-O(3) = 1.960(3)	O(3)-V-O(6) = 91.15(11)
V-O(4) = 1.991(3)	O(6)-V-O(5) = 87.81(11)
V-O(5) = 1.966(4)	O(3)-V-O(1) = 178.29(12)
V-O(6) = 1.973(3)	O(2)-V(1)-O(1) = 85.7(2)

Complex of $[Al(acac)_2(THF)_2]_2[AlCl_4]$ (2.5)

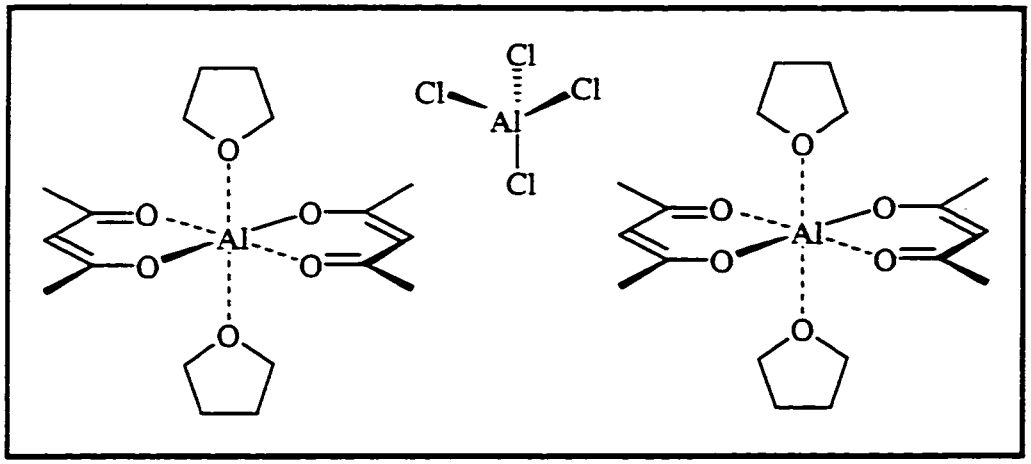

The structure consists of two distinct ionic fragments (Figure 2.3). The cation is formed by an octahedral aluminium atom surrounded by two *acac* ligands [Al(1)-O(3) = 1.846(4) Å. Al(1)-O(4) = 1.843(4) Å] and two molecules of THF [Al-O(6) = 1.953(4) Å] in an overall regular octahedral coordination geometry [O(3)-Al(1)-O(4) = 92.8(2)°. O(3)-Al-O(6) = 90.1(2)°, O(4)-Al-O(6) = 90.1(2)°, O(3)-Al(1)-O(4a) = 87.2(2)°]. The two *acac* ligands define the symmetry-generated equatorial plane of the octahedron [O(3)-Al(1)-O(3a) = 180.0°. O(4)-Al(1)-O(4A) = 179.997(1)°], while the two molecules of THF are lying trans to each other on the vertical axis [O(6)-Al(1)-(O6a) = 180.0°]. The anion is a regular tetrahedral $AlCl_4^-$ anion [Al(3)-Cl(1) = 2.100(3) Å, Cl(1)-Al(3)-Cl(2) = 109.6(2)°]. The structure of **2.5** is another of the few examples of cationic aluminium species.

Figure 2.3 ORTEP of $[Al(acac)_2(THF)_2]_2[AlCl_4]$ (2.5)

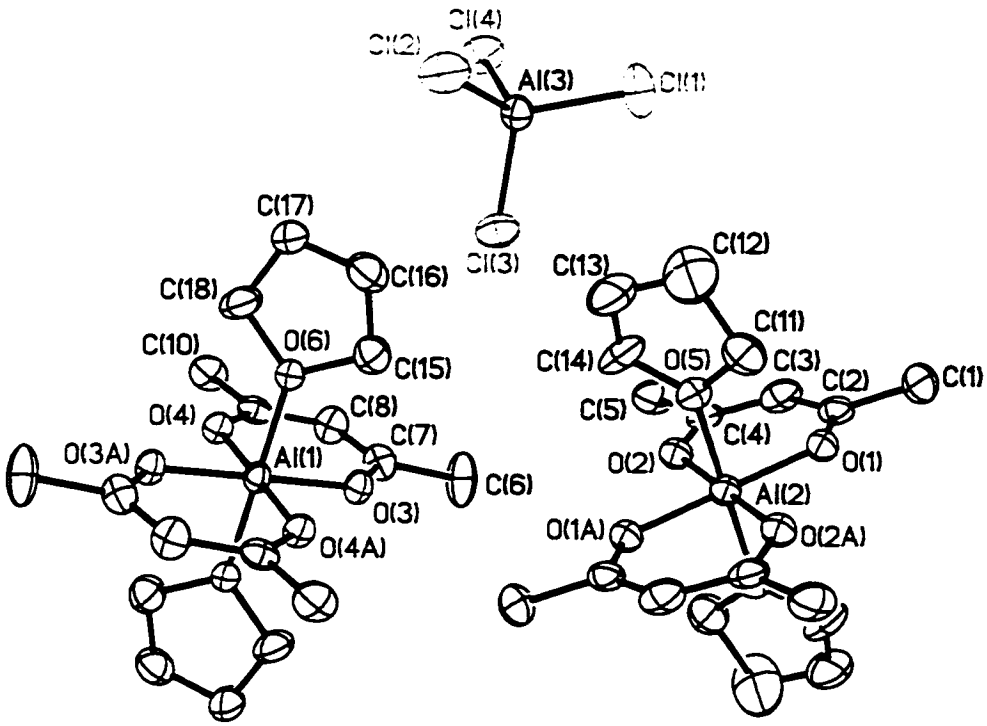

Selected Bond Lengths (Å) and Angles (°) of Complex 2.5

Distances	Angles
Al(1)-O(4) = 1.843(4)	O(4a)-Al(1)-O(4) = 179.997(1)°
Al(1)-O(3) = 1.846(4)	O(4a)-Al(1)-O(3) = 92.8(2)°
Al(1)-O(6) = 1.953(4)	O(4)-Al(1)-O(3a) = 87.2(2)°
Al(3)-Cl(1) = 2.100(3)	O(4a)-Al(1)-O(3) = 87.2(2)°
Al(3)-Cl(2) = 2.119(3)	O(4)-Al(1)-O(3) = 92.8(2)°
Al(3)-Cl(3) = 2.125(3)	O(3)-Al(1)-O(3) = 180.0°
Al(3)-Cl(4) = 2.130(3)	Cl(1)-Al(3)-Cl(3) = 109.6(2)°
	Cl(1)-Al(3)-Cl(4) = 109.8(2)°
	Cl(2)-Al(3)-Cl(4) = 108.23(13)°
	Cl(1)-Al(3)-Cl(3) = 110.08(14)°

Figure 2.4 ORTEP of $[V_2Cl_3(THF)_6][AlCl_4]$

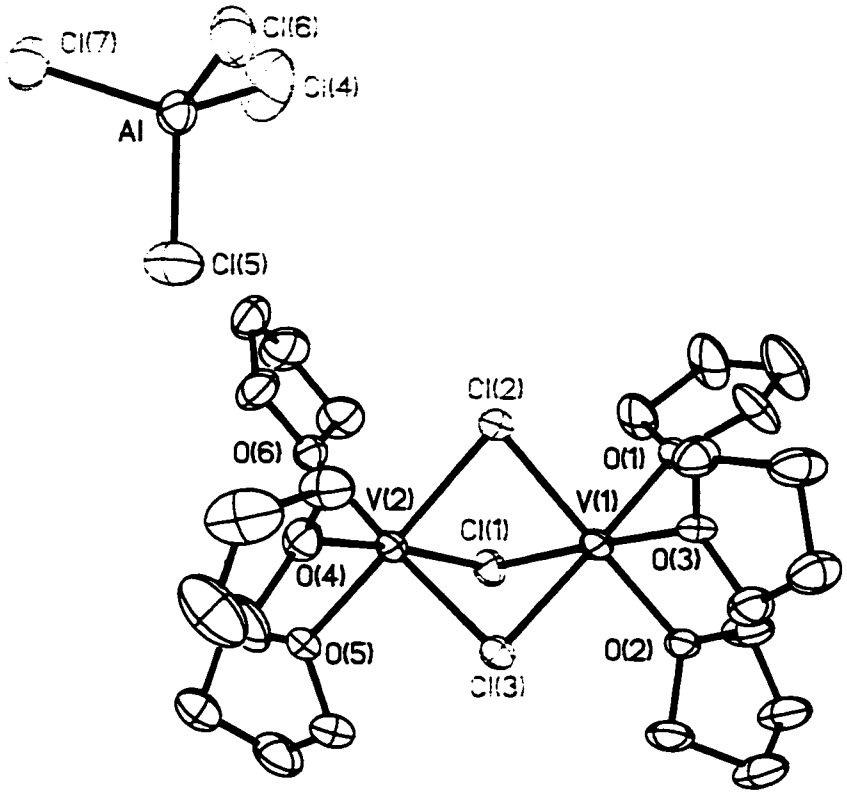

Selected bond lengths (Å) and angles (°) of complex 2.6

Distances	Angles
V(1)-O(2) = 2.125(7)	O(2)-V(1)-O(3) = 87.1(2)
V(1)-O(3) = 2.156(8)	O(2)-V(1)-O(1) = 88.6(3)
V(1)-O(1) = 2.159(6)	O(2)-V(1)-Cl(2) = 179.2(2)
V(1)-Cl(1) = 2.505(4)	O(2)-V(1)-Cl(1) = 91.5(2)
V(1)-Cl(2) = 2.450(4)	O(2)-V(1)-Cl(3) = 93.0(2)
V(1)-Cl(3) = 2.493(3)	V(1)-Cl(1)-V(2) = 73.51(11)
Al-Cl(4) = 2.103(8)	V(1)-Cl(2)-V(2) = 74.58(10)
Al-Cl(5) = 2.105(7)	V(1)-Cl(3)-V(2) = 73.32(8)
Al-Cl(6) = 2.106(8)	Cl(4)-Al-Cl(5) = 110.1(4)
Al-Cl(7) = 2.132(4)	Cl(4)-Al-Cl(6) = 109.9(4)
	Cl(4)-Al-Cl(7) = 107.9(4)

Complex of V(*acac*)$_2$(TMEDA) (2.7a).

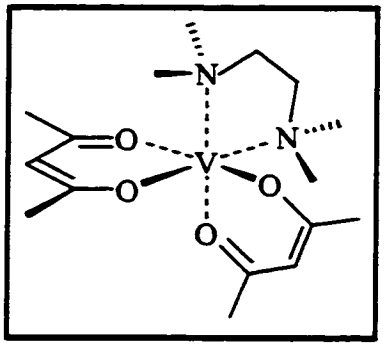

The crystal structure is composed of discrete monomeric units containing a vanadium atom in a slightly distorted octahedral environment. Two *acac* ligands [V-O(1) = 2.057(4) Å, V-O(2) = 2.051(4) Å, V-O(3) = 2.065(4) Å, V-O(4) = 2.042(4) Å] and one TMEDA [V-N(1) = 2.243(5) Å, V-N(2) = 2.239(4) Å] defined the coordination octahedron [O(1)-V-O(2) = 88.0(2)°, O(1)-V-N(1) = 92.2(2)°, O(1)-V-O(3) = 92.0(2)°, O(1)-V-O(4) = 94.2(2)°, O(1)-V-N(1) = 92.2(2)°, O(1)-V-N(2) = 171.9(2)°].

Figure 2.5 ORTEP of V(*acac*)$_2$(TMEDA) (2.7a)

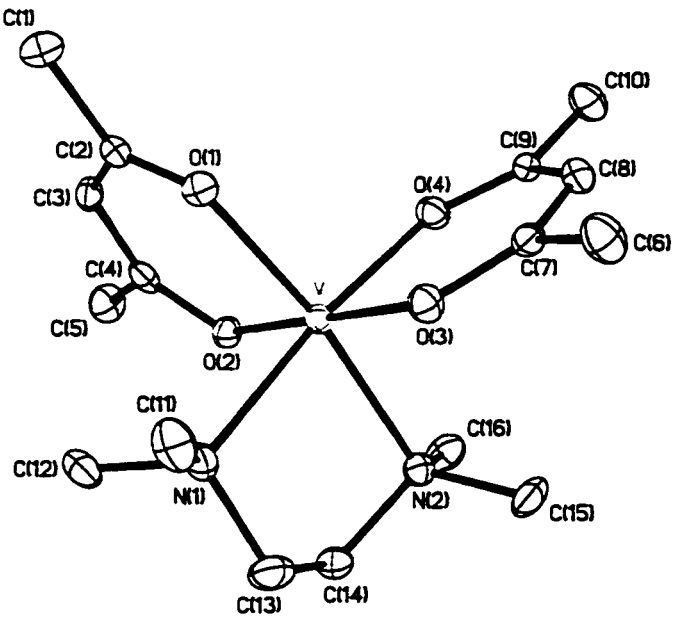

Selected Bond Lengths (Å) and Angles (°) Complex 2.7a

Distances	Angles
V-O(4) = 2.042(4)	O(4)-V-O(2) = 91.4(2)°
V-O(2) = 2.051(4)	O(4)-V-O(1) = 94.2(2)°
V-O(1) = 2.057(4)	O(2)-V-O(1) = 88.0(2)°
V-O(3) = 2.065(4)	O(4)-V-O(3) = 88.4(2)°
V-N(2) = 2.239(4)	O(2)-V-O(3) = 179.8(2)°
V-N(1) = 2.243(5)	O(1)-V-O(3) = 92.0(2)°
	O(4)-V-N(2) = 92.6(2)°
	O(2)-V-N(2) = 87.4(2)°
	O(1)-V-N(2) = 171.9(2)°
	O(3)-V-N(2) = 92.6(2)°
	O(4)-V-N(1) = 173.3(2)°
	O(2)-V-N(1) = 90.6(2)°
	O(1)-V-N(1) = 92.2(2)°
	O(3)-V-N(1) = 89.7(2)°
	N(2)-V-N(1) = 81.1(2)°

Complex of [V(*t-Bu-acac*)$_2$(TMEDA)][ZnCl$_4$] (2.8)

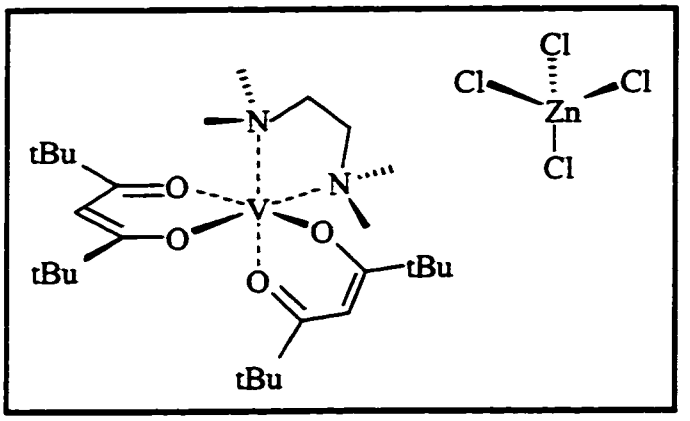

The structure consists of three separate ionic units. The two identical cationic vanadium moieties are octahedral, with two *acac* ligands and one TMEDA defining the vertexes of a distorted octahedron [O(1)-V-O(2) = 87.31(18)°, O(1)-V-O(3) = 96.03(18)°, O(1)-V-O(4) = 88.71(18)°, N(1)-V-N(2) = 82.4(2)°, O(1)-V-N(1) = 91.3(2)°, O(1)-V-N(2) = 173.3(2)°]. Both the V-N and V-O bond distances [V-N(1) = 2.172(6) Å, V-O(1) = 1.963(4) Å, V-O(2) = 1.961(4) Å] and angles are as expected and compare well with those of V(*acac*)$_3$.[3] The anion is formed by a zinc atom surrounded by four chlorine atoms defining a rather regular tetrahedron with normal bond distances [Zn-Cl(1) = 2.277(2) Å] and angles [Cl(1)-Zn-Cl(2) = 11.07(8)°] (Figure 2.6). The relatively large thermal parameters of some of the methyl carbon atoms and of the TMEDA CH_2 groups are probably indicative of some rotational and conformational disorder.

Figure 2.6 ORTEP of [V(*t-Bu-acac*)$_2$(TMEDA)][ZnCl$_4$] (2.8)

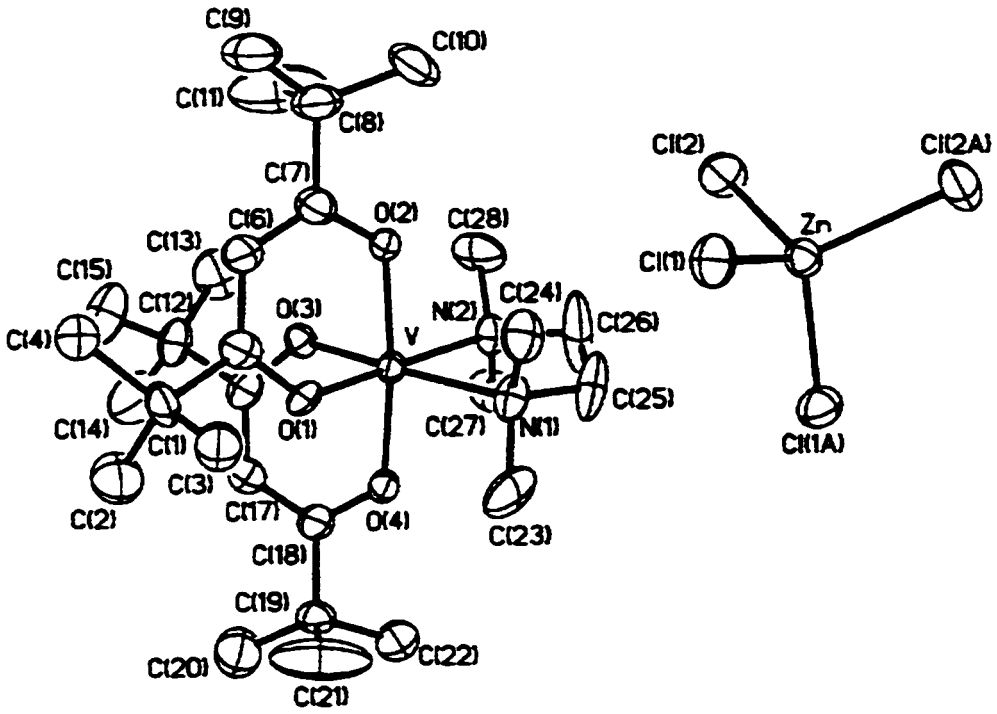

Selected Bond Lengths (Å) and Angles (°) Complex 2.8

Distances	Angles
V-O(3) = 1.936(4)	O(3)-V-O(4) = 87.82(18)
V-O(4) = 1.957(4)	O(3)-V-O(2) = 87.97(19)
V-O(2) = 1.961(4)	O(4)-V-O(2) = 173.87(18)
V-O(1) = 1.963(4)	O(3)-V-O(1) = 96.03(18)
V-N(2) = 2.169(6)	O(4)-V-O(1) = 88.71(18)
V-N(1) = 2.172(6)	O(2)-V-O(1) = 87.31(18)
O(1)-C(5) = 1.272(8)	O(3)-V-N(2) = 90.3(2)
O(2)-C(7) = 1.307(8)	O(4)-V-N(2) = 93.8(2)
O(3)-C(16) = 1.285(9)	O(2)-V-N(2) = 90.7(2)
O(4)-C(18) = 1.289(8)	O(1)-V-N(2) = 173.3(2)
Zn-Cl(1) = 2.277(2)	O(3)-V-N(1) = 172.6(2)
Zn-Cl(2) = 2.279(2)	O(4)-V-N(1) = 91.5(2)
	O(2)-V-N(1) = 93.3(2)
	O(1)-V-N(1) = 91.3(2)
	N(2)-V-N(1) = 82.4(2)

Complex of [V(*t-Bu-acac*)$_2$(TMEDA)][$CuCl_2$] (2.9)

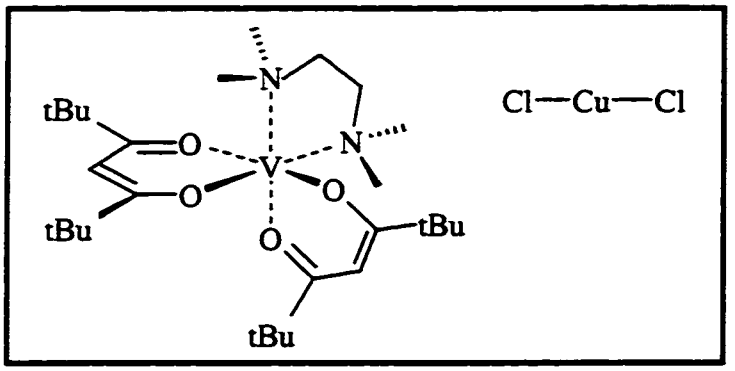

The complex is iso-morphous with **2.8** except for the anionic fragment which consists of a linear $CuCl_2$ anion [Cu-Cl(1) = 2.0863(13) Å, Cl(1)-Cu-Cl(1a) = 180.00(8)°]

Figure 2.7 ORTEP of [V(*t-Bu-acac*)$_2$(TMEDA)][$CuCl_2$]

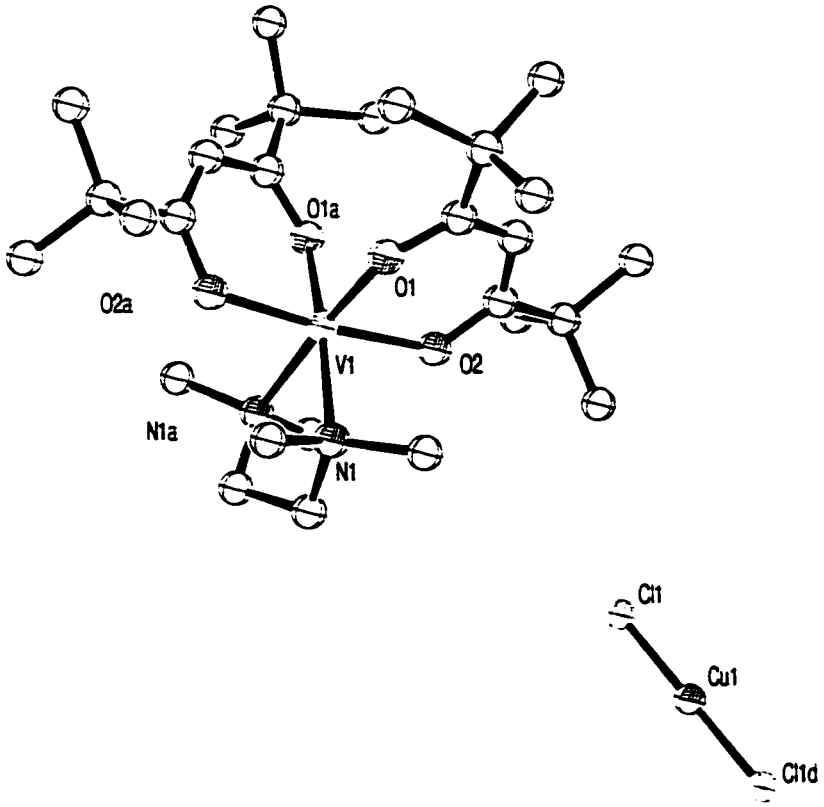

Selected bond lengths (Å) and angles (°) of complex 2.9

Distances	Angles
V-O(1) = 1.9497(17)	O(1)-V-O(1A) = 94.62(10)
V-O(2) = 1.9601(17)	O(1)-V-O(2) = 87.28(7)
V-N(1) = 2.188 (2)	O(1)-V-O(2A) = 88.89(7)
Cu-Cl(1) = 2.0863	O(1)-V-N(1) = 91.64(8)
	O(1)-V-N(1A) = 173.72(7)
	Cl(1)-Cu-Cl(1A) = 180.00(8)

2.5 Results and Discussion

Four V(*R-acac*)$_3$ complexes were prepared (Scheme 2.2) in order to study the effect of the steric and electronic features of the various ligands on catalyst activity. By selecting the *Cy-acac* ligand we expected to obtain higher solubility while preserving almost unchanged the steric and electronic properties of the basic *acac* ligand.

It was hoped that higher solubility would give better chances for isolating the catalytically active species in crystalline form. By using the *t-Bu-acac* ligand we expected to be able to evaluate the influence of steric factors on the catalytic process. The fluorinated F-acac ligand was expected to modify mainly the electronic features while maintaining the steric bulk of the catalyst very close to that of *t-Bu-acac*. The vanadium β-ketodionate complexes employed in this study were prepared following standard procedures and were characterised by combustion analysis, IR spectroscopy, and single-crystal X-ray analysis. Magnetic moments consistent with the high-spin d^2 electronic configuration were obtained in all cases.

Scheme 2.2 Vanadium (III) Substituted Acetylacetonate Derivatives

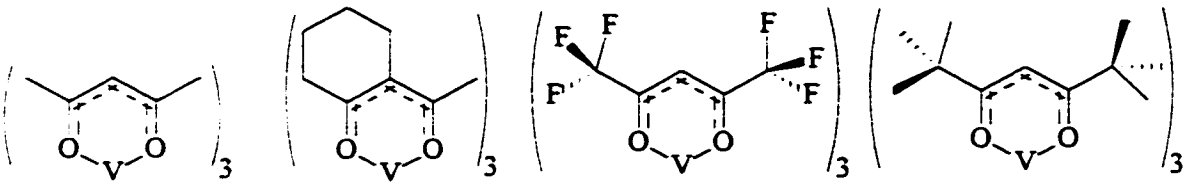

V(acac)$_3$ **(2.1)** ***V(Cy-acac)$_3$*** **(2.2)** ***V(F-acac)$_3$*** **(2.3)** ***V(t-Bu-acac)$_3$*** **(2.4)**

The catalytic activity of the various complexes was tested for ethylene-propylene co-polymerisation in the presence of catalyst reactivator. The results are summarised in Table 2.1.

Table 2.1 Ethene/Propene Co-polymerization Results

	V(*acac*)$_3$ (2.1)		V(*Cy-acac*)$_3$ (2.1a)		V(*t-Bu-acac*)$_3$ (2.3)		V(*F-acac*)$_3$ (2.4)	
	DEAC	*EASC*	*DEAC*	*EASC*	*DEAC*	*EASC*	*DEAC*	*EASC*
activity[a]	994	980	1168	990	746	622	762	800
M_w ($\times 10^3$)	219	702	218	716	290	1265	277	801
M_w/M_n	2.3	2.5	2.3	2.2	2.2	2.4	2.2	2.3
% ethylene	62	52	59	53	65	57	63	54

[a] kg EP elastomer produced in 30 min by 1 mol of vanadium catalyst; DEAC = Et_2AlCl, EASC = $Et_3Al_2Cl_3$ with a V:Al of 1:40 in 200 ml of cyclohexane and pressures of 1 atm.

The results clearly indicated that the activities of **2.1** and **2.2** are comparable in the presence of DEAC and EASC and are only slightly higher with respect to the two more crowded **2.3** and **2.4**. Surprisingly, the chlorine content of the co-catalyst and the steric hindrance of the *R-acac* ligand have only minor effects on the catalytic activity. Even more surprising, complexes of the two bulky *t-Bu-acac* and *F-acac* ligands show comparable activity despite considerably different electronegativity.

Examination of the data in Table 2.1 reveals that the propylene content in the EP elastomers decreases in the case of the sterically encumbered **2.4** and **2.3** catalysts but, again, only to a very modest extent.

The insensitivity of both the catalyst activity and polymer composition to a large variation of ligand steric hindrance and electronic features strongly indicates that the catalytic site is widely open and probably far from the β-diketonate ligand. Thus, a primary role of the aluminium co-catalyst is that of abstracting at least two if not all three

acac ligands from the vanadium centre. The variation of only 5-10% in polymer composition observed by changing the co-catalyst Lewis acidity is also in line with this rationale. A relatively minor increase of the Lewis acidity of the co-catalyst as in the case of EASC probably increases the extent of migration of the *acac* ligand from vanadium. thus decreasing further the selectivity.

The polymerisation reactions were typically carried out in hydrocarbon solvents since the employment of coordinating solvents such as ethers is well known to quench the polymerisation. For this reason, attempts to isolate and characterise the catalytically active species were carried out by mixing together catalyst and co-catalyst in toluene in different ratios and without exposure to reactivators. Similar results were also obtained in hexane. This was of course an over simplification of the real catalytic system, which requires the presence of reactivating substances for higher catalyst productivity. Nevertheless, we felt that this strategy might help to evaluate the intriguing role of these substances and to shed some light on the structure of the catalyst.

Different from the catalytic system where a large excess of co-catalyst is imperative to enhance catalyst efficiency, the nature of the isolated product proved to be rather insensitive to the stoïchiometric ratio. Typically, reactions carried out in the ratios of 1:1, 1:3 or higher produced the same poorly soluble, brown and paramagnetic material in 78% yield based on the proposed formulation (Scheme 2.3). The magnetic moment of this compound [$\mu_{eff} = 3.75$ BM] is also consistent with the d^3 electronic configuration of a V(II) centre. This solid is pyrophoric and reacts with moisture to yield negligible amounts of ethane. Although combustion analysis data were inconclusive due to the extreme air-sensitivity of this solid, XRF data consistently yielded a V/Cl/Al ratio of 1:5:2.

Scheme 2.3 Deactivation and Reactivation of the V(*acac*)$_3$ Pro-catalysts

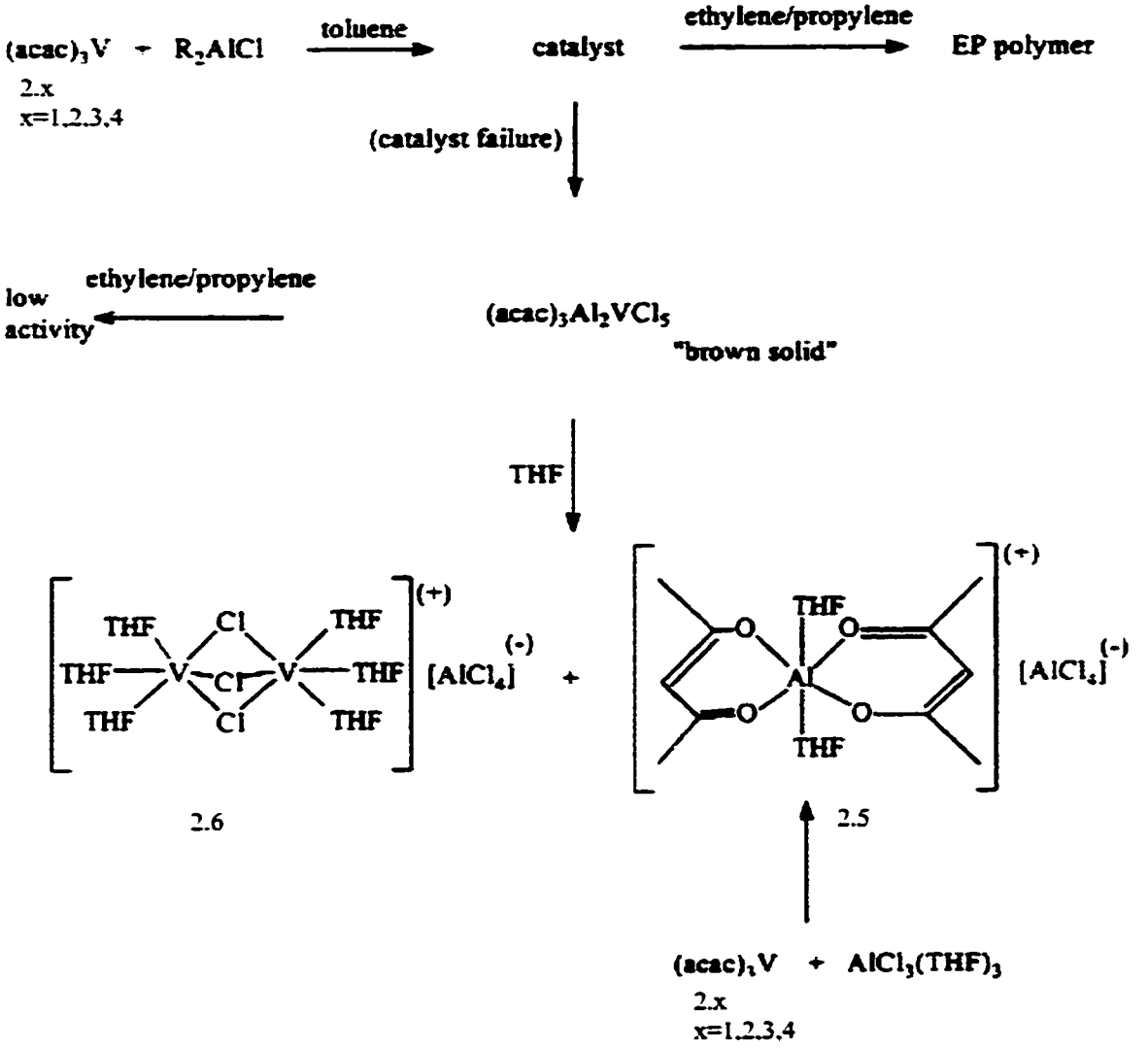

The IR spectrum clearly indicated the presence of the *acac* ligand. Once placed in cyclohexane or toluene and exposed to a mixture of ethylene and propylene, this solid displayed a minimal polymerisation activity without need of additional co-catalyst and of catalyst reactivator. Further addition of co-catalysts did not affect the catalytic activity.

These observations together with the high yield indicate that the brown solid is a deactivated catalyst. Unfortunately, repeated attempts to grow suitable crystals for X-ray analysis created great frustration due to low solubility in hydrocarbon solvents. In attempt

to indirectly identify the nature of this species degradation experiments were conducted (Scheme 2.3). Treatment of the "brown solid", obtained from the direct reaction of the catalyst with the aluminium co-catalyst, with THF yielded a bright green solution, from which a green crystalline mass, mixed together with white crystals, was obtained. The structures of both compounds (**2.5**) and (**2.6**) were elucidated by X-ray analysis. The mint green crystals are $[V_2Cl_3(THF)_6][AlCl_4]$ which contain vanadium in the formal oxidation state +2 and whose crystal structure was previously reported[16] with the wrong space group since the crystals were twinned. The white crystals are the unprecedented ionic $[Al(acac)_2(THF)_2][AlCl_4]$ complex. This species was also conveniently prepared in analytically pure form by reacting $V(acac)_3$ with $AlCl_3$ or, more simply, through direct treatment of $AlCl_3(THF)_3$ with one equivalent of Na-*acac* in THF.

These findings indicate that the co-catalyst plays the dual role of (1) completely abstracting the *acac* ligands from the vanadium centre and (2) reducing vanadium to its divalent state. In fact, the treatment of the "brown solid" with THF is unlikely to trigger a redox process, although the possibility that the divalent **2.6** might be generated by a disproportionation reaction cannot be categorically excluded at this stage. However, the neatness of the reaction and the fact that the visible region of the UV-visible spectrum of the mother liquor was basically identical to that of **2.6** discourage the idea that other high-valent vanadium species may be present in significant amount in the reaction mixture. By reducing vanadium, the aluminium co-catalyst deactivates the catalyst. On the basis of the XRF and the results of the above degradation experiment, we speculate that the brown deactivated catalyst has the formulation $\{[(\beta\text{-diketonate})AlCl_2][VCl_2][\beta\text{-diketonate})_2AlCl]\}$. The reduction of the vanadium centre can be envisioned as occurring

via β-hydrogen elimination from the corresponding V(III) alkyl derivative (Scheme 2.3). This is suggested by the presence of small amounts of hydrogen and ethane in the reaction mixtures obtained upon reacting in preparative scales the catalyst with a stoïchiometric amount of co-catalyst. Obviously the structures of both catalyst and deactivated catalyst are purely putative. However, they are consistent with all the findings described above.

They contain the appropriate ratio of heavy elements. The absence of *acac* ligands on the vanadium centre is furthermore consistent with the relative insensitivity of the catalyst activity and polymer composition to the nature of the *acac* ligand.

Since the brown product isolated from the reaction pro-catalyst/co-catalyst is a very poor catalyst, at first glance this seems to contradict the claims that V(II) species might be active catalysts.[11b] We have tested the activity of $[V_2Cl_3(THF)_6][AlCl_4]$ and of other V(II) derivatives [e.g., $VCl_2(TMEDA)_2$, $V_2Cl_5(TMEDA)^{3+}$, $V(BH_4)_2(THF)_3$] under the usual reaction conditions, finding only a negligible amount of polymerisation in comparison to the β-diketonate V(III) complexes used in this work. Some activity was observed in the presence of reactivator, but the overall polymerisation capability always remained very low. While it is very possible that the presence of THF in the coordination sphere of vanadium is responsible in this particular case for the lack of catalytic activity, on the other hand, the "brown solid" is a much less efficient catalyst in comparison with the catalysts prepared in situ. Therefore, the "brown solid" is a deactivated form of the catalyst, and since vanadium is present in this species in the oxidation state +2, reduction of the metal centre indeed corresponds to catalyst deactivation. In an attempt to substantiate this hypothesis, we have attempted the preparation of a V(II) complex

containing the *acac* ligand and to study its behaviour in the presence of co-catalysts and with or without reactivators. The $(R\text{-}acac)_2V(TMEDA)$ complexes [R = *H* (**2.7a**), *Cy* (**2.7b**), *t-Bu* (**2.7c**)] were prepared as described in Scheme 3 via straightforward chlorine replacement reaction on $VCl_2(TMEDA)_2$ by the corresponding β-diketonate sodium salt. The complexes were isolated in good yield and crystalline form after suitable work-up. These unprecedented species were characterised on the basis of combustion analysis data, while the connectivity was elucidated by an X-ray crystal structure in the case of **2.7a**. The complex displays a value of the magnetic moment as expected for the d^3 electronic configuration.

Scheme 2.4 Preparation of V(II) Acetylacetonato Complexes

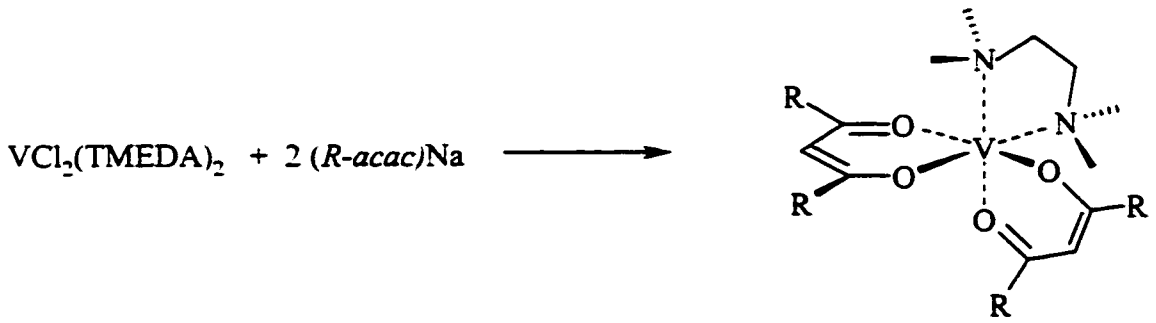

R = H **(2.7a)**, Cy **(2.7b)**, tBu **(2.7c)**

Complexes **2.7x** are certainly not an ideal substrate to model the catalyst reactivation process. Two ligands are still attached to the vanadium atom, while this is unlikely to happen during the catalytic cycle, where the transition metal probably retained no more than one *acac* (if any). Furthermore, the presence of co-ordinated TMEDA in the coordination sphere of vanadium, necessary to prevent rapid disproportionation toward the formation of $(acac)_3V$, could be detrimental to the catalytic process. Nevertheless, we expected that the excess co-catalyst would easily abstract TMEDA, thus overturning its

undesirable presence. Also, the presence of the β-diketonate ligand is certainly necessary to the catalytic cycle since simple vanadium (II) and (III) halide salts display much lower or no activity.[11c]

As expected, complex **2.7** does not polymerise olefins under the usual reaction conditions in the presence of co-catalyst and in the absence of reactivating substances. This reinforces the idea that V(II) species, formed during the catalytic cycle, poorly polymerise, and thus their formation indeed accounts for the catalyst failure during the cycle. Conversely, treatment of toluene solutions of complexes **2.7** with reactivator (for example, 1,1,2-trichloroethane) suddenly changed colour from blue to brown-red, and subsequent addition of excess DEAC gave a moderate polymerisation activity (153 kg polymer/ mol of V cat./20 min) despite the detrimental presence of one equivalent of TMEDA in the mixture (Scheme 2.5).

Scheme 2.5 Reactivation Processes Using Alternative Methods

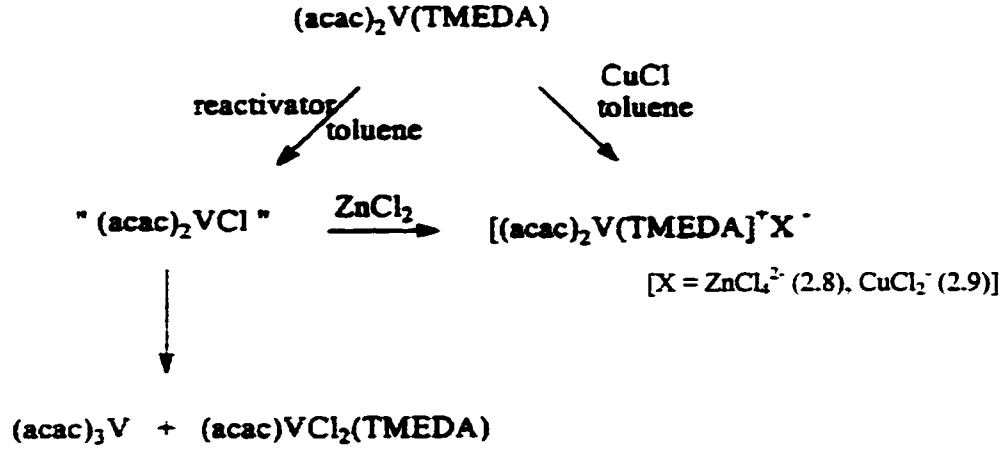

Attempts to isolate the product of the reaction were carried out in the case of **2.7b**. The reaction with ethyl trichloroacetate yielded a mixture of the green VCl_2(*Cy*-

acac)(TMEDA) and the red-brown V(*Cy-acac*)$_3$, which were separated and identified. We propose that both products arise from ligand disproportionation of the intermediate VCl(*acac*)$_2$(TMEDA). In fact, a similar reaction of **2.7a** with reactivators carried out in the presence of $ZnCl_2$ afforded red crystals of [V(*acac*)$_2$(TMEDA)]$_2$[$ZnCl_4$] (**2.8**). This new compound is paramagnetic and provides satisfactory analytical data consistent with the formulation revealed by the X-ray crystal structure.

Similarly, oxidation of **2.7a** with excess CuCl in hot toluene led to the formation of an ionic complex [V(*acac*)$_2$(TMEDA)][$CuCl_2$] (**2.9**) also containing the same cation of complex **2.8**.

2.6 Conclusions

While further work will be necessary in the future to elucidate the structure of the catalyst and fully understand the reactivation step in the catalytic cycle, the results described above have allowed the clarification of some aspects of the vanadium-catalysed ethylene-propylene co-polymerisation. The nature of the *acac* ligand has a surprisingly minor effect on the catalyst activity, thus indicating that an almost complete migration of the ligand from the vanadium centre occurs during the process. With this respect, one of the roles of the aluminium co-catalyst is certainly that of abstracting the ligand from the metal centre. This work reiterated the idea that V(II) species, largely produced during the polymerisation process, are inactive in polymerisation. The role of the reactivating substances is that of restoring the original trivalent oxidation state of vanadium and perhaps to reform the $V(acac)_3$ catalyst via ligand scrambling.

2.7 References

1. For recent review-articles on this vast topic see for example:

(a) Toto, M.; Cavallo, L.; Corradini, P.; Moscardi, G.; Resconi, L.; Guerra, G., *Macromolecules*, **1998**, *31*, 3431.

(b) Galimberti, M.; Piemontesi, F.; Fusco, O.; Camurati, I.; Destro, M.; *Macromolecules* **1998**, *31*, 3409.

(c) Kaminsky, W. J.; *Chem. Soc., Dalton Trans.*, **1998**, 1413.

(d) Mitchell, J. P.; Hajela, S.; Brookhart, S. K.; Hardcastle, K. I.; Henling, L. M.; Bercaw, J. E.; *J. Am. Chem. Soc.* **1996**, *118*, 1045.

2.(a) Bernardi, F.; Bottoni, A.; Miscione, G. P.; *Organometallics* **1998**, *17*, 16.

(b) Stehling, U. M.; Stein, K. M.; Kesti, M. R.; Waymouth, R. M.; *Macromolecules* **1998**, *31*, 2019.

(c) Mcknight, A. L.; Masood, M. A. Waymouth, R. M.; *Organometallics*, **1997**, *16*, 2879.

(d) Koo, K. M.; Marks, T. J.; *J. Am. Chem. Soc.*, **1998**, *120*, 4019.

(e) Beck, S.; Prosenc, M. H.; Brintzinger, H. H.; *J. Mol. Catal.*, **1998**, *128*, 41.

(f) Beck, S.; Brintzinger, H. H.; *Inorg. Chim. Acta;* **1998**, *270*, 376.

(g) Sacchi, M. C.; Barsties, E.; Tritto, I.; Locatelli, P.; Brintzinger, H. H.; Stehling, U.; *Macromolecules;* **1997**, *30*, 3955.

(h) Gilchrist, J.; Bercaw, J.; *J. Am. Chem. Soc.;* **1996**, *118*, 12021.

(i) Beck, S.; Prosenc, M. H.; Brintzinger, H. H.; Goretzki, R.; Herfert, N.; Fink, G.; *J. Mol. Catal.;* **1996**, *111*, 67.

(j) Chen, Y.-X.; Stern, L. C.; Yang, S.; Marks, T. J.; *J. Am. Chem. Soc.*, **1996**, *118*, 12451.

(k) Johnson, L. K.; Killian, C. M.; Brookhart, M., *J. Am. Chem. Soc.*, **1995**, *117*, 6414.

(l) Scollard, J. D.; McConville, D. H., *J. Am. Chem. Soc.*, **1996**, *118*, 10008.

(m) Thiyagarajan, B.; Jordan, R. F.; Young, V. G. *Organometallics*, **1998**, *17*, 281.

(n) Yu, P.; Montero, L. M.; Barnes, C. E.; Roesky, H. W.; Usón, I.; *Inorg. Chem.*; **1998**, *37*, 2595.

(o) Jordan, R. F.; Dasher, W. E.; Echols,S. F., *J. Am. Chem. Soc.*; **1986**, *108*, 1718.

(p) Guram, A. S.; Jordan, R. F.; Comprehensive Organometallic Chemistry; Abel, E. W., Stone, F. G. A., Wilkinson, G., Eds.; *Pergamon*: New York, **1995**, and references therein.

3 Coles, M. P.; Jordan, R. F.; *J. Am. Chem. Soc.*; **1997**, *119*, 8125.

4. (a) Small, B. L.; Brookhart, M.; Bennett, A. M. A.; *J. Am. Chem. Soc.*; **1998**, *120*, 4049 and references therein.

(b) Gibson, V. C.; Kimberley, B. S.; White, A. J. P.; Williams, D. J.; Howard, P.; *J. Chem. Soc., Chem. Commun.*; **1998**, 313, and references therein.

5. (a) Sinn, H.; Kaminski, W.; Advances in Organometallic Chemistry; Stone, F. G. A., West, R., Eds.; *Academic Press*: New York, **1980**.

(b) Doi, Y.; Tokuhiro, N.; Nunomura, M.; Miyake, H.; Suzuki, S.; Soga, K.; Transition Metals and Organometallics as Catalysts for Olefin Polymerization; Kaminsky, W., Sinn, H., Eds.; *Springer-Verlag*: Berlin, **1988**.

(c) Carrick, W. L.; *J. Am. Chem. Soc.* **1958**, *80*, 6455.

(d) Christman, D. L.; *J. Polym. Sci., Part A-1*, 1972, 471.

(e) Pasquon, I. G.; Giannini, U.; Catalysis; Anderson, J. R., Boudart, M., Eds.; *Springer-Verlag*: Berlin, **1984**.

(f) Carrick, W. L.; Kluiber, R. W.; Bonner, E. F.; Wartman, L. H.; Rugg, F. M.; Smith J. J.; *J. Am. Chem. Soc.* **1960**, *82*, 3883

(g) Lehr, M. H.; *Macromolecules;* **1968**, *1*, 178.

(h) Christman, D. L.; Keim, G. I.; *Macromolecules*; **1968**, *1*, 358.

(i) von Junghanns, E.; Gumboldt, A.; Bier, G.; *Makromol. Chem.*; **1967**, *101*, 229.

(j) Lehr, M. H.; Carmen, C. J.; *Macromolecules;* **1969**, *2*, 217

(k) Duck, E. W.; Grant, D.; Horder, J. R.; Jenkins, D. K.; Marlow, A. E.; Wallis, S. R.; Doughty, A. G.; Maradon, J. M.; Skinner, G. A.; *Eur. Polym. J.*; **1974**, *10*, 481

(l) Feher, F. J.; Blanski, R. L.; *J. Am. Chem. Soc.;* **1992**, *114*, 5886.

(m) Feher, F. J.; Walzer, J. F.; Blanski, R. L.; *J. Am. Chem. Soc.*, **1991**, *113*, 3618.

(n) Feher, F. J.; Blanski, R. L.; *Organometallics*, **1993**, *12*, 958.

(o) Feher, F. J.; Walzer, J. F. *Inorg. Chem.* **1991**, *30*, 1689.

(p) Cucinella, S.; Mazzei A. U.S. Patent 3,711,455, CI. 260-85.3, 1973.

(q) Boor, J., Jr.; Youngman, E. A.; *J. Polym. Sci., Part A-1* **1966**, *4*, 1861.

(r) Zambelli, A.; Natta, G.; Pasquon, I.; *J. Polym. Sci., Part C*; **1964**, *4*, 411.

(s) Pino, P.; Mulhaupt, R.; *Angew. Chem., Int. Ed. Engl.* **1980**, *19*, 857.

6. (a) Witte, P. T.; Meetsma, A.; Hessen, B.; *J. Am. Chem. Soc.;* **1997**, *119*, 10561.

(b) Murphy, V. J.; Turner, H. *Organometallics;* **1997**, *6 (12)*, 2495-2497.

(c) Schuere, S.; Fisher, J.; Kress, J.; *Organometallics*. **1995**, *14*, 2627.

(d) Zambelli, A.; Proto, A.; Longo, P.; Ziegler-Natta Catalysis; Fink, G., Mulhaupt, R., Brintzinger, H. H., Eds.; *Springer-Verlag*: Berlin, **1995**.

(e) Kim, W. K.; Fevola, M. J.; Liable-Sands, L. M.; Rheingold, A. L.; Theopold, K. H. *Organometallics*, **1998**, *17*, 4541

(f) Feher, K. J.; Walzer, J. F.; Blanski, R. L.; *J. Am. Chem. Soc.*, **1991**, *113 (3)*, 3618.

7.(a) Czaja, K.; Bialek, M.; *Macromol. Rapid Commun.*; **1998**, *19 (3)*, 163-166.

(b) Buhl, M.; *Angew. Chem., Int. Ed;*. **1998**, *37 (1-2)*, 142-144.

(c) Chan, M. C. W.; Cole, J. M.; Gibson, V. C.; Howard, J. A. K.; *J. Chem. Soc., Chem. Commun.*; **1997**, 2345.

8. See for example:

(a) Doi, Y.; Suzuki, S.; Soga, K.; *Macromolecules*; **1986**, *19*, 2896.

(b) Ouzumi, T.; Soga, K.; *Makromol. Chem.*: **1992**, *193*, 823.

(c) Gumboldt, A.; Helberg, J.; Schleitzer, G.; *Makromol. Chem.*; **1967**, *101*, 229.

(d) Adisson, E.; *J. Polym. Sci., Part A: Polym. Chem.*; **1994**, *32*, 1033.

(e) Davis, S. C.; von Hellens, W.; Zahalka, H.; Polymer Material Encyclopedia Vol. 3 ; Salamone, J. C., Ed.; *CRC Press Inc.*: Boca Raton, FL, **1996**.

9. See for example:

(a) Fan, L.; Harrison, D.; Woo, T. K.; Ziegler, T.; *Organometallics*; **1995**, 14, 2018.

(b) Woo, T. K.; Margl, P. M.; Lohrenz, J. C. W.; Bloch, P. E.; Ziegler, T.; *J. Am. Chem. Soc.*; **1996**, *118*, 13021.

(c) Bernardi, F.; Bottoni, A.; Miscione, G. P.; *Organometallics*;**1998**, *17*, 16.

10.(a) Gambarotta, S.; Floriani, C.; Chiesi-Villa, A.; Guastini, C.; *J. Chem. Soc., Chem. Commun.*; **1984**, 886.

(b) Buijink, J. K.; Meetsma, A.; Teuben, J. H.; *Organometallics*; **1993**, *12*, 2004.

(c) Berno, P.; Gambarotta, S.; Richeson, D.; Comprehensive Organometallic Chemistry II; Abel, E. W., Stone, F. G. A.; Wilkinson, G., Eds.; *Oxford*, **1995**, and references therein.

11.(a) Cramail, H.; Dolatkhani, M.; Deffieux, A.; New EPDM's Based on Linear Dienes: Conventional Versus Metallocene Catalysis; Metallocenes 1995 International Congress on Metallocene Polymers; Scotland Business Research: Skillman, NJ; **1995**; pp 227-241.

(b) Cann, K. G.; Nicoletti, J. W.; Bai, X.; Hussein, F. D.; Lee, K. H.; Zilker, D. P.; Goeke, G. L.; *Polym. Prepr.*; **1998**, *39*, 192.

(c) Smith, P. D.; Martin, J. L.; Huffman, J. C.; Bansemer, R. L.; Caulton, K. G.; *Inorg. Chem.*; **1985**, *24*, 2997.

12.(a) Chan, M. C. W.; Cole, J. M.; Gibson, V. C.; Howard, J. A. K.; *J. Chem. Soc., Chem. Commun.*; **1997**, 2345, and references therein.

(b) Coles, M. P.; Gibson, V. C. Polym. Bull. 1994, 33, 529.

(c) Henrici-Olive, G.; Olive, S. *Angew. Chem., Int. Ed. Engl.*; **1971**, *10*, 776.

(d) Evens, G. G.; Pijpers, E. M. J.; Seevens, R. H. M.; Transition Metal Catalyzed Polymerization; Quirk, R. P., Ed.; *Cambridge University Press*: Cambridge, **1988**; p 782.

(e) Doi, Y.; Suzuki, S.; Hizai, G.; Soga, K. Transition Metal Catalyzed Polymerization; Quirk, R. P., Ed.; *Cambridge University Press:* Cambridge, **1988**; p 182.

(f) Ver Strate, G.; Encyclopedia of Polymer Science and Engineering, 2nd ed.; *J. Wiley*: New York, **1985**: Vol. 6, p 543.

13.(a) Giannetti, E.; Mazzocchi, R.; Albizzatti, E.; Fiorani, T.; *Makromol. Chem.*, **1984**, *185*, 2133.

(b) Cooper, T. A.; *J. Am. Chem. Soc.*, **1973**, *95:13*, 4158.

14. Edema, J. J. H.; Staudhamer, W.; Gambarotta, S.; Meetsma, A.; vanBolhuis, F., *Inorg. Chem.*, **1990**, *29*, 1302.

15. Manzer, L. E., *Inorg. Synth.*, **1982**, *21*, 138.

16. Morosin, B.; Montgomery, H.; *Acta Crystallogr.*, **1969**, *25*, 1354, and references cited therein.

17. Calderazzo, F.; de Benedetto, G. E.; Pampaloni, G.; Mossmer, C. M.; Strahle, J.; Wurst, K., *J. Organomet. Chem.*, **1993**, *451*, 73.

18. Mabbs, M. B.; Machin, D., *Magnetism and Transition Metal Complexes*; Chapman and Hall: London, 1973.

19. Foese, G.; Gorter, C. J.; Smits, L. J.; *Constantes Sélectionnées: Diamagnétisme. Paramagnétisme. Relaxation Paramagnétique*; Mason; Paris, 1957.

20. Doi, Y.; Suzuki, S.; Hizai, G.; Soga, K., *Transition Metal Catalyzed Polymerisation*; Quirk, R. P., Ed.; Cambridge University Press; Cambridge, 1988. p.182.

Life and Death of an Active Ethylene Polymerization Catalyst. Ligand Involvement in Catalyst Activation and Deactivation. Isolation and Characterization of Two Unprecedented Neutral and Anionic Vanadium(I) Alkyls.

Abstract

The focus of ***Chapter 3*** *is to describe the catalytic activation and deactivation of {2,6-bis[2,6-(i-Pr)$_2$PhN=C(Me)]$_2$ (C$_5$H$_3$N)}VCl$_3$·1.3(CH$_2$Cl$_2$)* ***(3.2)****. The reaction of {2,6-bis[2,6-(i-Pr)$_2$PhN=C(Me)]$_2$(C$_5$H$_3$N)}VCl$_3$·1.3(CH$_2$Cl$_2$)* ***(3.2)*** *with stoïchiometric amounts of methylalumoxane (PMAO) in toluene resulted in the methylation of the pyridine ring ortho position affording {2,6-bis[2,6-(i-Pr)$_2$PhN=C(Me)]$_2$(2-MeC$_5$H$_3$N)}VCl$_2$·0.5 (toluene)* ***(3.3)****. In the process the ligand became an anionic amide, the metal centre eliminated one chlorine atom, and the vanadium coordination number decreased by one unit. This new trivalent compound is a potent ethylene polymerization pre-catalyst, and polymers produced by the complex activated with PMAO showed a bimodal character in the GPC. Its bimodality is tentatively explained with the existence of two catalytically active species (mono and dialkylation of the vanadium centre). Further attack of a strong alkylating agent such as MeLi occurs at the pyridine ring to either remove the methyl group, or to place an additional methyl group on the ring meta position. Both processes imply two-electron reduction of the metal centre and formation of the corresponding V(I) derivatives {2,6-bis[2,6-(i-Pr)$_2$PhN=C (Me)]$_2$(C$_5$H$_3$N)}V(CH$_3$)(μ-CH$_3$)Li(Et$_2$O)$_3$* ***(3.4)*** *and the ionic [{2,6-bis[2,6-(i-Pr)$_2$PhN=C(Me)]$_2$ (2,3-Me$_2$C$_5$H$_3$N)}V(CH$_3$)$_2$] [Li(THF)$_2$(TMEDA)$_2$] ·0.5(Et$_2$O)* ***(3.5)*** *which were isolated in crystalline form.*

3.1 Introduction

Recent findings that a diimine/pyridine ligand system[1] spectacularly enhances the reactivity of electron-rich late-transition metals toward Ziegler-Natta olefin polymerization have attracted considerable attention in the literature. The very high activity of these catalysts and especially of those discovered by Brookhart[2] and Gibson[3] poses some fascinating questions about which particular ligand-to-metal bonding features may be responsible for the tremendous activity of these systems. Another point of interest

arises from the nature of the polymer. Typically, these catalysts produce highly linear polymers with variable polydispersities.[4] Questions thus arise about which processes may determine chain initiation, termination, and molecular weight distribution in these highly active systems.

Recent work from our group on divalent samarium supported by tetradentate Schiff base ligands has indicated that it is possible for a coordinated diimine to be alkylated by nucleophilic agents.[5] As a result of the nucleophilic attack, the ligand became an anionic organic amide and as a result the nature of the metal-ligand interaction was completely modified. In view of these findings, and since amide ligands have been proven to support Ziegler-Natta catalysts of early transition metals[6] and especially of vanadium,[7] we became thus interested in studying the catalytic activity of medium-valent vanadium complexes of neutral Schiff bases. For this work we have selected the same 2,6-bis[1-(2,6-dimethylphenylimino) ethyl]pyridine ligand[2,3] successfully used by Brookhart and Gibson for late transition metals. Our aim was two-fold. First we wanted to probe the robustness of the particular diimine/pyridine ligand system mentioned above and its possible involvement in some of the transformations occurring during the catalytic cycle. Second, we wished to expand our understanding of the ability of d^2 vanadium complexes to function as olefin polymerization catalysts. It should be reiterated that, although a trivalent vanadium complex is one of the catalysts commercially used for the production of EPDM elastomers,[8] information remains surprisingly limited.[9]

Recently, we found that V(III) aryloxides work as potent Ziegler-Natta catalysts.[10] In close analogy to the catalytic system based on tris-diketonate vanadium, which is employed for the manufacture of EPDM rubber, the vanadium centre undergoes

reduction to the divalent state during the catalytic cycle. Formation of divalent vanadium typically results in catalyst failure and deactivation, and is a direct consequence of ligand abstraction by the Al co-catalyst as previously discussed in chapter 2.[11] In contrast, vanadium amide catalysts are more robust and are not so susceptible to reduction.[7c] One of the goals of this study was to verify the possibility that a ligand system containing a pyridine ring and two imino functions remains strongly bonded to the metal centre during the cycle. By preventing ligand abstraction and consequent metal reduction, a considerable increase of the catalytic activity of the vanadium center could be reasonably anticipated.

In this chapter, we describe the preparation and characterization of a trivalent vanadium diimine/pyridine complex as well as a preliminary assessment of its activity as a Ziegler-Natta pre-catalyst and an evaluation of the possible role played by the ligand in chain termination and catalyst deactivation.

3.2 Experimental Section

All operations were performed under inert atmosphere by using standard Schlenk type techniques. $VCl_3(THF)_3$[12] and 2,6-bis[1-(2,6-dimethylphenylimino)ethyl]pyridine[2] were prepared according to published procedures. Polymethylalumoxane solution (13.5% Al) in toluene (PMAO-IP, AKZO) was used as received. Infrared spectra were recorded on a Mattson 9000 and Nicolet 750-Magna FTIR instruments from Nujol mulls prepared in a dry-box. Samples for magnetic susceptibility measurements were weighed inside a dry-box equipped with an analytical balance and sealed into calibrated tubes. Magnetic measurements were carried out with a Gouy balance (Johnson Matthey) at room temperature. Magnetic moments were calculated following standard methods,[13] and corrections for underlying diamagnetism were applied to data.[14] Elemental analyses were carried out with a Perkin-Elmer 2400 CHN analyzer. Data for X-ray crystal structure determination were obtained with a Bruker diffractometer equipped with a SMART CCD area detector.

Preparation of {2,6-bis[2,6-(i-Pr)$_2$PhN=C(Me)]$_2$(C_5H_3N)}VCl_3 (CH_2Cl_2)$_{1.3}$ (3.2).

A solution of $VCl_3(THF)_3$ (1.6 g, 4.1 mmol) in anhydrous THF (100 ml) was treated with 2,6-bis[1-(2,6-di-isopropylphenylimino)ethyl]pyridine (2.0 g, 4.1 mmol). The solution was heated to 70 °C for 1 h and then stirred overnight at room temperature. The colour of the solution changed from cherry-red to burgundy. The solvent was evaporated under reduced pressure to yield a dark red solid, which was redissolved in anhydrous CH_2Cl_2 (75 ml). Dark red crystals of **3.2** were obtained after allowing the resulting solution to stand 3 days at room temperature (2.77 g, 3.7 mmol, yield 90%). IR (Nujol mull, cm^{-1}):

3163 (m), 3059 (s), 2012 (w), 1936 (w), 1876 (w), 1574 (s), 1328 (m), 1317 (m), 1267 (s), 1206 (s), 1179 (m), 1149 (w), 1105 (m), 1057 (m), 1038 (m), 980 (w), 954 (w), 937 (m), 905 (w), 834 (w), 815 (m), 797 (s), 777 (s), 758 (w), 746 (m), 723 (w), 697 (w), 651 (w), 618 (w), 560 (w). Anal. Calcd (found) for $C_{34.33}H_{45.67}Cl_{5.67}N_3V$: C 54.81 (54.73), H 6.12 (6.01), N 5.59 (5.47). $\mu_{eff} = 2.94\ \mu_{BM}$.

Preparation of {2,6-bis[2,6-(i-Pr)$_2$PhN=C(Me)]$_2$(2-MeC$_5$H$_3$N)}VCl$_2$ 0.5 (hexane) (3.3).

A suspension of **3.2** (2.1 g, 3.3 mmol) in anhydrous toluene (150 ml) was treated with PMAO (0.8 mL, 13% Al solution in toluene, 6.6 mmol). The colour rapidly changed from red to green. The mixture was gently heated and allowed to stir for 16 h at room temperature. The resulting suspension was filtered to eliminate a small amount of insoluble material. After the solvent was evaporated in vacuo, the green, solid residue was dissolved in anhydrous CH_2Cl_2 (40 ml) and layered with hexane (40 ml). Dark green crystals of **3.3** (0.63 g, 0.95 mmol, yield 29%) separated upon standing undisturbed at room temperature for 14 days. IR (Nujol mull, cm^{-1}): 3187 (s), 1612 (m), 1588(w), 1565 (m), 1517 (m), 1414 (w), 1364 (m), 1351 (m), 1324 (w), 1308 (w), 1260 (s), 1187 (m), 1146 (m), 1099 (s), 1054 (s), 1022 (s), 934 (w), 909 (w), 863 (m), 804 (s), 772 (s), 754 (w), 720 (m), 695 (m), 672 (m), 650 (w), 570 (w). Anal. Calcd (found) for $C_{37}H_{53}N_3VCl_2$: C 67.16 (66.93), H 8.07 (7.84), N 6.35(6.21). $\mu_{eff} = 2.87\ \mu_{BM}$.

Method B

A solution of **3.2** (1.31 g, 2.0 mmol) in anhydrous toluene (100 ml) was cooled to -78 °C. The addition of a solution of MeLi in ether (1.43 ml, 1.4 M, 2.0 mmol) to the mixture

immediately changed the colour from red to green. The solution was allowed to warm slowly to room temperature and then stirred for 4 h at room temperature. The solvent was removed in vacuo to yield a dark green, solid residue, which was redissolved in ether (100 ml). The resulting solution was filtered to remove a small quantity of insoluble material, and a small amount of hexane was added. Dark green crystals of **3.3** separated upon standing at -30 °C for 72 h (0.68 g, 1.1 mmol, 54%).

Preparation of {2,6-bis[2,6-(i-Pr)$_2$PhN=C(Me)]$_2$(C$_5$H$_3$N)}V(CH$_3$)(CH$_3$)Li(Et$_2$O)$_3$ (3.4).

A solution of **3.2** (1.3 g, 2.0 mmol) in anhydrous toluene (100 ml) was cooled to -78 °C. The addition of a solution of MeLi in ether (5.7 ml, 1.4 M, 8.0 mmol) immediately changed the colour of the mixture from red to dark brown. The solution was allowed to warm slowly to room temperature and then stirred for additional 4 h. The solvent was then removed in vacuo to yield a dark brown solid, which was redissolved in freshly distilled ether (100 ml). The solution was filtered to remove a small quantity of insoluble material. Dark brown crystals of **3.4** separated upon allowing the solution to stand at room temperature for 72 h (0.83 g, 1.0 mmol, yield 50%). IR (Nujol mull, cm^{-1}): 3167 (m), 3050 (m), 1611 (m), 1585(w), 1457(s), 1378 (m), 1312 (m), 1246 (s), 1199 (m), 1189 (m), 1174 (w), 1153 (w), 1102 (w), 1092 (m), 1055 (s), 1042 (s), 986 (w), 952 (m), 934 (w), 889 (w), 861 (w), 825 (w), 803 (m), 775 (m), 758 (m), 738 (m), 722 (m), 694 (w), 682 (w), 629 (w). Anal. Calcd (found) for C$_{47}$H$_{79}$O$_3$N$_3$VLi: C 71.27 (71.02), H 10.05 (9.89), N 5.31 (5.26). μ_{eff} = 2.50 μ_{BM}.

Preparation of [{2,6-bis[2,6-(i-Pr)$_2$PhN=C(Me)]$_2$(2,3-Me$_2$C$_5$H$_3$N)}V(CH$_3$)$_2$][Li(THF)$_2$ (TMEDA)$_2$] (Et$_2$O)$_{0.5}$ (3.5).

A solution of **3.2** (1.3 g, 2.0 mmol) in anhydrous toluene (100 ml) was cooled to -78 °C. The addition of a solution of MeLi in ether (5.7 ml, 1.4 M, 8.0 mmol) changed immediately the colour of the mixture from red to dark brown. The solution was allowed to warm slowly to room temperature and then stirred for additional 72 h. The solvent was then removed in vacuo to yield a dark brown solid which was redissolved in freshly distilled ether (100 ml) followed by the addition of TMEDA (2 ml) and THF (10 ml). The resulting solution was filtered to remove a small amount of insoluble material. Dark brown crystals of **3.5** were obtained upon allowing the resulting solution to stand at room temperature for 72 h. (0.78 g, 0.86 mmol, yield 44%). IR (Nujol mull, cm^{-1}): 3168(m), 3050(m), 2924(s), 2853(s), 1585(m), 1457(s), 1378(s), 1312(m), 1245(s), 1200(w), 1190(w), 1174(w), 1154(w), 1102(m), 1099(s), 1092(m), 1055(m), 1042(w), 986(w), 953(m), 934(m), 890(w), 861(w), 825(m), 803(m), 775(m), 758(m), 738(w), 722(m), 695(w), 682(w), 629(w). Anal. Calcd (found) for $C_{53}H_{92}N_5O_{2.5}VLi$: C 70.95(70.88), H 10.34 (10.11), N 7.81(7.65). $\mu_{eff} = 2.64\ \mu_{BM}$.

3.3 General Polymerization Procedure

Ethylene (99.5%, polymer grade, Praxair) was purified by passage through the bench scale reactor's gas purification units (13× molecular sieves, alumina and oxygen removal columns). Anhydrous toluene was purchased from Aldrich and purified over molecular sieves prior to use. PMAO-IP was purchased from Akzo-Nobel and contained 13.5 wt % of Al. $B(C_6F_5)_3$ was purchased from Boulder Scientific Inc. and used without further purification. A bench scale reactor was used in the polymerization experiments. The reactor uses a programmable logic control (PLC) system with Wonderware 5.1 software for process control. Ethylene polymerizations were performed in the 500 mL Autoclave Engineers Zipperclave reactor equipped with an air driven stirrer and an automatic temperature control system. All of the chemicals were fed into the reaction batch wise except for ethylene, which was fed on demand.

Conditions for polymerization are as summarized above, the control temperature was 50°C for a slurry polymerization and 140°C for solution polymerization experiments. The polymerization time varied from 10 to 30 min. Adding 5 mL of methanol to the reactor terminated the reaction, and the polymer was recovered by evaporation of the toluene in vacuo. The polymerization activities were calculated based upon weight of polymer produced (Table 3.1). Polymer molecular weights and molecular weight distributions were measured by GPC (Waters 150-C) at 140 °C in 1,2,4-trichlorobenzene calibrated using polyethylene standards. DSC was conducted on a DSC 220 C from Seiko Instruments. The heating rate was 10 °C/min from 0° to 200°C. In a typical polymerization experiment, the solvent was pre-saturated with ethylene in the reactor at the desired temperature. The co-catalyst was injected in the reactor followed by

introduction of the pre-catalyst. In the mixed-activator experiment the two co-catalysts were premixed and injected in the reactor prior to introduction of the pre-catalyst. 1-octene was introduced in the reactor and premixed with ethylene before heating. Reproducibility of catalyst activity and reactor operation was checked by regularly running polymerization experiments using a standard zirconium catalyst and by repeating the experiments under identical reaction conditions. Errors and deviation were always below 5.9%.

Table 3.1 Polymerisation Results of Complex 3.2

entry	T (°C)	activation (Al:V)	run time (min)	yield (g)	activity (1) g PE/mmol cat h	activity (2) g PE/mmol cat [C_2] h	M_w ($x10^{-3}$)	PD
1	50	PMAO (600)	15	22.8	1415.6	652.4	67.4	11.54
2[a]	50	PMAO (60)	30	24.2	2243.5	3309.9	174.2	50.79
3	140	PMAO (600)	10	6.6	611.7	788.8	277.6	40.35
4	140	PMAO (60)	10	6.3	583.9	752.9	178.9	35.92
5[b]	140	PMAO (60)	10	5.6	519	669.2	179.2	30.90
6[c]	140	PMAO (20) $B(C_6F_5)_3$ (B/V=1.05)	10	3.3	305.0	393.3	58.3	8.46

[a] In this particular case the catalyst concentration was 100 mol/L instead of 300 mol/L in all other cases. The ethylene total pressure was 100 psig. The temperature was controlled within 5 °C. [b] 40 mL of 1-octene was added into reactor in a batch. 3.9 Br/1000C were detected by FT-IR; polymer melting point was 127.4 °C. PMAO and the catalyst (Al/V = 20) was pre-mixed before injected into the reactor. The catalyst and $B(C_6F_5)_3$ solution were injected into the reactor simultaneously.

Table 3.2 Polymerisation Conditions

	slurry phase	solution phase
Toluene	216 mL	216 mL
Catalyst concentration	300 μmol/L	300 μmol/L
PMAO	Al/V = 600 (mol/mol)	Al/V = 60, 600 (mol/mol)
Reaction temperature	50 °C	140 °C
reactor pressure	300 psig total	286 psig total

3.4 X-ray Crystallographic Structural Studies.

Suitable crystals were selected, mounted on thin glass fibres using paraffin oil and cooled to the data collection temperature. Data were collected on a Bruker AX SMART 1k CCD diffractometer using 0.3° ω-scans at 0°, 90°, and 180° in ϕ. Unit-cell parameters were determined from 60 data frames collected at different sections of the Ewald sphere. Semi-empirical absorption corrections based on equivalent reflections were applied. Systematic absences in the diffraction data and unit-cell parameters were consistent, uniquely, with the reported space group for **3.2**, **3.3**, and **3.5** and with $Pna2_1$ ($Pn2_1a$), and *Pnma* for **3.4**. Solution in *Pnma* yielded chemically reasonable and computationally stable results of refinement for **3.4**. The structures were solved by direct methods, completed with difference Fourier syntheses and refined with full-matrix least squares procedures based on F^2. Three symmetry-unique but chemically equivalent molecules of the complex and four molecules of methylene chloride solvent, one of which is disordered with a 60/40-site occupation distribution were located in the asymmetric unit of **3.2**. A molecule of hexane solvent was located in **3.3** disordered at an inversion center and was refined with half site occupancy. A half molecule of diethyl ether solvent and a lithium counter ion, coordinated with one TMEDA and two THF ligand molecules, were located in **3.5**. A lithium ion, coordinated to three diethyl ether molecules, was located within interacting distance of one of the methyl ligands of the anionic complex in **3.4**. All non-hydrogen atoms were refined with anisotropic displacement parameters. All hydrogen atoms were

treated as idealized contributions. All scattering factors and anomalous dispersion factors are contained in the SHEXTL 5.03 program library. Crystal data and relevant geometrical parameters are reported in Appendix 2 and Appendix 3.

Complex of 2,6-bis(2,6-diisopropylphenylimino)ethyl]pyridine (3.1)

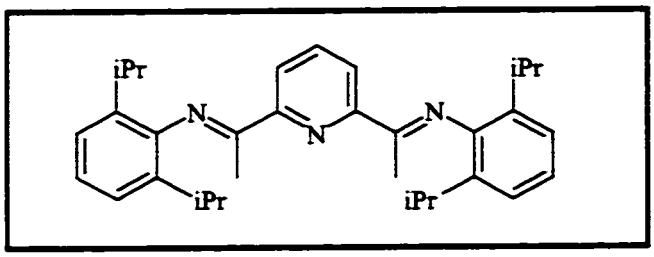

Structure of **3.1** consists of the 2,6-bis[1-(2,6-dimethylphenylimino)ethyl]pyridine ligand used in the synthesis of the following vanadium, chromium, titanium and manganese complexes. The single crystal x-ray structure has not yet been reported by Gibson or Brookhart and is described below (Figure 3.1). Excluding the sp^3 hybridized carbons of the two isopropyl groups and the two methyl groups, all other carbons have an sp^2 coordination geometry which is confirmed by carbon-carbon bond distances which fall in the order of 1.37-1.40 Å and bond angles in the range of 117°-122°. The C-N distance of the imino functional group also falls in the expected range for carbon-nitrogen double bonds [C(20)-N(3) = 1.273(5)Å, N(1)-C(13) = 1.267(5)Å] . This structure will play a role in comparing angular and distal deformations of the ligand upon binding of the metal to the ligand.

Figure 3.1 ORTEP of 2,6-bis(2,6-diisopropylphenylimino)ethyl]pyridine (3.1)

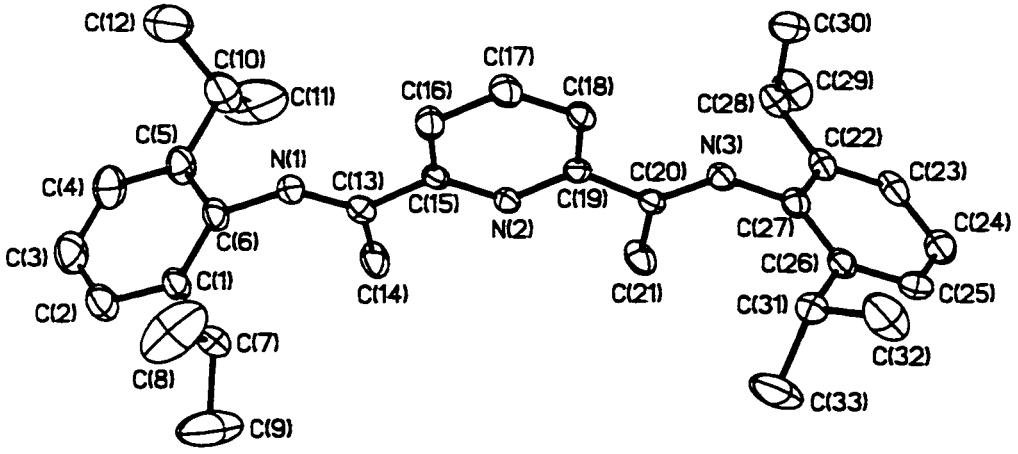

Selected Bond Lengths (Å) and Angles (°) for Complex 3.1

Distances	Angles
N(1)-C(6) = 1.434(5)	C(6)-N(1)-C(13) = 122.7(4)
N(1)-C(13) = 1.267(5)	N(1)-C(13)-C(15) = 117.2(4)
C(13)-C(15) = 1.485(5)	C(13)-C(15)-N(2) = 116.8(4)
N(2)-C(15) = 1.344(5)	C(15)-N(2)-C(19) = 117.8(4)
N(2)-C(19) = 1.357(5)	N(2)-C(19)-C(18) = 123.1(4)
C(19)-C(20) = 1.489(5)	C(19)-C(18)-C(17) = 118.9(4)
C(20)-N(3) = 1.273(5)	C(18)-C(17)-C(16) = 119.3(4)
N(3)-C(27) = 1.434(5)	N(2)-C(19)-C(20) = 114.9(4)
C(19)-C(20) = 1.489(5)	C(19)-C(20)-N(3) = 116.8(4)
C(18)-C(17) = 1.376 (5)	C(20)-N(3)-C(27) = 121.4(4)

Complex of {2,6-bis[2,6-(i-Pr)$_2$PhN=C(Me)]$_2$(C_5H_3N)}VCl_3 (3.2)

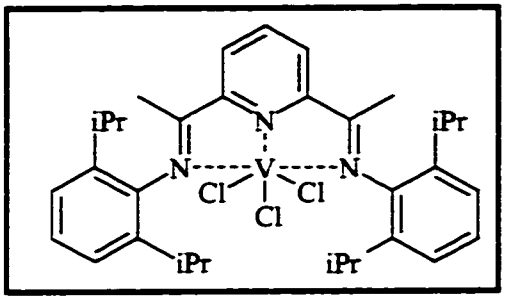

The structure of **3.2** consists of a vanadium atom surrounded by the pyridine/diimine ligand and three chlorine atoms (Figure 3.2). The coordination geometry around the metal center is distorted octahedral with the equatorial plane defined by the three nitrogen atoms of the ligand [N(1)-V(1)-N(2) = 74.61(13)°, N(2)-V(1)-N(3) = 75.46(13)°, N(1)-V(1)-N(3) = 150.03(12)°] and one chlorine atom [N(1)-V(1)-Cl(1)= 106.07(10)°, N(3)-V(1)-Cl(1) = 103.90(10)°, N(2)-V(1)-Cl(1) = 177.43(11)°]. The other two chlorine atoms are placed on the two axial positions and form a significantly bent Cl-V-Cl vector [Cl(2)-V(1)-Cl(3) = 166.38(6)°]. The V-Cl distances [V(1)-Cl(1) = 2.2739(14) Å, V(1)-Cl(2) = 2.2924(14) Å, V(1)-Cl(3) = 2.3552(14) Å] are slightly different from each other but fall in the expected range for terminal V-Cl bonds. The V-N distances are also normal. The two V-N distances formed by the two imino functions [V(1)-N(1) = 2.242(3) Å, V(1)-N(3) = 2.212(3) Å] are longer than that formed with the pyridine nitrogen atom [V(1)-N(2) = 2.067(3) Å] possibly suggesting the presence of some extent of V-pyridine -bonding. The C-N bonds of the two imine groups are only slightly longer than expected [N(1)-C(13) = 1.283(5) Å, N(3)-C(20) = 1.288(5) Å]. The pyridine ring is co-planar with the molecular equatorial plane whereas the two terminal phenyl groups attached to the two imino nitrogens lay on perpendicular planes.

Figure 3.2 ORTEP of {2,6-bis[2,6-(i-Pr)$_2$PhN=C(Me)]$_2$(C$_5$H$_3$N)}VCl$_3$ (3.2)

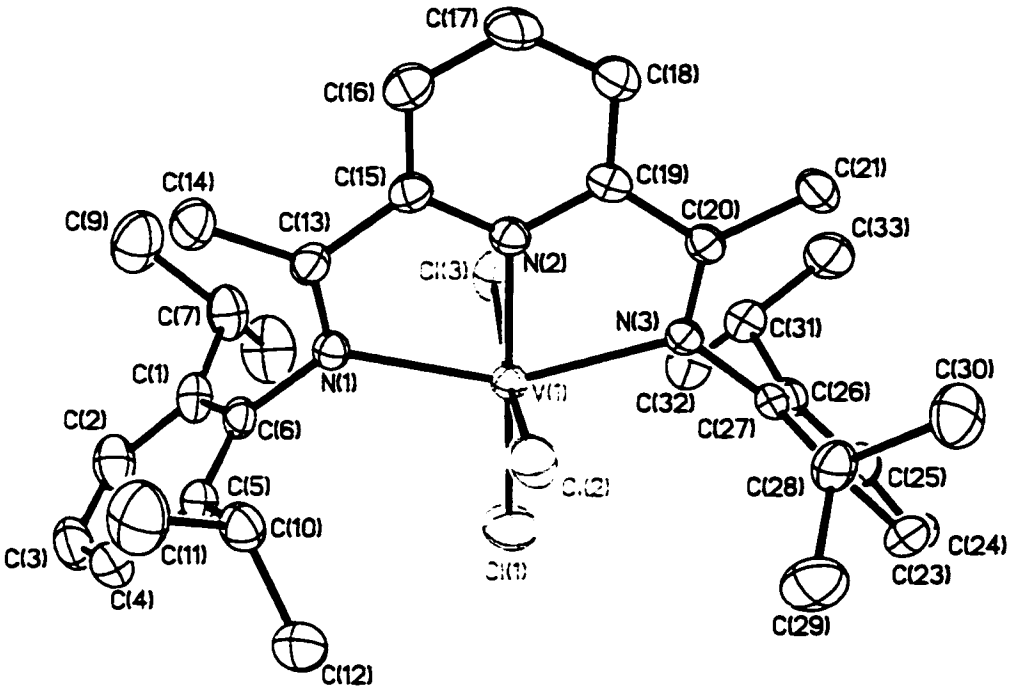

Selected Bond Lengths (Å) and Angles (°) for Complex 3.2

Distances	Angles
V(1)-Cl(1) = 2.2739(14)	N(1)-V(1)-Cl(1) = 106.07(10)
V(1)-Cl(2) = 2.2924(14)	N(1)-V(1)-Cl(2) = 88.96(9)
V(1)-Cl(3) = 2.3552(14)	N(1)-V(1)-Cl(3) = 89.25(9)
V(1)-N(1) = 2.242(3)	N(1)-V(1)-N(2) = 74.61(13)
V(1)-N(2) = 2.067(3)	N(2)-V(1)-Cl(1) = 177.43(11)
V(1)-N(3) = 2.212(3)	Cl(2)-V(1)-Cl(3) = 166.38(6)
N(1)-C(13) = 1.283(15)	N(3)-C(20)-C(19) = 116.9(4)
N(3)-C(20) = 1.288(5)	C(2)-V-N(3) = 92.9(4)
	N(1)-V-N(3) = 150.5(4)
	N(2)-C(17)-C(18) = 106.4(10)
	N(2)-C(17)-C(15) = 104.4(11)

Complex of ({2,6-bis[2,6-(i-Pr)$_2$PhN=C(Me)]$_2$(2-MeC$_5$H$_3$N)}VCl$_2$ (3.3)

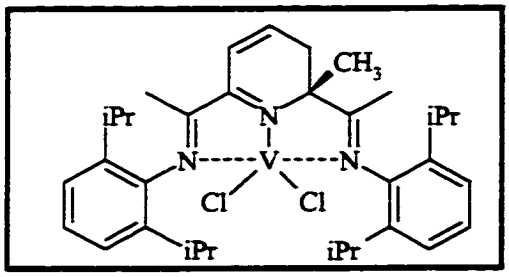

The coordination geometry of vanadium in this complex can be described as distorted trigonal bipyramidal and is defined by two chlorine atoms and by the three nitrogen donor atoms of the tridentate ligand (Figure 3.3). Two chlorines and the nitrogen atom of the methylated pyridine ring define with the metal centre the molecular equatorial plane [Cl(1)-V-Cl(2) = 112.10(9)°, Cl(1)-V-N(2) = 113.69(18)°, Cl(2)-V-N(2) = 134.18(19)°]. Two nitrogens of the two imino functions are located on the axial position forming a significantly bent N-V-N vector [N(1)-V-N(3) = 154.2(3)°]. Apart from the deviation from the planarity of the methylated pyridine ring, the diimine/pyridine ligand does not display additional distortion with respect to complex **3.2**. Even the V-Cl [V-Cl(1) = 2.257(2) Å, V-Cl(2) = 2.259(2) Å] as well as the V-N bond distances [V-N(1) = 2.162(6) Å, V-N(3) = 2.156(6) Å] compare well to those of complex **3.2**. Conversely, the V-N distance with the distorted ring [V-N(2) = 1.886(6) Å] is shorter as a result of the change of the nature of the V-N interaction and the presence of a formal negative charge on the ring. Similar to complex **3.2** the orientation of the two peripheral phenyl rings is perpendicular to the V-N(1)-N(2)-N(3) plane. The decrease of the vanadium coordination number with respect to **3.2** does not significantly affect the geometry of the vanadium/diimine core.

Figure 3.3 ORTEP of ({2,6-bis[2,6-(i-Pr)$_2$PhN=C(Me)]$_2$(2-MeC$_5$H$_3$N)}VCl$_2$ (3.3)

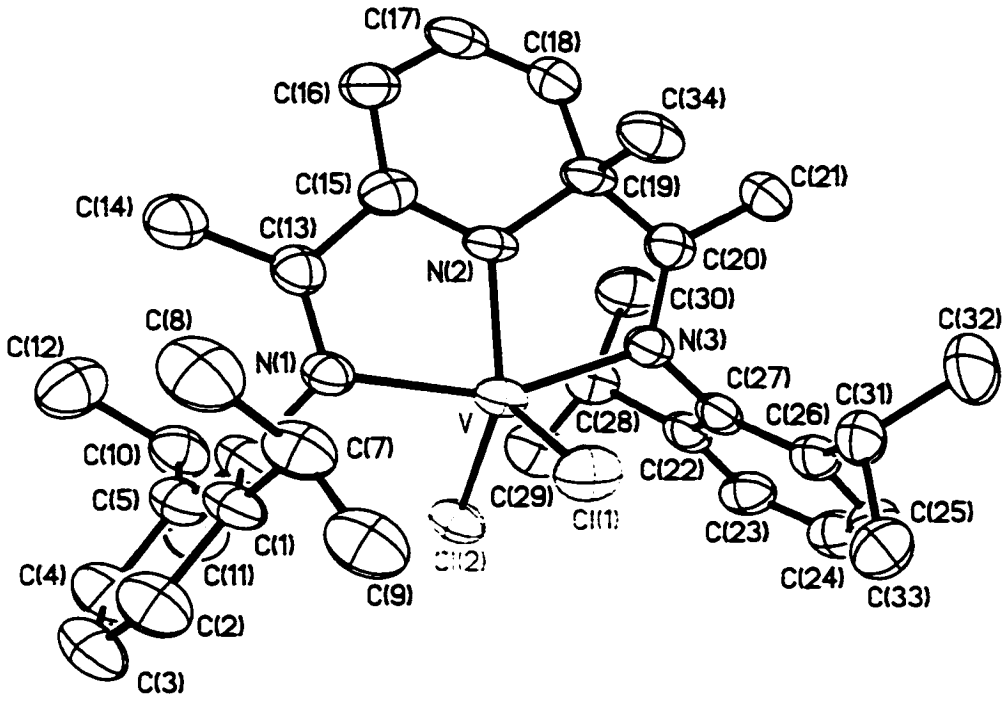

Selected Bond Lengths (Å) and Angles (°) for Complex 3.3

Distances	Angles
V-Cl(1) = 2.257(2)	N(1)-V-N(3) = 154.2(3)
V-Cl(2) = 2.259(2)	N(1)-V-N(2) = 78.6(3)
V-N(1) = 2.162(6)	N(1)-V-Cl(1) = 98.74(18)
V-N(2) = 1.886(6)	N(1)-V-Cl(2) = 96.30(17)
V-N(3) = 2.156(6)	Cl(1)-V-Cl(2) = 112.10(9)
C(19)-C(34) = 1.561(9)	Cl(1)-V-N(2) = 113.69(18)
	Cl(2)-V-N(2) = 134.18(19)
	N(1)-V(1)-N(3) = 150.03(12)
	N(2)-V(1)-N(3) = 75.46(13)

Complex of {2,6-bis[2,6-(iPr)$_2$PhN=C(Me)]$_2$(C$_5$H$_3$N)}V(CH$_3$)$_2$Li(Et$_2$O)$_3$ (3.4).

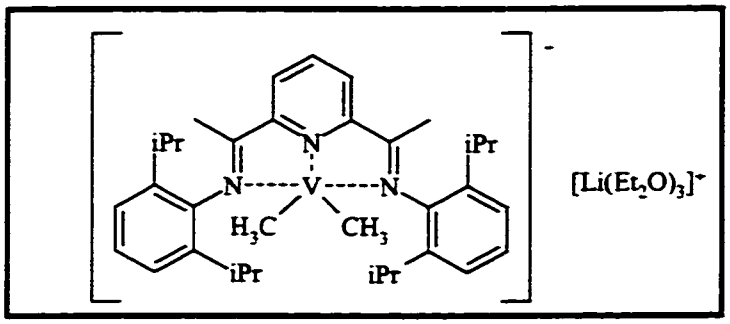

The coordination geometry around the vanadium centre is in this case better described as square pyramidal (Figure 3.4) and is strongly reminiscent of the recently reported structure of the $FeCl_2$ adduct of the same ligand.[2] The three nitrogen donor atoms of the ligand and one terminal methyl group define the basal plane [N(1)-V-N(2) = 77.53(13)°, N(1)-V-C(2) = 143.5(3)°, N(2)-V-C(2) = 95.71(15)°, N(2)-V-N(2a) = 151.1(2)°]. The vanadium atom is slightly elevated above the plane [distance from the plane 0.51 Å] while a second methyl group occupies the axial position. The V-N distances [V-N(2) = 2.046(4) Å] are normal and compare well with those of complex **3.2**. The pyridine ring forms a V-N distance [V-N(1) = 1.911(6) Å] which is longer than in complex **3.3** but which compares well to that of **2.2**. The V-C distances [V-C(1) = 2.118(7) Å, V-C(2) = 2.093(9) Å] slightly differ from each other as a probable result of the different positions in the coordination polyhedron (basal versus axial). One tetrahedral lithium atom attached to three molecules of coordinated ether [Li-O(1) = 1.934(15) Å] is also bonded to the axial methyl group [Li-C(1) = 2.514(18) Å] forming a significantly bent Li-C-V vector [V-C(1)-Li = 151.4(5)°].

Figure 3.4 **ORTEP of {2,6-bis[2,6-(iPr)$_2$PhN=C(Me)]$_2$(C$_5$H$_3$N)}V(CH$_3$)$_2$Li(Et$_2$O)$_3$ (3.4)**

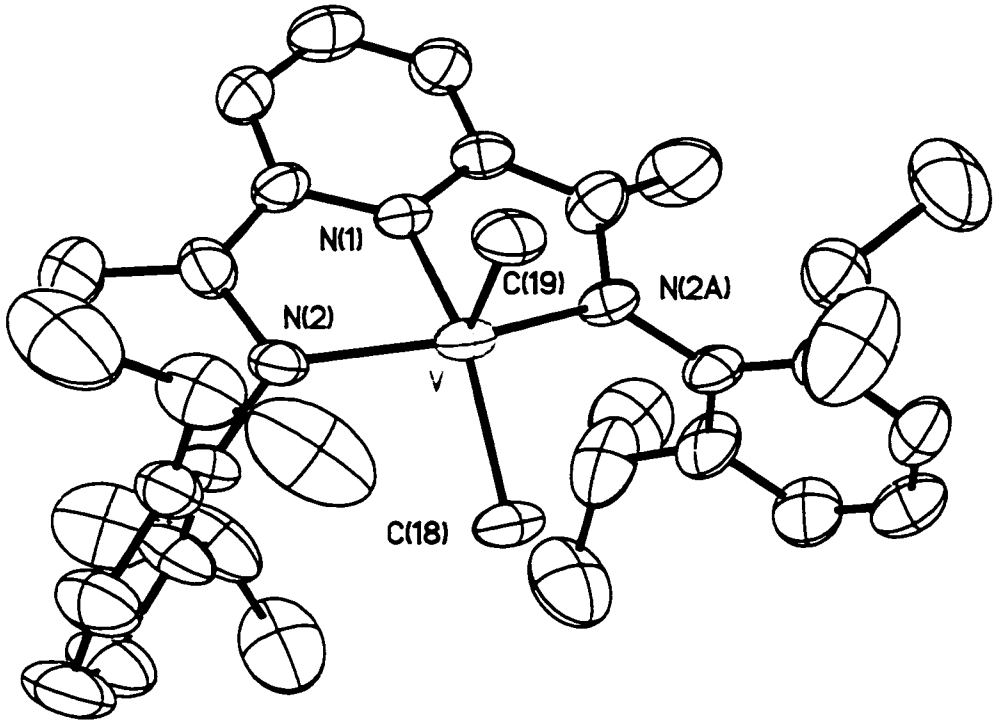

Selected Bond Lengths (Å) and Angles (°) for Complex 3.4

Distances	Angles
V-C(1) = 2.118(7)	V-C(1)-Li = 151.4(5) *
V-C(2) = 2.093(9)	C(1)-V-C(2) = 119.9(3)
V-N(1) = 1.911(6)	C(1)-V-N(1) = 96.6(3)
V-N(2) = 2.046(4)	C(1)-V-N(2) = 98.55(13)
Li-C(1) = 2.514(18)	C(2)-V-N(2) = 95.71(15)
	C(2)-V-N(1) = 143.5(3)
	N(2)-V-N(1) = 77.53(13)
	N(2)-C(19)-C(34) = 109.1(6)
	C(20)-C(19)-C(18) = 114.6(7)
	N(3)-C(20)-C(19) = 115.5(7)

*the Li counter-cation was omitted for clarity purposes.

Complex of [{2,6-bis[2,6-(i-Pr)$_2$PhN=C(Me)]$_2$(2,3-Me$_2$C$_5$H$_3$N)}V(CH$_3$)$_2$] [Li(THF)$_2$ (TMEDA)] (3.5)

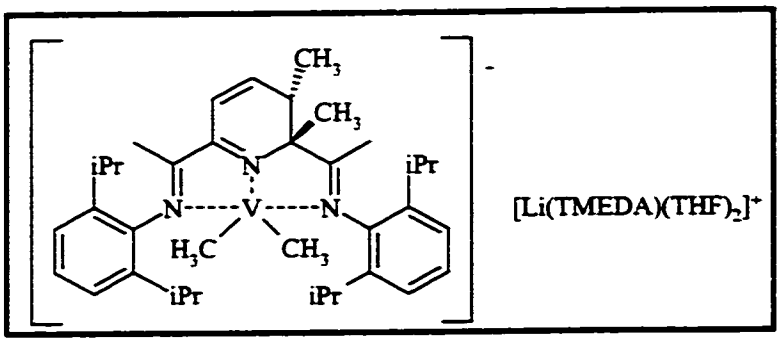

Despite the considerable distortion of the diimine ligand pyridine ring introduced by the double methylation, the coordination geometry around the vanadium centre (Figure 3.5) is very similar to that observed in complex **3.4** [N(1)-V-N(2) =79.7(4)°, N(1)-V-N(3) = 150.5(4)°, N(1)-V-C(2) = 93.8(4)°, N(2)-V-C(2) = 146.0(4)°, N(3)-V-N(2) = 78.7(4)°, N(3)-V-C(2) = 92.9(4)°]. Even in this case, the coordination geometry around the metal center is square pyramidal with the three nitrogen donor atoms [V-N(1) = 1.986(9) Å, V-N(2) = 1.872(9) Å, V-N(3) = 2.005(9) Å] and one methyl group [V-C(2) = 2.115(10) Å] defining the basal plane. The vanadium atom is elevated above the basal plane [distance from the plane 0.50 Å] and all of the bond distances and angles compare rather well to those of **3.4**. The second methyl is placed on the axial position [C(1)-V-C(2) = 111.4(5)°, C(1)-V-N(1) = 108.2(4)°, C(1)-V-N(2) = 102.3(4)°, C(1)-V-N(3) = 95.9(4)°] forming a V-C distance [V-C(1) = 2.075(11) Å], which compares well with that of complex **3.4**. This is in spite of the fact that the lithium counter-cation is solvated by one molecule of TMEDA [Li-N(4) = 2.11(3) Å] and two molecules of THF [Li-O(1) = 1.93(2) Å] and does not form a direct bonding interaction with the anionic vanadium moiety.

Figure 3.5 **ORTEP of [{2,6-bis[2,6-(i-Pr)$_2$PhN=C(Me)]$_2$(2,3-Me$_2$C$_5$HN)}V(CH$_3$)$_2$] [Li(THF)$_2$ (TMEDA)$_2$] (3.5)**

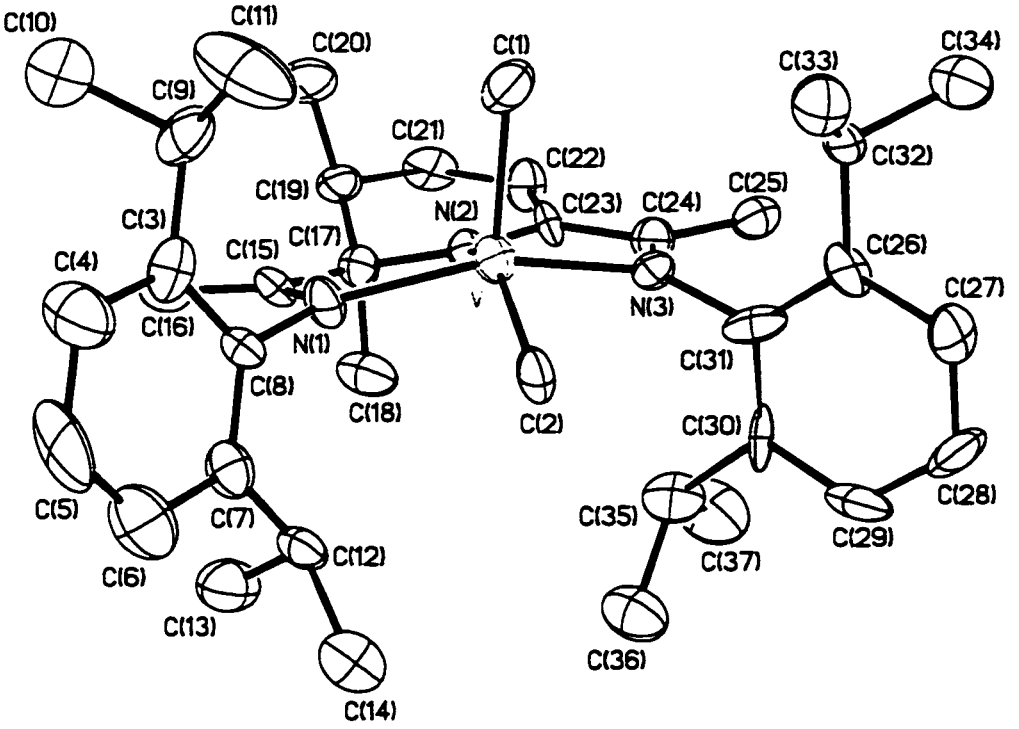

Selected Bond Lengths (Å) and Angles (°) for Complex 3.5

Distances	Angles
V-C(1) = 2.075(11)	C(1)-V-C(2) = 111.4(5)
V-C(2) = 2.115(10)	C(1)-V-N(3) = 95.9(4)
V-N(1) = 1.986(9)	C(1)-V-N(2) = 102.3(4)
V-N(2) = 1.872(9)	C(1)-V-N(1) = 108.2(4)
V-N(3) = 2.005(9)	C(2)-V-N(1) = 93.8(4)
C(17)-C(18) = 1.602(15)	C(2)-V-N(2) = 146.0(4)
C(19)-C(20) = 1.552(14)	N(2)-V-N(2a) = 151.1(2)

*The Li counter cation was omitted for clarity.

3.5 Results and Discussion

Reaction of $VCl_3(THF)_3$ with 2,6-bis[1-(2,6-dimethylphenylimino)ethyl]pyridine in toluene afforded a dark red, scarcely soluble solid of the trivalent and mononuclear adduct 2.6-$[(2.6\text{-}(i\text{-}Pr)_2C_6H_3N)C(CH_3)]_2C_5H_3NVCl_3$ (**3.2**) (Scheme 3.1). The complex is paramagnetic and shows a magnetic moment as expected for the d^2 electronic configuration of the trivalent vanadium center. Not surprising, complex **3.2** is a potent ethylene polymerization catalyst precursor (Table 3.1). However, when comparing the activity to literature data, it appears that when **3.2** is activated with methylalumoxane (PMAO), the catalyst productivity is somewhat lower than that displayed by the related Fe derivative recently reported by Brookhart and Gibson.[4] Upon mixing a red toluene solution of **3.2** with excess of methylalumoxane co-catalyst, the colour immediately turned emerald green and vigorous ethylene uptake took place to form linear high density polyethylene as indicated by the melting point of the polymer (132.1 °C). When complex **3.2** was activated with PMAO at 50 °C and with a ratio Al/V = 600 (entry 1), the polymerization under slurry conditions started immediately and the temperature of the reaction mixture increased from 50 to about 85 °C within 20 s. The initial polymerization rate was high, but ethylene consumption slowed after about 2 min. However, the catalyst remained active throughout the 15 min run. This phenomenon might be caused by embedding of the catalytic sites in the solid polyethylene produced during the first few minutes. The GPC showed polymers with high polydispersities (Table 3.1). Deconvolution of the GPC curves (Figure 3.6) as the Al:V ratio decreased revealed one main peak, which, can be attributed to the presence of chain transfer of the growing

polymer chain to aluminium at higher Al:V ratios and to a single-site active catalyst species.

Figure 3.6 Gel Permeation Chromatography of Polyethylene Produced by 3.1 at 140°C (entries 3, 4, 6)

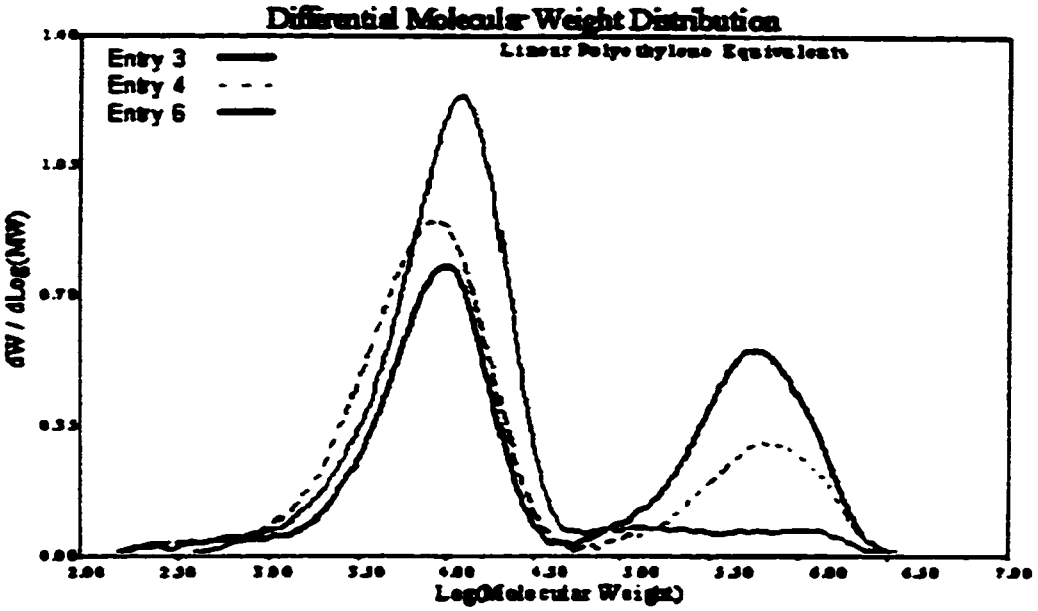

A comparison of the runs conducted at different temperatures and under two different reaction conditions (slurry and solution phase see Table 3.2) showed that the overall polymerization productivity is similar. However, the reactions carried out at two different temperatures displayed totally different kinetic profiles. The catalyst showed an extended life at 50 °C but was deactivated within 1 min at 140 °C. A bimodal character is clearly apparent in the GPC curves for polymers obtained at 140 °C using PMAO as co-catalyst (Figure 3.6). We observed that a higher Al/V ratio favoured the formation of the catalytic species responsible for the formation of low-molecular-weight polymer. The low-molecular-weight peak decreased upon decreasing of the Al to V ratio and increased at higher temperatures. The bi-modal behaviour of the system arises from high chain

transfer rates to the aluminium co-catalyst at higher Al to V ratios yielding the low-molecular weight fraction after β-H elimination. Reducing the Al to V ratio as observed in Figure 3.6 can eliminate this second low-molecular weight fraction. The diminished overall polymer productivity observed for the ethylene and 1-octene co-polymerization run (Table 3.1, Entry 5) may be attributed to steric congestion around the vanadium centre. It might also result from the formation of dormant sites after the insertion of 1-octene. In *situ* alkylation of the complex with PMAO and use of $B(C_6F_5)_3$ as a co-activator led to a drop in the overall catalyst productivity as indicated in entry 6. We also observe that this additive suppresses the formation of high-molecular-weight polymer (Figure 3.6).

The formation of an intense emerald-green colour observed upon mixing a solution of the vanadium species **3.2** with either small or large excess of PMAO co-catalyst clearly indicates the formation of a new species. Reactions carried out in preparative scale by mixing the catalysts and co-catalyst in the V : Al ratio of 1 : 2 afforded emerald green crystals of the new trivalent {2,6-bis [2,6-$(i\text{-}Pr)_2$PhN=C(Me)]$_2$(2-MeC_5H_3N)}VCl_2 compound (**3.3**) (Scheme 3.1) in reasonable yield (31%).

The isolated yield of compound was significantly improved to 65% by concentrating and cooling the reaction mother liquor. The X-ray diffraction pattern of the bulk solid was identical to that of the single crystal, thus confirming the analytical purity of complex **3.3**. The relatively low yield of isolated crystalline **3.3** is probably the result of its fairly high solubility. A comparison of the UV-vis spectrum of a freshly prepared solution of analytically pure **3.3** with that of the mother liquor did not show any significant difference, thus indicating the absence of other vanadium complexes in the

reaction mixture. The fact that no other products seem to be present in significant amounts possibly indicates that in contrast to other vanadium-based Ziegler-Natta catalysts,[15] the present system has only little or no possibility of having the ligand abstracted from the vanadium center by the Al co-catalyst.

Scheme 3.1 Pathway to Catalyst Activation

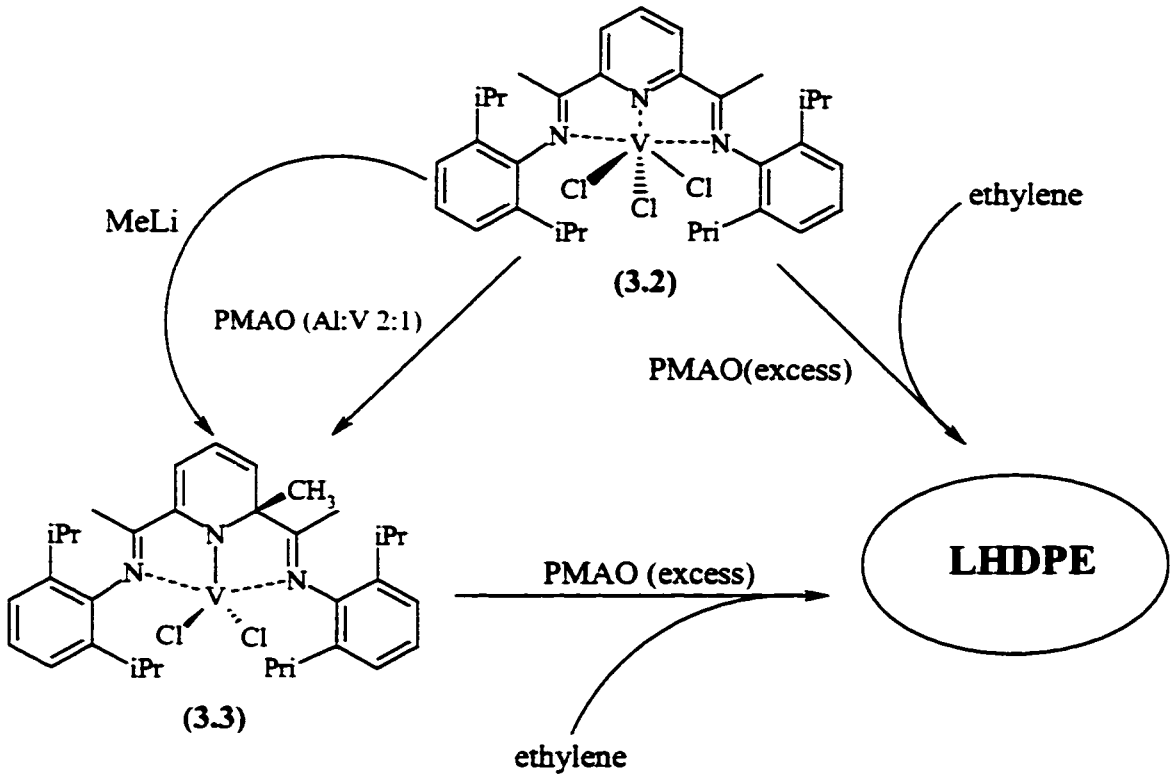

Compound **3.3** was also conveniently prepared in similar yield upon treatment of **3.2** with an equimolar amount of MeLi. The magnetic moment calculated for the formulation as determined by the crystal structure was consistent with the high spin d^2 electronic configuration of trivalent vanadium.

The connectivity of this new vanadium complex, as demonstrated by X-ray crystallography, showed that an important reorganization of the ligand had taken place as

a result of the pre-catalyst/co-catalyst interaction. The formation of **3.3** is the result of an unusual chloride abstraction reaction by M-Me [M = Li, AlO] where the alkyl group was delivered to one of the two *ortho* carbon atoms of the pyridine ring rather than to the metal center (Scheme 3.1). As part of the same process, a chlorine atom was removed from vanadium. Thus the reaction resulted in a considerable release of steric hindrance around vanadium, which decreased the coordination number by one unit (from 6 to 5) and adopted a trigonal bipyramidal coordination geometry. In the process, the ring acquires a negative charge, and the neutral diimine/pyridine ligand is *transformed into a diimine/anionic amide*. In other words, the interaction of catalyst with co-catalyst results in: (1) the transformation of the ligand in an anionic amide and (2) the creation of an empty coordination site around vanadium. This behaviour has two related precedents in the chemistry of zirconium.[16]

There are two possible and different driving forces that combine to push the reaction along this unusual pathway. The total electronic density distribution, as generated by the ZINDO/INDO/1 wave functions calculations (Nucleophilic Susceptibility subroutine of the CaChe software package)[17] was evaluated for a model compound with the atomic coordinates of **3.2**. Figure 3.7 shows the superimposition of the three-dimensional surface over one of the two possible resonance structures of **3.2**. The result of the calculation clearly indicated that the part of the molecule most positively charged and thus more susceptible to nucleophilic attack are indeed the two pyridine *ortho* carbon atoms (Figure 3.7). In addition, the alkylation of the pyridine ring generated a diene/amido system whose extensive conjugation with the metal center might well provide the stabilization energy necessary to balance the loss of the aromatic character of

the pyridine ring.[18] In agreement with this proposal, the V-$N_{pyridine}$ distance in complex **3.3** is significantly shorter than in **3.2** thus indicating an increase of V-N π-bonding.

Figure 3.7 **Superimposition of the structure of complex (3.2) over the 3-D surface representation of the total electron density distribution map indicating the most nucleophilic site on complex (3.2)**

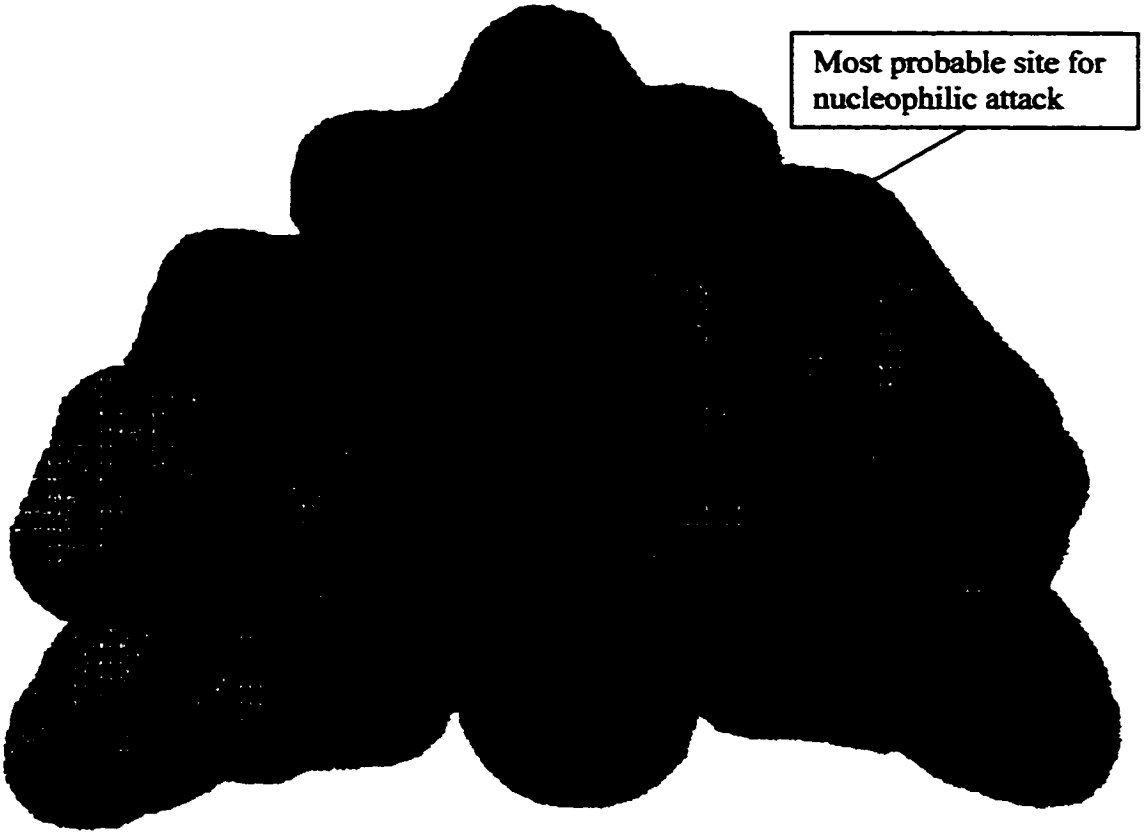

As mentioned above, the reaction of **3.2** with PMAO, Me_3Al, or MeLi seems to exclusively produce the catalyst precursor **3.3**. However, only upon using PMAO as co-catalyst does the system polymerize ethylene since no appreciable olefin polymerization was observed with Me_3Al. The activity of **3.3** was the same as with complex **3.2** and produced ethylene polymers with the same characteristics and quality.[19] On the basis of

these observations, it seems legitimate to conclude that complex **3.2** is the precursor of **3.3**, which is in turn the precursor of the catalytically active species. The fact that the presence of a co-catalyst is necessary for the catalytic activity of **3.3** rules out the possibility that the alkylation of the pyridine ring might perhaps be a reversible process with the methyl being transferred to the vanadium atom to start the polymerization reaction.

The possibility that cationic vanadium alkyls or other neutral species with different nuclearity may be the catalytically active species, as well as any other mechanistic possibility is entirely plausible and cannot be ruled out at this stage. Thus, attempts to isolate the catalytically active species were carried out by reacting **3.3** with excess PMAO. The reactions led only to unreacted **3.3** with no evidence for the formation of other products. A similar result was obtained at higher temperatures. The solution of mixtures of catalyst/co-catalyst were indefinitely stable in the range 50-100°C (appreciable decomposition occurred only at 120°C). In all cases, unreacted **3.3** was the only detectable compound. Therefore, if the subsequent role of the PMAO co-catalyst, after modifying the diimino/pyridine ligand, is perhaps that of replacing one or two of the residual chlorine atoms to form the corresponding coordinatively unsaturated vanadium alkyl derivatives, it is well possible that only a small fraction of **3.3** is actually activated. This observation prompted us to investigate the reaction of **3.3** with stronger methylating agents. Reaction of either **3.2** with 4 equivalents or of **3.3** with 3 equivalents of MeLi yielded two different compounds, which were separated via addition of TMEDA to the reaction mixture (Scheme 3.2). Work-up in the absence of TMEDA afforded the unprecedented monovalent and anionic vanadium dialkyl complex {2,6-bis[2,6-(i-

$Pr)_2PhN=C(Me)]_2(C5H_3N)\}V(CH_3)(-CH_3)Li(Et_2O)_3$ (**3.4**). The most striking feature of this compound is the absence of the methyl group originally present on the pyridine ortho carbon atom. The crystallographic features of this compound indicate that the regular geometry of the diimine/pyridine ring was restored during the reaction via elimination of the methyl group, while the vanadium oxidation state was lowered to +1 during the process. The vanadium centre bears two methyl groups, which together with the ligand provide the metal with a strange square pyramidal geometry.[20] The magnetic moment measured for analytically pure samples and calculated according to the formula as provided by the crystal structure indicates that the vanadium atom is in an intermediate-spin d^4 electronic configuration.

Scheme 3.2 Deactivation Pathways via Alkylation in the *Ortho* Position and Methyl Radical Coupling

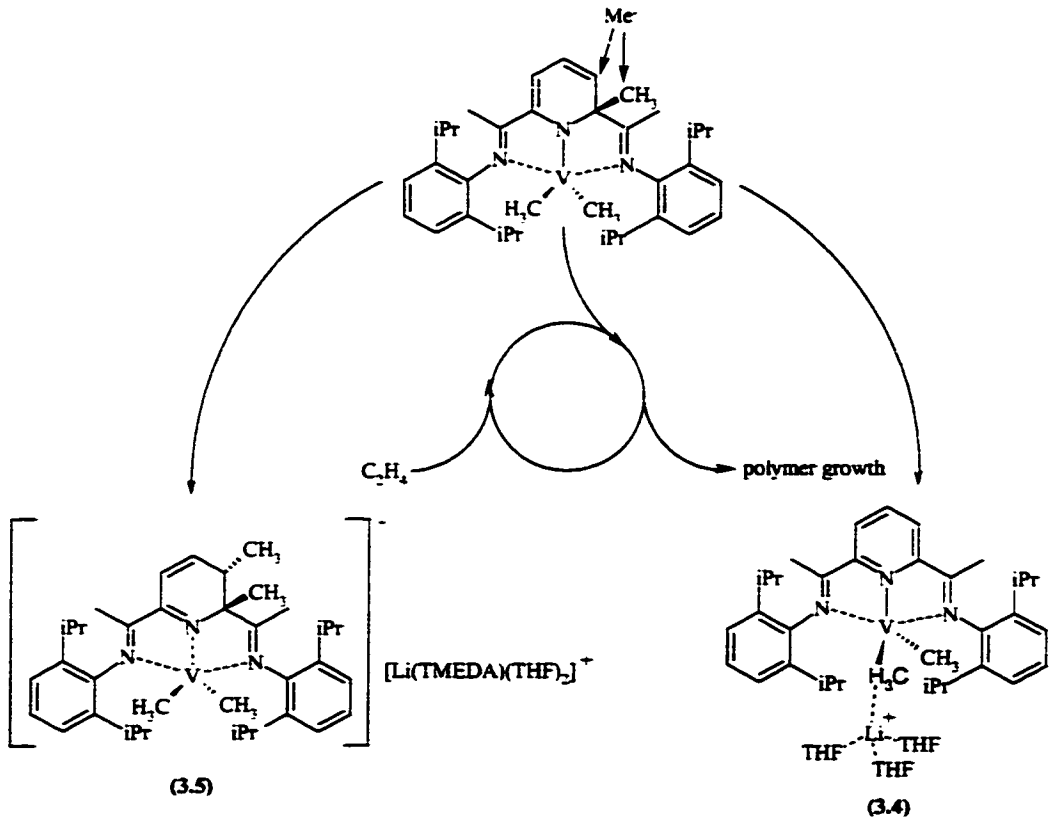

The second product that was isolated upon addition of TMEDA to the reaction mixture is also an anionic monovalent vanadium dimethyl derivative [{2,6-bis[2,6-(i-$Pr)_2$PhN=C(Me)]$_2$ (2,3-$Me_2C_5H_3N$)}V$(CH_3)_2$][Li$(THF)_2(TMEDA)_2$] (**3.5**). One minor difference with respect to **3.4** is that the lithium counter-cation is separated and fully solvated by one molecule of TMEDA and two molecules of THF and does not form bonding contacts with the vanadium anionic moiety. The most surprising difference, however, is the presence of a second methyl group on the ring *meta* position adjacent to the already alkylated carbon atoms. The two methyl groups are located on the two opposite sides of the molecular plane (Figure 3.4). Even in this case, the ligand involvement in the reaction resulted in a two-electron reduction of vanadium.

While it is unlikely that simple absence or presence of TMEDA is responsible for driving the reaction toward either the *dealkylation* or second ring alkylation pathways, two simultaneous processes probably form the two compounds **3.4** and **3.5**. The presence/absence of TMEDA simply afforded crystallization of one species in favour of the other. In complexes **3.4** and **3.5** the ligand is no longer an anionic organic amide. The ligand was transformed respectively into a neutral diimine/pyridine and a diimine/azadiene ligand. Although these two species are considerably different, both arise from similar two-electron reduction processes of the vanadium atom. The process can be envisioned as the result of a nucleophilic attack on either the methyl group attached to the *ortho* carbon atom, or at the *meta* carbon atom (Scheme 3.2). In the first case, the attack resulted in methyl abstraction and formation of ethane (identified in the gas chromatogram of the reaction mixture) while the pyridine ring was reformed. Two electrons were transferred in the process from the ring to the vanadium center, which

consequently reduced its oxidation state from +3 to +1. A similar reduction occurred in the second case during the formation of **3.5** when a methyl group attacked the ring *meta* position. Even in this case, the reaction implies a two-electron transfer to the vanadium center and consequent reduction to the monovalent state. As expected, the monovalent complexes **3.4** and **3.5** either with or without co-catalyst and activators are inert toward ethylene polymerization. Thus, their isolation shows that should a similar process occur (even at minor extent) with milder alkylating agents such as PMAO, this will provide a possible reduction pathway of the metal center with consequent chain termination.

3.6 Conclusion

Involvement of the ligand directly in the reactivity of the metal center is the key to understanding the high activity of this catalytic system. First of all, the alkylation of the pyridine ring transforms the initial coordination complex **3.2** into a covalent transition metal amide **3.3**, the process being accompanied by a decrease in the coordination number of the metal center. Steric hindrance is probably the factor responsible for the very poor co-monomer incorporation observed with this system. Further attack on the ligand, which reduces the metal toward an inactive V(I) species, is very fast with MeLi and might also occur at smaller extent with PMAO. Finally, despite its involvement in the reactivity of the metal center, the ligand is strongly bound to the transition metal with no evidence that the Al co-catalyst could abstract it. This is certainly an important factor, which in combination with the unique ability of this ligand to stabilize vanadium alkyls is probably responsible for the high activity observed in this system.

3.7 References

1. See, for example:

(a) Johnson, L. K.; Mecking, S.; Brookhart, M. S.; *J. Am. Chem. Soc.;* **1996**, *118*, 267

(b) Johnson, L. K.; Killian, C. M.; Tempel, D. J.; Brookhart, M. S.; *J. Am., Chem. Soc.* **1996**, *118*, 11664

(c) Johnson, L. K.; Killian, C. M.; Brookhart, M. S.; *Organometallics;* **1997**, *16*, 2005

(d) Guerin, F.; McConville, D. H.; Vittal, J. J.; Yap, G. P. A.; *Organometallics;* **1998**, *17*, 5172.

(e) Etkin, N.; Ong, C. M.; Stephan, D. W. *Organometallics* 1998, 17, 3656.

2. Johnson, L. K.; Killian, C. M.; Brookhart, M. S.; *J. Am. Chem. Soc.*; **1995**, *117*, 6414.

3. Gibson, V. C.; Kimberley, B. S.; White, A. P. J.; Williams, D. J.; Howard, P. J.; *Chem. Soc., Chem. Commun.;* **1998**, 313.

4. (a) Small, B. L.; Brookhart, M. S.; Bennett, A. M. A.; *J. Am. Chem. Soc.;* **1998**, *120*, 4049.

(b) Britovsek, G. J. P.; Gibson, V. C.; Kimberley, B. S.; Maddox, P. J.; McTavish, S. J.; Solan, G. A.; White A. J. P.; Williams, D. J. J.; *Chem. Soc., Chem. Commun.* **1998**, 849.

5. Dubé, T.; Gambarotta, S.; Yap, G. P. A.; *Organometallics;* **1998**, *17*, 3967.

6. (a) Boisson, C.; Berthet, J. C.; Ephritikhine, M.; Lance, M.; Nierlich, M.; *J. Organomet. Chem.*; **1997**, *531*, 115

(b) Witte, P. T.; Meetsma, A.; Hessen, B.; Budzelaar, P. T. H.; *J. Am. Chem. Soc.*; **1997**, *119*, 10561

(c) Kim, I.; Nishihara, Y.; Jordan, R. F.; Rogers, R. D.; Rheingold, A.; Yap, G. P. A.; *Organometallics;* **1997**, *16*, 3314

(d) Male, N. A. H.; Thornton-Pett, M.; Bochmann, M.; *J. Chem. Soc., Dalton Trans.*; **1997**, 2487.

(e) Kim, I.; Jordan, R. F.; *Macromolecules*; **1996**, *29*, 489

(f) Scollard, J. D.; McConville, D. H.; *J. Am. Chem. Soc.*; **1996**, *118*, 10008.

7. (a) Kim, W. K.; Fevola, M. J.; Liable-Sands, L. M.; Rheingold, A. L.; Theopold, K. H. I.; *Organometallics;* **1998**, *17*, 4541.

(b) Brussee, E. A. C.; Meetsma, A.; Hessen, B.; Teuben, J. H.; *Organometallics 1998, 17*. 4090

(c) Desmangles, N.; Gambarotta, S.; Bensimon, C.; Davis, S.; Zahalka, H.; *J. Organomet. Chem.*; **1997**, *562*, 53.

(d) Murphy, V. J.; Turner, H. *Organometallics;* **1997**, *16*, 2495.

8. (a) Doi, Y.; Suzuki, S.; Soga, K.; *Macromolecules;* **1986**, *19*, 2896.

(b) Ouzumi, T.; Soga, K.; *Makromol. Chem.*; **1992**, *193*, 823.

(c) Gumboldt, A.; Helberg, J.; Schleitzer, G.; *Makromol. Chem.;* **1967**, *101*, 229.

(d) Adisson, E.; *J. Polym. Sci., Part A: Polym. Chem.*; **1994**, *32*, 1033.

(e) Davis, S. C.; von Hellens, W.; Zahalka, H.; In Polymer Material Encyclopedia; Salamone, J. C., Ed.; *CRC Press Inc.*, **1996**; Vol. 3.

9. (a) Schuere, S.; Fisher, J.; Kress, J.; *Organometallics;* **1995**, *14*, 2627.

(b) Zambelli, A.; Proto, A.; Longo, P. In Ziegler Natta Catalysis; Fink, G.,

Mulhaupt, R., Brintzinger, H. H., Eds.; *Springer-Verlag*: Berlin, **1995**.

(c) Kim, W. K.; Fevola, M. J.; Liable-Sands, L. M.; Rheingold, A. L.; Theopold, K. H.; *Organometallics;* **1998**, *17*, 4541.

(d) Feher, K. J.; Walzer, J. F.; Blanski, R. L.; *J. Am. Chem. Soc.;* **1991**, *113*, 3618.

(e) Czaja, K.; Bialek, M.; *Macromol. Rapid Commun.;* **1998**, *19(3)*, 163-166.

(f) Buhl, M.; *Angew. Chem. Int. Ed.;* **1998**, *37(1-2)*, 142-144.

(g) Chan, M. C. W.; Cole, J. M.; Gibson, V. C.; Howard, J. A. K.; *J. Chem. Soc. Chem. Commun.*; **1997**, 2345.

10. Kasani, A.; Ruppa, K. B.; Gambarotta, S.; Yap, G. P. A., manuscript in preparation.

11. Ma, Y.; Reardon, D.; Gambarotta, S.; Yap, G. P. A.; Zahalka, H.; Lemay, C. *Organometallic*, **1999**, *18*, 2773-2781.

12. Manzer, L. E. *Inorg. Synth.*, **1982**, *21*, 138.

13. Mabbs, M. B.; Machin, D. Magnetism and Transition Metal Complexes; *Chapman and Hall*; London, **1973**.

14. Foese, G.; Gorter, C. J.; Smits, L. J., Constantes Selectionnées Diamagnetisme, Paramagnetisme, Relaxation Paramagnetique; *Masson*: Paris, **1957**.

15. (a) Cramail, H.; Dolatkhani, M.; Deffieux, A.; New EPDM's Based on Linear Dienes: Conventional Versus Metallocene Catalysis; Metallocenes '95 Int. Congr. Metallocene Polym. Scotland Business Research: *Skillman*, NJ; **1995**, pp 227-241.

(b) Cann, K. G.; Nicoletti, J. W.; Bai, X.; Hussein, F. D.; Lee, K. H.; Zilker, D. P.; Goeke, G. L.; *ACS Polym. Prepr.* **1998**, *39*, 192.

(c) Smith, P. D.; Martin, J. L.; Huffman, J. C.; Bansemer, R. L.; Caulton, K. G.; *Inorg. Chem.;* **1985**, *24*, 2997.

(d) Chan, M. C. W.; Cole, J. M.; Gibson, V. C.; Howard, J. A. K. *J. Chem. Soc., Chem. Commun.* 1997, 2345 and refs therein.

(e) Coles, M. P.; Gibson, V. C.; *Polym. Bull.*, **1994**, *33*, 529.

(f) Henrici-Olive, G.; Olive, S.; *Angew. Chem., Int. Ed. Engl.;* **1971**, *10*, 776.

(g) Evens, G. G.; Pijpers, E. M. J.; Seevens, R. H. M. In Transition Metal Catalyzed Polymerization; Quirk, R. P., Ed.; *Cambridge University Press*, Cambridge, **1988**; p 782.

(h) Doi, Y.; Suzuki, S.; Hizai, G.; Soga, K.; In Transition Metal Catalyzed Polymerization; Quirk, R. P., Ed.; *Cambridge University Press*: Cambridge, **1988**; p 182.

(i) Ver Strate, G.; In Encyclopedia of Polymer Science and Engineering, 2nd ed.; *Wiley*: New York, **1985**; Vol. 6, p 543.

16. (a) Bei, X.; Swenson, D. C.; Jordan, R. F.; *Organometallics*; **1997**, *16*, 3282

(b) Kobriger, L. M.; McMullen, A. K.; Fanwick, P.E.; Rothwell, I. P.; *Polyhedron* **1989**, *8*, 77.

17. Quantum CAChe 2.0 for Windows software package, Oxford Molecular Group 1997.

18. See for example: Berno, P.; Gambarotta, S.; *Organometallics;* **1994**, *13*, 2569.

19. A comparison of the relative activity of **2.2** and **2.3** and their qualitative polymer characteristics, was obtained by carrying out two simultaneous polymerization experiments by using 5 mM solution of the catalyst, a V/Al = 60 and ethylene P =

1 atm. The two systems produced respectively 6.1 and 6.3 g of polymer in a 20 min run. The polymer quality was also very comparable.

20. However, the coordination geometry of the vanadium center is very similar to that of the d^6 Fe(II) compound reported by Brookhart.[4]

Chapter 4

Titanium(III), Chromium(III), Manganese(II) Complexes Supported by a Bis(imino)pyridyl Ligand System. Insight into the Effect of Electronic Configuration of the Metal Centre on Ethylene Polymerization Activity. Isolation and Characterization of a Novel Manganese(I) Alkyl.

Abstract

Chapter 4 *outlines the reactions of {2,6-bis[2,6-(i-Pr)$_2$PhN=C(Me)]$_2$(C$_5$H$_3$N)} with MnCl$_2$(THF)$_2$, TiCl$_3$(THF)$_3$ and CrCl$_3$(THF)$_3$ afforded the expected {2,6-bis[2,6-(i-Pr)$_2$PhN=C(Me)]$_2$(C$_5$H$_3$N)}MnCl$_2$* ***(4.1)****, {2,6-bis[2,6-(i-Pr)$_2$PhN=C(Me)]$_2$(C$_5$H$_3$N)}TiCl$_3$* ***(4.3)*** *and {2,6-bis[2,6-(i-Pr)$_2$PhN=C(Me)]$_2$(C$_5$H$_3$N)}CrCl$_3$* ***(4.4)*** *products following the methodology used to prepare complex* ***3.2****. Alkylation of* ***4.1*** *using two equivalents of MeLi lead to the reduced product {2,6-bis[2,6-(i-Pr)$_2$PhN=C(Me)]$_2$(C$_5$H$_3$N)}MnCH$_3$* ***(4.2)****, the first Mn(I) alkyl complex which is not supported by Cp or CO ancillary ligands. It is suspected that the pathway to the reduced species is done via a radical coupling mechanism. All four complexes were tested for their activity towards polymerization to understand how Ti(III), Cr(III), Mn(II) and Mn(I) with the d^1, d^3, d^5, d^6 electronic configurations respectively, affect the catalytic activity. Complexes* ***4.3*** *and* ***4.4*** *were the only complexes that had moderate activity towards polymerization of ethylene. Surprisingly,* ***4.2*** *has the same electronic configuration as the Fe(II) complex reported by Gibson and Brookhart and does not possess the ability to polymerize ethylene when activated with PMAO.*

4.1 Introduction

In the past few years, efforts to develop alternatives to group IV metallocene single site olefin polymerisation catalysts have multiplied affording major breakthroughs in the field. For example, the groups of Gibson, Brookhart and Bennett have independently developed catalytic systems based on late transition metals complexes such as Fe(II), Co(II) [1,2,3], Ni(II), Pd(II)[4], Ru(II), Rh(II)[5] and Al(III)[6] incorporating sterically hindered α-diimine ligand systems. The tremendous success of the Fe(II) and Co(II) catalysts relies chiefly on the coordinating planar tridentate bis(imino)pyridine ligand which seems to possess the right electronic properties to maintain a low energy

ethylene insertion barrier while maintaining a relatively high energy barrier for the β-H transfer and β-H elimination termination steps,[7] the later two processes being controlled by the steric bulk of the 2,6-disubstituted phenyl groups.

In order to better understand the properties of this neutral tridentate bis(imino)pyridine ligand system, our group has embarked on a project aiming to elucidate its capabilities as an early transition metal supporting ligand. In particular, our investigations on vanadium have proven to be fruitful in the event that a powerful vanadium (III) catalyst was developed and better understanding of the activation of the vanadium catalytic species through alkylation was obtained. More specifically, this catalytic system demonstrated ligand involvement in the activation process of the pro-catalyst via alkylation of the *ortho* position of the pyridine ring upon treatment with PMAO[12]. Interestingly, deactivation of the vanadium catalytic species has exposed the versatility of the ligand showing that the ligand is able to support V(I) alkyl complexes that had never previously been seen in non-Cp supported vanadium chemistry. In the present study our group has continued its investigation into the role of the ligand and its properties on early transition metals such as Ti(III), Cr(III), Mn(II). The aim was to further test the capacity of this particular ligand system to stabilize other metals in unusual oxidation states and electronic configurations.

As result of alkylation reactions of the Mn(II) bis(imino)pyridine complex, the ligand system has demonstrated once again its robustness and its ability to stabilize rare low-valent transition metal alkyl complexes. This chapter describes the isolation of the first low-valent Mn(I) alkyl complex not supported by *Cp* or CO ligands but rather by nitrogen donor-based bis(imino)pyridyl ligand system.

4.2 Experimental Section

All operations were performed under inert atmosphere by using standard Schlenk type techniques. $MnCl_2(THF)_2$[8], $TiCl_3(THF)_3$[8], $CrCl_3(THF)_3$[8] and 2,6-bis[1-(2,6-diisopropylphenylimino)ethyl]pyridine[9] were prepared according to published procedures. Infrared spectra were recorded on a Mattson 9000 and Nicolet 750-Magna FTIR instruments from Nujol mulls prepared in a dry-box. Samples for magnetic susceptibility measurements were weighed inside a dry-box equipped with an analytical balance and sealed into calibrated tubes. Magnetic measurements were carried out with a Gouy balance (Johnson Matthey) at room temperature. Magnetic moments were calculated following standard methods,[10] and corrections for underlying diamagnetism were applied to data.[11] Elemental analyses were carried out with a Perkin-Elmer 2400 CHN analyser. Data for X-ray crystal structure determination were obtained with a Bruker diffractometer equipped with a SMART CCD area detector.

Preparation of {2,6-bis[2,6-(i-Pr)$_2$PhN=C(Me)]$_2$(C_5H_3N)}$MnCl_2$ (4.1)

A solution of 2,6-bis[1-(2,6-diisopropylphenylimino)ethyl]pyridine (2g, 4.16mmol) in toluene (100 ml) was treated with $MnCl_2(THF)_2$ (1.12g, 4.16 mmol). The mixture was refluxed overnight, upon which the yellow suspension changed to an orange solution. The solution was evaporated to dryness yielding an orange solid, which was then dissolved in 20 ml of methylene chloride. The orange solution was filtered and layered with hexane yielding orange crystals of **4.1** over a period of 2 weeks. (1.79 g, 2.95 mmol, yield 71%). IR (Nujol mull, cm^{-1}): 3055(m), 2906(s), 1570(m), 1458(s), 1379(s), 1321(m), 1302(w), 1255(m), 1236 (m), 1146(w), 1103(m), 1078 (w), 995(w), 960(w), 868(w), 824(m),

800(w), 769(s), 723(m), 688(w). Anal. Calcd (found) for $C_{33}H_{43}Cl_3N_3Mn$: C 65.24 (63.71), H 7.13 (6.96), N 6.92 (6.64). $\mu_{eff} = 5.74\ \mu_{BM}$.

Preparation of {2,6-bis[2,6-(i-Pr)$_2$PhN=C(Me)]$_2$(C$_5$H$_3$N)}MnCH$_3$ (4.2)

A solution of **4.1** (1.52g, 2.50 mmol) in freshly distilled diethyl ether (100 ml), was treated with two equivalents of MeLi (3.5 ml of 1.4 M solution in diethyl ether, 5 mmol). The solution was left to stir for 2 days upon which the colour changed from orange to maroon. The solution was filtered and the solvent was reduced to 15 ml to crystallize for 4 days upon which, burgundy crystals of **4.2** suitable for single crystal X-ray analysis were obtained (0.71 g, 1.28 mmol, yield 51%). IR (Nujol mull, cm^{-1}): 3058(w), 2923(s), 2854(w), 1586(s), 1462(s), 1378(s), 1319(w), 1255(m), 1236(m), 1145(w), 1104(m), 1091 (m), 997(w), 950 (m), 854(m), 822(w), 798(w), 772(m), 756(m), 724(m), 694(m), 502 (m). Anal. Calcd (found) for $C_{34}H_{46}N_3Mn$: C 74.02 (74.18), H 8.40 (8.72), N 7.62 (7.41). $\mu_{eff} = 4.82\ \mu_{BM}$

Preparation of {2,6-bis[2,6-(i-Pr)$_2$PhN=C(Me)]$_2$(C$_5$H$_3$N)}TiCl$_3$ (4.3)

A solution of 2,6-bis[1-(2,6-diisopropylphenylimino)ethyl]pyridine (2.6g, 5.3 mmol) in toluene (100 ml) was treated with $TiCl_3(THF)_3$ (2.0g, 5.3 mmol). The mixture was refluxed overnight (110ºC), upon which the pale blue suspension changed to a brown/orange colour yielding an orange microcrystalline material. The solution was evaporated to dryness and the solvent was replaced with 20 ml of methylene chloride upon which the solution changed colour to a dark emerald green. The solution was filtered and layered with hexane yielding green crystals of **4.3** over a period of 2 weeks.

(2.60 g, 4.1 mmol, yield 77%). IR (Nujol mull, cm^{-1}): 3224(m), 2924(s), 2853(s), 1643(m), 1574(s), 1456(s), 1379(m), 1330(s), 1302(w), 1259(w), 1203(w), 1178(w), 1099(s), 1078(m), 1057(m), 1022(m), 980(m), 935(w), 885(w), 860(w), 798(s), 775(s), 766(s), 742(m), 721(s), 692(w), 613(w). Anal. Calcd (found) for $C_{34}H_{45}Cl_5N_3Ti$: C 56.65 (55.03), H 6.29 (6.14), N 5.83 (5.61). μ_{eff}= 1.693 μ_{BM}.

Preparation of {2,6-bis[2,6-(i-Pr)$_2$PhN=C(Me)]$_2$(C$_5$H$_3$N)}CrCl$_3$ (4.4)

A solution of 2,6-bis[1-(2,6-diisopropylphenylimino)ethyl]pyridine (2.0g, 4.16 mmol) in toluene (100 ml) was treated with $CrCl_3(THF)_3$ (1.55g, 4.16 mmol). The mixture was refluxed overnight (110ºC). The solution was evaporated to dryness and the solvent was replaced with 20 ml of methylene chloride upon which the solution changed colour to a dark green. The solution was filtered and layered with hexane yielding green crystals of **4.4** over a period of 2 weeks. (2.39 g, 3.3 mmol, yield 79%). IR (Nujol mull, cm^{-1}): 3168(m), 2954(s), 2879(s), 1620(w), 1576(m), 15.14(m), 1464(s), 1379(s), 1323(w), 1259(m), 1209(w), 1171(w), 1149(w), 1101(m), 1055(w), 1039(m), 982(w), 935(w), 891(w), 839(w), 796(s), 777(m), 760(w), 723(m), 700(w), 654(w). Anal. Calcd (found) for $C_{34}H_{45}Cl_5N_3Cr$: C 56.33 (54.73), H 6.26 (6.11), N 5.80 (5.98). μ_{eff}= 3.83 μ_{BM}.

4.3 General Polymerization Procedure

Ethylene (99.5%, polymer grade, Praxair) was purified by passage through the bench scale reactor's gas purification units (13× molecular sieves, alumina and oxygen removal columns). Anhydrous toluene was purchased from BDH and purified over molecular sieves prior to use. PMAO-IP was purchased from Akzo-Nobel and contained 13.5 wt % of Al. DMAC, TMA were purchased from Aldrich and were used as received. A bench scale reactor was used in the polymerization experiments. Conditions for polymerization are as summarized below. The polymerization time varied from 30 to 60 min. Adding 10 ml of a 10% solution of HCl in methanol to the reactor terminated the reaction, and the polymer was recovered by filtration and then the polymer was dried in vacuo. The polymerization activities were calculated based upon weight of polymer produced (Table 5.1). Polymer molecular weights and molecular weight distributions were measured by GPC (Waters 150-C) at 140 °C in 1,2,4-trichlorobenzene calibrated using polyethylene standards. In a typical polymerization experiment, the solvent was pre-saturated with ethylene in the reactor at the desired temperature. The co-catalyst was injected in the reactor followed by introduction of the pro-catalyst Reproducibility of catalyst activity and reactor operation was checked by regularly running polymerization experiments using a standard zirconium catalyst and by repeating the experiments under identical reaction conditions. Errors and deviation were always below 6%.

Table 4.1 Polymerisation Results

Pro-catalyst	T (°C)	Activation (Al:M)	Time (min)	Yield (g)	Activity[b]	M_w (x 10^3)	PD
$(C_{33}H_{43}N_3)TiCl_3$[a]	25	PMAO (1000)	20	1.57	89	*	*
	25	DMAC (40)	20	1.14	65		
	25	TMA (40)	20	0.75	42		
$(C_{33}H_{43}N_3)CrCl_3$[a]	25	PMAO (1000)	20	1.00	57	57.2	33.0

[a] Conditions: 0.10g of pro-catalyst; 200 ml of toluene; 5 psig of ethylene.
[b] g PE $mmol^{-1}$ cat^{-1} h^{-1}
* M_w and PD of these polymers are not available due to insolubility.

4.4 X-ray Crystallographic Studies.

The experimental parameters for the structural determination of complexes **4.1**, **4.2**, **4.3** and **4.4** are described in the next paragraph. Suitable crystals were selected, mounted on thin, glass fibres using paraffin oil and cooled to the data collection temperature. Data were collected on a Bruker AX SMART 1k CCD diffractometer using 0.3° ω-scans at 0, 90, and 180° in ϕ. Unit-cell parameters were determined from 60 data frames collected at different sections of the Ewald sphere. Semi-empirical absorption corrections based on equivalent reflections were applied (Blessing, R., *Acta Cryst.*, **1995**, A51, 33-38).

No symmetry higher than triclinic was observed for **4.1** and solution in the centric space group option produced chemically reasonable and computationally stable results of refinement. Systematic absences in the diffraction data and unit-cell parameters were uniquely consistent for consistent with *P*21/*c* for **4.2**, **4.3**, and **4.4**. The structures were solved by direct methods, completed with difference Fourier syntheses and refined with full-matrix least squares procedures based on *F*2. The atomic coordinates of **4.3** were used as an initial trial solution for the isomorphic **4.4**. Structures **4.3** and **4.4** each have three independent molecules of the respective compound and four molecules of co-

crystallized methylene chloride solvent in the asymmetric unit. All non-hydrogen atoms were refined with anisotropic displacement parameters. All hydrogen atoms were treated as idealized contributions. All scattering factors are contained in the SHEXTL 5.10 program library (Sheldrick, G. M., Bruker AXS, Madison, WI, 1997). Crystal data and relevant geometrical parameters are reported in Appendix 4 and Appendix 5.

Complex of $(C_{33}H_{43}N_3)MnCl_2$ (4.1)

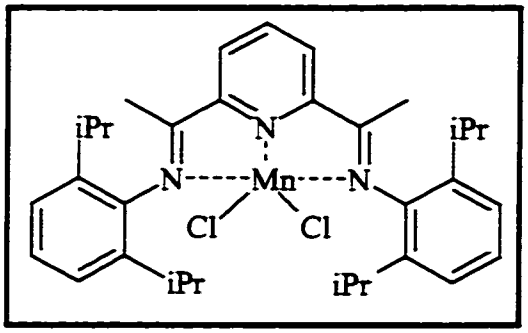

The coordination geometry of manganese in this complex can be described as distorted trigonal bipyramidal and is defined by two chlorine atoms and by the three nitrogen donor atoms of the tridentate ligand (Figure 4.1). Two chlorines and the nitrogen atom of the pyridine ring define with the metal center the molecular equatorial plane [Cl(1)-Mn-Cl(2) = 119.68(9)°, Cl(1)-Mn-N(2) = 98.93(17)°, Cl(2)-Mn-N(2) = 141.36(18)°]. Two nitrogens of the two imino functions occupy the axial position forming a significantly bent N-Mn-N vector [N(1)-Mn-N(3) = 135.4(2)°]. The Mn-Cl [Mn-Cl(1) = 2.350(3) Å, Mn-Cl(2) = 2.313(2) Å] as well as the Mn-N bond distances [Mn-N(1) = 2.333(5) Å, Mn-N(3) = 2.318(5) Å, Mn-N(2) = 2.201(5) Å] compare well to those found in the literature. Similar to complex **3.2** (V(III) analog) the orientation of the two peripheral phenyl rings is perpendicular to the Mn-N(1)-N(2)-N(3) plane.

Figure 4.1 ORTEP of $(C_{33}H_{43}N_3)MnCl_2$ (4.1)

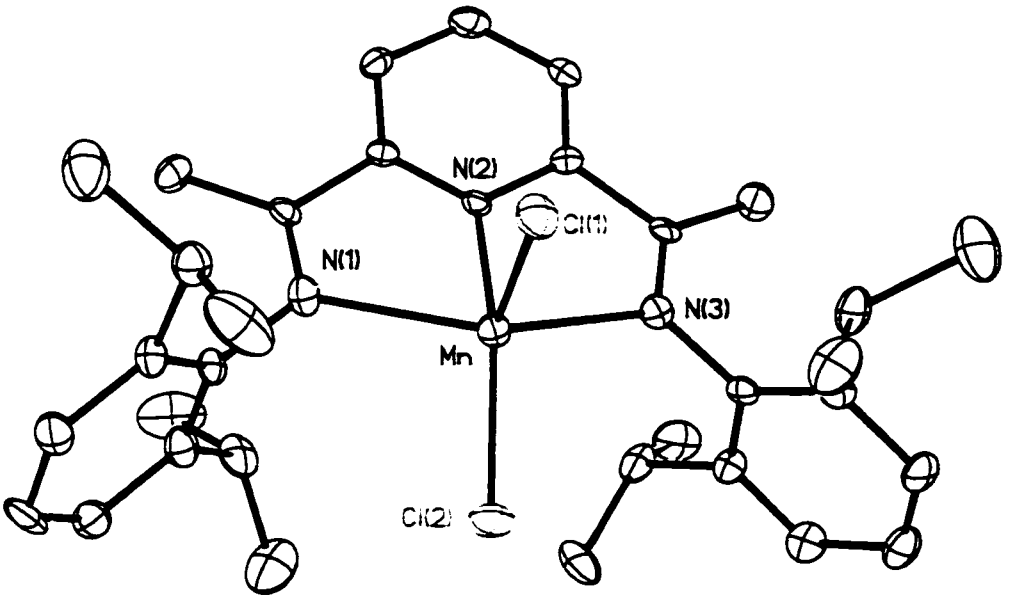

Selected Bond Lengths (Å) and Angles (°) for $(C_{33}H_{43}N3)MnCl_2$ (4.1)

Distances	Angles
Mn-Cl(1) = 2.350(3)	N(1)-Mn-Cl(1) = 103.25(17)
Mn-Cl(2) = 2.313(2)	N(1)-Mn-Cl(2) = 100.47(16)
Mn-N(1) = 2.156(6)	N(1)-Mn-N(2) = 69.71(19)
Mn-N(2) = 2.201(5)	N(2)-Mn-Cl(1) = 98.93(17)
Mn-N(3) = 2.318(5)	N(1)-Mn-N(3) = 135.4(2)
N(1)-C(13) = 1.273(8)	Cl(1)-Mn-Cl(2) = 119.68(9)
N(3)-C(20) = 1.279(8)	N(2)-Mn-Cl(2) = 141.36(18)

Complex of $(C_{33}H_{43}N_3)MnCH_3$ (4.2)

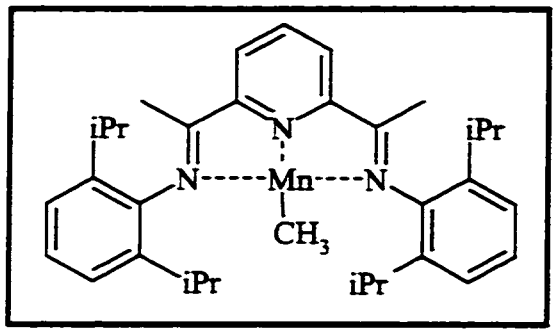

The coordination geometry of manganese in this complex can be described as distorted square planar and is defined by one methyl group and by the three nitrogen donor atoms of the tridentate ligand (Figure 4.2). The methyl group and the three nitrogen atoms of the ligand define the distorted molecular equatorial plane comprising the metal center [C(34)-Mn-N(2) = 163.3(3)°, N(1)-Mn-N(3) = 143.09(13)°, C(34)-Mn-N(3) = 110.6(2)°, N(2)-Mn-N(3) = 74.96(12)]. The diimine/pyridine ligand does not display additional distortion with respect to complex **4.1**. The Mn-N bond distances [Mn-N(1) = 2.175(3) Å, Mn-N(3) = 2.160(3) Å, Mn-N(2) = 2.039 Å] compare well to those of complex **4.1** even after alkylation and reduction of the Mn metal center. As opposed to complex **3.2** the manganese complex is not subject to alkylation in the *ortho* position of the pyridine ring as seen in the chemistry of the analogous vanadium complex and presents a Mn-C bond well within the norm of manganese-carbon distances [Mn-C(34) = 2.086(7) Å]. Similar to complex **4.1** the orientation of the two peripheral phenyl rings is perpendicular to the Mn-N(1)-N(2)-N(3) plane. The decrease of the manganese coordination number with respect to **4.1** does not significantly affect the geometry of the manganese/diimine core.

Figure 4.2 ORTEP of $(C_{33}H_{43}N_3)MnCH_3$ (4.2)

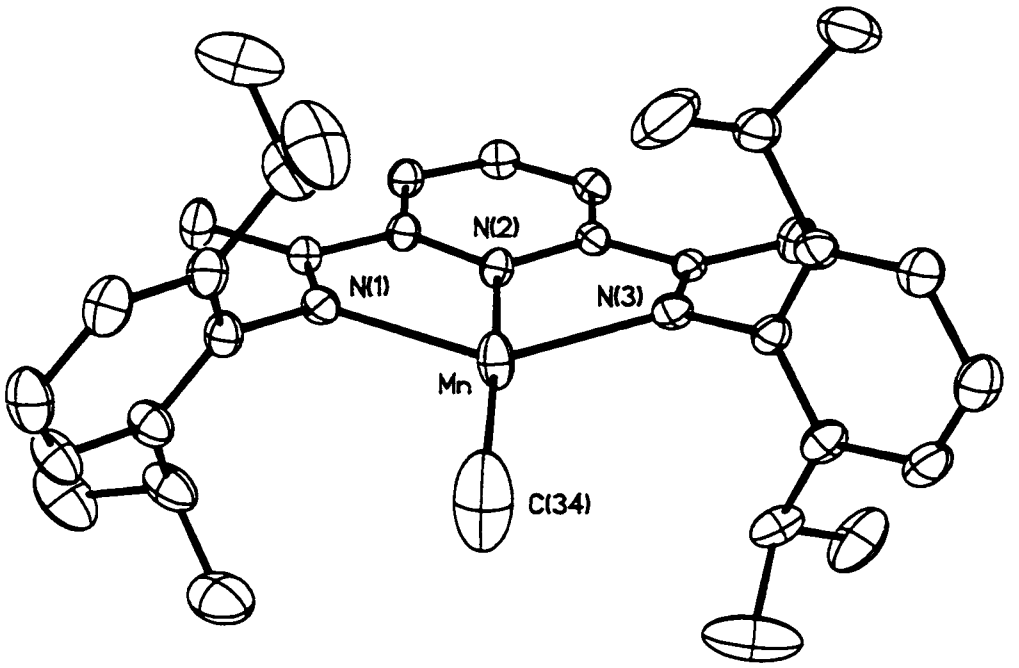

Selected Bond Lengths (Å) and Angles (°) for $(C_{33}H_{43}N_3)MnCH_3$ (4.2)

Distances	Angles
Mn-C(34) = 2.086(7)	N(2)-Mn-C(34) = 163.3(3)
Mn-N(1) = 2.175(3)	N(1)-Mn-N(3) = 143.09(13)
Mn-N(2) = 2.039(3)	N(1)-Mn-N(2) = 74.18(12)
Mn-N(3) = 2.160(3)	N(1)-Mn-C(34) = 104.8(2)
N(1)-C(13) = 1.320(5)	
N(3)-C(20) = 1.333(5)	

Complex of $(C_{33}H_{43}N_3)TiCl_3$ (4.3)

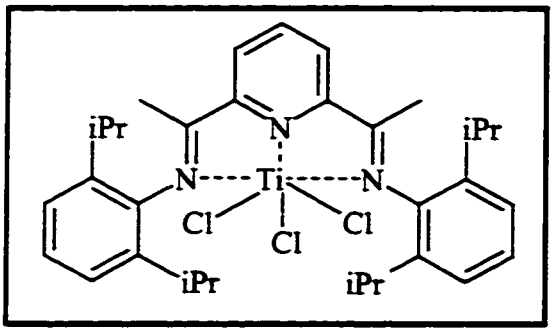

The structure of **4.3** consists of a titanium atom surrounded by the pyridine/diimine ligand and three chlorine atoms (Figure 4.3). The coordination geometry around the metal center is distorted octahedral with the equatorial plane defined by the three nitrogen atoms of the ligand [N(1)-Ti(1)-N(2) = 72.33(12)°, N(2)-Ti(1)-N(3) = 72.26(12)°, N(1)-Ti(1)-N(3) = 143.26(12)°] and one chlorine atom [N(1)-Ti(1)-Cl(1)= 99.66(9)°, N(3)-Ti(1)-Cl(1) = 116.95(9)°, N(2)-Ti(1)-Cl(1) = 166.45(10)°]. The other two chlorine atoms are placed on the two axial positions and form a significantly bent Cl-Ti-Cl vector [Cl(2)-Ti(1)-Cl(3) = 172.81(5)°]. The Ti-Cl distances [Ti(1)-Cl(1) = 2.3102(12) Å, Ti(1)-Cl(2) = 2.4410(13) Å, Ti(1)-Cl(3) = 2.3411(13) Å] are slightly different from each other but fall in the expected range for terminal Ti-Cl bonds. The Ti-N distances are also normal. The two Ti-N distances formed by the two imino functions [Ti(1)-N(1) = 2.223(3) Å, Ti(1)-N(3) = 2.267(3) Å] are longer than that formed with the pyridine nitrogen atom [Ti(1)-N(2) = 2.143(3) Å]. Furthermore, the C-N bonds of the two imino groups are only slightly longer than expected [N(1)-C(13) = 1.289(5) Å, N(3)-C(20) = 1.297(5) Å]. The pyridine ring is co-planar with the molecular equatorial plane whereas the two terminal phenyl groups attached to the two imino nitrogens lay on perpendicular planes.

Figure 5.3 ORTEP of $(C_{33}H_{43}N_3)TiCl_3$ (4.3)

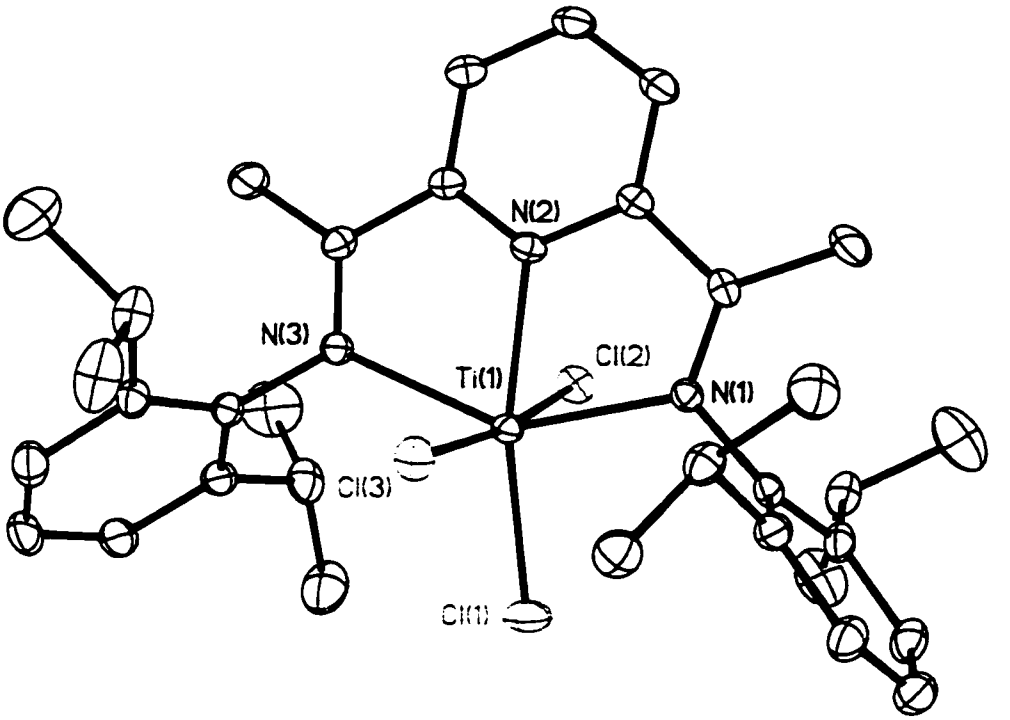

Selected Bond Lengths (Å) and Angles (°) for $(C_{33}H_{43}N_3)TiCl_3$ (4.3)

Distances	Angles
Ti(1)-Cl(1) = 2.3102(12)	N(1)-Ti(1)-Cl(1) = 99.66(9)
Ti(1)-Cl(2) = 2.4410(13)	N(1)-Ti(1)-Cl(2) = 93.57(9)
Ti(1)-Cl(3) = 2.3411(13)	N(1)-Ti(1)-Cl(3) = 90.63(9)
Ti(1)-N(1) = 2.223(3)	N(1)-Ti(1)-N(2) = 72.33(12)
Ti(1)-N(2) = 2.143(3)	N(2)-Ti(1)-Cl(1) = 166.45(10)
Ti(1)-N(3) = 2.267(3)	Cl(2)-Ti(1)-Cl(3) = 172.81(5)
N(1)-C(13) = 1.289(5)	N(1)-Ti-N(3) = 143.26(12)
N(3)-C(20) = 1.297(5)	

Complex of $(C_{33}H_{43}N_3)CrCl_3$ (4.4)

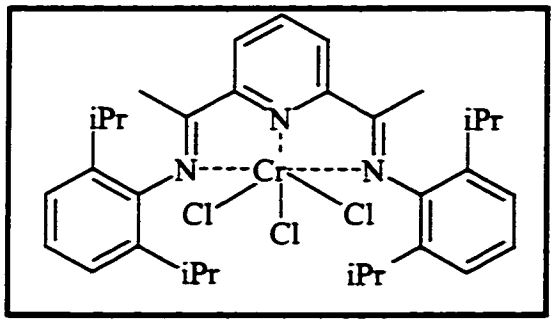

The structure of **4.4** consists of a chromium atom surrounded by the pyridine/diimine ligand and three chlorine atoms (Figure 4.4). The coordination geometry around the metal center is distorted octahedral with the equatorial plane defined by the three nitrogen atoms of the ligand [N(1)-Cr(1)-N(2) = 76.7(2)°, N(2)-Cr(1)-N(3) = 76.5(2)°, N(1)-Cr(1)-N(3) = 152.1(2)°] and one chlorine atom [N(1)-Cr(1)-Cl(1)= 100.35(15)°, N(3)-Cr(1)-Cl(1) = 107.24(16)°, N(2)-Cr(1)-Cl(1) = 171.59(17)°]. The other two chlorine atoms are placed in the two axial positions and form a significantly bent Cl-Cr-Cl vector [Cl(2)-Cr(1)-Cl(3) = 176.38(8)°]. The Cr-Cl distances [Cr(1)-Cl(1) = 2.295(2) Å, Cr(1)-Cl(2) = 2.350(2) Å, Cr(1)-Cl(3) = 2.273(2) Å] are slightly different from each other but fall in the expected range for terminal Cr-Cl bonds. The Cr-N distances are also normal. The two Cr-N distances formed by the two imino functions [Cr(1)-N(1) = 2.156(6) Å, Cr(1)-N(3) = 2.161(6) Å] are longer than that formed with the pyridine nitrogen atom [Cr(1)-N(2) = 1.996(5) Å] possibly suggesting the presence of some extent of Cr-pyridine π back-bonding. The C-N bonds of the two imino groups are only slightly longer than expected [N(1)-C(13) = 1.296(9) Å, N(3)-C(20) = 1.291(8) Å]. The pyridine ring is co-planar with the molecular equatorial plane whereas the two terminal phenyl groups attached to the two imino nitrogens lay on perpendicular planes.

Figure 4.4 ORTEP of $(C_{33}H_{43}N_3)CrCl_3$ (4.4)

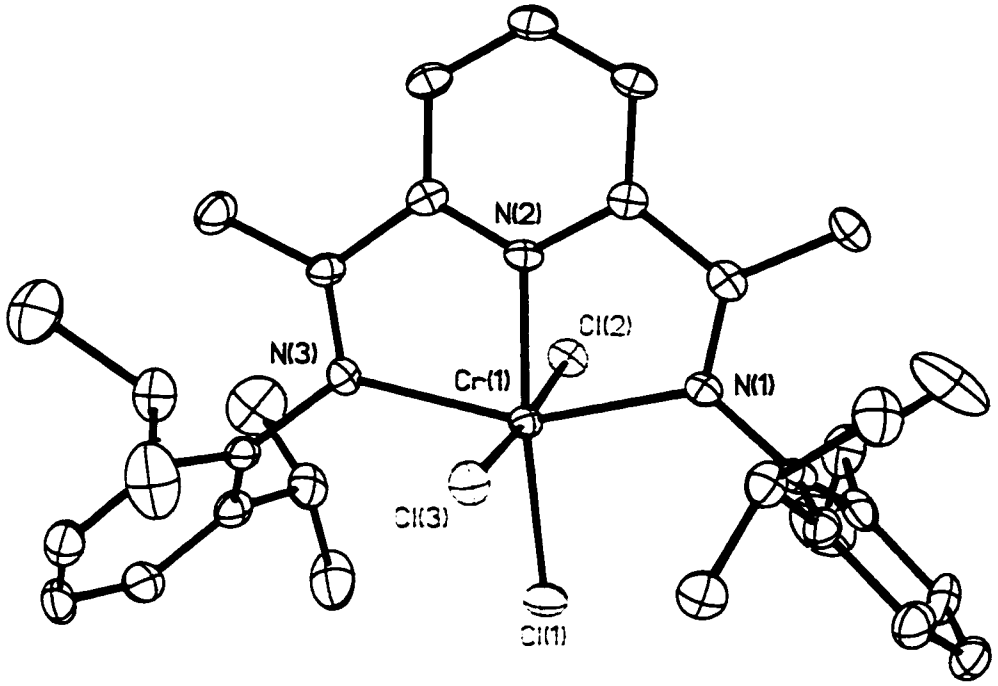

Selected Bond Lengths (Å) and Angles (°) for $(C_{33}H_{43}N_3)CrCl_3$ (4.4)

Distances	Angles
Cr(1)-Cl(1) = 2.295(2)	N(1)-Cr(1)-Cl(1) = 100.35(15)
Cr(1)-Cl(2) = 2.350(2)	N(1)-Cr(1)-Cl(2) = 92.74(15)
Cr(1)-Cl(3) = 2.273(2)	N(1)-Cr(1)-Cl(3) = 81.94(15)
Cr(1)-N(1) = 2.156(6)	N(1)-Cr(1)-N(2) = 76.7(2)
Cr(1)-N(2) = 1.996(5)	N(2)-Cr(1)-Cl(1) = 171.59(17)
Cr(1)-N(3) = 2.161(6)	Cl(2)-Cr(1)-Cl(3) = 176.38(8)
N(1)-C(13) = 1.289(5)	N(1)-Cr-N(3) = 152.1(2)
N(3)-C(20) = 1.296(9)	

4.5 Results and Discussion

In close analogy with the Fe(II) and Co(II) bis(imino)pyridine complexes developed by the Gibson and Brookhart groups, the Mn(II) compound **(4.1)** shares a distorted square pyramidal geometry. The Fe(II) and Co(II) complexes have a high spin d^6 and a high spin d^7 electronic configuration respectively whereas the Mn(II) has a high spin d^5 configuration with 5 unpaired electrons. Unlike the late transition metal complexes of Fe(II) and Co(II), the Mn(II) complex **(4.1)** does not exhibit any activity towards ethylene polymerization upon activation with methylalumoxane (Mn:Al 1:1000) in toluene under one atmosphere of ethylene at room temperature. Since the supporting bis(imino)pyridine ligand system is the same in all cases and that the polymerization conditions are comparable we can conclude that the lack of catalytic activity of complex **4.1** can be ascribed exclusively to the high spin d^5 electronic configuration (μ_{eff} = 5.74 μ_{BM} for complex **4.1**) and its lack of Lewis acidity. In the light of this result, an attempt to reduce complex **4.1** to obtain a Mn(I), d^6 electronic configuration species like the successful Fe(II) complex was pursued. Complex **4.2** was obtained from the reduction reaction carried out with two equivalents of MeLi yielding the first non-Cp or CO supported Mn(I) methyl complex. (Scheme 4.1)

Scheme 4.1 Synthesis of Complex 4.2

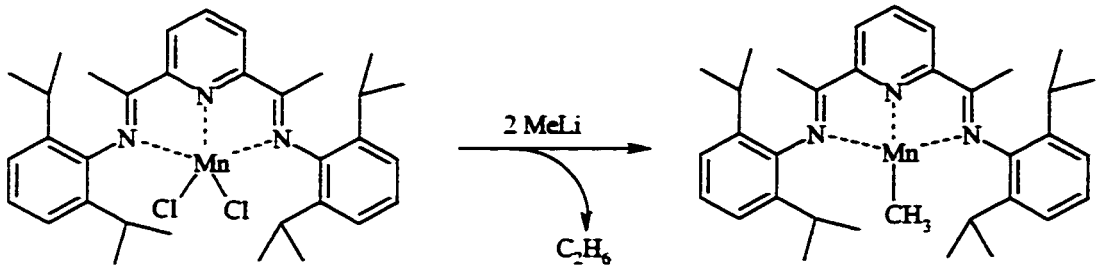

4.1 **4.2**

The reduction of the metal center is not particularly surprising given that Mn(II) complexes are used as radical initiators in radical polymerization processes. It is therefore quite easy to foresee the possibility of a methyl radical coupling mechanism liberating ethane gas and reducing the manganese metal center to the +1 oxidation state. Complex **4.2** has a distorted square pyramidal geometry with the central Mn atom is surrounded by three coordinating nitrogens from the bis(imino)pyridine ligand and one methyl group. The magnetic moment is consistent with a d^6 high-spin electronic configuration thus accounting for the distorted square pyramidal geometry.

Ethylene as well as styrene polymerization experiments were conducted on the neutral complex **4.2** and in the presence of methylalumoxane, lead to no polymer formation. This may indicate that the system does not possess a sufficiently strong Lewis acidity to afford insertion of the ethylene monomer into the metal-carbon bond.

On the other hand complexes **4.3** and **4.4** based on Ti(III) and Cr(III) with high spin d^1 and d^3 electronic configurations are iso-structural with the octahedral d^2 V(III) complex previously reported.[12] Both complexes **4.3** and **4.4** do exhibit some activity (Table 4.1) under similar conditions although a few orders of magnitude lower than the high spin V(III) complex with a d^2 electronic configuration. This behaviour is in line with theoretical calculations done by Ziegler's group on early transition metals bearing similar ligand systems with electronic configurations ranging between d^0 and d^4 and pointing out the overall versatility of the d^2 electronic configuration. This study also demonstrated that complexes with a d^2 electronic configuration maintained a relatively low insertion energy barrier with respect to the higher energy barriers of the chain termination steps involving β-H chain transfer to the monomer and β-H elimination of the polymeric chain[13].

4.6 Conclusion

The present study presents the first Mn(I) alkyl complex not supported by Cp or CO ancillary ligands. Furthermore, polymerization tests have demonstrated the inability of the high spin d^5 Mn(II) and the high spin d^6 Mn(I) complexes supported by a bis(imino)pyridine ligand to polymerize ethylene. These results are quite surprising given the high activity observed on the high spin d^6 Fe(II) and the high spin d^7 Co(II) complexes.

The Cr(III), d^3 and the Ti(III), d^1 complexes are octahedral complexes were also tested for polymerization and demonstrated average catalytic activity when compared to the V(III) d^2 complex previously reported. The differences in catalytic activity seem to be dependent on the orbital steering influence of the bis(imino)pyridine ligand system on the available electronic orbitals of the metal center and on the interaction between the pro-catalyst and the co-catalyst.

4.7 References

1.(a) Small, B. L.; Brookhart, M.; Bennett, A. M. A.; *J. Am. Chem Soc.;* **1998**, *120*, 4049.

(b) Small, B. L.; Brookhart, M.; *Polymer Prep. (Am. Chem. Soc., Div. Polym. Chem.)*, **1998**, *39*, 213.

2.(a) Britovsek, G. J. P.; Gibson, V. C.; Kimberley, B. S., Maddox, P. J.; McTavish, S. J.; Solan, G. A.; White, A. J. P.; Williams, D.; *Chem.Comm.*, **1998**, *120*, 849.

(b) Britovsek, G. J. P.; Bruce, M.; Gibson, V. C.; Kimberley, B. S.; Maddox, P. J.; Mastroianni, S.; McTavish, S. J.; Redshaw, C.; Solan, G. A.; Strömberg, S.; White, A. J. P.; Williams, D. J.; *J. Am. Chem. Soc.*, **1999**, *121*, 8728.

(c) Britovsek, G. J. P.; Dorer, B. A.; Gibson, V. C.; Kimberley, B. S.; Solan, G. A., (BP Chemicals Limited), WO 99/12981, **1999** [*Chem Abstr.* **1999**, *130*, 252793].

3.(a) Bennett, A. M. A. (DuPont), WO 98/27124, **1998**, [*Chem Abstr.* **1998**, *129*, 122973x]

(b) Bennett, A. M. A., *CHEMTECH*, **1999**, *July*, 24-28

4.(a) Johnson, L. K.; Killian, C. M.; Brookhart, M.; *J. Am. Chem. Soc.*, **1995**, *117*, 6414.

(b) Johnson, L. K.; Mecking, S.; Brookhart, M.; *J. Am. Chem. Soc.*, **1996**, *118*, 267.

(c) Killian, C. M.; Tempel, D. J., Johnson, L. K.; Brookhart, M.; *J. Am. Chem. Soc.*, **1996**, *118*, 11664.

(d) Johnson, L. K.; Killian, C. M.; Arthur, S. D.; Feldman, J.; McCord, E. F.; McLain, S. J.; Kreutzer, K. A.; Bennett, M. A.; Coughlin, E. B.; Ittel, S. D.;

Parthasarathy, A.; Tempel, D. J.; Brookhart, M. S. (DuPont); WO 96/23010, **1996**, [*Chem. Abstr.* **1996**, *125*, 222773t]

(e) Schleis, T.; Spaniol, T. P.; Okuda, J.; Heinemann, J.; Mülhaupt, R.; *J. Organomet. Chem.*, **1998**, *569*, 159.

(f) De Bruin, B.; Eckhard, B.; Bothe, E.; Weyhermüller, T.; Wieghardt, K.; *Inorg. Chem.*, **2000**, *39 (13)*, 2936.

5. (a) Dias, E. L.; Brookhart, M.; White, P. S.; *Chem. Comm.*; **2001**, 423.

6. Bruce, M.; Gibson, V. C.; Redshaw, C.; Solan, G. A.; White, J. P. A.; Williams, D. J.; *Chem. Comm.*, **1998**, 2523.

7. Margl, P., Deng, L., Ziegler, T., *Organometallics*, **1999**, *18*, 5701

8. Manzer, L. E. *Inorg. Synth.*, **1982**, *21*, 138.

9. Johnson, L. K.; Killian, C. M.; Brookhart, M. S., *J. Am. Chem. Soc.*, **1995**, *117*, 6414.

10. Mabbs, M. B.; Machin, D. *Magnetism and Transition Metal Complexes*; Chapman and Hall; London, 1973.

11. Foese, G.; Gorter, C. J.; Smits, L. J., *Constantes Selectionnées Diamagnétisme, Paramagnétisme, Relaxation Paramagnétique*; Masson: Paris, 1957.

12. Reardon, D.; Conan, F.; Gambarotta, S.; Yap, G. P. A.; Wang, Q.; *J. Am. Chem. Soc.*, **1999**, *121 (40)*, 9318- 9325.

13. Schmid, R.; Ziegler, T.; *Organometallics*, **2000**, *19*, 2756

Chapter 5

Vanadium-Promoted Aldol Condensation and Pinacolic Coupling of Acetylpyrrole: Formation of Two New Potent Catalysts for Olefin Co-Polymerization.

Abstract

Chapter 5 *describes the reaction of $VCl_3(THF)_3$ with three equivalents of the potassium salt of acetylpyrrole $[CH_3CO(\alpha\text{-}C_4H_3N)]K$ affording the dinuclear $[(\alpha\text{-}C_4H_3N)C(O)CH_2C(\alpha\text{-}C_4H_3N)(CH_3)O]_2\{[CH_3CO(\alpha\text{-}C_4H_3N)]_2V_2[K(THF)]_2\}$ **(5.1)**, where four acetylpyrrolide anions from two vanadium moieties have undergone an aldol condensation. The two pyrrolyl-acetylacetonate units so generated work as tetradentate binucleating ligands holding together the dinuclear structure. A similar reaction carried out on the divalent $[V_2Cl_3(THF)_6]_2[Zn_2Cl_6]$ salt afforded the dinuclear and trivalent $[(\alpha\text{-}C_4H_3N)(CH_3)(O)C\text{-}C(O)(CH_3)(\alpha\text{-}C_4H_3N)]\{[(\alpha\text{-}C_4H_3N)C(O)CH_3]VK(THF)\}_2$ **(5.2)** where two acetylpyrrolide ligands, one per vanadium atom, have undergone a reductive coupling to form a pinacol. Even in this case the dipyrrolylpinacol works as a tetradentate binucleating ligand holding together the dinuclear frame. Attempts to perform the same reaction on another V(II) salt such as $VCl_2(TMEDA)_2$ afforded instead the corresponding divalent derivative $[(\alpha\text{-}C_4H_3N)C(O)CH_3]_2V(TMEDA)$ **(5.3)** where the acetylpyrrolide anions remained intact. Both **5.1** and **5.2** are potent olefin co-polymerization catalyst upon activation with diethyl aluminium chloride while **5.3** displays low but not negligible activity.*

5.1 Introduction

Most research in the field of Ziegler-Natta catalysis has traditionally focused on group IV elements and more recently on late metals whereas group V derivatives have largely been ignored. Information about performance of group V metal catalysts has remained confined mainly within the patent literature.[1] Only recently the appearance of a few reports such as those described in chapter 2 and chapter 3 of this thesis may have contributed to the rejuvenation of interest for vanadium-based Ziegler-Natta catalysis.[2] Nonetheless, the field remains underdeveloped and the current paucity of this literature

strikingly contrasts with the fact that vanadium catalysts are widely used for the industrial production of ethylene-propylene-diene elastomers (EPDM).[3]

The ability of vanadium catalysts to perform random co-polymerizations makes these species well suited for synthetic rubber manufacture[4]. The only drawback for using these catalysts is the rather characteristic low activity, which on average is a few orders of magnitude lower than that displayed by group IV catalysts. While theoretical calculations have recently predicted that a particularly high level of activity should be expected for d^2 V(III) complexes,[5] an intrinsic instability of vanadium alkyls towards formation of inactive divalent vanadium species is likely to be responsible for the generally observed low activity.[6] Accordingly, we have demonstrated in chapter 2 and chapter 3 that in the case of both, the commercially-used V(*acac*)$_3$[6] and the potent olefin polymerization catalyst VCl_3(diiminopyridinato),[7] the alkylation process indeed affords inactive low-valent vanadium complexes. In the particular case of the V(*acac*)$_3$ catalytic system, the catalyst deactivation is a direct consequence of the ability of the alkyl aluminium co-catalyst to completely strip the vanadium atom of the *acac* ligands (leaching).[6] The abstraction of ligand diminishes the stability of the V-C function and the consequent reduction to the divalent state is responsible for the deactivation observed with this and other vanadium-based catalytic systems.

Given this rationale, we have embarked on the preparation of new complexes of trivalent vanadium to relate catalytic activity to stability of trivalent organometallic vanadium species. To this end, nitrogen-donor-based ligands seem to be particularly promising for improving the stability of the V-C bonds[7, 8] and display a lower affinity for aluminium species with consequent reduced possibility of "leaching". However, recent

studies have indicated that partial or complete replacement of the oxygen donor atoms with nitrogen, as in the so-called *acnac* or *nacnac* ligands[9, 10], resulted in a significant decrease of catalytic activity. Therefore, we became interested in examining the behaviour of the N and O donor-based acetylpyrrolide chelating anion, which displays low possibility of being leached. Like the *acac* ligands, it possesses a π-electron system while the aromatic character of the pyrrolyl anion moiety may reasonably be expected to act as an electron-withdrawing group. Thus, by increasing the Lewis acidity of the metal center the acetylpyrrolide anion might ultimately promote the ability of vanadium to interact with olefins. Last but not least; should the pyrrolide anion adopt a η^5-bonding mode with respect to the metal center (Cp-type), the vanadium catalyst might gain a geometry closely reminiscent of the tremendously successful single-site constrained-geometry catalysts (Scheme 5.1)[11]. Herein we report our observations.

5.2 Experimental Section

All operations were performed under inert atmosphere by using standard Schlenk type techniques. $VCl_3(THF)_3$[12], $[V_2Cl_3(THF)_6]_2[Zn_2Cl_6]$[13], $VCl_2(TMEDA)_2$[14], were prepared according to published procedures. Diethylaluminium chloride (1 M solution in hexane), trimethylaluminium (1 M solution in toluene), dimethylaluminium chloride (2 M solution in toluene) and acetylpyrrole were obtained from Aldrich and were used as received.

Propylene (99.5%, polymer grade, Praxair) and ethylene (99.5%, polymer grade, Praxair) were purified by passage of the gas through a gas purification system (P_2O_5 column and oxygen removal column containing a QS catalyst). 1-Hexene was distilled over metallic sodium. Infrared spectra were recorded on a Mattson 9000 and Nicolet 750-Magna FTIR instruments from Nujol mulls prepared in a dry-box. NMR spectra were recorded on a Bruker DRX 500 instrument. Samples for magnetic susceptibility measurements were weighed inside a dry-box equipped with an analytical balance, and sealed into calibrated tubes. Magnetic measurements were carried out with a Gouy balance (Johnson Matthey) at room temperature. Magnetic moments were calculated following, standard methods[14], and corrections for underlying diamagnetism were applied to data.[15] Elemental analyses were carried out with a Perkin Elmer 2400 CHN analyzer. Data for X-ray crystal structure determination were obtained with a Bruker diffractometer equipped with a Smart CCD area detector.

Synthesis of $[CH_3CO(C_4H_3N)]K(THF)$

A solution of acetylpyrrole (2.0 g, 18.3 mmol) in THF (50 ml) was treated with KH (0.4 g, 9.2 mmol) at –78°C. The solution was allowed to stir for 1 hour while warming to room temperature. The solution was filtered, concentrated and slowly cooled to –30°C upon which needle shaped colourless crystals of the corresponding potassium salt separated (2.2 g, 15.2 mmol, 83%,). IR (Nujol mull, cm^{-1}) ν: 3533 (m), 3172 (w), 2949 (s), 2868 (s), 2729 (w), 2671 (w), 1734 (w) 1716 (w), 1699 (m), 1684 (w), 1653 (m), 1616 (m), 1558 (s), 1464 (s), 1377 (s), 1338 (w), 1319 (w), 1267 (m), 1184 (w), 1153 (w), 1130 (w), 1068 (w), 1034 (m), 1018 (w), 966 (w), 914 (w), 881 (w), 870 (w), 839 (w), 798 (w), 766 (m), 746 (m), 735 (m), 721 (m), 694 (w), 667 (w), 633 (w), 625 (w). Anal Calcd (found) for C_6H_6ONK: C, 48.97 (47.05); H, 4.07 (4.21); N, 9.51 (8.96): ^{1}H-NMR (500 MHz, THF-d_8, 298 K) δ: 7.03 (d, 1H, C-H pyr), 6.90 (d, 1H, C-H pyr), 6.00 (t, 1H, C-H pyr), 3.58 (m, 4H, THF), 2.25 (s, 3H, CH_3): ^{13}C-NMR (500 MHz, THF-d_8, 298 K) δ: 188.72 (s, C=O), 141.18 (s, C-pyr), 138.19 (s, C-H), 120.40 (s, C-H), 110.74 (s, C-H), 25.30 (s, CH_3).

Preparation of $[(\alpha\text{-}C_4H_3N)C(O)CH_2C(\alpha\text{-}C_4H_3N)(CH_3)O]_2\{[CH_3CO(C_4H_3N)]_2V_2[K(THF)]_2\}$ (5.1)

A solution of $[CH_3CO(C_4H_3N)]K$ (2.5 g, 10.4 mmol) in THF (50 ml) was treated with $VCl_3(THF)_3$ (1.3 g, 3.4 mmol). The resulting dark orange red solution was filtered to eliminate a small amount of insoluble material. The solution was evaporated to dryness and the residue redissolved in ether. The solution was allowed to stand at room temperature for four days upon which crystalline **5.1** separated (2.13 g, 2.3 mmol, 68%).

IR (Nujol mull, cm^{-1}) v: 1591 (w), 1550 (vs), 1532 (s), 1498 (m), 1460 (vs), 1446 (vs), 1432 (w), 1384 (vs), 1368 (w), 1313 (m, s), 1287 (vs), 1273 (w), 1203 (s), 1188 (s), 1154 (vs), 1121 (m), 1110 (m), 1063 (s), 1043 (vs), 1028 (s), 980 (m), 965 (w), 943 (vs), 920 (m), 891 (m), 867 (s), 831 (m), 795 (m), 757 (w), 744 (s), 728 (vs), 710 (w), 697 (s), 668 (s), 652 (m), 629 (m), 608 (s), 582 (s), 550 (m), 529 (m). Anal Calcd (found) for $V_2K_2C_{36}H_{44}N_6O_8$: C, 53.22 (54.01), H 5.14 (5.93), N 8.30 (8.58), μ_{eff} = 4.19 μ_{BM} per formula unit.

Preparation of $[(\alpha\text{-}C_4H_3N)(CH_3)(O)C\text{-}C(O)(CH_3)(\alpha\text{-}C_4H_3N)]\{[(\alpha\text{-}C_4H_3N)C(O)CH_3]VK(THF)\}_2$ (5.2)

A solution of $[V_2Cl_3(THF)_6]_2[Zn_2Cl_6]$ (2.0 g, 1.2 mmol) in THF (70 ml) was treated with $[CH_3CO(C_4H_3N)]K$ (2.2 g; 14.8 mmol). The resulting dark brown-greenish solution was centrifuged to eliminate KCl After evaporation of the solvent in vacuo, the solid residue was redissolved in ether and the resulting brown solution was allowed to stand at room temperature for four days upon which a burgundy red microcrystalline solid separated. The solid was collected and redissolved in toluene (10 ml). Reddish-brown crystals of **5.2** were obtained upon cooling at -40ºC (0.9 g, 0.9 mmol. 38%). IR (Nujol, cm^{-1}): 1734 (w), 1684 (w), 1643 (s), 1547 (vs), 1506 (m), 1464 (vs), 1379 (vs), 1286 (vs), 1261 (s), 1236 (m), 1203 (m), 1182 (m), 1163 (w), 1147 (m), 1118 (m), 1107 (w), 1086 (m), 1039 (s), 987 (m), 956 (m), 929 (s), 912 (m), 841 (w), 802 (w), 754 (s), 744 (s), 727 (s), 696 (s), 687 (m), 650 (m), 621 (m), 604 (m), 550 (w). Anal Calcd (found) for $K_2V_2C_{47}H_{52}N_6O_8$: C 55.95 (56.30), H 5.19 (5.55), N 8.33 (8.64). μ_{eff} = 5.88 μ_{BM} per formula unit.

Preparation of $[CH_3CO(C_4H_3N)]_2V(TMEDA)$ (5.3).

Method A. A light blue solution of $VCl_2(TMEDA)_2$ (1.8 g, 5.2 mmol) in THF (100 ml), was reacted with $[CH_3CO(C_4H_3N)]K$ (2.5 g; 10.4 mmol). The resulting dark-blue solution was evaporated to dryness and the resulting residue was redissolved in freshly distilled ether (75 ml). The solution was filtered and allowed to stand at –20°C where blue crystals of **5.3** separated (0.9 g, 2.3 mmol, 44%). IR (Nujol, cm^{-1}) v: 1734 (w), 1685 (m), 1637 (s), 1539 (s), 1462 (vs), 1377 (vs), 1279 (vs), 1259 (s), 1199 (m), 1138 (m), 1097 (s), 1063 (s), 1032 (s), 1003 (s), 955 (m), 924 (s), 889 (m), 870 (m), 796 (s), 739 (s), 696 (s), 667 (w), 644 (m), 613 (m), 588 (w). Anal Calcd (found) for $VC_{18}H_{28}N_4O_2$: C 56.39 (56.69), H 7.36 (7.68), N 14.61 (14.75). $\mu_{eff} = 3.68\ \mu_{BM}$.

Method B.

A solution of $[V_2Cl_3(THF)_6]_2[Zn_2Cl_6]$ (2.0 g, 1.23 mmol) in THF (70 ml) was treated with $[CH_3CO(C_4H_3N)]K$ (1.4 g; 9.8 mmol). The resulting dark blue solution was centrifuged to eliminate KCl and subsequently treated with TMEDA (0.6 g, 4.9 mmol). The solvent was evaporated in vacuo and the residue redissolved in ether (20 ml). The solution was centrifuged concentrated and allowed to stand at -20ºC upon which dark blue crystals of analytically pure **5.3** separated.

5.3 General Polymerization Procedure.

Catalysts were evaluated by co-polymerizing ethylene-propylene in cyclohexane solutions at 2 bar total pressure and 22°C. Experiments were carried out in 150 ml of anhydrous toluene in magnetically agitated glass reactors using a continuous flow of 1000 sccm ethylene and/or 1000-sccm propylene. After equilibration with the feed, 0.2 mmol of DEAC co-catalyst were added followed by addition of 5 μmole vanadium catalyst A chlorinated ester such as ethyl trichloroacetate (Aldrich) was used for the *in situ* oxidation of **3.3**. The total amount of reactivating substance added to the reaction mixture was 20 μmole. Polymerization reactions were carried out for 30 minutes followed by addition of 5ml ethanol and depressurization. The EP rubber and PP polymers were recovered by solvent evaporation, dried in a vacuum oven at 60°C. PE polymers were collected by filtration, washed and sonicated in diluted HCl, and dried at 60°C. The polymer composition of EP rubber was determined by FTIR using the ratio of peak heights of the bands at 1155 and 720 cm^{-1} after calibration with standard samples. The molecular weights were determined by GPC at 140°C by using trichlorobenzene as a solvent. The molecular weights are reported as polystyrene equivalents.

Table 5.1 Polymerization Results of Complex 5.1

Feed	T (°C)	Activator	run time (min)	yield (g)	Activity (g/mmol cat./h)	M_w ($x10^3$)	PD
Ethylene	25	DMAC	60	6.31	3786		
		DMAC	60	4.31	2590*	54	25.5
		DEAC	20	2.70	1620		
Ethylene / Propylene	25	DMAC	20	2.61	2490	580	4.96
		DEAC	20	4.15	1566		
Ethylene / Propylene / Norbornylene	25	DMAC	20	2.75	1650	88	3.48
Ethylene / Norbornylene	25	DMAC	20	6.00	3600	65.4	2.51
Ethylene / 1-hexene	25	DMAC	20	3.21	1926	526	2.60

*the reaction was done with 1:2 V:ETA (ETA = ethyl-1,1,1-trichloroacetate) which was used as a chlorinating agent.

Table 5.2 Polymerization Results of Complex 5.2

Feed	T (°C)	Activator	run time (min)	Yield (g)	Activity (g/mmol cat. h)	Mw ($x10^3$)	PD
Ethylene	25	DMAC	60	5.78	3466		
	25	DMAC	60	14.21	8526*	73	23.0
	25	DEAC	20	2.40	1600		
Ethylene / Propylene	25	DMAC	20	4.40	2933	1230	2.79
Ethylene / Propylene / Norbornylene	25	DMAC	20	3.84	2560	465	18.4
Ethylene / Norbornylene	25	DMAC	20	5.58	3720	630	4.4
Ethylene / 1-hexene	25	DMAC	20	4.71	3140	295	6.17

*the reaction was done with 1:2 V:ETA (ETA = ethyl-1,1,1-trichloroacetate) which was used as a oxidizing agent.

5.4 X-Ray Crystallographic Structural Studies

Suitable crystals were selected, mounted on thin, glass fibres using paraffin oil and cooled to the data collection temperature. Data were collected on a Bruker AX SMART 1k CCD diffractometer using 0.3° ω-scans at 0, 90, and 180° in ϕ. Unit-cell parameters were determined from 60 data frames collected at different sections of the Ewald sphere. Semi-empirical absorption corrections based on equivalent reflections were applied (Blessing, R., *Acta Cryst.*, **1995**, A51, 33-38). Systematic absences in the diffraction data and unit-cell parameters were uniquely consistent with the reported space groups. The structures were solved by direct methods, completed with difference Fourier syntheses and refined with full-matrix least squares procedures based on F^2. The molecule was located at a two-fold rotation axis in complex **5.2** and at an inversion centre in complex **5.1**. Attempts to model several peaks located away from the molecule in complex **5.1** as a chemically reasonable, co-crystallized solvent molecule failed. These apparent solvent atoms were assigned arbitrary carbon atom identities and refined isotropically with partial occupancies. All remaining non-hydrogen atoms were refined with anisotropic displacement parameters. All hydrogen atoms were treated as idealized contributions. All scattering factors and anomalous dispersion factors are contained in the SHELXTL 5.10 program library (Sheldrick, G. M., Bruker AXS, Madison, WI, 1997). Crystal data for the three complexes are given in Appendix 6.

Complex of $[(\alpha\text{-}C_4H_3N)C(O)CH_2C(\alpha\text{-}C_4H_3N)(CH_3)O]_2$ $\{[CH_3CO(C_4H_3N)]_2V_2[K(THF)]_2\}$ (5.1)

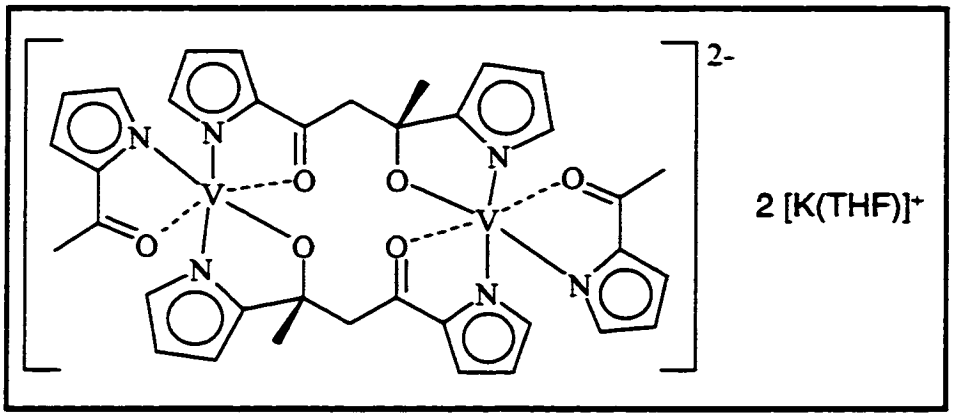

The complex is dinuclear and consists of two identical V(acetylpyrrolide) units bridged by two 1,3-di-(α-pyrrolyl)-3-hydroxyl-butan-1-one trianions (Figure 5.1). Two potassium atoms, each solvated by one molecule of THF, complete the dinuclear structure. The coordination geometry around each vanadium is distorted octahedral [O(1)-V(1)-N(1) = 82.25(11)°, O(1)-V(1)-N(3) = 108.40(11)°, O(1)-V(1)-O(2) = 92.30(10)°, O(1)-V(1)-N(2) = 164.17(11)°, O(1)-V(1)-O(3) = 89.89(10)°] and is defined by one intact acetylpyrrolide ligand which occupy two adjacent coordination sites with the nitrogen of the pyrrolide ligand [V(1)-N(3) = 2.030(3) Å] and the oxygen atom of the acetyl group [V(1)-O(3) = 2.135(3) Å]. The oxygen atom, however is also bonded to one potassium atom [K(1)-O(3) = 2.871(3) Å]. The two tetradentate 1,3-di-(α-pyrrolyl)-3-hydroxyl-butan-1-one trianions bridge the two vanadium centres. Each trianion uses the nitrogen atom of one of the two pyrrolyl ligand and the carbonyl group [C(11)-O(2) = 1.275(4) Å] to bond the first vanadium [V(1)-N(2) = 2.111(3) Å , V(1)-O(2) = 2.077 (2) Å] and the N atom of the second pyrrolyl and the contiguous deprotonated hydroxyl

oxygen atom to bond the second vanadium atom [V(1A)-N(1A) = 2.024(3) Å , V(1A)-O(1A) = 1.890 (2) Å]. The overall, the *fac*-octahedral coordination geometry of each vanadium centre is defined by three nitrogen atoms of three σ-bonded pyrrolyl moieties and three oxygen atoms and more specifically one oxygen/nitrogen couple from an intact acetylpyrrolide and the other two from two pyrrolyl hydroxyl butanone ligands). Each potassium atom is π-bonded to one butanone pyrrolyl ring σ-bonded to one vanadium and to the three oxygen atoms bonded to the second vanadium forming a planar V_2K_2 tetrametallic core [V-K-V-K torsion angle = 0°].

Figure 5.1 **ORTEP of $[(\alpha\text{-}C_4H_3N)C(O)CH_2C(\alpha\text{-}C_4H_3N)(CH_3)O]_2$ $\{[CH_3CO(C_4H_3N)]_2V_2[K(THF)]_2\}$ (5.1)**

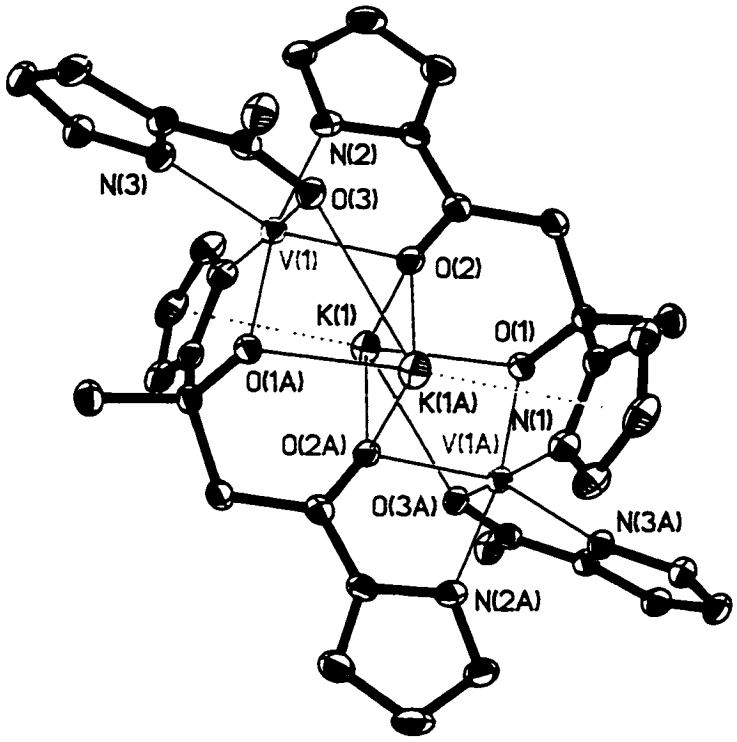

Selected Bond Distances (Å) and Angles (deg) for Complex 5.1

Distances	Angles
V(1)-N(3) = 2.030(3) Å	O(1)-V(1)-N(1) = 82.25(11)
V(1)-O(3) = 2.135(3) Å	O(1)-V(1)-N(3) = 108.40(11)°
K(1)-O(3) = 2.871(3) Å	O(1)-V(1)-O(2) = 92.30(10)°
C(11)-O(2) = 1.275(4) Å	O(1)-V(1)-N(2) = 164.17(11)°
V(1)-N(2) = 2.111(3) Å	O(1)-V(1)-O(3) = 89.89(10)°
V(1)-O(2) = 2.077 (2) Å	
V(1A)-N(1A) = 2.024(3) Å	
V(1A)-O(1A) = 1.890 (2) Å	

Complex of $[(\alpha\text{-}C_4H_3N)(CH_3)(O)C\text{-}C(O)(CH_3)(\alpha\text{-}C_4H_3N)]\{[(\alpha\text{-}C_4H_3N)\ C(O)CH_3]VK(THF)\}_2$ (5.2)

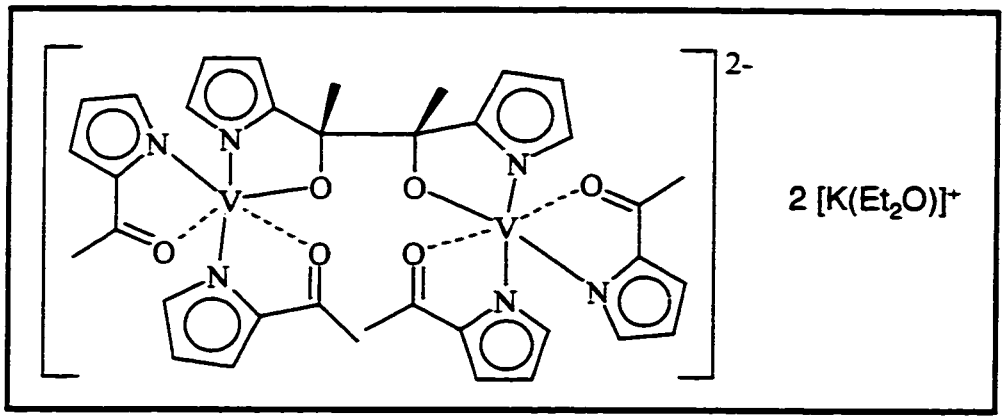

This complex is also a symmetry generated dimer with two identical V(acetylpyrrolide)$_2$ units bridged by one 2,3-di-(α-pyrrolyl)-2,3-butandiolate tetra-anion. The coordination geometry around each vanadium atom is slightly distorted octahedral [O(1)-V(1)-N(1) = 81.0(2)°, O(1)-V(1)-N(3) = 103.4(2)°, O(1)-V(1)-O(2) = 97.0(2)°, O(1)-V(1)-O(3) = 89.1(2)°, O(1)-V(1)-N(2) = 172.3(2)°] and is defined by the oxygen and nitrogen atoms of two σ-bonded acetylpyrrolyl ligands and by one oxygen and nitrogen atoms of the bridging tetra-anion [V(1)-N(3) = 2.045(6) Å, V(1)-N(2) = 2.119(6) Å, V(1)-O(3) = 2.123(4) Å , V(1)-O(2) = 2.070(5) Å]. The bridging interaction is realized with the four donor atoms, each couple of contiguous N and O atoms bonding each vanadium [V(1)-O(1) = 1.859(4) Å, V(1)-N(1) = 2.041(5) Å]. Thus even in this case, three oxygen and three nitrogen atoms define the overall *fac*-octahedral coordination geometry of each vanadium centre. Two potassium atoms are each connected to the three oxygen atoms attached to one vanadium and π-bonded to one pyrrolyl ring which is in turn σ-bonded to the second vanadium atom. The network of bridging interaction creates a tetrametallic V_2K_2 cluster with a planar core [torsion angle = 13.9º].

Figure 5.2 **ORTEP of $[(\alpha\text{-}C_4H_3N)(CH_3)(O)C\text{-}C(O)(CH_3)(\alpha\text{-}C_4H_3N)]\{[(\alpha\text{-}C_4H_3N)C(O)CH_3]VK(THF)\}_2$ (5.2)**

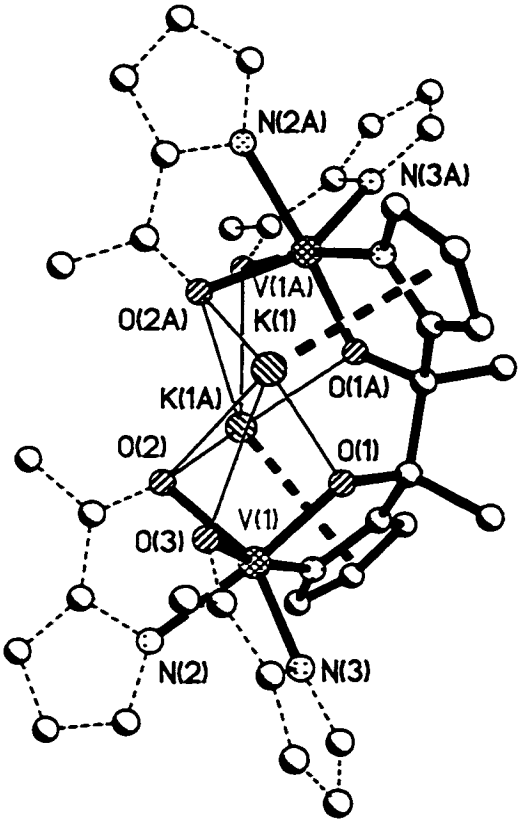

Selected Bond Distances (Å) and Angles (deg) for Complex 5.2

Distances	Angles
V(1)-N(3) = 2.045(6) Å	O(1)-V(1)-N(1) = 81.0(2)°
V(1)-N(2) = 2.119(6) Å	O(1)-V(1)-N(3) = 103.4(2)°
V(1)-O(3) = 2.123(4) Å	O(1)-V(1)-O(2) = 97.0(2)°
V(1)-O(2) = 2.070(5) Å	O(1)-V(1)-O(3) = 89.1(2)°
V(1)-O(1) = 1.859(4) Å	O(1)-V(1)-N(2) = 172.3(2)°
V(1)-N(1) = 2.041(5) Å	
C(5)-O(1) = 1.433(7) Å	
C(17)-O(3) = 1.284(8) Å	
C(11)-O(2) = 1.277(8) Å	
K(1)-O(4) = 2.674(6) Å	

Complex of $[CH_3CO(C_4H_3N)]_2V(TMEDA)$ (5.3)

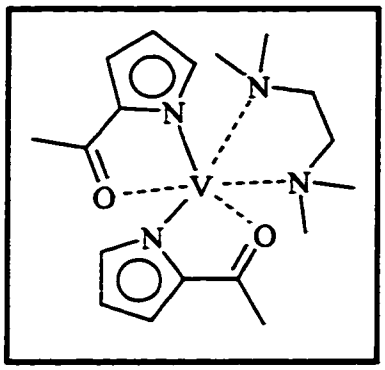

The complex is formed by discrete monomeric units containing vanadium in a distorted octahedral environment [O(1)-V-N(2) = 97.1(2)°, O(1)-V-O(2) = 173.7(1)°, O(1)-V-N(1) = 77.8(2)°, O(1)-V-N(4) = 96.9(2)°, O(1)-V-N(3) = 88.7(2)°]. The coordination geometry around the metal is defined by the oxygen [V-O(1) = 2.12(4) Å, V-O(2) = 2.11(3) Å] and nitrogen [V-N(1) = 2.12(5) Å, V-N(2) = 2.11(4) Å] donor atoms of two intact acetylpyrrolide anions and the two nitrogen atoms of one TMEDA molecule [V-N(3) = 2.25(5) Å, V-N(4) = 2.23(4) Å]. The two oxygen atoms are located on the axis while the four N atoms bound the equatorial plane [N(4)-V-N(3) = 81.4(2)°, N(4)-V-N(2) = 163.7(2)°, N(4)-V-N(1) = 91.3(2)°]. The bond distances and angles of the coordinated anions compare well with those in complexes **5.1** and **5.2**.

Figure 5.3 ORTEP of $[CH_3CO(C_4H_3N)]_2V(TMEDA)$ (5.3)

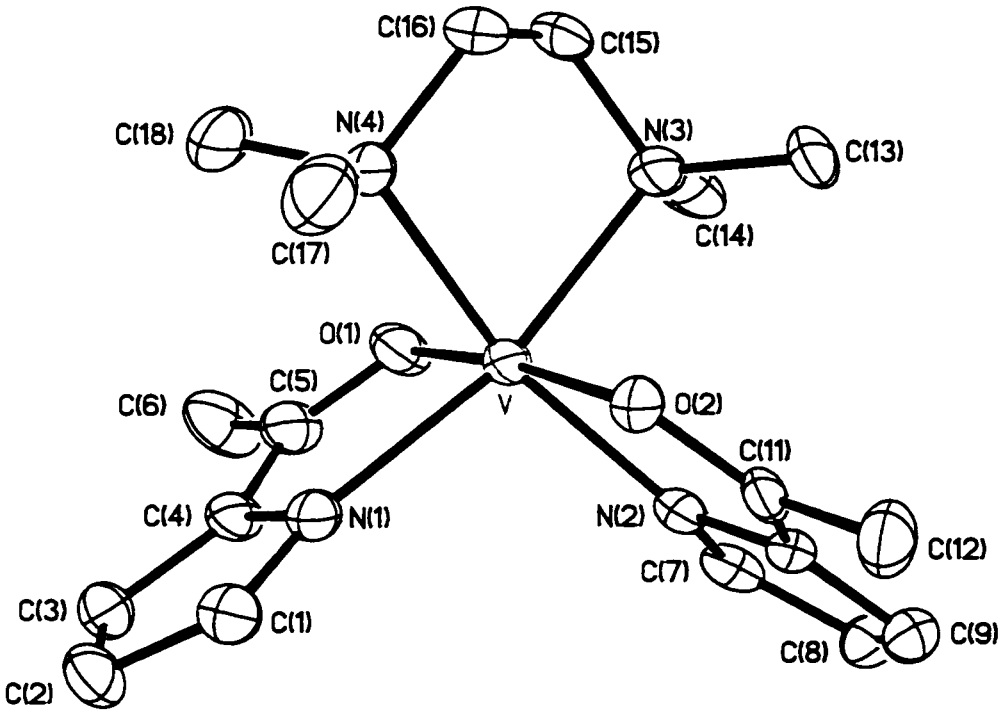

Selected Bond Distances (Å) and Angles (deg) for complex 5.3

Distances	Angles
O(1)-V-N(2) = 97.1(2)°	V-O(1) = 2.12(4) Å
O(1)-V-O(2) = 173.7(1)°	V-O(2) = 2.11(3) Å
O(1)-V-N(1) = 77.8(2)°	V-N(1) = 2.12(5) Å
O(1)-V-N(4) = 96.9(2)°	V-N(2) = 2.11(4) Å
O(1)-V-N(3) = 88.7(2)°	V-N(3) = 2.25(5) Å
	V-N(4) = 2.23(4) Å
	N(4)-V-N(3) = 81.4(2)°
	N(4)-V-N(2) = 163.7(2)°
	N(4)-V-N(1) = 91.3(2)°

5.5 Results and Discussion

The potassium salt $[(\alpha\text{-}C_4H_3N)C(O)CH_3]K(THF)$ was readily prepared via reaction of acetylpyrrole with KH in THF. The reaction was accompanied by vigorous gas evolution and the salt was isolated in good yield and in crystalline form as colourless needles. The crystals rapidly desolvate upon drying and meaningful analytical data in agreement with the formulation $[(\alpha\text{-}C_4H_3N)C(O)CH_3]K$ were obtained only from samples previously exposed to vacuum for a few hours. The ^{1}H-NMR spectrum showed the expected pattern with three slightly broadened singlets for the pyrrolyl CH groups and one sharp singlet for the methyl group with the correct relative intensities. The ^{13}C-NMR spectrum also showed the expected six-line spectrum.

Scheme 5.1 Modes of Bonding of the Acetylpyrrolide Ligand

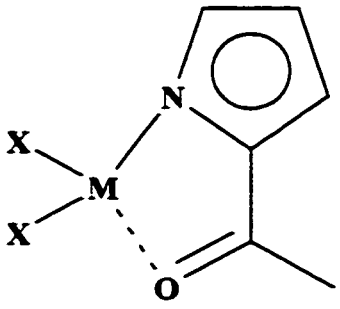

η^1-bound pyrrolide ring

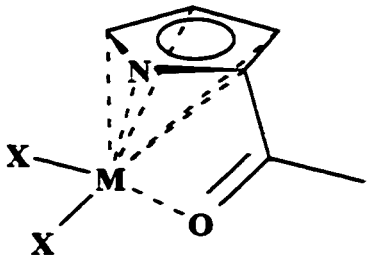

η^5-bound pyrrolide ring

Given the excellent activity and versatility of the commercially used $V(acac)_3$ catalyst, attempts to prepare a monomeric V(acetylpyrrolide)$_3$ complex of similar octahedral structure were initially carried out by reacting the potassium salt of acetylpyrrole $K[(\alpha\text{-}C_4H_3N)C(O)CH_3]$ with $VCl_3(THF)_3$ in THF at room temperature and by using a stoïchiometric ratio of ligand/vanadium of 3:1. The reaction afforded instead

the $\{[(\alpha\text{-}C_4H_3N)C(O)CH_3]VK(THF)\}_2[(\alpha\text{-}C_4H_3N)C(O)CH_2CO(CH_3)(\alpha\text{-}C_4H_3N)]_2$ **(5.1)** complex (Scheme 5.2).

Scheme 5.2 Synthesis of complex 5.1

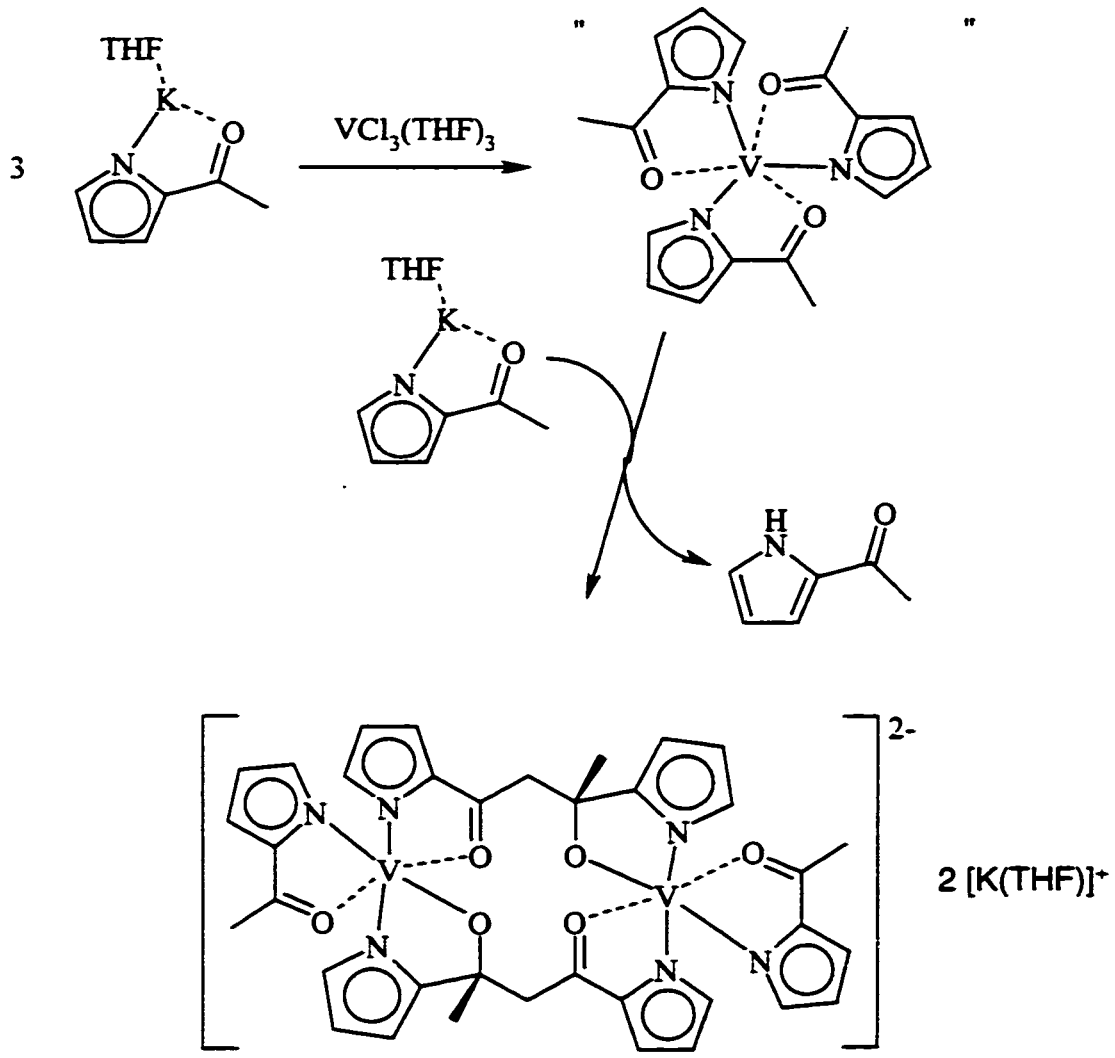

The two bridging 1,3-di-(α-pyrrolyl)-3-hydroxy-butan-1-one trianionic ligands bridging the two vanadium centres arise from the aldol condensation of two acetylpyrrole units. Although this type of process typically requires the intervention of a base, we found no sign for this transformation during the initial deprotonation of acetylpyrrole by KH. This was verified by a DEPT ^{13}C NMR experiment resulting in the absence of a

secondary carbon (-CH_2-) signal, which is present in the ligand, which has undergone the "aldol" condensation. By contrast, reaction of analytically pure [(α-C_4H_3N)C(O)CH_3]K with $VCl_3(THF)_3$ yielded **5.1** as the only product which could be isolated and identified from the reaction mixtures. This suggests that vanadium acts as a templating agent by triggering the aldol condensation of two of the three acetylpyrrolide anions. Nonetheless, the formal elimination of one proton from the acetylpyrrolide anion, as required by the aldol condensation, can be obtained only with the intervention of a base provided by a *fourth* equivalent of acetylpyrrolide potassium (Scheme 5.2). Accordingly, reactions carried out with excess [(α-C_4H_3N)C(O)CH_3]K gave a substantial improvement of the reaction yield (from 25% to 68%).

Complex **5.1** is a versatile catalyst for ethylene homo-, co- and ter-polymerization (Table 5.1). For this study the investigation was limited to propylene, norbornene and 1-hexene as co-monomers. The activity of the catalyst activated by either DEAC or DMAC and calculated on the basis of the amount of isolated polymer places this complex amongst the most active vanadium catalysts reported so far[1,6-9]. For example, the activity for the formation of ethylene-propylene copolymer is substantially higher than that reported for the commercially used V(*acac*)$_3$ [994 g EP/mmol/30 min].[6] In addition, the average molecular weight of the polymer was substantially higher while the polydispersity and composition remained comparable. Just the polyethylene samples displayed rather low molecular weight and broad polydispersity. The diagram of the ethylene uptake as a function of time recorded for an ethylene homo-polymerization experiment (Figure 5.4) clearly indicated that the catalyst is active only in the first 16-17 minutes. By assuming that even in this case the deactivation was the result of the

reduction of the vanadium center to the divalent state, attempts to extend catalyst life were done by carrying out polymerization experiments in the presence of ethyl trichloroacetate (ETA) as a reactivating substance.

Figure 5.4 Ethylene Consumption versus Time of Complex 5.1

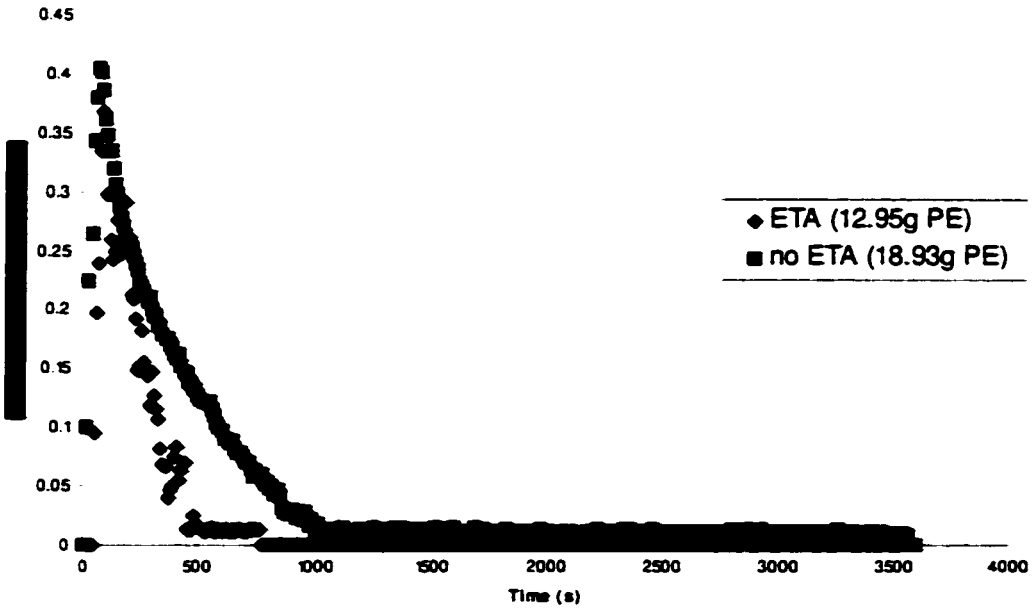

Polymerization Conditions: 15μmol of catalyst; 1:40 V:Al (DMAC); 1:2 V:ETA; 600 ml of toluene; 25°C; 10 psig ethylene

The role of this particular compound is believed to be that of reoxidizing intermediate V(II) species to trivalent state capable of re-entering the catalytic cycle as seen in chapter 2 scheme 2.1. To our surprise, the activity was substantially decreased indeed indicating that a complete and irreversible catalyst deactivation occurred after only eight minutes. Accordingly, the amount of polymer produced was also substantially lower. The detrimental effect of ETA suggests that a) the divalent species resulting from the deactivation process is either not reoxidized by ETA or produces an inactive species upon

oxidation and b) the striking difference of behaviour with the V(*acac*)$_3$ catalyst (where the employment of ETA is necessary to optimize catalyst performance) can only be ascribed to the presence of the acetylpyrrolide ligand which, therefore, is likely to remain connected to the vanadium center. Finally, the nature of the aluminium alkyl co-catalyst (DMAC versus DEAC) has a rather strong influence on the activity, which can be explained in terms of relative stability of the corresponding intermediate vanadium alkyl initiators (i.e. a V-Me function is likely to have a longer life-time than the corresponding V-Et).

The rapid drop in catalytic activity of **5.1** observed after the initial burst, is a rather common feature among vanadium-based Ziegler-Natta catalysts.[7] As mentioned above, in chapter 2 and in chapter 3, this behaviour is usually attributed to reduction of the metal centre to the inactive lower oxidation states of vanadium and whose formation is in turn ascribed to poor stability of the vanadium/carbon bond generated during the catalytic cycle. In an attempt to verify these hypotheses or at least to gain some insight into the reactivation process, we have attempted the synthesis of novel divalent vanadium complexes of the acetylpyrrolide ligand system. The aim was two-fold: a) to verify the inability of the divalent state to promote olefin polymerization under Ziegler-Natta conditions; b) to understand the anomalous behaviour of **5.1** with respect to the reoxidation by ETA.

The reaction of $[V_2Cl_3(THF)_6]_2[Zn_2Cl_6]$ with $[(\alpha\text{-}C_4H_3N)C(O)CH_3]K(THF)$ proceeded in two different manners depending on the reaction stoïchiometry. Reactions carried out with an excess of ligand afforded the dinuclear trivalent vanadium complex

$[(\alpha\text{-}C_4H_3N)(CH_3)(O)C\text{-}C(O)(CH_3)(\alpha\text{-}C_4H_3N)]$ $\{[(\alpha\text{-}C_4H_3N)C(O)CH_3]$ V K $(THF)\}_2$ $(toluene)_{0.5}$ (**5.2**) (Scheme 5.3).

Scheme 5.3 Synthesis of complex 5.2 and 5.3

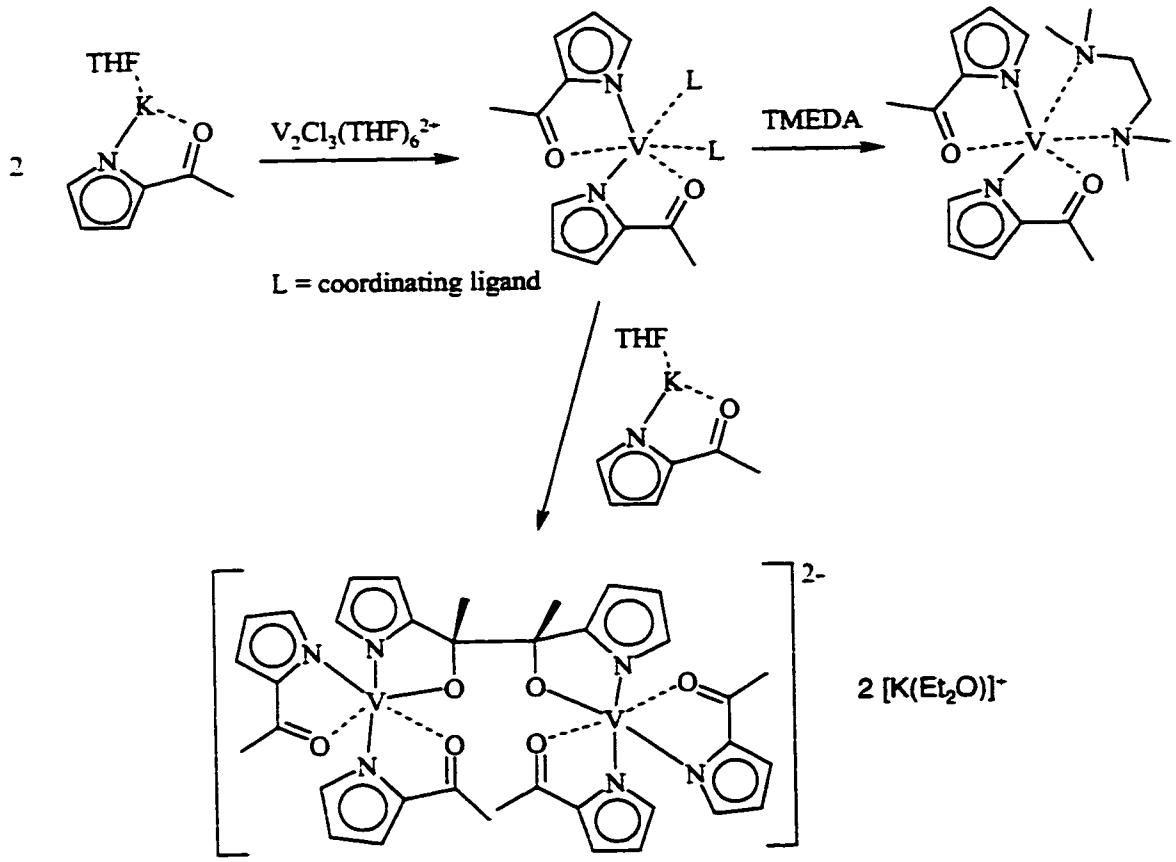

The $[(\alpha\text{-}C_4H_3N)(CH_3)(O)C\text{-}C(O)(CH_3)(\alpha\text{-}C_4H_3N)]^{4-}$ tetra-anion which bridges the two vanadium centres is the result of the pinacolic condensation of two acetylpyrrolide ligands. Given the strength of divalent vanadium as a reducing agent, the reduction of one acetylpyrrolide ligand to the corresponding pinacol is not particularly surprising.[17] Thus, it is conceivable that a divalent species produced by the normal deactivation process may undergo an internal reoxidation reaction at the expense of the

acetylpyrrolide ligand reforming a trivalent complex ready to re-enter the catalytic cycle. As a fascinating possibility, the high catalytic activity of **5.1** might be a direct consequence of this behaviour. Accordingly, complex **5.2** also is an active catalyst for ethylene homo- and co-polymerization although slightly less active than **5.1** (Table 5.2). However, the kinetic profile of the ethylene polymerization reaction showed that the catalyst is active only during the first three minutes after which the activity suddenly comes to an end (Figure 5.5). However, when the polymerization reaction was carried out in the presence of ETA as a reactivating substance, the catalyst remained active for up to 45-46 minutes and the production of polyethylene was the highest ever observed for a vanadium catalyst (8.526 g/mole/20 min).

Figure 5.5 Ethylene Consumption versus Time for Complex 5.2

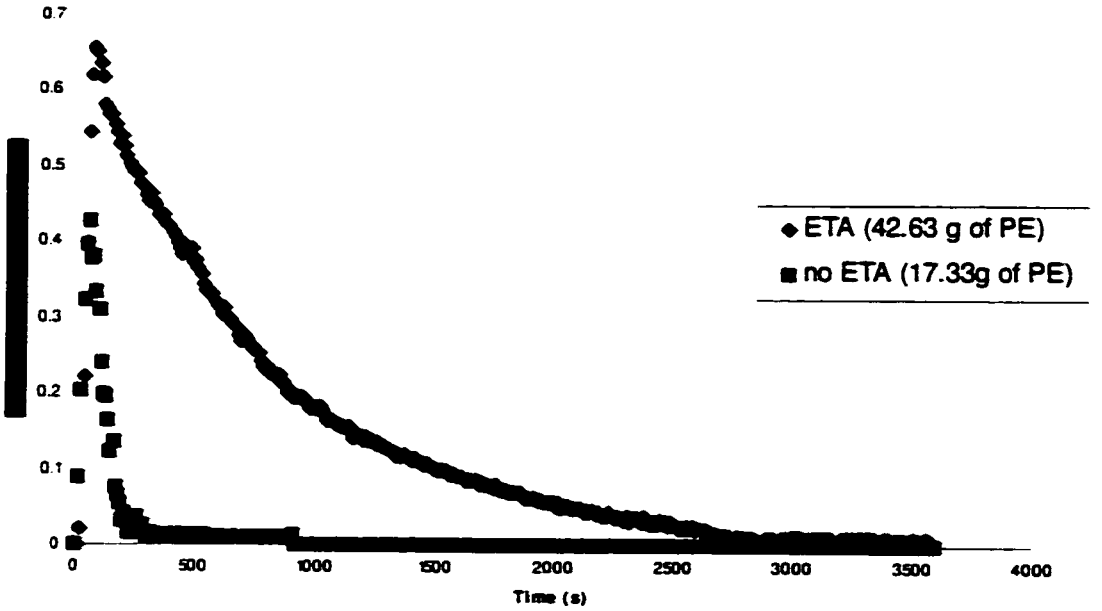

Polymerization Conditions: 15 μmol of catalyst; 1:40 V:Al (DMAC); 1:2 V:ETA; 600 ml of toluene; 25°C; 10 psig of ethylene

Unfortunately, repeated attempts to isolate intermediate complexes deriving from the direct interaction between the three complexes reported in this paper and a variety of alkyl aluminium derivatives and even $AlCl_3$ as a model only afforded non-crystalline materials. Therefore, we can only speculate about the identity of the intermediate species and the factors responsible for the high activity of **5.1** and **5.2**. At this stage we can conclude that the unusually high catalytic activity displayed by **5.1** and **5.2** and their contrasting behaviour with respect to the treatment with an oxidizing agent is the result of the combination of a few factors, which favourably concurred. The reduction of **5.1** to the divalent state as naturally occurs during the olefin polymerization reaction as a result of chain termination processes, does not seems to be responsible for the deactivation of **5.1**. In fact, a simple pinacolic type of reaction will regenerate another active catalyst that, by being more robust and more resistant to oxidizing agents, may last even longer. In addition, a divalent complex of this ligand system is also catalytically active thus opening interesting perspectives for further research.

5.6 References

1. (a) Sinn, H.; Kaminski, W. *Advances in Organometallic Chemistry*; Stone, F. G. A., West, R., Eds.; Academic Press: New York, 1980.

(b) Doi, Y.; Tokuhiro, N.; Nunomura, M.; Miyake, H.; Suzuki, S.; Soga, K. *Transition Metals and Organometallics as Catalysts for Olefin Polymerization*; Kaminsky, W., Sinn, H., Eds.; Springer-Verlag: Berlin, 1988.

(c) Carrick, W. L. *J. Am. Chem. Soc.* **1958**, *80*, 6455,

(d) Christman, D. L. *J. Polym. Sci., Part A-1* **1972**, 471.

(e) Pasquon, I.G.; Giannini, U. *Catalysis*; Anderson, J. R., Boudart, M., Eds.; Springer-Verlag: Berlin, 1984.

(f) Carrick, W. L.; Kluiber, R. W.; Bonner, E. F.; Wartman, L. H.; Rugg, F. M.; Smith J. J. *J. Am. Chem. Soc.* **1960**, *82*, 3883.

(g) Lehr, M. H. *Macromolecules* **1968**, 1, 178,

(h) Christman, D.L.; Keim, G. I. , *Macromolecules* **1968**, 1, 358,

(i) von Junghanns, E.;Gumboldt, A.; Bier, G. *Makromol. Chem.* **1967**, *101*, 229,

(j) Lehr, M. H.; Carmen, C. J. *Macromolecules* **1967**, 2, 217.

(k) Duck, E. W.; Grant, D.; Horder, J. R.; Jenkins, D. K.; Marlow, A. E.; Wallis, S. R.; Doughty, A. G.; Maradon, J. M.; Skinner, G. A. *Eur. Polym.* J. **1974**, *10*, 481,

(l) Feher, F. J.; Blanski, R. L. *J. Am. Chem. Soc.* **1992**, *114*, 5886.

(m) Feher, F. J.; Walzer, J. F.; Blanski, R. L. *J. Am. Chem. Soc.* **1991**, *113*, 3618,

(n) Feher, F. J.; Blanski, R. L. *Organometallics* **1993**, *12*, 958,

(o) Feher, F. J.; Walzer, J. F. *Inorg. Chem.* **1991**, *30*, 1689.

(p) Cucinella, S.; Mazzei A. U.S. Patent 3,711,455, Cl. 260-85.3, 1973.

(q) Boor, J., Jr.; Youngman, E. A. *J. Polym. Sci., Part A-1* **1966**, 4, 1861.

(r) Zambelli, A.; Natta, G.; Pasquon, I. *J. Polym. Sci., Part C* **1964**, 4, 411.

(s) Pino, P.; Mulhaupt, R. *Angew. Chem., Int. Ed. Engl.* **1980**, *19*, 857.

2. (a) Witte, P. T.; Meetsma, A.; Hessen, B. *J. Am. Chem. Soc.*, **1997**, *119*, 10561.

(b) Murphy, V. J.; Turner, H. *Organometallics*, **1997**, *6* (12), 2495-2497.

(c) Schuere, S.; Fisher, J.; Kress, J. *Organometallics*, **1995**, *14*, 2627.

(d) Zambelli, A.; Proto, A.; Longo, P. *Ziegler Natta Catalysis*; Fink, G., Mulhaupt, R., Brintzinger, H. H., Eds.; Springer-Verlag: Berlin, 1995.

(e) Kim, W. K.; Fevola, M. J.; Liable-Sands, L. M.; Rheingold, A. L.; Theopold, K. H., *Organometallics*, **1998**, *17*, 4541.

(f) Feher, K. J.; Walzer, J. F.; Blanski, R. L.; *J. Am. Chem. Soc.*, **1991**, *113* (3), 3618.

(g) Czaja, K.; Bialek, M. *Macromol. Rapid Commun.* **1998**, *19* (3), 163-166.

(h) Buhl, M. *Angew. Chem., Int. Ed.* **1998**, *37* (1-2), 142-144.

(i) Chan, M. C. W.; Cole, J. M.; Gibson, V. C.; Howard, J. A. K. *J. Chem. Soc., Chem. Commun.* **1997**, 2345. and references therein.

(j) Gibson, V. C., Redshaw, C., Elsegood, M. R. J, *J. Chem. Soc. Dalton Trans.*, **2001**, 767-769.

(k) Henderson, R. A., Hughes, D. L., Janas, Z., Richards, R. L., Sobota, P., Szafert, S., *J. Organomet. Chem.*, **1998**, *554*, 195-201.

(l) Choukroun, R.; Moumboko, P.; Chevalier, S.; Etienne, M.; Donnadieu, B.; *Angew. Chem. Int. Ed.*, **1998**, *37(22)*, 3169-3172.

(m) Lorber, C.; Donnadieu, B; Choukroun, R.; *Organometallics*; **2000**; *19(10)*; 1963-1966.

(n) Hagen, H.; Bezemer, C.; Boersma, J.; Kooijman, H.; Lutz, M.; Spek, A. L.; van Koten, G.; *Inorg. Chem.*; **2000**; *39(18)*; 3970-3977.

3. See for example:

(a) Doi, Y.; Suzuki, S.; Soga, K. *Macromolecules*,**1986**, *19*, 2896.

(b) Ouzumi, T.; Soga, K. *Makromol. Chem.* **1992**, *193*, 823.

(c) Gumboldt, A.; Helberg, J.; Schleitzer, G. *Makromol. Chem.*,**1967**, *101*, 229.

(d) Adisson, E. *J. Polym. Sci., Part A: Polym. Chem.*, **1994**, *32*, 1033.

(e) Davis, S. C.; von Hellens, W.; Zahalka, H. *Polymer Material Encyclopedia Vol. 3:* Salamone, J. C., Ed.; CRC Press Inc.; Boca Raton, FL, 1996.

4. Elston patent

1. Schmid, R.; Ziegler, T.; *Organometallics*, **2000**, *19*, 2756-2765

6. Ma, Y.; Reardon, D.; Gambarotta, S.; Yap, G. E.; Zahalka, H.; Lemay, C.; *Organometallics*, **1999**, *18*, 2773-2781.

7. Reardon, D.; Conan, F.; Gambarotta, S.; Yap, G. E.; Wang, Q.; *J. Am. Chem. Soc.*, **1999**, *121 (40)*, 9318- 9325.

8. Desmangles, N.; Gambarotta, S.; Bensimon, C.; Davis, S.; Zahalka, H., *J. Organomet. Chem.* **1997**, *562*, 53.

9. Theopold, K. H, *Organometallics*; **1998**; *17(21)*; 4541-4543

10. unpublished results

11. Witte, P.T.; Meetsma, A.; Hessen, B.; *Organometallics*, **1999**, *18*, 2944-2946

12. Manzer, L. E. *Inorg. Synth.* **1982**, *21*, 138.

13. Reinder, J.B., Teuben, J. H., Beukema, W.R., Bansemer, R.L., Huffman, J.C., Caulton, K.G., *Inorg. Chem.*, **1984**, *23*, 2715-2718.

14. Edema, J.J.H.; Stauthamer, W.; van Bolhuis, F.; Gambarotta, S.; Smeets, W. J.J.; Spek, A. L.; *Inorg. Chem.*, **1990**, *29*, 1302-1306

15. Mabbs, M. B., Machin, D., *Magnetism and Transition Metal Complexes;* Chapman and Hall; London, 1973.

16. Foese, G., Gorter, C. J.; Smits, L. J.; *Constantes Sélectionnées Diamagnétisme, Paramagnétisme, Relaxation Paramagnétique*, Masson, Paris, 1957.

17.(a) Hirao, T.; Hatano, B.; Imamoto, Y.; Ogawa, A.; *J. Org. Chem.*; **1999**; *64(20)*; 7665-7667.

(b) Ogawa, A.; *J. Org. Chem.*; **1998**; *63(25)*; 9604-9604.

(c) Hirao, T.; *J. Org. Chem.*; **1998**; *63(25)*; 9421-9424.

(d) Ogawa, A.; *J. Org. Chem.*; **1998**; *63(9)*; 2812-2813.

Chapter 6

Stability of Metal-Carbon Bond versus Metal Reduction During Ethylene Polymerization Promoted by a Vanadium Complex: the Role of the Aluminium Co-Catalyst

Abstract

In ***chapter*** *6, the dinuclear and trivalent complex* $\{[(Me_3Si)NCH_2CH_2]_2N(Me_3Si)\}_2V_2(\mu\text{-}Cl)_2$ ***(6.3)*** *is the precursor to mono- and dinuclear alkyl derivatives that are thermally stable. For example, treatment with MeLi gives a stable methyl derivative, probably iso-structural with* ***6.3****, which upon further treatment with pyridine affords the mononuclear complex* $\{[(Me_3Si)NCH_2CH_2]_2N(Me_3Si)\}V(CH_3)$*(pyridine)* ***(6.4a)****. However, reaction of* ***6.3*** *with* Me_2AlCl, $AlMe_3$ *or PMAO-IP yields the tetrametallic species* $\{[(Me_3Si)NCH_2CH_2]_2N(Me_3Si)\}_2V_2(\mu\text{-}Cl)_2(AlMe_2)_2$ ***(6.7)*** *where the central core of* ***6.3*** *is preserved except for the vanadium centres which have been reduced to the divalent state. The two* Me_2Al *residues are now coordinated to the amido ligand. The reduction of vanadium to the divalent state relates to the drop in catalytic activity of* ***6.3*** *as an ethylene polymerization catalyst. A similar reaction of* ***6.3*** *with* $AlCl_3$ *resulted in disproportionation forming the tetravalent complex* $\{[(Me_3Si)NCH_2CH_2]_2N(Me_3Si)\}VCl_2AlCl_3$ ***(6.5)*** *and the pentanuclear mixed-valent V(II)/V(III) species* $[(AlCl_2)\{[(Me_3Si)NCH_2CH_2]_2N(Me_3Si)\}V]_2[(\mu\text{-}Cl)_6V]\cdot(toluene)_2$ ***(6.6)****. The fact that complex* ***6.6*** *contains a divalent vanadium atom stripped of its ligand system indicates that two different reaction mechanisms are operating to reduce the vanadium centre and that the differing Lewis acidity of the two aluminium species is the determining factor.*

6.1 Introduction

Research into the area of Ziegler-Natta olefin polymerization has traditionally focused on the group 4 metals since these catalysts tend to be both efficient and selective.[1] In addition, most of the industrially successful catalysts are based on Cp and its derivatives as these ligands are both robust and highly tunable. Nevertheless, some non-metallocene systems have found industrial applications. Particularly relevant to this

work is the V(*acac*)$_3$ catalyst used for the commercial production of ethylene-propylene-diene elastomers (EPDM).[2]

A recent study of this system in our group highlighted a number of problems with the process.[3] The investigation confirmed that the Al co-catalyst plays a pivotal role in the catalyst activation by generating, in addition to the V-R function, empty coordination sites on vanadium (otherwise coordinatively saturated) via removal of one or more of the *acac* ligands. However, the co-catalyst also serves to deactivate the catalyst. By stripping the metal of the remaining *acac* ligands, the co-catalyst decreases the stability of the V-R bond. Consequently, the vanadium metal is rapidly reduced to the divalent state resulting in complete catalyst failure. In spite of this drawback, vanadium catalysts remain irreplaceable in EPDM manufacture. Thus, we were interested in developing new catalysts that might avoid the problems encountered with the above system. To prevent ligand leaching, it was decided to change the donor set from oxygen to nitrogen atoms. With such a system one might reasonably expect that the lower affinity of aluminium for nitrogen would reduce migration of the ligand from the vanadium center.

A direct consequence of ligand leaching is the reduction of the metal to V(II) which is a rather common deactivation pathway for vanadium catalysts. This is thought to be a result of a variety of events including β-H elimination of the alkyl polymer growing chain[4] and C-H σ-bond metathesis,[4] and relates to an intrinsic instability of the V-C bond once the ligand system has been abstracted from the vanadium center. Although a number of V(III) alkyl complexes have been successfully synthesized,[5,6] nevertheless, these complexes generally employ sterically bulky alkyl ligands or bulky supporting ligands. By analogy, we felt that a large chelating ligand would also be desirable for a vanadium

catalyst since it should extend catalyst's life. Moreover, it was hoped that a polydentate chelating ligand might also contribute to the aggregation of both vanadium and aluminium in the same molecular structure providing insight into the catalyst/co-catalyst interaction.

In view of these considerations the bulky N,N,N-*tris*-trimethylsilyl diethylenediamidoamino ligand[7] was selected for this study as it has already been successfully employed for different purposes, including one spectacular case of dinitrogen cleavage,[8] with a range of metals including V,[6] Ti,[9] Zr[10] and Nb.[11] The resulting vanadium complexes prepared in the course of this investigation and their catalytic behaviour, including their interaction with the Al co-catalyst, are now presented.

6.2 Experimental Section

All operations were performed under inert atmosphere by using standard Schlenk type techniques. Polymethylalumoxane solution (13.5% Al) in toluene (PMAO-IP, AKZO), $AlMe_3$ (Aldrich) was used as received without further purification. $VCl_3(THF)_3$[12], was synthesised according to published procedures and $AlCl_3$ was sublimed under reduced pressure before use. Infrared spectra were recorded on a Mattson 9000 and Nicolet 750-Magna FTIR instruments from Nujol mulls prepared in a dry box. Samples for magnetic susceptibility measurements were weighed inside a dry box equipped with an analytical balance and sealed into calibrated tubes. Magnetic measurements were carried out with a Gouy balance (Johnson Matthey) at room temperature. Magnetic moments were calculated following standard methods[13], and corrections for underlying diamagnetism were applied to data[14]. Elemental analyses were carried out with a Perkin-Elmer 2400 CHN analyser. NMR analysis were carried out on Varian Gemini 200 and Bruker AMX-500 spectrometers using vacuum sealed NMR tubes prepared inside a dry-box.

Preparation of $[(TMS)NHCH_2CH_2]_2NTMS$ (6.1)

A solution of DABCO (diaminebicyclooctane 50 g, 0.45 mol) in ether (700 ml) was treated with chorotrimethylsilane (62.17 ml, 0.45 mol) at room temperature. Upon mixing the colour of the solution changed from colourless to white. After stirring for 1 hour, diethyltriamine (15.3 ml, 0.15 mol) was added to the mixture and stirring was continued overnight. The solution was then filtered and ether was removed under vacuum to yield yellow oil. DABCO was removed by sublimation and the amine was distilled to give a

colourless oil (21 g, 65 mmol, 43%). IR (Nujol mull, cm^{-1}) ν: 3450 (m), 1330 (s), 850 (s), 660 (s), 592 (s). ^{1}H NMR ($CDCl_3$, 200 MHz, 25°C): δ 01. (m, 9H, TMS), 2.7 (m, 4H, CH_{ethyl}). ^{13}C-NMR ($CDCl_3$, 200 MHz, 25°C): δ 42 (s, TMS), 52 (s, TMS), 54 (s, CH_{ethyl}).

Preparation of $[(TMS)NLiCH_2CH_2]_2NTMS$ (6.2)

The addition of butyl lithium (52 ml, 0.13 mol, 2.5M) to a solution of **6.1** (21g, 65 mmol) in hexane (150 ml) at –80°C afforded a white precipitate. The solution was allowed to warm to room temperature, stirred for 1 hour, and filtered to collect the di-lithiated complex. (19.3g, 58 mmol, 89%). IR (Nujol mull, KBr, cm^{-1}) ν: 1258 (m), 1083 (m), 944 (w), 884 (w), 8.25 (m), 7.29 (w). ^{1}H-NMR ($CDCl_3$, 200 MHz, 25 °C): δ 0.15 (s, 9H, TMS), 0.34 (s, 18H, TMS), 2.9 (m, 4H, CH_{ethyl}).

Preparation of $\{[(TMS)NCH_2CH_2]_2N(TMS)\}_2V_2(\mu\text{-}Cl)_2$ (6.3)

A solution of $VCl_3(THF)_3$ (5.8g, 15.5 mmol) in THF (100 ml) was treated with one equivalent of **6.2** (5.2g, 15.5 mmol) at room temperature. The colour of the solution immediately darkened upon mixing and stirring was continued for 30 minutes. THF was removed in vacuo and the resulting red powder was redissolved in hexane (150 ml). The solution was then filtered to eliminate LiCl and allowed to stand at 0°C, for 24 hours, upon which dark red crystals of the complex separated. (5.1g, 6.2 mmol, 80%). IR (Nujol mull, KBr, cm^{-1}) ν: 1377 (m), 1250 (s), 1074 (s), 937 (s), 911 (s), 825 (s). Anal Calcd. (Found): C, 38.64 (38.53); 8.73 (8.61); N 10.40 (10.34). μ_{eff}: 2.93 μ_{BM}.

Preparation of {[(TMS)NCH$_2$CH$_2$]$_2$N(TMS)}V(CH$_3$)(pyridine) (6.4a)

A solution of complex **6.3** (1.1g, 1.4 mmol) in ether (100 ml) was treated with one equivalent of methyl lithium (2 ml 1.4 M) at room temperature. After mixing the colour of the solution changed to pink red and stirring was continued for 30 minutes. The solvent was removed in vacuo, the solid residue was redissolved in hexane (50 ml) and the solution was filtered to eliminate LiCl. The addition of dry pyridine (5 ml) turned the colour of the solution to purple. The mixture was allowed to stand at –80°C for 36 hours upon which dark purple crystals of the complex separated. (0.98g, 2.1 mmol, 75%). μ_{eff} = 2.90 μ_{BM}. The extreme air-sensitivity prevented IR analysis as well as combustion analysis determinations.

Preparation of {[(TMS)NCH$_2$CH$_2$]$_2$N(TMS)}VCl$_2$AlCl$_3$ (6.5) and {[(TMS) (AlCl$_2$) NCH$_2$CH$_2$]$_2$N(TMS)V}(μ-Cl)$_3$V(μ-Cl)$_3${[(TMS) (AlCl$_2$) NCH$_2$CH$_2$]$_2$N(TMS)V} (6.6)

A solution of complex **6.3** (1.0g, 1.23 mmol) in toluene (150 ml) was treated with two equivalents of trichloroaluminium (0.37g, 2.8 mmol) at room temperature. After mixing the colour of the solution changed to brown and stirring was continued for 1 hour. The solution was then filtered (to eliminate excess $AlCl_3$) and the volume was reduced to crystallize. The mixture was allowed to stand at room temperature, for 24 hours, upon which red crystals of **6.5** separated (0.2g, 0.35 mmol, 28%). IR (Nujol, KBr, cm^{-1}) v: 1377 (m), 1255 (s), 1089 (m), 1051 (m), 1001 (m), 912 (s), 891 (s), 840 (s), 759 (m), 721 (w), 669 (w), 634 (w). μ_{eff}: 1.83 μ_{BM}. Among the red crystals thin green plates were observed. X-ray analysis of the latter confirmed the molecular connectivity of **6.6**.

Unfortunately, only small amounts of complex **6.6** were obtained and no further characterization was possible.

Preparation of $\{[(TMS)NCH_2CH_2]_2N(TMS)\}_2V_2(\mu\text{-}Cl)_2(AlMe_2)_2$ (6.7)

Method A:

A solution of **6.3** (0.9g, 1.14 mmol) in hexane (100 ml) was treated with 1 ml of PMAO (13% Al solution in toluene) at room temperature. Upon addition a green precipitate separated from the red solution. It took roughly 54 equivalents of Al (PMAO) to yield a colourless solution. Crystals of the precipitate were obtained by layering a solution of PMAO in toluene over a solution of **6.3** in hexane. This mixture was allowed to stand at room temperature for 3 days, upon which emerald green crystals of the complex separated (0.2 g, 0.22 mmol, 19%). IR (Nujol, KBr, cm^{-1}) v: 2722 (w), 2701 (w), 1377 (m), 1247 (s), 1197 (s), 1126 (m), 1099 (s), 1054 (s), 904 (s), 836 (s), 765 (s), 674 (s). μ_{eff}: 3.9 μ_{BM}. Anal. Calcd. for $C_{30}H_{82}N_6Si_6V_2Al_2Cl_2$ (Found): C 39.07(38.88); H 8.96 (8.71); N 9.11 (8.97).

Method B:

A solution of **6.3**(1.23g, 1.6 mmol) in hexane (150 ml) was treated with two equivalents of trimethylaluminium (3 ml, 2.0 M) at room temperature. After mixing the colour of the solution changed to dark red and stirring was continued for 30 minutes. The mixture was allowed to stand at 4 °C, for 2 days, upon which emerald green crystals of the complex separated from a brown solution (0.3g, 0.33 mmol, 20%).

Preparation of $\{[(TMS)NCH_2CH_2]_2N(TMS)\}VCl_2$ (6.8)

A solution of **6.3** (1.0g, 1.23 mmol) in toluene (150 ml) was treated with one equivalent per vanadium dimer of triphenylphosphine dichloride (0.2g, 0.6 mmol) at room temperature. After mixing the colour of the solution changed to brown and stirring was continued for one hour. The solution was then filtered and the solvent was reduced to dryness. Freshly distilled hexane was added (30 ml). The mixture was allowed to stand at –40°C, for 24 hours, upon which brown crystals of $\{[(TMS)NCH_2CH_2]_2N(TMS)\}VCl_2$ (0.22g, 0.5 mmol, 41%). IR (Nujol, KBr, cm^{-1}) ν: 1377 (m), 1255 (s), 1089 (m), 1051 (m), 1001 (m), 912 (s), 891 (s), 840 (s), 759 (m), 721 (w), 669 (w), 634 (w). μ_{eff}: 1.83 μ_{BM}. Anal. Calcd. for $C_{13}H_{35}N_3Si_3VCl_2$ (Found): C 35.52 (35.49); H 8.03 (7.95); N 9.58 (9.53).

Preparation of $\{[(TMS)NHCH_2CH_2]_2N\}VCl_2$ (6.9)

A solution of **6.1** (2.246g, 2.54 ml, 7.07 mmol; 0.883 g/ml) was prepared in 50 ml of ether and was treated with ^{n}Bu-Li (7.07 mmol; 1.6 M solution in hexane; 4.42 ml). The solution was stirred for one hour liberating butane gas and leaving a clear colourless solution. A suspension of VCl_4(DME) (2g, 7.07 mmol) in ether was also prepared to which was slowly cannulated over a period of 30 minutes, the solution of **6.2**. The dark brown solution was left to stir overnight and was then filtered to eliminate LiCl. The volume of the solution was reduced and was left to crystallize at –20°C (2.15g, 4.9 mmol, 69%). IR (Nujol, KBr, cm^{-1}) ν: 2949 (s), 2851 (s), 1495 (m), 1462 (s), 1409 (w), 1378 (m), 1339 (m), 1318 (w), 1288 (m), 1255 (s), 1215 (s), 1156 (w), 1127 (m), 1061 (s),

1024 (w), 932 (s), 905 (s), 843 (s), 800 (s), 752 (s), 696 (s), 684 (s), 635 (m), 552 (s). μ_{eff}: 1.98 μ_{BM}. Anal. Calcd. (Found): C, 27.26 (27.22); H, 6.16 (6.23); N, 7.33 (7.28).

Reaction of complex 6.3 with $VCl_3(THF)_3$

A dark red solution of complex **6.3** (0.57g, 0.71 mmol) in 30 ml of toluene was mixed with a 70 ml toluene suspension of $VCl_3(THF)_3$ (0.54g, 1.45 mmol) and was stirred for 2 hours upon which the colour changed to a dark brown. The solvent was reduced to dryness and replaced by 50 ml of freshly distilled diethyl ether. The solution was filtered to yield a brown microcrystalline solid (0.32g; yield 51%) at –40ºC after 2 days, which was characterized as complex **6.8**. The filtrate was redissolved in toluene and treated with 0.44 ml of TMEDA (0.34 g; 2.9 mmol), which rapidly changed colour to a dark blue. The solid was then identified as $VCl_2(TMEDA)_2$ (0.24g, 38%) upon characterization.

6.3 General Polymerization Procedure

A bench scale reactor was used in the polymerization experiments. The reactor uses a programmable logic control (PLC) system with Wonderware 5.1 software for process control. Ethylene polymerizations were performed in the 500 ml Autoclave Engineers Zipperclave reactor equipped with an air driven stirrer and an automatic temperature control system. All the chemicals were fed into the reaction batch-wise except for ethylene that was fed on demand.

Conditions for polymerization:

	Slurry phase	Solution phase
Toluene	216 mL	216 mL
Catalyst concentration	300 μmol/L	300 μmol/L
PMAO or Me_3Al	Al/V=60 (mol/mol)	Al/V=60 (mol/mol)
Reaction temperature	50 °C	140 °C
Reactor pressure	300 psig total	286 psig total

As summarized above the control temperature were 50 °C for the slurry polymerization and 140 °C for solution polymerization experiments. The polymerization time varied from 10 to 30 min. Adding 5 mL of methanol to the reactor terminated the reaction and the polymer was recovered by evaporation of the toluene *in vacuo*. The polymerization activities were calculated based upon weight of polymer produced.

Polymer molecular weights and molecular weight distributions were measured by GPC (Waters 150-C) at 140 °C in 1,2,4-trichlorobenzene calibrated using polyethylene standards. DSC was conducted on a DSC 220 C from Seiko Instruments. The heating rate was 10 °C/min from 0 to 200 °C.

In a typical polymerization experiment, the solvent was pre-saturated with ethylene in the reactor at the desired temperature. The co-catalyst was injected in the reactor followed by introduction of the pre-catalyst. In the mixed-activator experiment the two co-catalysts were pre-mixed and injected in the reactor prior to introduction of the pre-catalyst. 1-octene was introduced in the reactor and premixed with ethylene before heating. Reproducibility of catalyst activity and reactor operation was checked by regularly running polymerization experiments using a standard zirconium catalyst and by

repeating the experiments under identical reaction conditions. Errors and deviation were always below 5.9%.

6.4 X-ray Crystallographic Studies

Structural determination of **6.3**, **6.4a**, **6.5**, **6.6**, and **6.7**. Suitable crystals were selected, mounted on thin glass fibres using viscous oil and cooled to the data collection temperature. Data were collected on a Bruker AX SMART 1k CCD diffractometer using 0.3° ω-scans at 0, 90, and 180° in ϕ. Unit-cell parameters were determined from 60 data frames collected at different sections of the Ewald sphere. Semi-empirical absorption corrections based on equivalent reflections were applied.[15]

No symmetry higher than triclinic was evident from the diffraction data of **6.5** and **6.7**. Solution in the centric option yielded chemically reasonable and computationally stable results of refinement. Systematic absences in the diffraction data and unit-cell parameters were uniquely consistent for the reported space groups for **6.3**, **6.4a** and **6.5**. The structures were solved by direct methods, completed with difference Fourier syntheses and refined with full-matrix least squares procedures based on F^2. The compound molecules for **6.5** and **6.7** are located on inversion centres. Two toluene solvent molecules were located co-crystallized in the asymmetric unit of **6.7**. All non-hydrogen atoms were refined with anisotropic displacement parameters. All hydrogen atoms were treated as idealized contributions. All scattering factors are contained in the SHEXTL 5.10 program library (Sheldrick, G. M., Bruker AXS, Madison, WI, 1997). Crystal data and relevant geometrical parameters are reported in Appendix 7 and Appendix 8.

Complex of [{V(Me$_3$Si)N{CH$_2$CH$_2$N(SiMe$_3$)}$_2$}$_2$(μ-Cl)$_2$] (6.3)

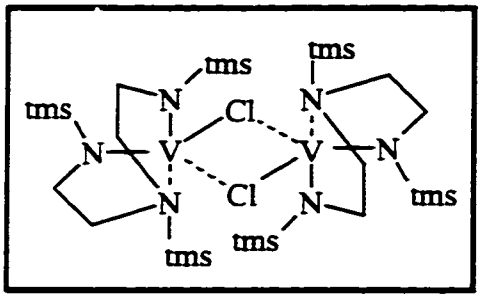

The crystal structure in Figure 6.1 shows a bimetallic complex with two distorted trigonal bipyramidal vanadium (III) centres bridged by two chlorides [V(1)-Cl(1)-V(2) = 97.36(6)°, V(1)-Cl(2)-V(2) = 97.44(6)°, Cl(2)-V(1)-Cl(1) = 82.03(6)°, Cl(2)-V(2)-Cl(1) = 82.11(6)°]. The equatorial plane of the trigonal bipyramidal vanadium is occupied by the two σ-bonded nitrogen atoms of the silylamino (disilylamido) ligand and a bridging chlorine atoms [N(1)-V(1)-N(3) = 117.91(26)°, N(1)-V(1)-N(2) = 84.69(22)°, N(1)-V(1)-Cl(1) = 119.98(19)°, N(1)-V(1)-Cl(2) = 100.98(17)°, N(4)-V(2)-N(6) = 118.03(24)°, N(4)-V(2)-N(5) = 84.76(21)°, N(4)-V(2)-Cl(1) = 100.72(17)°, N(4)-V(2)-Cl(2) = 121.96(18)°] while the co-ordinating nitrogen atom of the silylamino functionality and the second bridging chlorine atom [N(2)-V(1)-Cl(2) = 174.21(16)°, N(5)-V(2)-Cl(1) = 173.79(15)°] occupy the axial positions. The V-Cl distances are effectively equivalent and fall into the expected range for bridging chlorides [V(1)-Cl(1) = 2.373(2)Å, V(1)-Cl(2) = 2.459(2)Å, V(2)-Cl(1) = 2.462(2)Å, V(2)-Cl(2) = 2.373(2)Å]. The V-N bond lengths, are consistent with σ–bonded sylilamido donors [V(1)-N(1) = 1.906(5)Å, V(1)-N(3) = 1.899(5) Å, V(2)-N(4) = 1.905(5)Å, V(1)-N(6) = 1.902(5)Å] while the longer V-N bond lengths are indicative of a coordinated nitrogen [V(1)-N(2) = 2.179(5)Å, V(2)-N(5) = 2.193(5)Å]. All other bond distances and angles are unremarkable.

Figure 6.1 ORTEP of [{V(Me$_3$Si)N{CH$_2$CH$_2$N(SiMe$_3$)}$_2$}$_2$(μ-Cl)$_2$] (6.3)

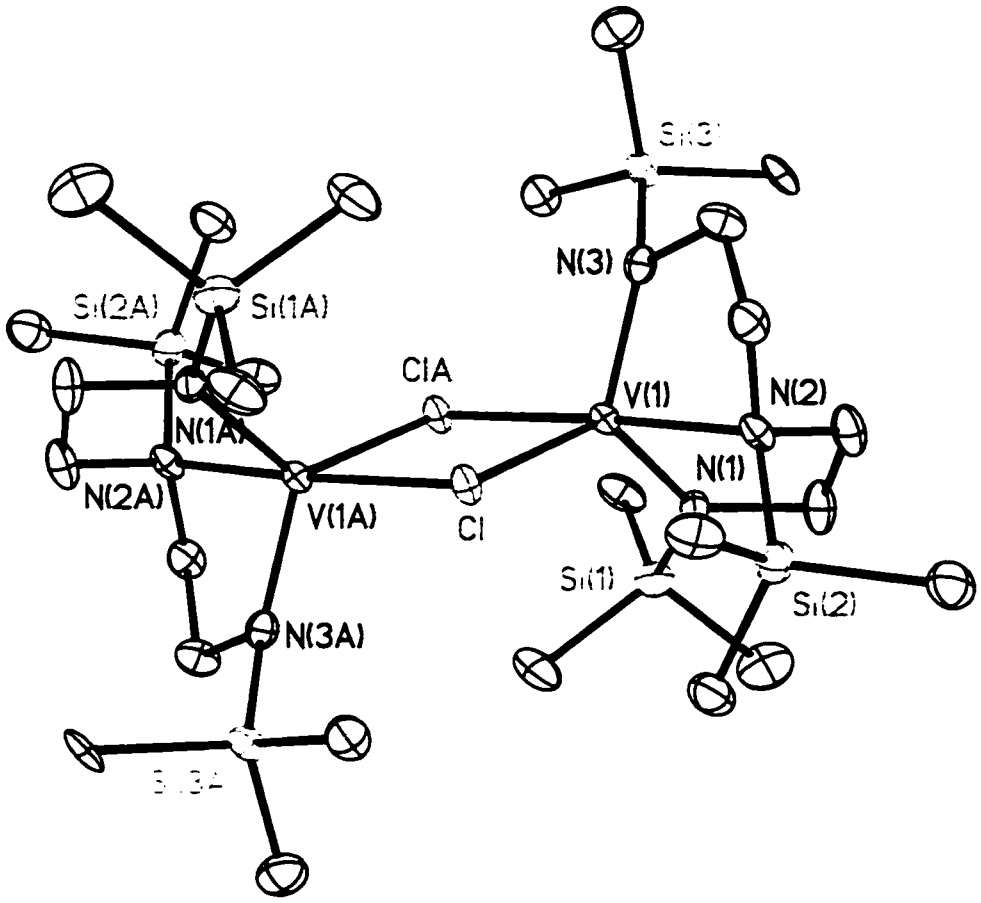

Selected Bond Distances (Å) and Angles (º)

Distances	Angles
V(1)-N(3) = 2.030(3)	O(1)-V(1)-N(1) = 82.25(11)
V(1)-O(3) = 2.135(3)	O(1)-V(1)-N(3) = 108.40(11)
K(1)-O(3) = 2.871(3)	O(1)-V(1)-O(2) = 92.30(10)
C(11)-O(2) = 1.275(4)	O(1)-V(1)-N(2) = 164.17(11)
V(1)-N(2) = 2.111(3)	O(1)-V(1)-O(3) = 89.89(10)
V(1)-O(2) = 2.077 (2)	
V(1A)-N(1A) = 2.024(3)	
V(1A)-O(1A) = 1.890 (2)	

Complex of $\{[(TMS)NCH_2CH_2]_2N(TMS)\}_2V(CH_3)(C_5H_5N)$ (6.4a)

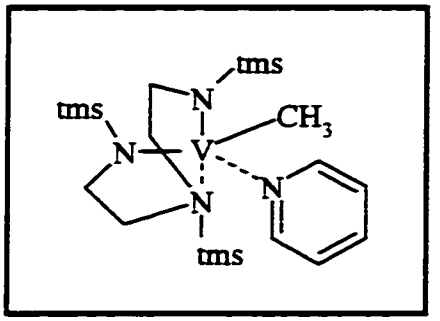

The molecule in figure 6.2 features a trigonal bipyramidal vanadium atom connected to a methyl group and a molecule of pyridine while the other three coordination sites are occupied by the ligand N atoms [C(19)-V-N(1) = 116.65(6)°, C(19)-V-N(3) = 113.85(7)°, C(19)-V-N(4) = 92.62(5)°, C(19)-V-N(2) = 100.94(5)°]. The coordination geometry around the terminal nitrogens is trigonal planar, suggesting a considerable extent of V-N π-donation. In agreement, the V-N distances are noticeably short [V-N(1) = 1.972(1)Å, V-N(3) = 1.925(2)Å] in spite of the considerable bulk of the TMS groups.

Figure 6.2 ORTEP of $\{[(TMS)NCH_2CH_2]_2N(TMS)\}_2V(CH_3)(C_5H_5N)$ (6.4a)

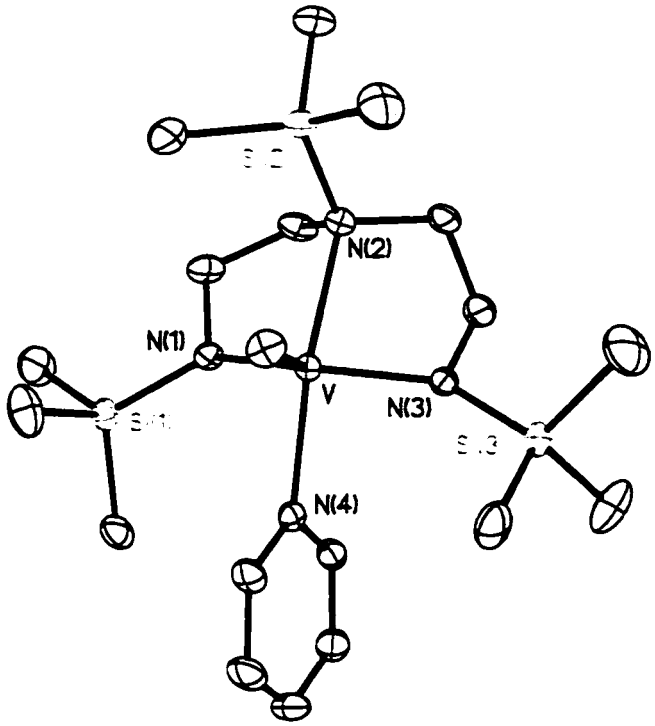

Selected Bond Distances (Å) and Angles (°)

Distances	Angles
V-C(19) = 2.118(3)	C(19)-V-N(1) = 116.65(6)
V-N(1) = 1.972(2)	C(19)-V-N(3) = 113.85(7)
V-N(2) = 2.264(2)	C(19)-V-N(4) = 92.62(5)
V-N(3) = 1.954(2)	C(19)-V-N(2) = 100.94(5)
V-N(4) = 2.157(2)	C(4)-N(1)-Si(1) = 112.9(2)
	C(4)-N(1)-V = 114.2(2)
	Si(1)-N(1)-V = 128.17(13)
	Si(2)-N(2)-V = 118.73(12)
	C(10)-N(3)-Si(3) = 112.6(2)
	C(10)-N(3)-V = 112.5(2)

Complex of $\{[(TMS)NCH_2CH_2]_2N(TMS)\}VCl_2AlCl_3$ (6.5)

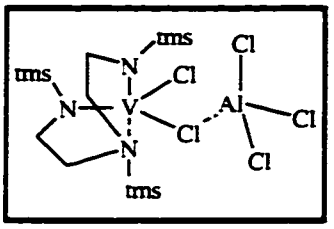

The bimetallic vanadium/aluminium complex has a distorted trigonal bipyramidal and tetrahedral coordination geometry around the vanadium and aluminium centres respectively with the metals being linked by a single bridging chlorine atom [V-Cl(1)-Al = 118.0(6)°] (Figure 6.3). The equatorial plane is comprised of two σ-bonded nitrogens from the silylamino(disilylamido) ligand and one terminal chlorine atom [N(1)-V-N(3) = 124.86(14)°, N(1)-V-N(2) = 79.80(12)°, N(2)-V-Cl(2) = 117.60(11)°, N(2)-V-Cl(1) = 95.71(10)°], while the bridging chlorine atom and the silylamine nitrogen occupy the axial positions [N(2)-V-Cl(1) = 170.63(8)°]. The tetrahedral environment around Al is composed of three σ-bonded chlorine atoms and one bridging atom [Cl(1)-Al-Cl(3) = 107.13(7)°, Cl(1)-Al-Cl(4) = 103.46(7)°, Cl(1)-Al-Cl(5) = 106.32(8)°]. The V-N distances [V-N(1) = 1.815(3)Å, V-N(3) = 1.832(3)Å] are normal and compare well with those of complex **6.3**. The vanadium silylamine distance [V-N(2) = 2.294(3) Å] is longer than in complex **6.3**. The V-Cl distances [V-Cl(1) = 2.4649(14) Å, V-Cl(2) = 2.2441(13) Å] differ slightly from each other probably because one of the chlorine atoms is bridging and the other is terminal. Al-Cl distances follow the same trend where terminal chlorine atoms have slightly shorter Al-Cl distances [Al-Cl(3) = 2.120(2)Å, Al-Cl(4) = 2.1070Å, Al-Cl(5) = 2.108(2)Å] than the bridging Al-Cl distance [Cl(1)-Al = 2.1971(18)Å].

Figure 6.3 ORTEP of $\{[(TMS)NCH_2CH_2]_2N(TMS)\}VCl_2AlCl_3$ (6.5)

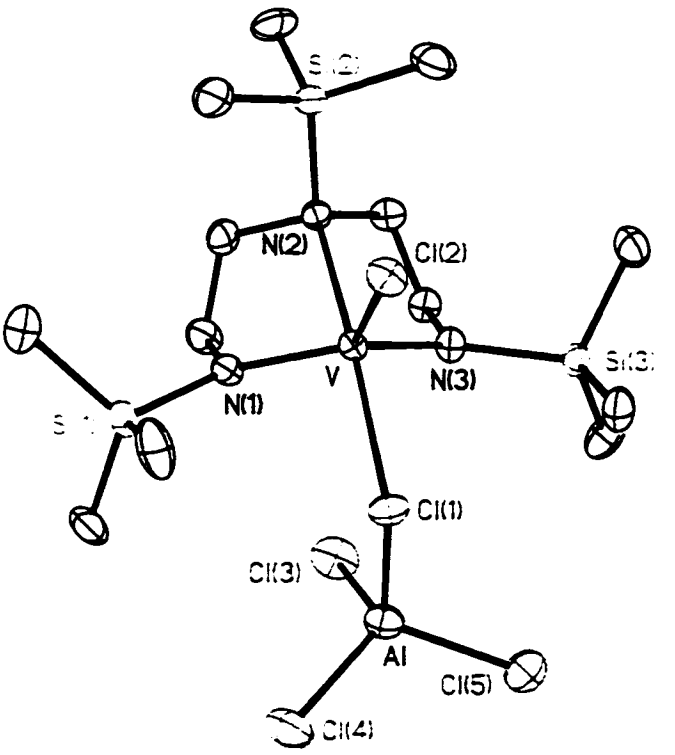

Selected Bond Distances (Å) and Angles (º)

Distances	Angles
V(1)-Cl(1) = 2.510(2)	N(2)-V(1)-Cl = 110.50(14)
V(1)-Cl = 2.4815(17)	N(2)-V(1)-N(3) = 81.6(2)
V(1)-N(1) = 2.217(5)	N(2)-V(1)-N(1) = 81.1(2)
V(1)-N(2) = 2.224(7)	Cl(1)-V(1)-N(1) = 167.9(2)
V(1)-N(3) = 2.233(5)	Cl(1)-V(1)-N(3) = 95.33(16)
Al-N(1) = 1.958(5)	N(1)-V(1)-Cl = 98.89(12)
Al-N(3) = 1.954(6)	Cl-V(1)-N(3) = 167.9(2)
Al-C(14) = 1.970(10)	Cl-V(1)-Cl(1) = 80.64(6)
Al-C(15) = 1.991(9)	V(1)-Cl(1)-V(2) = 99.36(6)
	N(1)-Al-N(3) = 97.3(2)
	N(1)-Al-C(14) = 112.4(3)
	N(1)-Al-C(15) = 111.3(4)

Complex of {[(TMS)($AlCl_2$)NCH_2CH_2]$_2$N(TMS)V} (μ-Cl)$_3$V(μ-Cl)$_3$ {[(TMS)($AlCl_2$)NCH_2CH_2]$_2$N(TMS)V} (6.6)

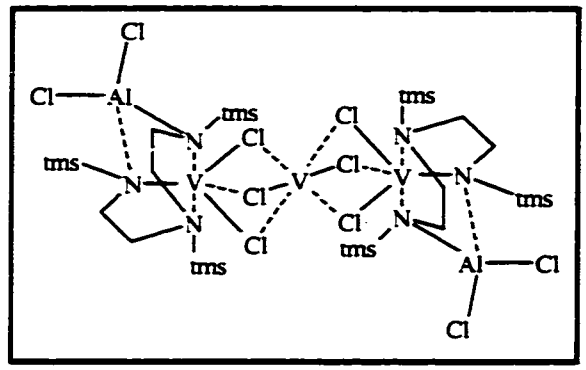

The vanadium/aluminium structure elucidated from X-ray analysis (figure 6.4) presents a symmetry generated complex through an inversion centre with three octahedral vanadium centres and two tetrahedral aluminiumdichloride units bound to the silylamino(disilylamido) ligand. The central vanadium is surrounded by six chlorides which fill the six coordination sites of the octahedron [Cl(1)-V(2)-Cl(2) = 82.74(7)°, Cl(1)-V(2)-Cl(3) = 83.62(8)°, Cl(1)-V(2)-Cl(1)#1 = 180.000(1)°] and is the inversion centre of the complex. The peripheral octahedral vanadium centres have three coordination sites occupied by chlorine atoms and the three others by the three nitrogen atoms of the ligand [Cl(1)-V(1)-N(1) =95.37(15)°, Cl(1)-V(1)-N(2) = 178.53(15)°, Cl(1)-V(1)-N(3) = 97.83(15)°, Cl(1)-V(1)-Cl(3) = 86.03(8)°]. The distorted tetrahedral aluminium centres are bound to two nitrogens from the ligand and to two chlorine atoms [Cl(4)-Al-N(1) = 113.12(19)°, Cl(4)-Al-N(3) = 113.57(18)°, Cl(4)-Al-Cl(5) = 195.97(11)°]. The V-Cl bonds of the central vanadium are within expected range [V(2)-Cl(1) = 2.453(2)Å, V(2)-Cl(2) = 2.456(2)Å, V(2)-Cl(3) = 2.460(2)Å] and are comparable to the values to the V-Cl distances bridging to the peripheral vanadiums [V(1)-Cl(1) = 2.412(2)Å, V(1)-Cl(2) = 2.389(2)Å, V(1)-Cl(3) = 2.389(2)Å]. The V-N distances are longer [V(1)-N(1) = 2.150(5)Å, V(1)-N(2) = 2.158(5)Å, V(1)-N(3) = 2.216(5) Å] than the V-N bonds of complex **6.3** which is most likely a result of the formation of Al-N bonds [Al-N(1) = 1.911(6)Å, Al-N(3) = 1.914(5)Å] which occurred upon the attack of aluminium with the ligand. All other bond distances fall within the expected range and are comparable to those of complex **6.3**.

Figure 6.4 ORTEP of $\{[(TMS)(AlCl_2)NCH_2CH_2]_2N(TMS)V\}$ $(\mu\text{-}Cl)_3V(\mu\text{-}Cl)_3$ $\{[(TMS)(AlCl_2)NCH_2CH_2]_2N(TMS)V\}$ (6.6)

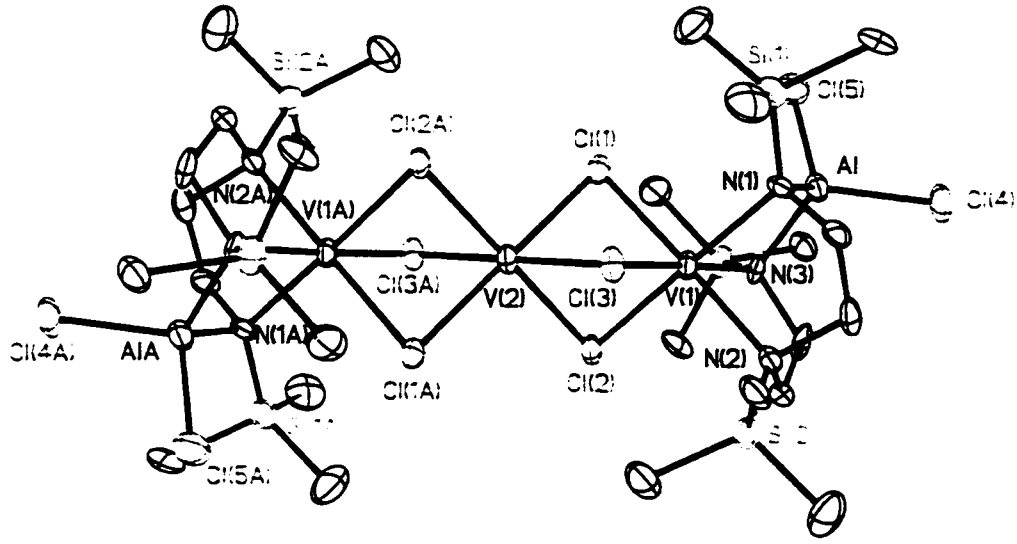

Selected Bond Distances (Å) and Angles (º)

Distances	Angles
V-N(1) = 1.815(3)	N(1)-V-N(3) = 124.86(14)
V-N(2) = 2.294(3)	N(1)-V-N(2) = 79.80(12)
V-N(3) = 1.832(3)	N(2)-V-Cl(2) = 117.60(11)
V-Cl(1) = 2.4649(14)	N(2)-V-Cl(1) = 95.71(10)
V-Cl(2) = 2.2441(13)	V-Cl(1)-Al = 118.0(6)
Al-Cl(3) = 2.120(2)	Cl(1)-Al-Cl(3) = 107.13(7)
Al-Cl(4) = 2.107(2)	Cl(1)-Al-Cl(4) = 103.46(7)
Al-Cl(5) = 2.108(2)	Cl(1)-Al-Cl(5) = 106.32(8)

Complex of {[(TMS) ($Al(CH_3)_2$) $NCH_2CH_2]_2N(TMS)\}_2$ $V_2(\mu\text{-}Cl)_2$ (6.7)

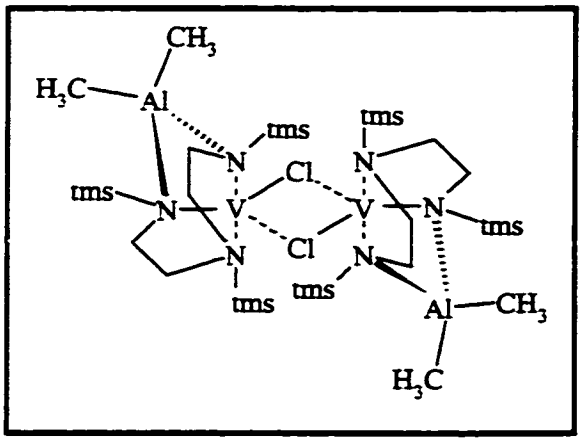

The crystal structure in figure **6.5** shows a vanadium/aluminium complex generated through an inversion centre with two pseudo-square pyramidal vanadium (III) centres bridged by two chlorides [V(1)-Cl(1)-V(2) = 99.36(6)°, Cl-V(1)-Cl(1) = 80.64(6)°] and is reminiscent of complex **6.3** with two additional dimethylaluminium tetrahedral units bound to the silylamino(disilylamido) ligand. The basal plane of each vanadium is defined by the bridging chlorine atoms and two nitrogen atoms of the silylamino (disilylamido) ligand [Cl-V(1)-N(1) = 98.89(12)°, Cl-V(1)-N(3) = 167.9(2)°, Cl-V(1)-Cl(1) = 80.64(6)°, Cl(1)-V(1)-N(3) = 95.33(16)°] and the apical position is occupied by the coordinating silylamine nitrogen of the ligand [N(2)-V(1)-Cl = 110.50(14)°, N(2)-V(1)-N(3) = 81.6(2)°, N(2)-V(1)-N(1) = 81.1(2)°]. The tetrahedral aluminium centre is bound to two methyl groups and to two nitrogen atoms of the tridentate nitrogen-based ligand [N(1)-Al-N(3) = 97.3(2)°, N(1)-Al-C(14) = 112.4(3)°, N(1)-Al-C(15) = 111.3(4)°]. The V-Cl distances are almost equivalent and fall into the expected range for bridging chlorides [V(1)-Cl(1) = 2.510(2)Å, V(1)-Cl = 2.4815(17)Å]. Surprisingly all three V-N bond lengths are quite similar even though formally speaking one nitrogen is σ-bonded and the two others are simply co-ordinated [V(1)-N(1) = 2.217(5)Å, V(1)-N(2) = 2.224(7)Å, V(1)-N(3) = 2.233(5)Å]. The lengthening of the V-N bonds, compared to complex **6.3**, are probably due to the fact that these nitrogens are also bridging to the aluminium atom which is σ–bonded to one nitrogen and co-ordinated to the other [Al-N(1) = 1.958(5)Å, Al-N(3) = 1.954(6)Å]. All other bond distances and angles are as expected.

Figure 6.5 ORTEP of {[(TMS) ($Al(CH_3)_2$) $NCH_2CH_2]_2N(TMS)\}_2$ $V_2(\mu$-$Cl)_2$ (6.7)

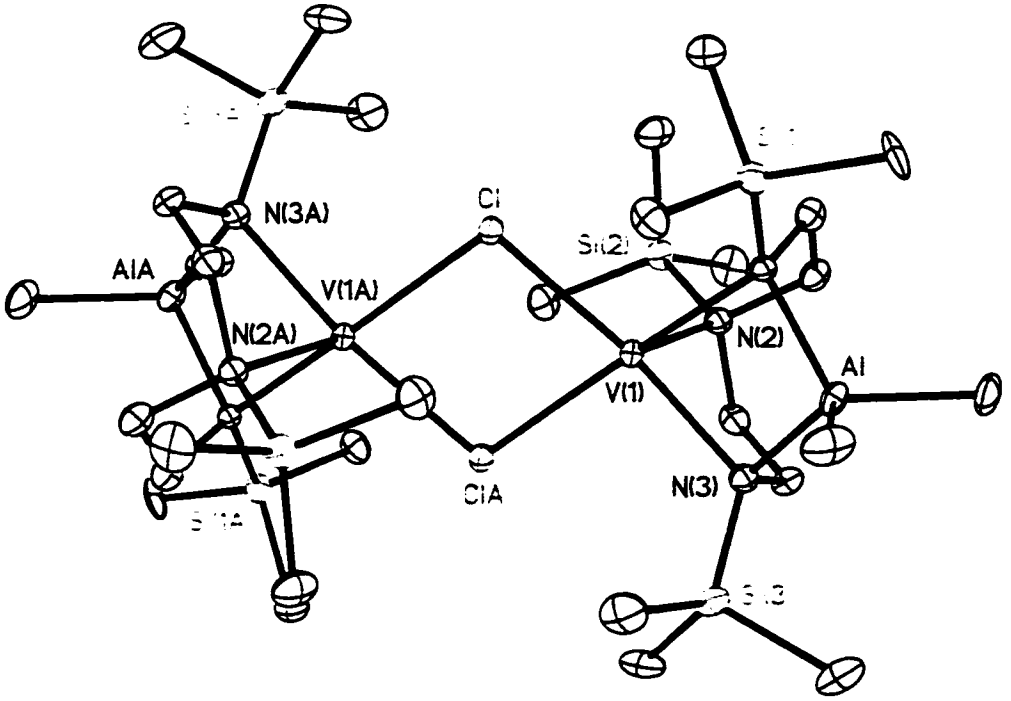

Selected Bond Distances (Å) and Angles (º)

Distances	Angles
V(1)-Cl(1) = 2.412(2)	Cl(1)-V(1)-N(1) =95.37(15)
V(1)-Cl(2) = 2.389(2)	Cl(1)-V(1)-N(2) = 178.53(15)
V(1)-Cl(3) = 2.389(2)	Cl(1)-V(1)-N(3) = 97.83(15)
V(2)-Cl(1) = 2.453(2)	Cl(1)-V(1)-Cl(3) = 86.03(8)
V(2)-Cl(2) = 2.456(2)	Cl(1)-V(2)-Cl(2) = 82.74(7)
V(2)-Cl(3) = 2.460(2)	Cl(1)-V(2)-Cl(3) = 83.62(8)
V(1)-N(1) = 2.150(5)	Cl(1)-V(2)-Cl(1)#1 = 180.00(1)
V(1)-N(2) = 2.158(5)	Cl(4)-Al-N(1) = 113.12(19)
V(1)-N(3) = 2.216(5)	Cl(4)-Al-N(3) = 113.57(18)
Al-N(1) = 1.911(6)	Cl(4)-Al-Cl(5) = 195.97(11)
Al-N(3) = 1.914(5)	

Complex $\{[(TMS)NHCH_2CH_2]_2N\}VCl_2$ (6.9)

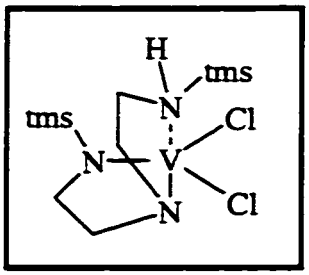

Complex **6.9** presented in figure 6.6 presents a distorted trigonal bipyramidal vanadium centre with two nitrogens in opposition in the two axial coordination sites [N(3)-V-N(1) = 162.23(9)º]. The other three coordination sites of penta-coordinate vanadium are occupied by two chlorides and one nitrogen atom [Cl(1)-V-N(2) = 117.28(8)º , Cl(1)-V-Cl(2) = 128.53(3)º, Cl(1)-V-N(3) = 90.27(7)º]. Unlike complex **6.3**, the V-N distances have clearly changed due to the loss of the trimethylsilyl fragment on the central coordinating nitrogen during the reaction. In the process the nitrogen has acquired an *amido* character which can be acknowledged by shortening of the vanadium/nitrogen bond length [V-N(2) = 1.836(2) Å] and a trigonal planar geometry [C(5)-N(2)-C(6) = 116.8(2)º, C(6)-N(2)-V = 121.9(2)º] with respect to the distance observed in complex **6.3.** A lengthening of the peripheral nitrogens has also been observed as a result of a second vanadium promoted modification to the ligand. Both tetrahedrally distorted nitrogens were hydrogenated and have gained a coordinating character to the vanadium centre [Si(1)-N(1)-V = 124.12(12)º, C(4)-N(1)-V = 102.02(16)º, C(4)-N(1)-Si(1) = 115.83 (18)º, Si(2)-N(3)-V = 121.83(12)º, C(7)-N(3)-V = 103.14(17)º, C(7)-N(3)-Si(2) = 117.17(19)º]. The V-Cl bond lengths are as expected and compare well with those observed in complex **6.3.**

Figure 6.6 ORTEP of {[(TMS)NHCH$_2$CH$_2$]$_2$N}VCl$_2$ (6.9)

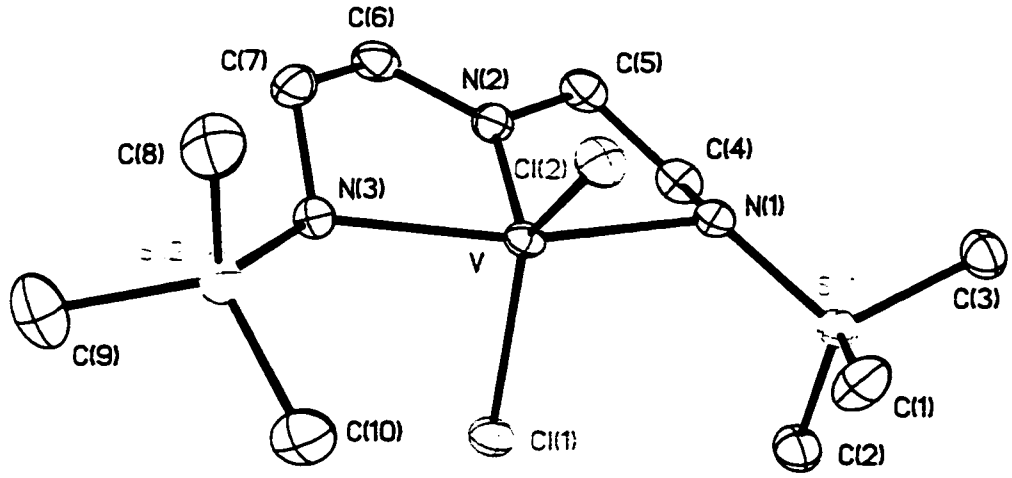

Selected Bond Distances (Å) and Angles (º)

Distances	Angles
V-Cl(1) = 2.3110(9)	Cl(1)-V-N(1) =95.37(15)
V-Cl(2) = 2.3073(8)	Cl(1)-V-N(2) = 178.53(15)
V-N(1) = 2.195(2)	Cl(1)-V-N(3) = 97.83(15)
V-N(2) = 1.836(2)	Cl(1)-V-Cl(2) = 86.03(8)
V-N(3) = 2.183(2)	N(1)-V-N(3) = 162.23(9)
	Si(1)-N(1)-V = 124.12(12)
	V-N(1)-C(4) = 102.02(16)
	C(5)-N(2)-V = 121.30(19)
	C(6)-N(2)-V = 121.9(2)
	C(7)-N(3)-V = 103.13(17)
	V-N(3)-Si(2) = 117.17(19)

6.5 Results and Discussion

The preparation of $[\{V(Me_3Si)N\{CH_2CH_2N(SiMe_3)\}_2\}_2(\mu\text{-}Cl)_2]$ **(6.3)** as a red-violet crystalline material was carried out according to the procedure recently described by Cloke[6.8] via room temperature reaction of $Li_2[(Me_3Si)N\{CH_2CH_2N(SiMe_3)\}_2]$ with $VCl_3(THF)_3$ in THF. The structure unequivocally confirmed the dinuclear nature of **6.3** with the two trigonal bipyramidal vanadium centres linked by two bridging chlorine atoms.

While activated by 60 equivalents of Me_2AlCl, Me_3Al or PMAO-IP, complex **6.3** displayed a substantial activity as an ethylene polymerization catalyst. The activity obtained with PMAO-IP activation (237 g of PE/mmol/hr) was 20 times higher than in the case of Me_3Al, while the highest activity was obtained with Me_2AlCl. The polymers obtained from the different activators and under comparable reaction conditions were very similar. The catalytic activity recorded for polymerization experiments carried out with Me_2AlCl at 50ºC and under 300 psig of ethylene was 660 g of PE/mmol/hr. The polyethylene showed catalyst uni-modality with average molecular weight of 721,000 and polydispersity of 2.3 (Figure 6.7). The melting point of the polymer (133.95°C) indicated that the polyethylene was essentially linear. Not surprising for a vanadium catalyst, the activity decreased at higher temperature (237 g of PE/mmol/hr at 140ºC, 286 psig). Also the polymer displayed lower average molecular weight (135,700) but similar polydispersity (2.7) and the presence of a significant fraction of higher molecular weight polymer (Figure 6.8) indicating that catalyst bimodality takes place at higher temperatures.

Figure 6.7 Differential Molecular Weight Distribution of Polyethylene Produced by Complex 6.3 at 50°C

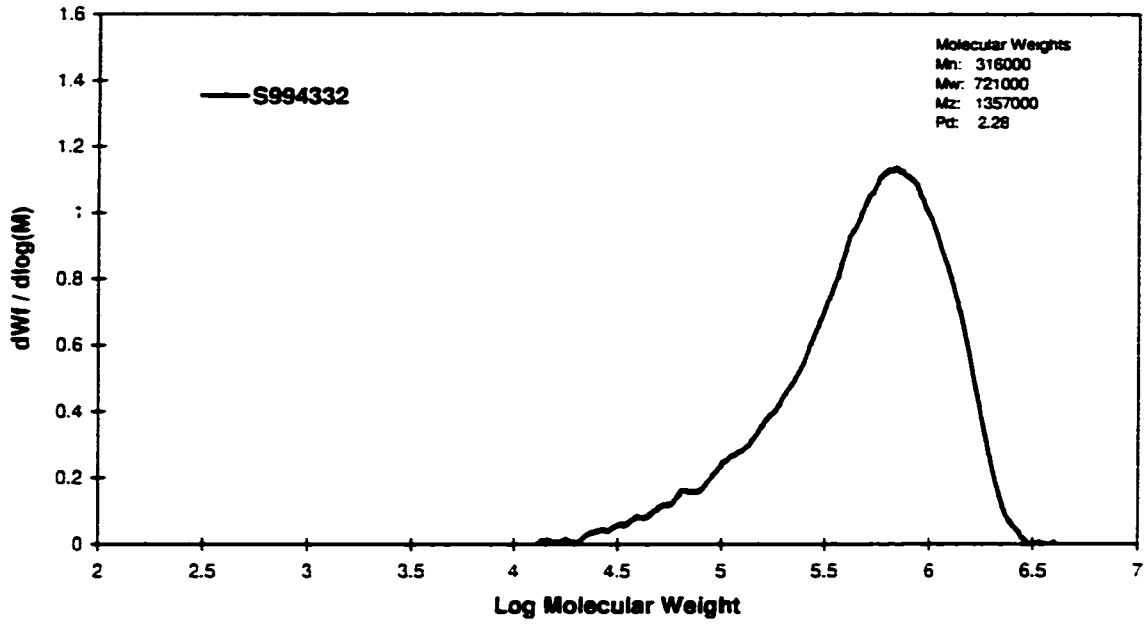

Figure 6.8 Differential Molecular Weight Distribution of Polyethylene Produced by Complex 6.3 at 140°C

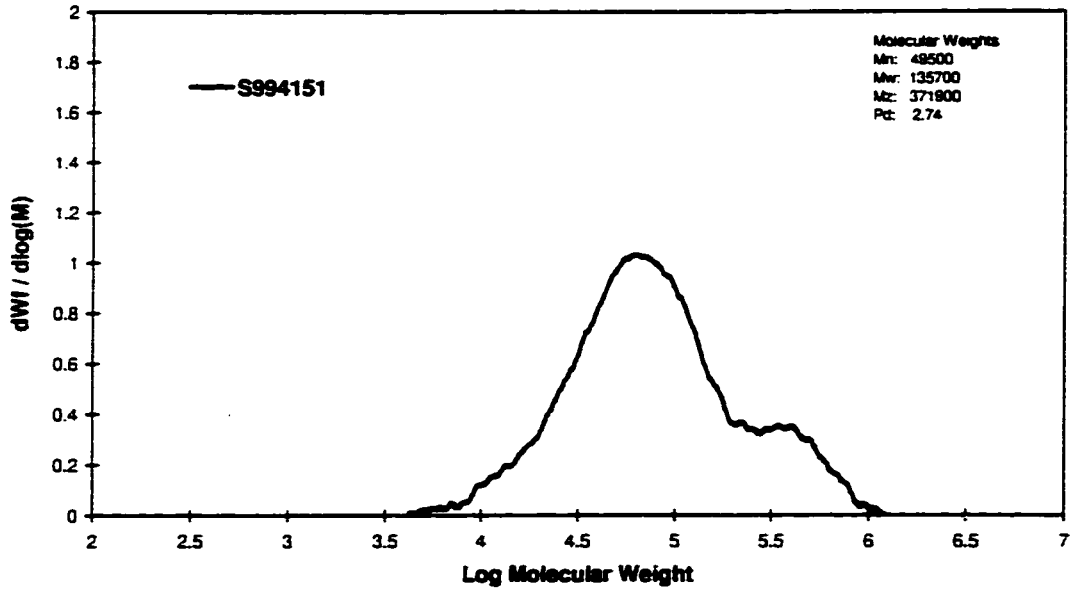

In common with other vanadium catalysts **6.3** is short lived at either 35ºC or 140ºC, typically not remaining active for more than 20-30 minutes, the longest catalyst life having been observed at 50ºC. Such deactivation is usually attributed to reduction of the vanadium center to the inactive divalent state. The reduction is thought to involve loss of the polymeric alkyl chain and is believed to be due to an intrinsic instability of the vanadium-carbon bond. However, we have reported that amide ligands may stabilize tetravalent vanadium alkyls[16] while, by using the silylamino(disilylamido) ligand, Cloke has isolated a mononuclear trimethylsilylmethyl derivative and successfully hydrogenolyzed to produce the corresponding dinuclear and trivalent vanadium hydride.[8] In all these reactions there was no indication of reduction of the vanadium center suggesting that amide ligands indeed provide sufficient stabilization to the V-C function.

Nevertheless, the rapid catalyst failure and the fact that the alkyl derivatives of this system reported before are particularly bulky prompted us to further investigate the ability of this versatile ligand system to support more standard vanadium-alkyls. Complex **6.3** undergoes a rapid reaction with MeLi in hexane resulting in the formation of a greyish precipitate (LiCl) and yielding a complex which was tentatively assigned as a methyl-bridged dimer $[\{V(Me_3Si)N\{CH_2CH_2N(SiMe_3)\}_2\}_2(\mu\text{-}Me)_2]$ probably of very similar structure to **6.3.** Unfortunately, despite repeated attempts we were unable to obtain crystals suitable for an X-ray diffraction study. However, given the release of nearly a stoïchiometric amount of methane gas during degradation experiments carried out with gaseous HCl in a closed vessel connected to a Toepler pump, a structure with methyl-bridges seems the most likely. Furthermore, treatment of the reaction solution with $AlCl_3$ reformed the starting material **6.3** in good yield (Scheme 6.1) and simple

addition of pyridine gave red crystals of $[(Me_3Si)N\{CH_2CH_2N(SiMe_3)\}_2V(Me)(Py)]$ (**6.4a**) in good yield.

Scheme 6.1 Activation Pathway of Complex 6.3

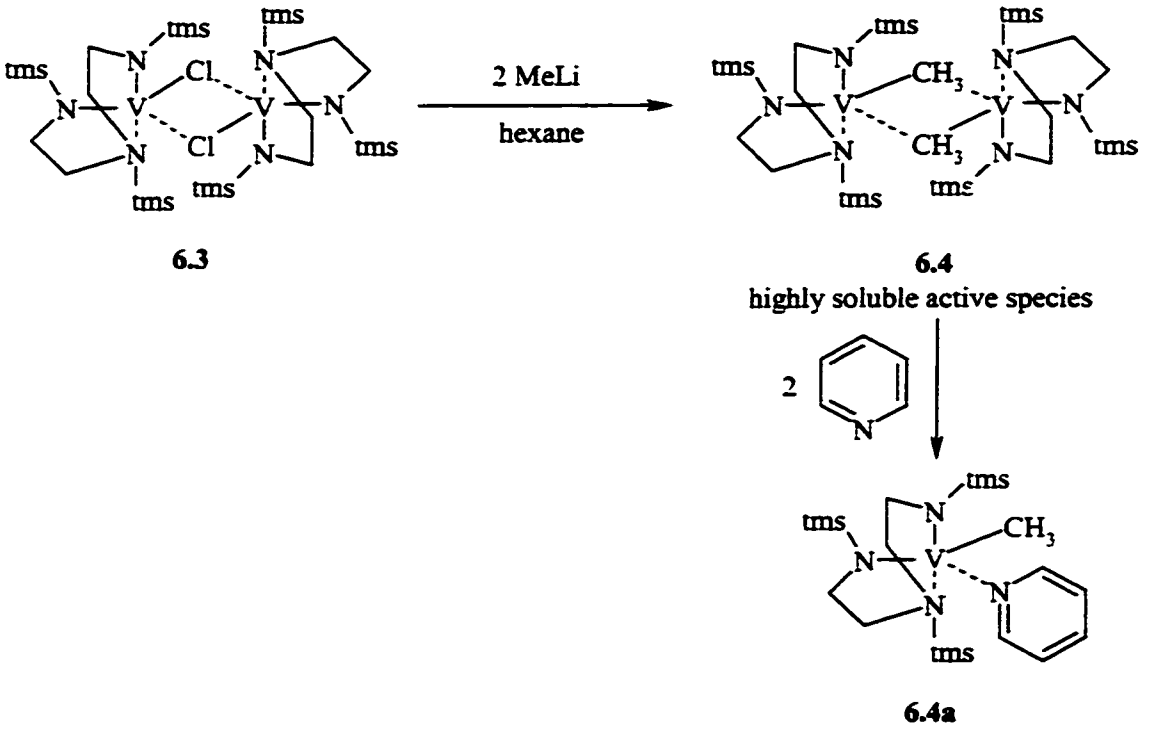

The X-ray crystal structure revealed that **6.4a** is mononuclear and that it has a terminally bonded Me group. Complex **6.4** and its precursor enlarge the meagre list of examples of stable V(III)-alkyl complexes.[5,8] Both are thermally robust since no decomposition was observed in boiling toluene and their unusual stability is likely to be ascribed to the particular nature of the amide ligand.

The versatility of the silylamino silyldiamide ligand to stabilize the vanadium carbon bond reiterates questions about the factors determining the catalyst failure. One possibility, although unlikely, is that the ligand might be leached out of the metal center

by the aluminium cocatalyst with a consequent decrease of the stability of the V-C bond. To rule out this possibility, we determined to study the interaction of **6.3** with the aluminium cocatalyst in the hope of trapping some vanadium-aluminium species. The reaction of **6.3** with either PMAO-IP, $AlMe_3$ or Me_2AlCl in hexane initially gave a red solution, which after a few days afforded emerald-green crystals of the tetrametallic ($\{[(Me_3Si)(Al\ Me_2)NCH_2CH_2]_2N(SiMe_3)\}_2V_2(\mu\text{-}Cl)_2$) (**6.7**) (Scheme 6.2).

Scheme 6.2 Catalyst/Co-catalyst Interaction Leading to Deactivation Over an Extended Period of Time

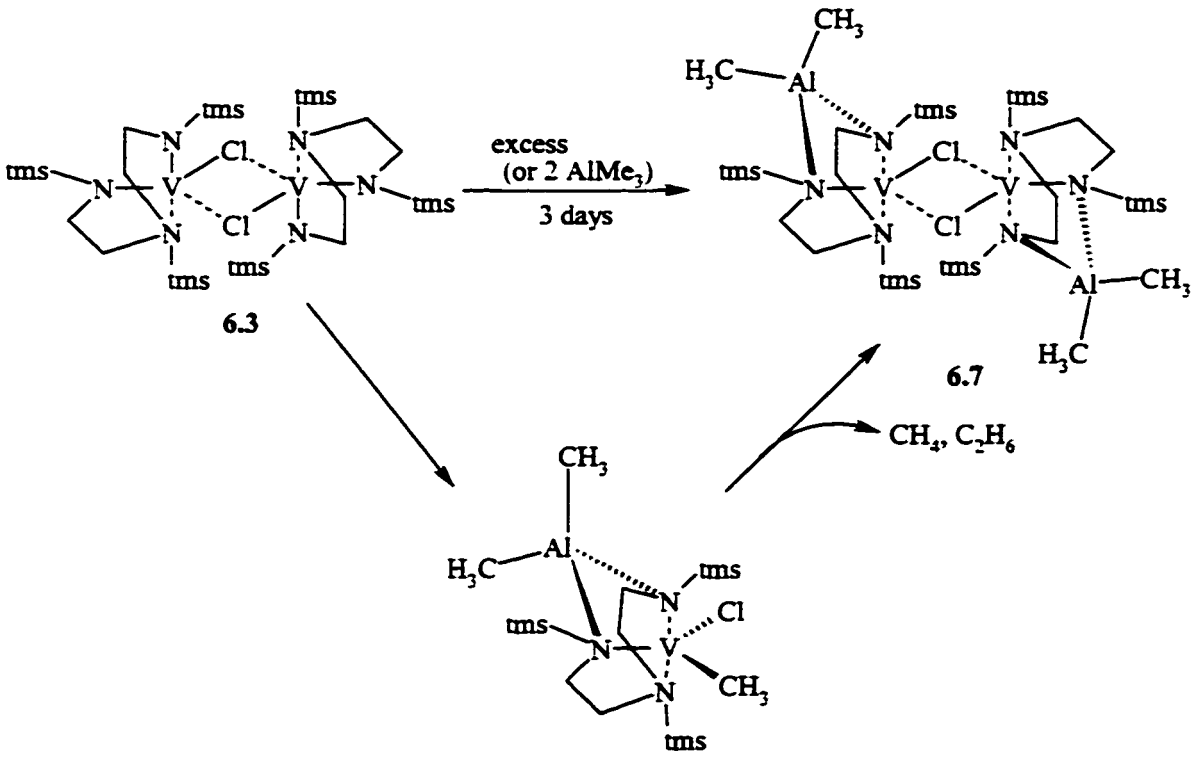

As expected, the best yield was obtained with Me_3Al. The X-ray crystal structure clearly showed that the ligand remains triply bound to the vanadium center. The main frame of the complex is virtually the same as in **6.3** with the two

($\{[(Me_3Si)NCH_2CH_2]_2N(SiMe_3)\}V$) moieties held together by two bridging chlorines. However, there are two major differences. Firstly, two Me_2Al residues are now coordinated each to one ligand's amide nitrogen atoms. Secondly, the vanadium center has been reduced to the inactive divalent state thus accounting for the catalyst failure. The magnetic moment of 3.9 μ_B/vanadium is as expected for the high-spin d^3 electronic configuration of a divalent vanadium center.

The isolation and characterization of **6.7** indicates that no ligand leaching occurs in the present catalytic system but rather aggregation with the co-catalyst. Yet, the vanadium center was reduced to the inactive divalent state. Thus, questions arise about how the reduction occurred given that simple chorine replacement by Me groups afforded thermally stable trivalent methyl derivatives.

In Ziegler-Natta catalysis, PMAO or AlR_3 in general play a dual role as both an alkylating agent and a Lewis acid. In order to separately analyze these two different aspects of the aluminium derivatives, we reacted **6.3** with $AlCl_3$, a pure Lewis acid, with no possibility of functioning as a reducing agent. The reaction was carried out in toluene and afforded a brown solution from which a mixture of two different compounds was obtained. X-ray diffraction of the crystals of the major component revealed the structure to be the hetero-bimetallic and tetravalent $[(Me_3Si)N\{CH_2CH_2N\ (SiMe_3)\}_2V(Cl)(\mu\text{-}Cl)AlCl_3]$ (**6.5**) which is basically the result of the coordination of $AlCl_3$ to the tetravalent $[(Me_3Si)N\{CH_2CH_2N(SiMe_3)\}_2VCl_2]$ via sharing of one of the two vanadium chlorine atoms. The tetravalent oxidation state of vanadium was also confirmed by the measurement of the magnetic moment, which is consistent with a d^1 electronic configuration (1.83 μ_{BM}).

The second component of the reaction mixture is particularly intriguing. The complex is a mixed valence V(II)/V(III) hetero-bimetallic pentamer [{[$(SiMe_3)(AlCl_2)N$ $CH_2CH_2]_2(Me_3Si)NV$}$(\mu\text{-}Cl)_3V(\mu\text{-}Cl)_3$[$(SiMe_3)(AlCl_2)NCH_2CH_2]_2(Me_3Si)NV$}] $(toluene)_2$ **(6.6)**, in which there are two vanadium atoms *formally* in the +3 oxidation state and one in the +2. Unfortunately, while complex **6.6** was obtained in analytically pure form, samples of **6.5** were invariably contaminated by variable amounts of **6.6** thus preventing a satisfactory analytical characterization.

The simultaneous formation of both **6.5** and **6.6** clearly indicates that $AlCl_3$ triggers a disproportionation reaction through which V(II) and V(IV) species are formed. The fact the central vanadium atom in complex **6.6** has been stripped of the ligand system clearly indicates that ligand leaching indeed occurred in spite of the ligand tridenticity and the higher affinity of vanadium for nitrogen donor atoms compared to aluminium. However, the fact that two $AlCl_2$ residues are connected to the periphery of the trimetallic cluster in a fashion which is identical to the coordination of the $AlMe_2$ residues in **6.7** indicates that: 1) the ligand leaching is only partial and probably governed by an equilibrium; 2) there is a common trend in the behaviour of **6.3** with both Me_3Al and $AlCl_3$. Complex **6.6** may be regarded as resulting from the *formal* aggregation of **6.3** with $AlCl_3$ and VCl_2 residues obviously generated as a partner of the oxidation to **6.5**. Thus it is tempting to rationalize the formation of the mixture of **6.5** and **6.6** in terms of initial partial reaction of **6.3** with $AlCl_3$ to afford VCl_3 and $[(Me_3Si)N\{CH_2CH_2N(SiMe_3)\}_2Al(Cl)]$ (Scheme 6.3). The association of VCl_3 with **6.3** triggers a disproportionation reaction to the tetravalent [$(Me_3Si)N\{CH_2$

$CH_2N(SiMe_3)\}_2VCl_2$ (**6.8**) and "VCl_2". This residue may react with both unreacted **6.3** and $AlCl_3$ to form **6.6**.

Scheme 6.3 Pro-catalyst/Co-catalyst Interaction using $AlCl_3$

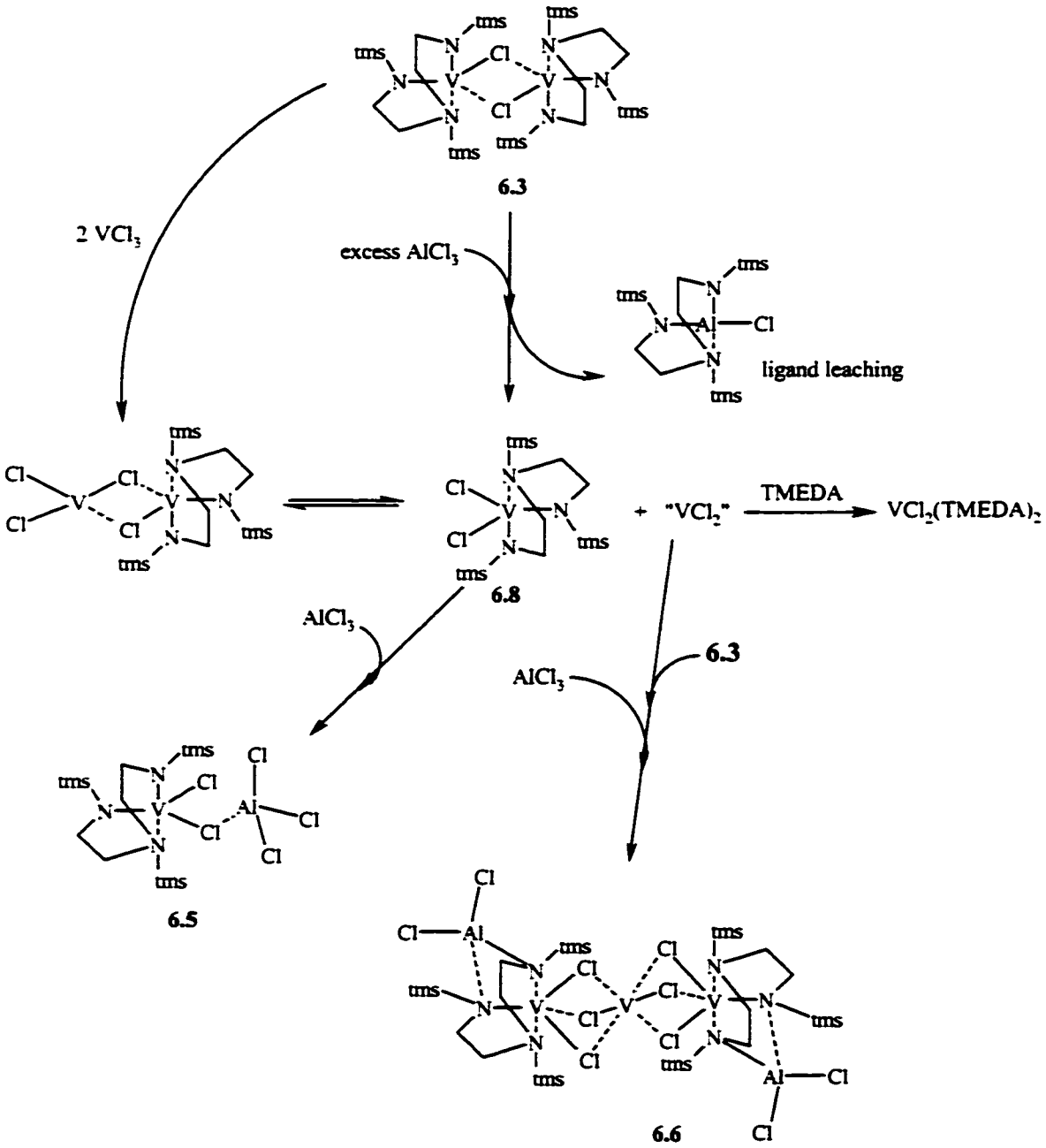

In agreement with this proposal, reaction of **6.3** with anhydrous VCl_3 in toluene indeed afforded a mixture of **6.8** (isolated from crystallization from hexane) and a poorly soluble residue which was redissolved in boiling THF and precipitated upon treatment with TMEDA as $VCl_2(TMEDA)_2$.[17] Finally, complex **6.8**, which was conveniently obtained via oxidation of **6.3** with Ph_3PCl_2, reacts with $AlCl_3$ to afford **6.6**.

Thus, the isolation of both tetra- and divalent vanadium species in the reaction of **6.3** with $AlCl_3$ clearly indicates that a disproportionation is at the basis of the reduction of the vanadium center. However, the fact that a vanadium atom in **6.5** has retained its ligand system and yet has been reduced strongly suggests that no ligand leaching occurred during the reaction of **6.3** with $AlMe_3$ as it should be expected given its lower Lewis acidity. Thus, the only possibility to explain the reduction of the metal center in the case of **6.5** is to assume that the addition intermediate $(Me_2Al)\{(Me_3Si)N[CH_2CH_2N(SiMe_3)]_2\}VClMe$, which is also likely to be the catalytically active species, has an intrinsic instability of the V-C bond (Scheme 6.2). Accordingly, a substantial amount of methane and a small amount of ethane was identified in the gas chromatograph of the reaction mother liquor.

Further reactivity was investigated with **6.1** to probe its reactivity with V(IV). Complex 6.1 was treated with one equivalent of ^{n}Bu-Li to make the monolithium salt of the ligand in attempt to induce the loss of one trimethylsilane group upon reaction with $VCl_4(DME)$. Brown crystals of complex **6.9** were obtained from diethyl ether and the single crystal x-ray structure revealed the loss of one trimethylsilane group yielding a tridentate dianionic ligand bound to a V(IV) metal center as observed through the magnetic susceptibility measurement bearing a value of 1.98 BM (see scheme 6.4).

Scheme 6.4 Preparation of Complex 6.9

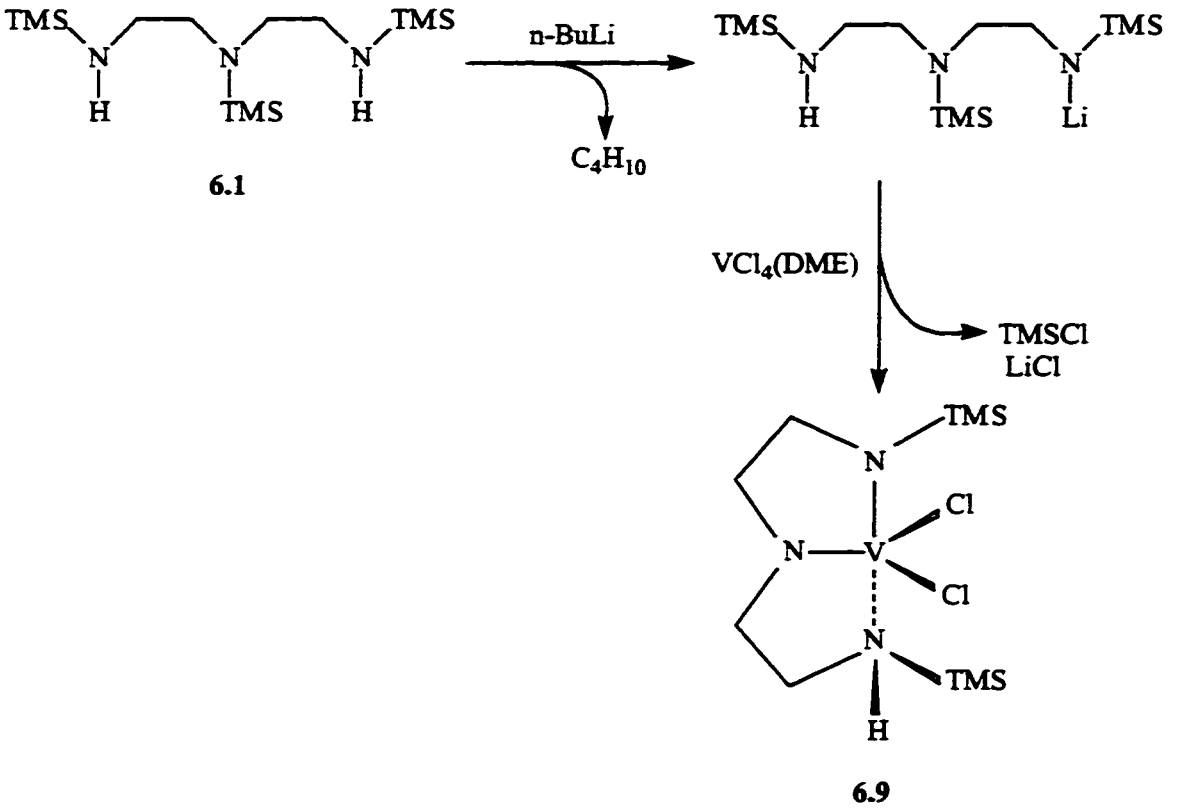

Preliminary ethylene polymerization studies were probed and yielded highly crystalline polyethylene, which was insoluble in conventional solvents used for room temperature gel permeation chromatography analysis. Activities for complex **6.9** were moderately low (82.2 g $mmol^{-1}$ atm^{-1} h^{-1}) when activated with $AlMe_3$ and slightly higher when activated with polymethylalumoxane (PMAO) where activities were in the range of 215 g $mmol^{-1}$ atm^{-1} h^{-1}). Further characterization of the polymer as well as activation reactions of complex **6.9** with alkylating reagents or with different co-catalysts will be the subject of additional experimental studies.

6.6 Conclusion

This work has allowed the isolation of a few novel vanadium aluminium clusters supported by the trimetylsylilamino(trimethylsilyldiamido) ligand. While the ligand system is capable of aggregating together vanadium and aluminium residues, the complete abstraction of ligand from vanadium, responsible for triggering disproportionation towards di- and tetravalent vanadium, is determined by the Lewis acidity of the aluminium co-catalyst, i.e. the chlorine content. In spite of the ability of this ligand system to stabilize both mono- and dinuclear trivalent vanadium alkyl derivatives and even in the event where ligand leaching did not occur, the vanadium atom was reduced. This is likely due to an intrinsic instability of the V-C bond of a alkyl/halide intermediate. Thus the search for long-lasting catalysts must be directed towards exploration for new ligand systems capable of stabilizing V-C functions even further.

6.7 References

1. See for example:

(a) Mohring, P. C.; Coville, N. J. *J. Organomet. Chem.*, 1994, **479**, 1.

(b) Erker, G.; Nolte, R.; Tsay, Y. H.; Kruger, C. *Angew. Chem.*, 1989, **28**, 628.

(c) Erker, G.; Nolte, R.; Aul, R.; Wilker, S.; Kruger, C.; Noe, R. *J. Am. Chem. Soc.*, 1991, **113**, 7594.

(d) Kaminsky, W.; Kulper, K.; Brintzinger, H. H.; Wild, R. W. P. *Angew. Chem. Int. Ed. Engl.*, 1985, **6**, 507.

(e) Coates, G. W.; Weymouth, R. M. *J. Am. Chem. Soc.*, 1991, **113**, 6270.

(f) Ewen, J. A. *J. Am. Chem. Soc.*, 1984, **106**, 6355.

(g) Guerra, G.; Cavallo, L.; Moscardi, G.; Vacatello, M.; Corradini, P. *J. Am. Chem. Soc.*, 1994, **116**, 2988.

(h) Jordan, R. F. *Adv. Organomet. Chem.* **1991**, *32*, 325.

(i) Brintzinger, H. H.; Fisher, D.; Mulhaupt, R.; Rieger, B.; Waymouth, R. M. *Angew. Chem. Int. Ed. Engl.* **1995**, *34*, 1143

(j) Bochmann, M. *J. Chem. Soc. Dalton Trans.* **1996**, 255.

2. See for example:

(a) Doi, Y., Suzuki, S.; Soga, K. *Macromolecules*, 1986, **19**, 2896.

(b) Ouumi, T.; Soga, K. *Makromol. Chem.*, 1992, **193**, 823.

(c) Gumbolt, A.; Helberg, J.; Schleitzer, G. *Makromol. Chem.*, 1967, **101**, 229.

(d) Adisson, E. *J. Polym. Sci., Part A: Polym. Chem.*, 1994, **32**, 1033.

(e) Davis, S. C.; von Hellens, W.; Zahalka, H. *Polymer Material Encyclopedia Vol. 3*; Salamone, J. C., Ed.; CRC Press Inc.; Boca Raton, FL, 1996.

(f) Sinn, H.; Kaminski, W. *Adv. Organomet. Chem.*; Stone, F.G.A.; West R. Eds.; Academic Press: New York, **1980.**

(g) Doi, Y.; Tokuhiro, N.; Nunomura, M.; Miyake, H.; Suuki, S.; Soga, K. *Transition Metals and Organometallics as Catalysts for Olefin Polymerization*; Kaminsky, W.; Sinn H. Eds.; Springer-Verlag: Berlin, **1988.**

(h) Carrick, W. L. *J. Am. Chem. Soc.* **1958**, *80*, 6455.

(i) Christman, D. L. *J. Polymer Sci.* **1972**, *A-1*, 471.

(j) Pasquon, I. G.; Giannini, U. *Catalysis*; Anderson, J. R.; Boudart, M. Eds.; Springer-Verlag: Berlin, **1984.**

(k) Carrick, W. L.; Kluiber, R. W.; Bonner, E. F.; Wartman, L. H.; Rugg, F. M.; Smith J. J. *J. Am. Chem. Soc.* **1960**, *82*, 3883.

(l) Lehr, M. H. *Macromolecules* **1968**, *1*, 178.

(m) Christman, D. L.; Keim, G. I. *Macromolecules* **1968**, *1*, 358.

(n) Lehr, M. H.; Carmen, C. J. *Macromolecules* **1969**, *2*, 217.

(o) Duck, E. W.; Grant, D.; Horder, J. R.; Jenkins, D. K.; Marlow A. E.; Wallis, S. R.; Doughty, A. G.; Maradon, J. M.; Skinner, G. A. *European Polymer J.* **1974**, *10*, 481.

(p) Schuere, S. : Fisher, J.; Kress, J. *Organometallics* **1995**, *14*, 2627.

(q) Feher, F. J.; Blanski, R. L. *J. Am. Chem. Soc.* **1992**, *114*, 5886.

(r) Feher, F. J.; Walzer, J. F.; Blanski, R. L. *J. Am. Chem. Soc.* **1991**, *113*, 3618.

(s) Feher, F. J.; Blanski, R. L. *Organometallics* **1993**, *12*, 958.

(t) Cucinella, S.; Mazzei A. U.S. Patent 3,711,455, CL 260-85.3 **1973.**

(u) Boor Jr., J.; Youngman, E. A. *J. Polymer Sci* **A-1**, **1966**, *4*, 1861.

(v) Zambelli, A.; Proto, A.; Longo, P. *Ziegler Natta Catalysis*; Fink, G.; Mulhaupt, R.; Brintzinger, H. H. Eds., Springer-Verlag Berlin, **1995.**

3. Ma, Y.; Reardon, D. F.; Gambarotta, S.; Yap, G. P. A. *Organometallics*, 1999, **18**, 2773.

4. Guram, A. S.; Jordan, R. F. in *Comprehensive Organomet. Chemistry*; Abel, E. W.; Stone F. G. A; Wilkinson, G. Eds. Pergamon **1995** and ref. cited therein.

5. Non-Cp and stable vanadium alkyls are rare compounds. See for example:

(a) Seidel, W., Kreiseli, G. *Z. Anorg. Allg. Chem.*, 1977, **435**, 146.

(b) Gambarotta, S.; Floriani, C.; Chiesi-Villa, A.; Guastini, G. *J. Chem. Soc.*, 1984, 886.

(c) Gambarotta, S.; Mazzanti, M.; Floriani, C.; Chiesi-Villa, A.; Guastini, G. *J. Chem. Soc.*, 1985, 829.

(d) Solari, E.; De Angelis, S.; Floriani, C.; Chiesi-Villa, A.; Rizzoli, C. *Inorg. Chem.*, 1992, **31**, 96.

(e) Wills, A. R.; Edwards, P. G. *J. Chem. Soc., Dalton Trans.*, 1989, 1253.

(f) Gambarotta, S.; Floriani, C.; Chiesi-Villa, A.; Guastini, C., *J. Chem. Soc. Chem. Commun.*, **1984**, 886:

(g) Buijink, J. K.; Meetsma, A.; Teuben, J. H. *Organometallics* **1993**, *12*, 2004;

(h) Berno, P.; Gambarotta, S.; Richeson, D. in *Comprehensive Organometallic Chemistry II*, Abel, E. W.; Stone, F. G. A.; Wilkinson, G. Eds.; Oxford 1995 and references cited therein.

6. Clancey, G. P.; Clark, H. C. S.; Clentsmith, G. K. B.; Hitchcock, P. B.; Cloke, F. G. N. *J. Chem. Soc., Dalton Trans.*, **1999**, 3345.

7. Gol'din, G. S.; Baturina, L. S.; Gavrilova, T. *Zh. Obshch. Khim.* **1975**, *45*, 2189.

8. Clentsmith, G. K. B.; Bates, V. M. E.; Hitchcock, P. B.; Cloke, F. G. N. *J. Am. Chem. Soc.*, 1999, **121**, 10444.

9.(a) Cloke, F. G. N.; Love, J. B.; Hitchcock, P. B. *J. Chem. Soc., Dalton Trans.*, **1995**, 25.

(b) Love J. B.; Clark, H. C. S.; Cloke, F. G. N.; Green, J. C.; Hitchcock, P. B. *J. Am. Chem. Soc.* **1999**, *121*, 6843.

10. Clark, H. C. S.; Cloke, F. G. N.; Hitchcock, P. B.; Love, J. B.; Wainright, A. P. *J. Organomet. Chem.*, **1995**, *503*, 333.

11. Horton, A. D.; De With, J.; Van de Linden, A. J.; Van de Weg, H. *Organometallics*, **1996**, *15*, 2672.

12. Manzer, L. E. *Inorg. Synth.*, **1982**, *21*, 138.

13. Mabbs, M. B.; Machin, D. *Magnetism and Transition Metal Complexes*; Chapman and Hall: London, 1973.

14. Foese, G.; Gorter, C. J.; Smits, L. J., *Constantes Selectionnées Diamagnetisme, Paramagnetisme, Relaxation Paramagnetique*; Masson: Paris, 1957.

15. Blessing, R., *Acta Cryst.*, **1995**, *A51*, 33-38.

16. Desmangles, N.; Gambarotta, S.,; Bensimon, C.; Davis, S.; Zahalka, H. *J. Organomet. Chem.* **1997**, *562*, 53.

17. Edema, J. J. H.; Stauthamer, W.; Gambarotta, S.; van Bolhuis, F.; Smeets, W. W. J.; Spek, A. *Inorg. Chem.* **1990**, *29*, 1302.

Chapter 7

Probing the Reactivity of *Meso*-Diphenyldipyrrolemethane Salts with Zr(IV), V(III), Cr(III) and Cr(II). Insight on How to Increase the Polymerization Potential of V(III) Polymerization Catalysts.

Abstract

***Chapter** 7 presents a preliminary study on the reactivity of the meso-diphenyldipyrrolidemethane ligand with Zr(IV), V(III), Cr(III) and Cr(II) which gave some insight into the different bonding modes of the pyrrolide moiety. The π-bonding mode is clearly presented in the structure of the Zr(IV) organometallic polymer with the following monomer unit, $\{[Ph_2C(C_4H_3N)_2]Zr_2Cl_7Li\}_n$ (7.4), formed upon reacting the ligand in a 2:1 stoïchiometry with $ZrCl_4$ in the absence of THF. Addition of THF, leads to the decomposition of the polymeric superstructure and leads to the formation of $[Ph_2C(C_4H_3N)_2]ZrCl_2(THF)_2$ (7.2). Reaction of the salt of the ligand with $VCl_3(THF)_3$ afforded dark reddish-brown crystals $[Ph_2C(C_4H_3N)_2VCl(THF)_2]_2$ (7.5) which was iso-structural with the Cr(III) complex, $[Ph_2C(C_4H_3N)_2CrCl(THF)_2]_2$ (7.7), obtained from the reaction of $CrCl_3(THF)_3$ and the ligand. Reactivity was also probed with $CrCl_2(THF)_2$ to yield $[Ph_2C(C_4H_3N)_2CrCl]_2 \cdot 2\ Li(THF)_4$ (7.8). In the case of 7.5, further reactivity was needed to render catalytic activity. This was done through the elimination of coordinated THF solvent molecules by replacing the chlorides with bulky oxygen-donor ligands that occupy the THF coordination sites as seen in the X-ray structure of complex 7.6. The structure of 7.6 demonstrates that the replacement of chlorides in complex 7.5 was a non-trivial reaction involving deoxygenation of one aryloxide. Complex 7.7 was treated in a similar fashion although the addition of the potassium salt of BHT lead to ligand scrambling yielding $[Ph_2C(C_4H_3N)_2]_2Cr(THF)_2K(THF)$ (7.9).*

7.1 Introduction

In the last five years, three of the major poly-α-olefin manufacturers (DSM, DOW, Exxon) have patented a new powerful single-site group IV catalyst supported by a ligand system combining a cyclopentadienyl ring with a pendant arm bearing a nitrogen donor amido functional group (constrained geometry complexes). The ligand system is an ingenious variation on the *ansa*-metallocene catalysts, which yield high polymerization

activities and narrow polydispersities, properties that are critical in tailoring polymers for specific industrial applications. This discovery encourages research of novel bulky ligand systems steering away from the *Cp*-based, group IV, d^0 complexes[1] popular in homo- and co-polymerization developed in the 1980's. More recently, a series of nitrogen based ligands have been developed which support high catalytic activity with both early[2] and late transition metals which use less or even no co-catalyst[3] and are less prone to deactivation by impurities in the polymerization medium.

In light of these findings, a novel ligand system based on pyrroles combines both: 1) the possibility of binding in an η^1 fashion through σ–electron donation or in an η^5-fashion via π-electron donation to the metal center and 2) the presence of a nitrogen donor group which acts as an amido upon deprotonation.

Scheme 7.1 Bonding Modes of the Pyrrole Ring

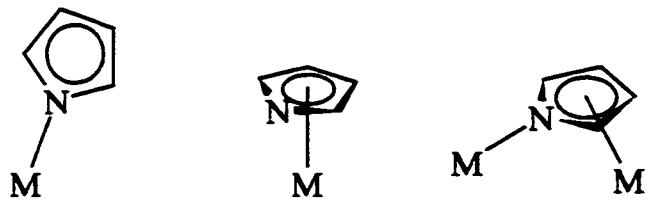

σ-bonding π-bonding σ/π-bridging

The chemistry of the *meso*-diphenyldipyrrolemethane as a supporting ligand system to low valent lanthanides was explored and has established a rich foundation in the chemistry of low-valent samarium clusters including the isolation of novel dinitrogen and hydrido cluster complexes[4] which exhibit the σ/π-bridging bonding mode. The mono-anionic pyrrolide ring acts to our knowledge in an η^5-bonding mode only in the

presence of "soft" metal atoms with diffuse orbitals. Other pyrrolide ligands such as porphirynogens demonstrate that the σ-bonding is the dominant binding mode to "harder" metal atoms, such as early transition metals[5]. In the case where a coordination site could be vacated the ligand could revert back and forth from a σ– to a π–donation to the metal center.

Another interesting feature of the pyrrolide moiety is the possibility of coordinating other ions such as K^+, Na^+, Li^+.[6] We were interested in this π-coordination feature since the cationic Ziegler-Natta process is an ionic process and would possibly lead to the isolation of the much sought after intermediate catalytic species which hypothetically would include the aluminium co-catalyst in some ionic form or another.

In the present study, we describe the result of a preliminary investigation of the reactivity of the *meso*-diphenyldipyrrolidemethane complexes of Zr(IV), V(III), Cr(III) and Cr(II).

7.2 Experimental Section

All operations were performed under inert atmosphere by using standard Schlenk type techniques. $ZrCl_4$ (Aldrich), pyrrole, benzophenone and the polymethylalumoxane solution (13.5% Al) in toluene (PMAO-IP, AKZO) were used as received without further purification. $VCl_3(THF)_3$[7], $ZrCl_4(THF)_2$[7], $CrCl_3(THF)_3$[7], $CrCl_2(THF)_2$[8] were synthesized according to published procedures. Infrared spectra were recorded on a Mattson 9000 and Nicolet 750-Magna FTIR instruments from Nujol mulls prepared in a dry box. Samples for magnetic susceptibility measurements were weighed inside a dry box equipped with an analytical balance and sealed into calibrated tubes. Magnetic measurements were carried out with a Gouy balance (Johnson Matthey) at room temperature. Magnetic moments were calculated following standard methods.[9] and corrections for underlying diamagnetism were applied to data.[10] Elemental analyses were carried out with a Perkin-Elmer 2400 CHN analyzer. Data for X-ray crystal structure determination were obtained with a Bruker diffractometer equipped with a SMART CCD area detector. NMR analysis were carried out on Varian Gemini 200 and Bruker AMX-500 spectrometers using vacuum sealed NMR tubes prepared inside a dry-box.

Preparation *meso*-diphenyldipyrromethane (7.1)[11]

In a 100 ml round-bottom flask filled with 60 ml of 99 % ethanol, 27 g (0.15 mol) of benzophenone and 0.5 ml of methanesulphonic acid was stirred and heated at 60-70° until benzophenone was completely dissolved. Then, neat pyrrole (10 ml, 0.14 mol) was added over a period of 30 minutes. The mixture was stirred at 60-70°C for 4 hours. The colour of the solution changed from dark-red to dark-brown. Stirring was discontinued and 100 ml of 99% EtOH were added. The solution was allowed to crystallize at 50°C.

The resulting red solid was filtered and washed with portions of warm absolute EtOH (100 ml, 50°C) until complete discoloration. The compound was dried in vacuo yielding analytically pure diphenyldipyrromethane (5.8 g, 19.5 mmol, 13%). m.p.:258°C. M.S.-E.I. m/e$^+$: 298. IR (KBr, Nujol mull, cm^{-1}) ν: 3412 (s), 3360 (s), 1660 (w), 1596 (m), 1544 (m), 1454 (vs), 1409 (m), 1377 (vs), 1255 (w), 1229 (w), 1184 (m), 1080 (s), 1029 (s), 887 (m), 797 (s), 733 (vs), 701 (vs), 624 (m), 514 (s). ^{1}H NMR ($CDCl_3$, 200 MHz, 25°C), δ (ppm): 7.92 (broad s, CH-phenyl, 2H), 7.25 (m, CH-phenyl, 8H), 7.10 (m, CH-pyrrole, 4H), 6.74 (m, CH-pyrrole, 2H), 6.17 (pseudo-quadruplet, CH-pyrrole, 2H), 5.93 (m, CH-pyrrole, 2H). ^{13}C NMR ($CDCl_3$, 500 MHz, 25°C) δ (ppm): 150.0 (s, C-phenyl), 149.0 (s, C-pyr), 128.8 (CH-phenyl), 128.5 (CH-phenyl), 127.4 (CH-phenyl), 117.1 (CH-pyrrole), 110.2 (CH-pyrrole), 108.6 (CH-pyrrole), 59.2 (C-aliphatic). Anal. Calcd (found) for $C_{21}H_{18}N_2$: C 84.53 (84.44), H 6.08 (5.99), N 9.39 (9.31).

Preparation of $[Ph_2C(C_4H_3N)_2]ZrCl_2(THF)_2$ (7.2)

Meso-diphenyldipyrromethane (1 g, 3.36 mmol) was dissolved in 100 ml of THF. The addition of two equivalents of KH (0.27 g, 6.72 mmol) at –78°C produced a vigorous gas evolution. The solution was stirred for one hour leaving a clear colourless solution. To this solution, one equivalent of $ZrCl_4(THF)_2$ (1.27 g, 3.36 mmol) was added at room temperature forming a yellow/orange solution which was stirred overnight. The solution was evaporated to dryness and the residue was suspended in 50 ml of dry toluene. The white precipitate (KCl), was filtered off and the clear solution was left to crystallize over a period of ten days. IR (Nujol mull, cm^{-1}): 3195 (m), 1595 (m), 1550 (w), 1456 (s), 1377 (m), 1308 (m), 1261 (m), 1230 (m), 1171 (m), 1155 (m), 1136 (w), 1097 (s), 1078 (s), 1045 (m), 1032 (m), 916 (m), 902 (m), 889 (w), 841 (m), 798 (m), 721 (s), 700 (m), 637

(w). ^{1}H NMR (THF-d_8, ppm): 7.15 (m, C*H*-phenyl, 6H), 7.03 (m, C*H*-phenyl, 4H), 6.70 (m, C*H*-pyrrolide, 2H), 5.98 (m, C*H*-pyrrolide, 2H), 5.73 (m, C*H*-pyrrolide, 2H), 3.58 (m, C*H*-THF, 4H), 1.73 (m, C*H*-THF, 4H). ^{13}C NMR (THF-d_8, ppm): 148.22 (q, C-pyrrolide), 136.51 (q, C-phenyl), 130.44 (*C*H-phenyl), 128.01 (*C*H-phenyl), 125.91 (*C*H-phenyl), 118.36 (*C*H-pyrrolide), 110.33 (*C*H-pyrrolide), 107.36 (*C*H-pyrrolide), 67.4 (*C*H-THF), 25.3 (*C*H-THF), 56.83 (q-*C*-methane).

Reaction of $ZrCl_4$ with dipotassium *meso*-diphenyldipyrrolidemethane (7.3)

A toluene solution (100 ml) of *meso*-diphenyldipyrromethane (1.1 g, 3.8 mmol) was treated with KH (0.3 g, 7.5 mmol) at –78ºC. Once the vigorous gas evolution ceased, the solution was stirred for 1 hour and the temperature increased slowly to reach room temperature. Anhydrous $ZrCl_4$ (1.3 g; 3.8 mmol) was then added at room temperature and an immediate colour change was observed to dark brown. The solution was filtered and the solvent was removed under reduced pressure. The resulting solid was characterized. IR (Nujol mull, cm^{-1}): 3184 (m), 1663.03 (w), 1594.3 (w), 1452.04 (s), 1377.6 (s), 1250 (s), 1149.64 (m), 1080.67 (s), 1030.77 (vs), 892.82 (m), 798.90 (s), 742.65 (vs). ^{1}H NMR (Toluene-d_8, ppm): 7.02 (m, C*H*-phenyl, 6H), 6.97 (m, C*H*-phenyl, 4H), 6.78 (m, C*H*-pyrrole, 2H), 5.93 (m, C*H*-pyrrole, 2H), 5.52 (m, C*H*-pyrrole, 2H). ^{13}C NMR (toluene-d_8, ppm): 153.10 (q C-pyrrole), 148.20 (q C-phenyl), 131.31 (CH-phenyl), 127.39 (CH-pyrrole), 126.84 (CH-phenyl), 125.37 (CH-phenyl), 110.41 (CH-pyrrole), 106.79 (CH-pyrrole), 60.02 (q C-methane). The above dry residue was dissolved in freshly distilled THF (100 ml) yielding an orange solution. A white precipitate (KCl) was filtered off and the volume of the solution was reduced to yield an orange solid (1.3 g, 2.9 mmol, 82%).

IR (KBr, Nujol mull, cm^{-1}) v: 3152 (s), 1592 (m), 1544 (m), 1261 (vs), 1183 (w), 1133 (s), 1100 (s), 1045 (vs), 977 (s), 893 (m), 842 (m), 802 (s), 742 (vs), 700 (s). ^{1}H NMR (THF-d_8, 200 MHz, 25°C), δ (ppm): 7.15 (m, C*H*-phenyl, 6H), 7.03 (m, C*H*-phenyl, 4H), 6.70 (m, C*H*-pyrrole, 2H), 5.98 (m, C*H*-pyrrole, 2H), 5.73 (m, C*H*-pyrrole, 2H). ^{13}C NMR (THF-d_8, 500 MHz, 25°C) δ (ppm): 148.22 (q, C-pyrrole), 136.51 (q, C-phenyl), 130.44 (CH-phenyl), 128.01 (CH-phenyl), 126.91 (CH-phenyl), 118.36 (CH-pyrrole), 110.33 (CH-pyrrole), 107.36 (CH-pyrrole), 56.83 (q, C-methane).

Preparation of $\{[Ph_2C(C_4H_3N)_2]Zr_2Cl_7Li\}_n$ (7.4)

A solution of *meso*-diphenyldipyrromethane (1.0 g, 3.5 mmol) in ether (100 ml) was cooled to –78°C. The addition of MeLi in ether (7.5 ml, 1.4 M, 7.0 mmol) caused a vigorous gas evolution. The solution was stirred at –78°C for 1 hour and allowed to warm slowly to room temperature. The addition of $ZrCl_4$ (1.6 g, 7.0 mmol) immediately changed the colour of the solution to yellow. After stirring overnight at room temperature the colour of the solution changed to a dark-brown. The solvent was then removed in vacuo to yield a dark-green solid. The residue was redissolved in toluene (100 ml) and stirred at room temperature for 2 hours. The colour changed from dark-green to dark-red. The solution was then filtered to remove a small quantity of insoluble material. Dark-red crystals of **7.4** separated upon allowing the solution to stand at room temperature for 72 hours (1.3 g, 1.6 mmol, 46%). IR (KBr, Nujol mull, cm^{-1}) v: 3348 (m), 1600 (w), 1542 (w), 1260 (m), 1147 (s), 1087.03 (m), 1053 (s), 988 (m), 831 (m), 742 (s), 723 (s). ^{1}H NMR (THF-d_8, 200 MHz, 25°C), δ (ppm): 7.18 (m, CH-phenyl, 6H), 7.06 (m, CH-phenyl, 4H), 6.68 (m, CH-pyrrole, 2H), 5.96 (m, CH-pyrrole, 2H), 5.71 (m, CH-pyrrole,

2H), 3.35 (m, CH_2-ether, 4H), 1.11 (t, CH_3-ether, 6H). ^{13}C NMR (THF-d_8, 500 MHz, 25°C) δ (ppm): 148.21 (q C-pyrrole), 136.49 (q C-phenyl), 130.43 (CH-phenyl), 129.99 (CH-phenyl), 126.90 (CH-phenyl), 118.35 (CH-pyrrole), 110.29 (CH-pyrrole), 107.30 (CH-pyrrole), 66.31 (CH_2-ether), 15.66 (q C-methane), 15.40 (CH_3-ether).

Preparation of $[Ph_2C(C_4H_3N)_2VCl(THF)_2]_2$ (7.5)

A solution of $Ph_2C(C_4H_3NH)_2$ (1.0 g, 3.5 mmol) in THF (100 ml) was treated with NaH (0.16 g, 7.0 mmol) upon which a vigorous evolution of hydrogen gas was observed. The mixture was stirred for one hour at room temperature and subsequently treated with $VCl_3(THF)_3$ (1.3 g, 3.5 mmol). The resulting dark-brown solution was allowed to stir overnight. The solvent was evaporated under reduced pressure and the solid was redissolved in freshly distilled toluene (50 ml). The resulting suspension was filtered to eliminate insoluble material (NaCl) and allowed to stand at room temperature overnight to yield dark reddish-brown crystals of **7.5** (2.14 g, 2.00 mmol, 58%). IR (KBr, Nujol mull, cm^{-1}) ν: 3195 (w), 1595 (m), 1550 (s), 1456 (m), 1377 (vs), 1308 (m), 1261 (m), 1203 (w), 1170 (s), 1155 (vs), 1136 (m), 1097 (m), 1045 (s), 1032 (vs), 1028 (s), 980 (m), 916 (m), 902 (m), 889 (s), 841 (m), 798 (m), 721 (vs), 700 (s), 654 (m). Anal. Calcd (found) for $V_2C_{58}H_{64}N_4O_4$: C, 72.61 (72.51), H 6.75 (6.56), N 5.21 (5.28). $\mu_{eff} = 5.42\ \mu_{BM}$ per dimer.

Preparation of $\{[Ph_2C(C_4H_3N)_2][2,6\text{-}(CCH_3)_2\text{-}4\text{-}(CH_3)(C_6H_2O)V\}_2(\mu\text{-}O)K(THF)$ (7.6)

Meso-diphenyldipyrromethane (1.60 g, 5.4 mmol) was dissolved in 50 ml of anhydrous THF and treated with 0.4 g (10.72 mmol) of KH. Upon addition, of the potassium hydride, a vigorous gas evolution was observed yielding a white suspension of the

potassium salt of the ligand. $VCl_3(THF)_3$ (2.0 g, 5.4 mmol) was added to this suspension and was allowed to react for 2 hours. A THF solution (50 ml) of 2,6-di-*tert*-butyl-4-methylphenol (1.8 g, 8.1 mmol) was also treated with KH (0.33 g, 8.1 mmol) to yield a clear colourless solution. The latter solution was allowed to react for 1 hour to liberate hydrogen and to form the potassium salt. The solution was then added drop-wise to the previous solution of $[Ph_2C(C_4H_3N)_2VCl(THF)_2]_2$ via cannula transfer. The colour of the solution changed immediately to brown-green. The solvent was evaporated to dryness and diethyl ether was added. The solution was filtered, removing KCl and was allowed to crystallize for 2 days upon which brown crystals of **7.6** were obtained. (2.7 g, 2.2 mmol, 40%). IR (KBr, Nujol mull, cm^{-1}) ν: 3053 (w), 2927 (s), 2855 (s), 1594 (m), 1550 (m), 1456 (s), 1414 (m), 1378 (s), 1313 (m), 1256 (m), 1231 (m), 1150 (m), 1118 (s), 1136 (m), 1081 (m), 1046 (m), 981 (w), 950 (w), 860 (s), 889 (s), 800 (m), 744 (s), 701 (s), 655 (m). Anal Calcd (found) for $C_{76}H_{90}N_4O_4V_2K$: C 72.19 (71.17), H 7.17 (7.23), N 4.43 (4.37). $\mu_{eff} = 3.45\ \mu_{BM}$ per dimer

Preparation of $[Ph_2C(C_4H_3N)_2CrCl(THF)_2]_2$ (7.7)

In 50 ml of anhydrous THF, 1.6 g (5.4 mmol) of *meso*-diphenyldipyrromethane were dissolved and treated with KH (0.43 g, 10.72 mmol). Upon addition the solution effervesced vigorously to yield a white suspension of the potassium salt of the ligand. $CrCl_3(THF)_3$, (2.0g, 5.4 mmol) of was added to the stirred suspension, and was allowed to react overnight. The solvent was evaporated to dryness and 75 ml of freshly distilled toluene were added. The dark orange-brown solution was filtered to remove insoluble material and allowed to stand at room temperature yielding orange crystals after 2 days.

(4.2 g, 3.4 mmol, 63%) IR (KBr, Nujol mull, cm^{-1}) ν: 3198 (w), 2986 (s), 2899 (s), 1599 (m), 1553 (s), 1454 (m), 1377 (vs), 1308 (m), 1261 (m), 1201 (w), 1170 (s), 1155 (vs), 1136 (m), 1097 (m), 1045 (s), 1032 (vs), 1028 (s), 982 (m), 916 (m), 902 (m), 891 (s), 844 (m), 798 (m), 721 (vs), 700 (s), 654 (m). Anal. Calcd (found) for $Cr_2C_{72}H_{80}N_4O_4Cl_2$: C, 69.72 (68.72), H 6.50 (6.57), N 4.52 (4.45). μ_{eff} = 7.36 μ_{BM} per dimer.

Preparation of $[Ph_2C(C_4H_3N)_2CrCl]_2 \cdot 2\ Li(THF)_4$ (7.8)

A solution of *meso*-diphenyldipyrromethane (1.00 g, 3.60 mmol) of was dissolved in 50 ml of anhydrous THF and was treated with 5.14 ml (7.20 mmol) of a 1.4 M solution of MeLi in ether. Upon addition, the solution effervesced vigorously to yield a white suspension of the lithium salt of the ligand. The solution was heated and was allowed to stir for 1 hour. $CrCl_2(THF)_2$ (0.96 g, 3.60 mmol) was added to the stirred suspension and allowed to react overnight. The solvent was evaporated to dryness and the residue was redissolved in 75 ml of freshly distilled toluene was added. The dark orange-brown solution was filtered to remove insoluble material and allowed to stand at room temperature to yield orange crystals after 4 days. (3.2 g, 2.5 mmol, 70%) IR (KBr, Nujol mull, cm^{-1}) ν: 3195 (m), 2987 (s), 1601 (m), 1555 (s), 1459 (m), 1376 (s), 1308 (m), 1263 (m), 1208 (w), 1165 (s), 1155 (s), 1136 (m), 1094 (m), 1045 (s), 1032 (s), 1028 (s), 980 (m), 916 (m), 902 (m), 885 (s), 851 (m), 798 (m), 721 (s), 700 (s), 654 (m). Anal. Calcd (found) for $Cr_2C_{74}H_{96}N_4O_8Li_2$: C, 69.04 (68.08), H 7.52 (7.57), N 4.35 (4.29). μ_{eff} = 9.52 μ_{BM} per dimer.

Preparation of $[Ph_2C(C_4H_3N)_2]_2Cr(THF)_2K(THF)$ (7.9)

Meso-diphenyldipyrromethane (1.6 g, 5.4 mmol) was dissolved in 50 ml of anhydrous THF and treated with 0.4 g (10.7 mmol) of KH. Upon addition, the solution effervesced to yield a white suspension of the potassium salt of the ligand. To this suspension, $CrCl_3(THF)_3$ (2.0 g, 5.4 mmol) of was added and allowed to react for 2 hours. A separate solution of 2,6-di-*tert*-butyl-4-methylphenol (1.2 g, 5.4 mmol) in 50 ml of THF was treated with KH (0.2 g, 5.4 mmol) to yield a clear solution. The solution was stirred for 1 hour and was then transferred via cannula to the previous solution. The colour of the solution changed immediately to brown-green. The solvent was evaporated to dryness and freshly distilled ether was added. The solution was filtered to remove KCl and was allowed to crystallize. (1.7 g, 1.9 mmol, 35%). IR (KBr, Nujol mull, cm^{-1}) ν: 3090 (m), 3053 (m), 1681 (w), 1632 (w), 1587 (m), 1562 (w), 1456 (s), 1409 (w), 1381 (s), 1347 (m), 1306 (w), 1281 (m), 1250 (m), 1222 (m), 1181 (m), 1145 (s), 1112 (m), 1078 (m), 1043 (s), 1012 (s), 998 (m), 983 (m), 949 (m), 924 (m), 899 (s), 854 (s), 788 (m), 761 (s), 745 (m), 718 (s), 696 (s), 656 (s), 625 (m), 610 (s). Anal. Calcd. (found) for $C_{54}H_{58}N_4O_3Cr$: C, 71.89 (70.48), H 6.48 (6.57), N 6.21 (6.09). $\mu_{eff} = 3.83\ \mu_{BM}$.

7.3 General Polymerization Procedure

A bench scale reactor was used in the polymerization experiments. The reactor uses a programmable logic control (PLC) system with Wonderware 5.1 software for process control. Ethylene polymerizations were performed in the 500 mL Autoclave Engineers Zipperclave reactor equipped with an air driven stirrer and an automatic temperature control system. All the chemicals were fed into the reaction batch-wise

except for ethylene that was fed on demand. The control temperature was 25 °C for the slurry polymerization experiments. The polymerization time varied from 10 to 30 min. Adding 5 mL of methanol to the reactor terminated the reaction and the polymer was recovered by evaporation of the toluene *in vacuo*. The polymerization activities were calculated based upon weight of polymer produced.

Polymer molecular weights and molecular weight distributions were measured by GPC (Waters 150-C) at 140 °C in 1,2,4-trichlorobenzene calibrated using polyethylene standards. DSC was conducted on a DSC 220 C from Seiko Instruments. The heating rate was 10 °C/min from 0 to 200 °C.

In a typical polymerization experiment, the solvent was pre-saturated with ethylene in the reactor at the desired temperature. The co-catalyst was injected in the reactor followed by introduction of the pre-catalyst. In the mixed-activator experiment the two co-catalysts were pre-mixed and injected in the reactor prior to introduction of the pre-catalyst. 1-octene was introduced in the reactor and premixed with ethylene before heating. Reproducibility of catalyst activity and reactor operation was checked by regularly running polymerization experiments using a standard zirconium catalyst and by repeating the experiments under identical reaction conditions. Errors and deviation were always below 5.9%.

Table 7.1 Polymerization Results[a]

Pro-catalyst	Feed	T (°C)	Activation (Al:M)	Time (min)	Yield (g)	Activity[b]	M_w (x 10^3)	PD
7.3	Ethene	25	PMAO (75)	30	0.8	7.23	*	*
7.3	Ethene	25	PMAO (958)	30	0.95	12.9		
7.6	Ethene	25	DMAC (40)	20	2.35	2073	*	*
7.6	Ethene	25	DEAC (40)	20	1.48	1305		
7.6	Ethene/ propene (50:50)	25	DMAC (40)	20	1.05	926	489	2.34

[a] Conditions: 5×10^{-6} moles of pro-catalyst; 200 ml of toluene: 10 psig of gas feed.
[b] units of activity are g PE/mmol cat h
* no characterization was obtained due to insolubility problems in conventional solvents

7.4 X-ray Crystallographic Structural Studies

Structural determination of complexes **7.3, 7.4, 7.5**·(toluene) **7.6, 7.7, 7.8** and **7.9** was done by selecting suitable crystals which were mounted on thin, glass fibres using paraffin oil and cooled to the data collection temperature. Data were collected on a Bruker AX SMART 1k CCD diffractometer using 0.3° ω-scans at 0, 90, and 180° in ϕ. Unit-cell parameters were determined from 60 data frames collected at different sections of the Ewald sphere. Semi-empirical absorption corrections based on equivalent reflections were applied (Blessing, R., *Acta Cryst.*, **1995**, A51, 33-38).

Systematic absences in the diffraction data and unit-cell parameters were uniquely consistent with the reported space groups. The structures were solved by direct methods, completed with difference Fourier syntheses and refined with full-matrix least squares procedures based on F^2. The polymeric structure in **7.4** is propagated by a screw axis.

In complexes **7.5** and **7.6**, systematic absences in the diffraction data and unit-cell parameters were consistent with *C2/c* and *Cc* for **7.6** and, uniquely, $P2_1/n$ for **7.5**. Refinement in the centro-symmetric space group options yielded computationally stable and chemically reasonable results of refinement. The structures were solved by direct methods, completed with difference Fourier syntheses and refined with full-matrix least squares procedures based on F^2. The compound molecule in **7.6** is located at a two-fold axis. A co-crystallized toluene solvent molecule was located in the asymmetric unit of **7.5**·(toluene).

No symmetry higher than triclinic was observed for **7.8**. Systematic absences in the diffraction data and unit-cell parameters were consistent with *C2/c* and *Cc* for **7.9** and, uniquely, $P2_1/n$ for **7.7**·(toluene). Refinement in the centro-symmetric space group

options yielded computationally stable and chemically reasonable results of refinement. The structures were solved by direct methods, completed with difference Fourier syntheses and refined with full-matrix least squares procedures based on F^2. The molecular anion of **7.8** and the compound molecule of **7.7**·2·(toluene) are located at inversion centres. The compound molecule in **7.9** is located at a two-fold axis. A co-crystallized toluene solvent molecule was located disordered in two positions with site occupancies of 75/25 in the asymmetric unit of **7.7**·2·(toluene).

All non-hydrogen atoms were refined with anisotropic displacement parameters. All hydrogen atoms were also treated as idealized contributions. All scattering factors and anomalous dispersion factors are contained in the SHEXTL 5.10 program library (Sheldrick, G. M., Bruker AXS, Madison, WI, 1997). Crystal data and relevant geometrical parameters are reported in Appendix 9 and Appendix 10.

Description of the Crystal Structures

Complex of $Ph_2C(C_4H_3N)_2ZrCl_2(THF)_2$ (7.3)

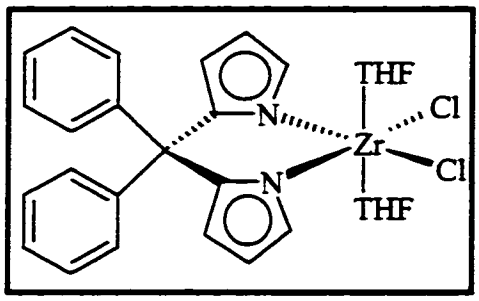

The molecular structure of $Ph_2C(C_4H_3N)_2ZrCl_2(THF)_2$ is shown in Figure 7.1 with selected bond distances and angles. The distorted octahedral geometry of the zirconium metal center is comprised of two chlorine atoms, two σ-bonded nitrogen atoms from the dipyrrolide ligand in the equatorial plane [N(1)-Zr-O(2) = 95.5(3)°, N(1)-Zr-N(2) = 83.3(4)°, N(1)-Zr-O(1) = 87.2(3)°, N(1)-Zr-Cl(1) = 172.0(3)°, N(1)-Zr-Cl(2) = 93.0(3)°], and two coordinated THF molecules located in the axial positions [O(1)-Zr-O(2) = 174.0(3)°]. The Zr-Cl distances [Zr-Cl(1) = 2.440(4)Å, Zr-Cl(2) = 2.464(4)Å] and the Zr-N distances [Zr-N(1) = 2.146(9)Å, Zr-N(2) = 2.179(9)Å] are as expected and comparable to those reported in the literature. The trigonal planar geometry of the nitrogen atom suggests the presence of some Zr-N π-bond character [C(1)-N(1)-Zr = 123.0(8)°, C(4)-N(1)-Zr = 129.8(8)°, C(8)-N(2)-Zr = 131.9(8)°, C(5)-N(2)-Zr = 122.6(8)°].

Figure 7.1 ORTEP of $Ph_2C(C_4H_3N)_2ZrCl_2(THF)_2$ (7.3)

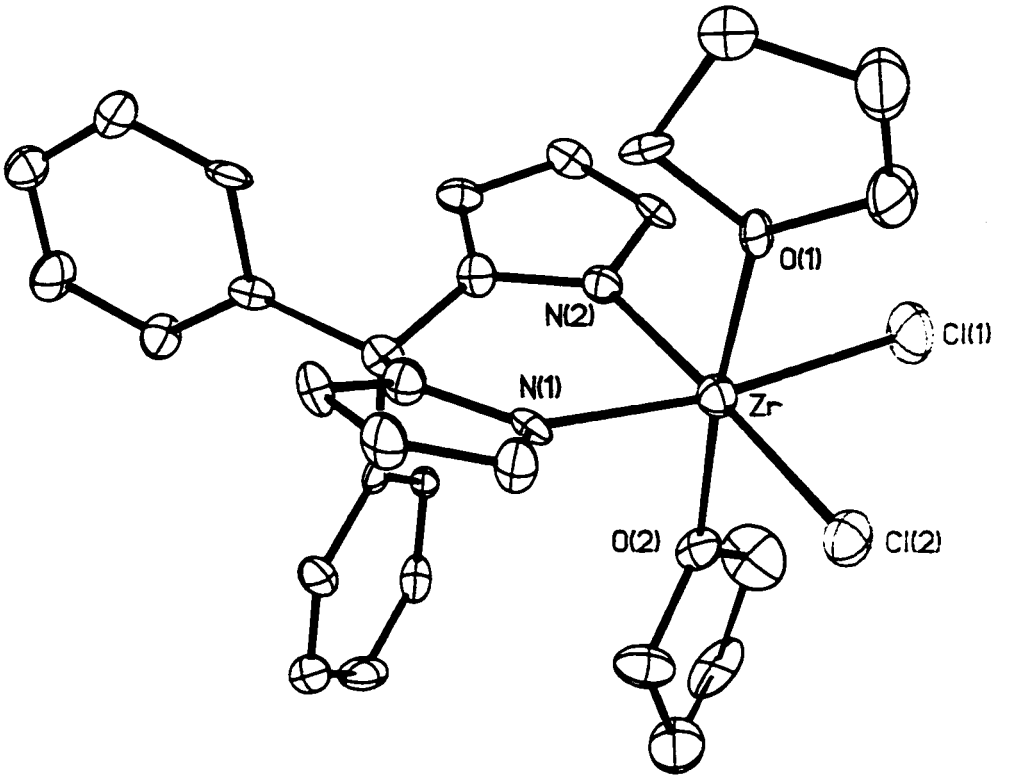

Selected Bond Distances (Å) and Angles (°) for $Ph_2C(C_4H_3N)_2ZrCl_2(THF)_2$ (7.3)

Distances	Angles
Zr-Cl(1) = 2.440(4)	N(1)-Zr-Cl(1) = 172.0(3)
Zr-Cl(2) = 2.464(4)	N(1)-Zr-Cl(2) = 93.0(3)
Zr-N(1) = 2.146(9)	N(1)-Zr-N(2) = 83.3(4)
Zr-N(2) = 2.179(9)	N(1)-Zr-O(1) = 87.2(3)
Zr-O(1) = 2.195(8)	N(1)-Zr-O(2) = 95.5(3)
Zr-O(2) = 2.152(8)	

Complex of $\{[Ph_2C(C_4H_3N)_2]Zr_2Cl_7Li\}_n$ (7.4)

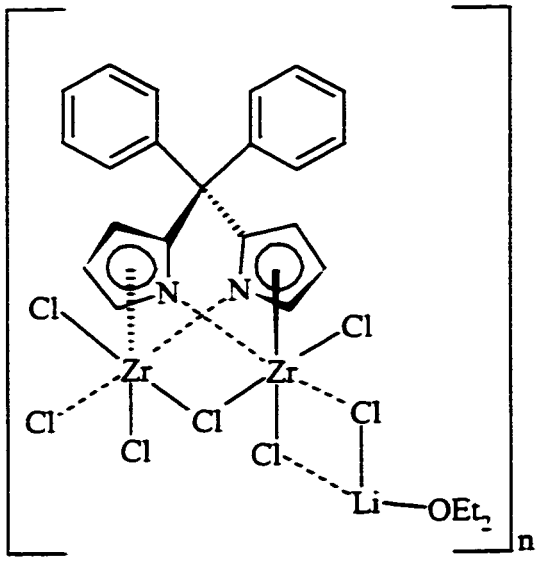

The molecular structure of **7.4** consists of two zirconium atoms, seven chlorine atoms and one diphenyldipyrrolidemethane ligand (Figure 7.2). The two zirconium atoms are bridged by one of the chlorine atoms [Zr(1)-Cl(7)-Zr(2) = 46.34 (3)°] and by the dipyrrolide ligand. One lithium atom bridges the chlorine atoms from two zirconium units thus forming an infinite array of bimetallic zirconium units (Figure 7.2). The inorganic polymer adopts an overall double helix conformation (Figure 7.2). The dipyrrole ring bridges two metal centres by using both σ and π-bonding modes. Each pyrrolyl ring is η^5–bound to one of the two Zr atoms forming slightly different Zr centroids [Zr(1)-ring centroid = 2.294(5) Å, Zr(2)- ring centroid = 2.267(5) Å]. Each ring is in turn σ-bonded to the second zirconium atom. The π-bonding mode is rather regular and the Zr-N distance with the second σ-bonded ring is also in the expected range. The coordination geometry around each zirconium metal center is distorted octahedral with

the equatorial plane defined by one σ-bonded pyrrole ring and three chlorine atoms [N(1)-Zr(2)-Cl(6) = 98.06 (10)°, N(1)-Zr(2)-Cl(4) = 159.21 (11)°, N(1)-Zr(2)-Cl(7) = 75.31(10)°]. The other chlorine atom is placed in one of the axial positions [N(1)-Zr(2)-Cl(5) = 81.63(11)°]. The second axial position is occupied by the centroid of a η^5-bonded pyrrolide ring [Zr(2)-ring centroid-Cl(5) = 171.1(17)°]. Three chlorine atoms and one molecule of ether surround lithium whose coordination geometry is distorted tetrahedral [Cl(3A)-Li-Cl(5) = 107.2(5)°, Cl(3A)-Li-Cl(4) = 121.6(5)°, Cl(5)-Li-Cl(4) = 89.4(4)°, O-Li-Cl(3A) = 114.1(5)°, O-Li-Cl(5) = 107.3(6)°, O-Li-Cl(4) = 112.9(6)°]. Both monomers are linked to each other by a two-fold screw axis between Zr(1) and Zr(1A). The Zr-Cl distances [Zr(1)-Cl(1) = 2.4035(15) Å, Zr(1)-Cl(2) = 2.4391(15)Å, Zr(1)-Cl(3) = 2.4211(14)Å] are slightly different from each other but fall in the expected range for terminal Zr-Cl bonds. The zirconium bonds with the bridging chlorine atoms are slightly longer [Zr(1)-Cl(7) = 2.6080(14)Å]. The Zr-N distances fall within normal range [Zr(1)-N(2) = 2.359(4)Å, Zr(2)-N(1) = 2.349(4)Å].

Figure 7.2a ORTEP of $\{[Ph_2C(C_4H_3N)_2]Zr_2Cl_7Li\}_n$ (7.4)

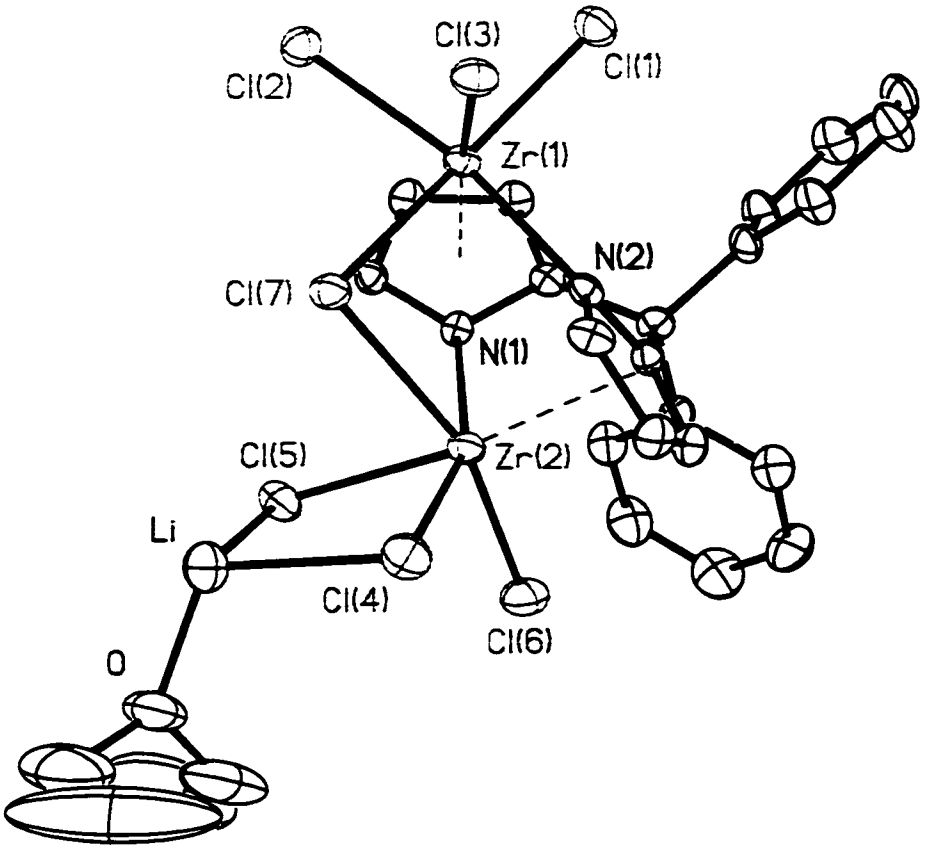

Selected Bond Distances (Å) and Angles (°) for $\{[Ph_2C(C_4H_3N)_2]Zr_2Cl_7Li\}_n$ (7.4)

Distances	Angles
Zr(1)-Cl(1) = 2.4035(15)	N(2)-Zr(1)-Cl(1) = 97.56(10)
Zr(1)-Cl(2) = 2.4391(15)	N(2)-Zr(1)-Cl(2) = 161.08(11)
Zr(1)-Cl(3) = 2.5211(14)	N(2)-Zr(1)-X(1A) = 88.5(1)
Zr(1)-Cl(7) = 2.6080(14)	N(2)-Zr(1)-Cl(3) = 81.90(11)
Zr(1)-N(2) = 2.359(4)	N(2)-Zr(1)-Cl(7) = 75.10(10)
Zr(1)-X(1A) = 2.292(4)	N(1)-Zr(2)-Cl(4) = 159.21(11)
Zr(2)-Cl(4) = 2.4749(15)	N(1)-Zr(2)-Cl(5) = 81.63(11)
Zr(2)-Cl(5) = 2.5190(15)	N(1)-Zr(2)-X(1B) = 89.9(1)
Zr(2)-Cl(6) = 2.3918(15)	N(1)-Zr(2)-Cl(6) = 98.06(10)
Zr(2)-Cl(7) = 2.6155(14)	N(1)-Zr(2)-Cl(7) = 75.31(10)
Zr(2)-N(1) = 2.349(4)	Zr(2)-Cl(5)-Li = 90.8(3)
Zr(2)-X(1B) = 2.267(4)	Zr(2)-Cl(4)-Li = 91.7(3)
Li-O = 1.834(12)	Cl(5)-Li-O = 107.3(6)
Li-Cl(5) = 2.405(12)	Cl(5)-Li-Cl(3A) = 107.2(5)
	Zr(1)-Cl(7)-Zr(2) = 87.49(4)

Figure 7.2b **Side and Top Views of the $\{[Ph_2C(C_4H_3N)_2]Zr_2Cl_7Li\}_n$ (7.4) Polymer.**

Side View

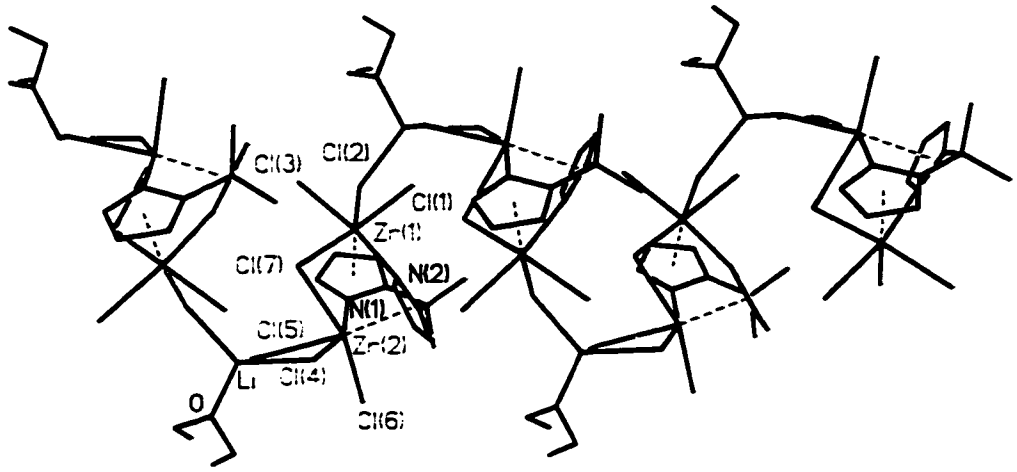

Top View

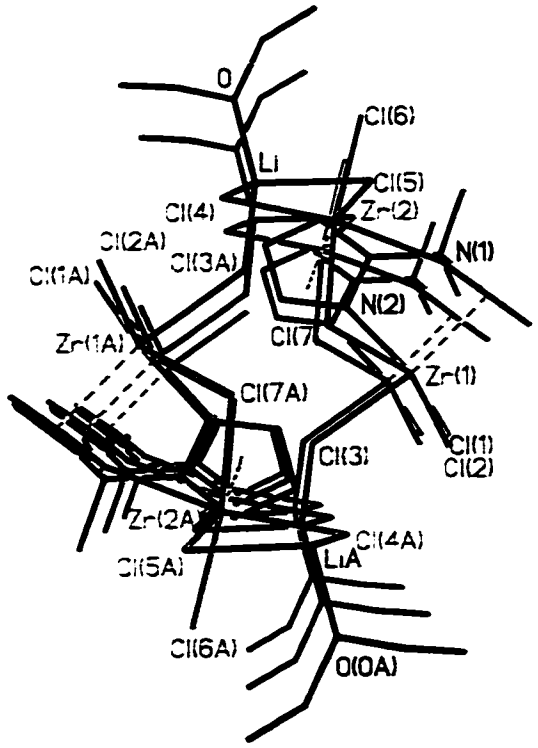

Complex of $[Ph_2C(C_4H_3N)_2VCl(THF)_2]_2$ (7.5)

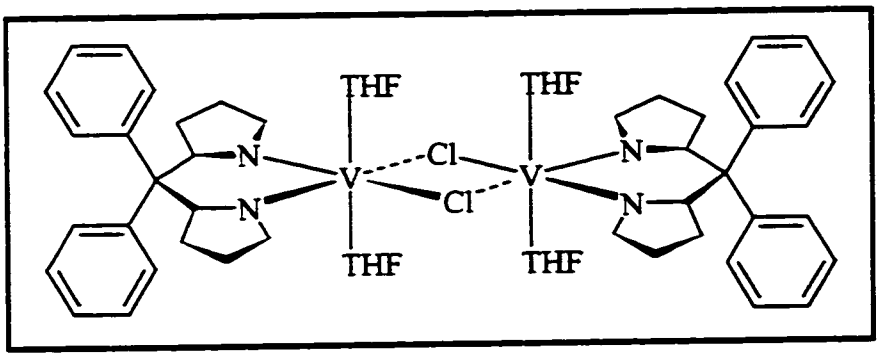

The crystal structure shows symmetry generated bimetallic complex with two distorted octahedral V(III) centres bridged by two chlorine atoms and adopting an overall edge-sharing bi-octahedral structure [V(#1)-Cl-V = 100.33(3)°, Cl(#1)-V-Cl = 79.67(3)°]. The octahedral coordination geometry around each vanadium is defined by the two bridging chlorine atoms and two σ-bonded nitrogen atoms of the dipyrrolide ligand [N(1)-V-N(2) = 91.98(9)°, N(1)-V-O(2) = 92.76(9)°, N(1)-V-O(1) = 90.48(9)°, N(1)-V-Cl = 174.30(7)°, N(1)-V-Cl(#1) = 94.70(7)°] defining the equatorial plane. Two molecules of coordinated THF are located on the axial positions on each of the vanadium atoms [O(2)-V-O(1) = 175.69(8)°]. The V-Cl distances are basically equivalent and fall into the expected range for bridging chlorides [V-Cl = 2.4999(9)Å, V-Cl(#1) = 2.4877(8)Å]. The V-N bond lengths are within normal ranges for values of single bonded nitrogens to vanadium [V-N(1) = 1.997(2)Å, V-N(2) = 2.009(2) Å]. The two pyrrolyl rings are nearly coplanar with the vanadium atom. All other bond distances and angles are as expected.

Figure 7.3 ORTEP of $[Ph_2C(C_4H_3N)_2VCl(THF)_2]_2$ (7.5)

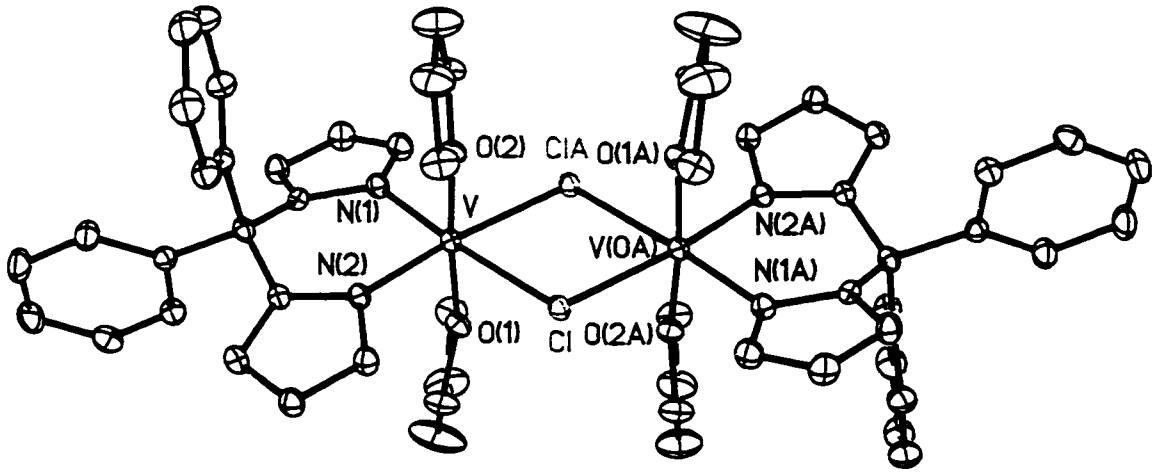

Selected Bond Distances (Å) and Angles (°) for $[Ph_2C(C_4H_3N)_2VCl(THF)_2]_2$ (7.5)

Distances	Angles
V-Cl = 2.4999(9)	N(1)-V-Cl = 174.30(7)
V-Cl(A) = 2.4877(8)	N(1)-V-Cl(A) = 94.70(7)
V-N(1) = 1.997(2)	N(1)-V-N(2) = 91.98(9)
V-N(2) = 2.009(2)	N(1)-V-O(1) = 90.48(9)
V-O(1) = 2.0621(19)	N(1)-V-O(2) = 92.76(9)
V-O(2) = 2.0179(19)	V-Cl-V(A) = 100.33(3)

Complex of $\{[Ph_2C(C_4H_3N)_2](C_{15}H_{23}O)V\}_2(\mu\text{-}O)K(THF)$ (7.6)

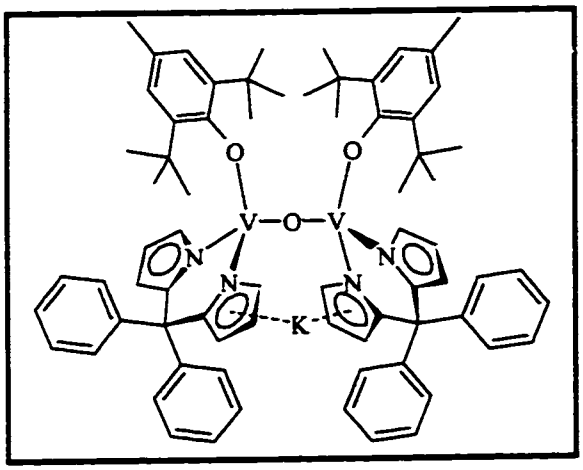

Complex **7.6** (Figure 7.4) is a C_2 symmetry generated dimer with each vanadium centre bearing one 2,6-di-*tert*-butyl-4-methylphenoxide and one *meso*-diphenyldipyrrolidemethane ligand. An oxygen atom bridges the two vanadium units while a potassium atom bridges two units through coordination in an η^5-fashion to two pyrrolide rings from two different ligands. The potassium atom is also ligated to one molecule of THF. The coordination geometry of each vanadium centre is distorted tetrahedral. Vanadium is σ–bonded to an aryloxide through the oxygen moiety and σ–bonded to one dianionic dipyrrolide ligand through the pyrrole nitrogens [O(1)-V(1)-N(1) = 117.17(15)°, O(1)-V(1)-N(2) = 120.01(17)°, O(1)-V(1)-O(2) = 115.88(18)°, O(2)-V(1)-N(1) = 104.21(18), O(2)-V(1)-N(2) = 106.35(14)°, N(1)-V(1)-N(2) = 89.33(18)°,]. The bond angle subtended at the aryloxide oxygen atom is nearly linear [V(1)-O(1)-C(27) = 166.2(3)°] and suggests some π-bonding character between the oxygen and the vanadium atoms. The fourth coordination site on each vanadium is occupied by a bridging oxygen [V(1)-O(2)-V(1A) = 169.5(3)°]. The V-N and V-O distances fall within the expected ranges for σ-bonded nitrogen and oxygen atoms bound to vanadium [V(1)-O(1) = 1.772(3)Å, V(1)-O(2) = 1.7878(10)Å, V(1)-N(1) = 1.958(4)Å, V(1)-N(2) = 1.940(4)Å].

Figure 7.4 ORTEP of {[$Ph_2C(C_4H_3N)_2$]($C_{15}H_{23}O$)V}$_2$(μ-O)K(THF) (7.6)

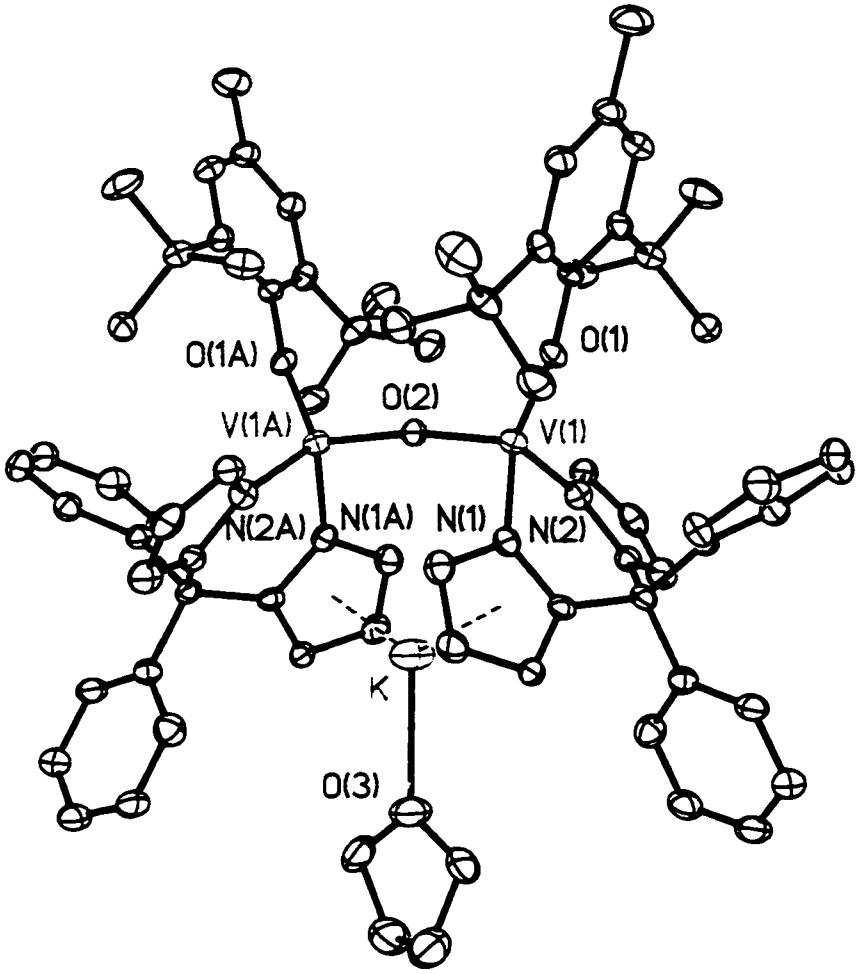

Selected Bond Distances (Å) and Angles (°) for Complex 7.6

Distances	Angles
V(1)-O(1) = 1.772(3)	N(1)-V(1)-O(1) = 117.17(15)
V(1)-O(2) = 1.7878(10)	N(1)-V(1)-O(2) = 104.21(18))
V(1)-N(1) = 1.958(4)	N(1)-V(1)-N(2) = 89.33(18)
V(1)-N(2) = 1.940(4)	V(1)-O(2)-V(1A) = 169.5(3)
K-O(3) = 2.679(6)	X1A-K-X1B = 142.7(3)
K-X1A = 2.840(6)	

Complex of $[Ph_2C(C_4H_3N)_2CrCl(THF)_2]_2$ (7.7)

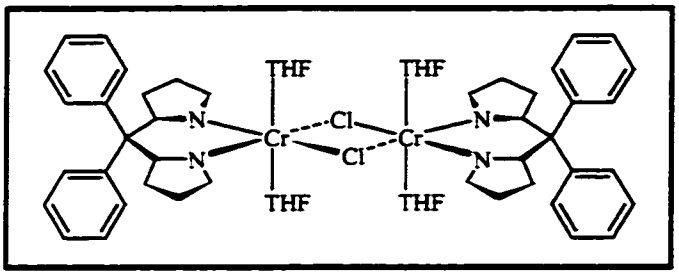

The crystal structure in Figure 7.5 shows a symmetry generated bimetallic complex with two distorted octahedral chromium (III) centres bridged by two chlorides and adopting an overall edge-sharing bi-octahedral structure [Cr(#1)-Cl-Cr = 100.065(19)°, Cl(#1)-Cr-Cl = 79.935(19)°]. The octahedral coordination geometry around each chromium is defined by the two bridging chlorine atoms and two σ-bonded nitrogen atoms of the dipyrrolide ligand [N(1)-Cr-N(2) = 92.45(7)°, N(1)-Cr-O(2) = 91.66(6)°, N(1)-Cr-O(1) = 89.10(6)°, N(1)-Cr-Cl = 174.38(5)°, N(1)-Cr-Cl(#1) = 94.60(5)°] defining the equatorial plane. Two molecules of coordinated THF are located in the axial positions on each of the chromium atoms [O(2)-Cr-O(1) = 176.46(6)°]. The Cr-Cl distances are practically equivalent and fall into the range expected for bridging chlorides [Cr-Cl = 2.4445(6)Å, Cr-Cl(#1) = 2.4323(6)Å]. The Cr-N bond lengths are within normal ranges for values of single bonded nitrogens to chromium [Cr-N(1) = 1.9779(16)Å, Cr-N(2) = 1.9719(16) Å] and compare well with those of other Cr-amido bonds. The two pyrrolyl rings are nearly co-planar with the chromium atom. All other bond distances and angles are as expected.

Figure 7.5 ORTEP of $[Ph_2C(C_4H_3N)_2CrCl(THF)_2]_2$ (7.7)

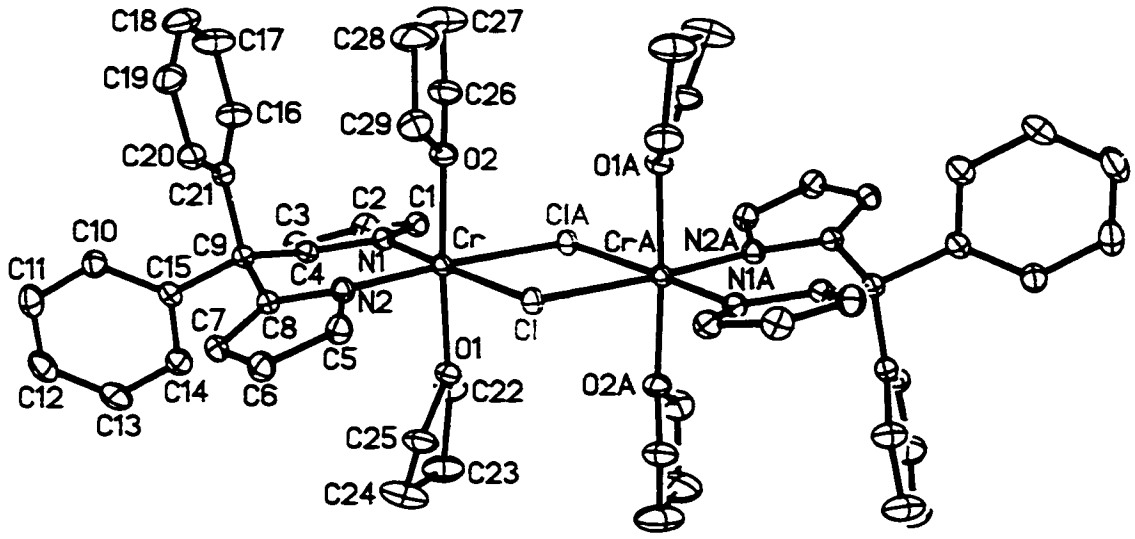

Selected Bond Distances (Å) and Angles (°) for $[Ph_2C(C_4H_3N)_2CrCl(THF)_2]_2$ (7.7)

Distances	Angles
Cr-Cl = 2.4445(6)	N(1)-Cr-Cl = 174.38(5)
Cr-Cl(A) = 2.4323(6)	N(1)-Cr-Cl(A) = 94.60(5)
Cr-N(1) = 1.9779(16)	N(1)-Cr-N(2) = 92.45(7)
Cr-N(2) = 2.9719(16)	N(1)-Cr-O(1) = 89.10(6)
Cr-O(1) = 2.0509(14)	N(1)-Cr-O(2) = 91.66(6)
Cr-O(2) = 2.0253(14)	Cr-Cl-Cr(A) = 100.065(19)

Complex of $[Ph_2C(C_4H_3N)_2CrCl]_2[Li(THF)_4]_2$ (7.8)

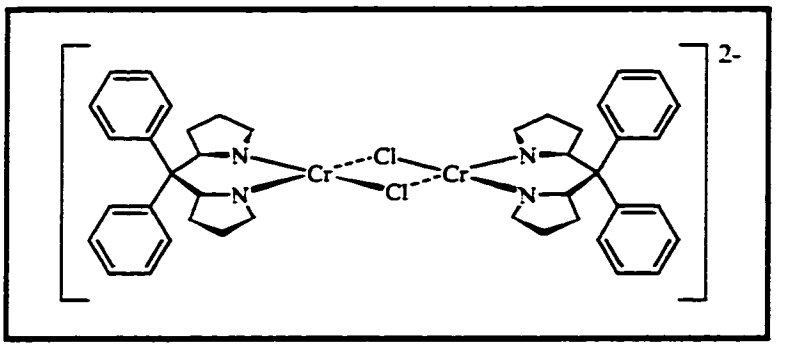

The C_2 symmetric molecular structure of complex **7.8** was elucidated by X-ray analysis and is shown in Figure 7.6. The complex is dimeric with two equivalent $Ph_2C(C_4H_3N)_2Cr$ units bridged by two chlorine atoms. The coordination geometry around each chromium is distorted square planar and is defined by one dipyrrolide ligand and the bridging chlorine atoms [N(2)-Cr-N(1) = 89.82(8)°, N(2)-Cr-Cl = 172.40(6)°, N(1)-Cr-Cl = 94.02(6)°, N(2)-Cr-C(#1) = 93.77(6)°, N(1)-Cr-Cl(#1) = 168.24(6)°]. The nitrogens σ-bonded to chromium have equivalent bond distances and are comparable to those of the Cr(III) and V(III) complexes and fall into the expected range [Cr-N = 2.011(2)Å]. The Cr-Cl bond distances are also normal [Cr-Cl = 2.4032(8)Å, Cr-Cl(#1) = 2.4137(8)Å]. Two tetrahedral, THF-solvated lithium cations are found in the crystal lattice, which are present to stabilize the dianionic chromium complex.

Figure 7.6 ORTEP of $[Ph_2C(C_4H_3N)_2CrCl]_2[Li(THF)_4]_2$ (7.8)

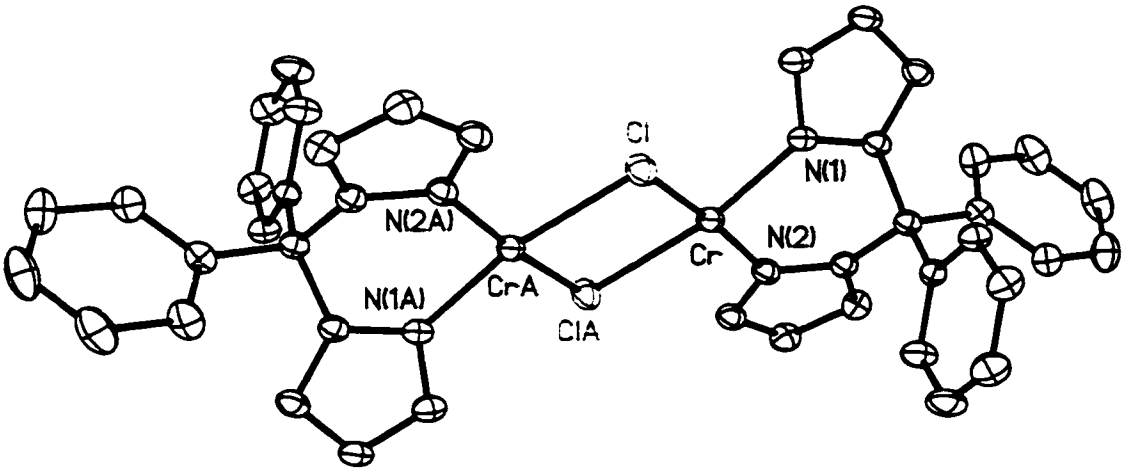

Selected Bond Distances (Å) and Angles (º) for $[Ph_2C(C_4H_3N)_2Cr]_2$ $[Li(THF)_4]_2$ (7.8)

Distances	Angles
Cr-Cl = 2.4032(8)	N(1)-Cr-Cl = 94.02(6)
Cr-Cl(A) = 2.4137(8)	N(1)-Cr-Cl(A) = 168.24(6)
Cr-N(1) = 2.011(2)	N(1)-Cr-N(2) = 89.82(8)
Cr-N(2) = 2.011(2)	Cr-Cl-Cr(A) = 96.23(3)

Complex of $[Ph_2C(C_4H_3N)_2]_2Cr(THF)_2{\cdot}K(Et_2O)$ (7.9)

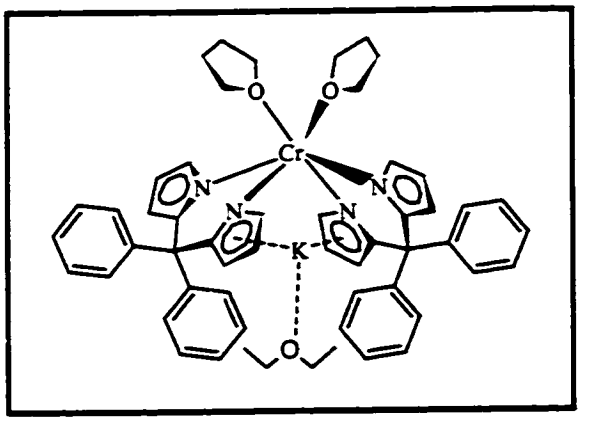

The molecular structure (Figure 7.7) shows a distorted octahedral chromium metal centre surrounded by two THF molecules, and two *meso*-diphenyldipyrrolidemethane ligands. The equatorial plane is comprised of two σ-bonded nitrogens from one dipyrrolide ligand, a coordinated oxygen from a THF molecule as wells as a σ-bonded nitrogen from a pyrrolide ring from the second dipyrrolide ligand [N(1)-Cr-N(2) = 88.56(9)°, N(2A)-Cr-O(1) = 85.34(8)°, N(2)-Cr-O(1) = 87.92(8)°, N(1)-Cr-N(2A) = 98.44(9)°]. The axial positions of the octahedron are occupied by a coordinated THF molecule and a nitrogen from the second pyrrolide ring of the diphenyldipyrrolide ligand [O(1A)-Cr-N(1A) = 175.80(8)°]. The complex also coordinates a potassium cation, which is bound in an η^5-fashion to two pyrrolide rings from two different diphenyldipyrrolide ligands and is solvated by one molecule of diethyl ether. The Cr-N σ-bonds and the Cr-O coordination bonds fall into the expected range when compared to the Cr(III) complex (7.7) reported above [Cr-N(1) = 2.004(2)Å, Cr-N(2) = 2.040(3)Å, Cr-O(1) = 2.1526(19)Å].

Figure 7.7 ORTEP of $[Ph_2C(C_4H_3N)_2]_2Cr(THF)_2 \cdot K$ (ether) (7.9)

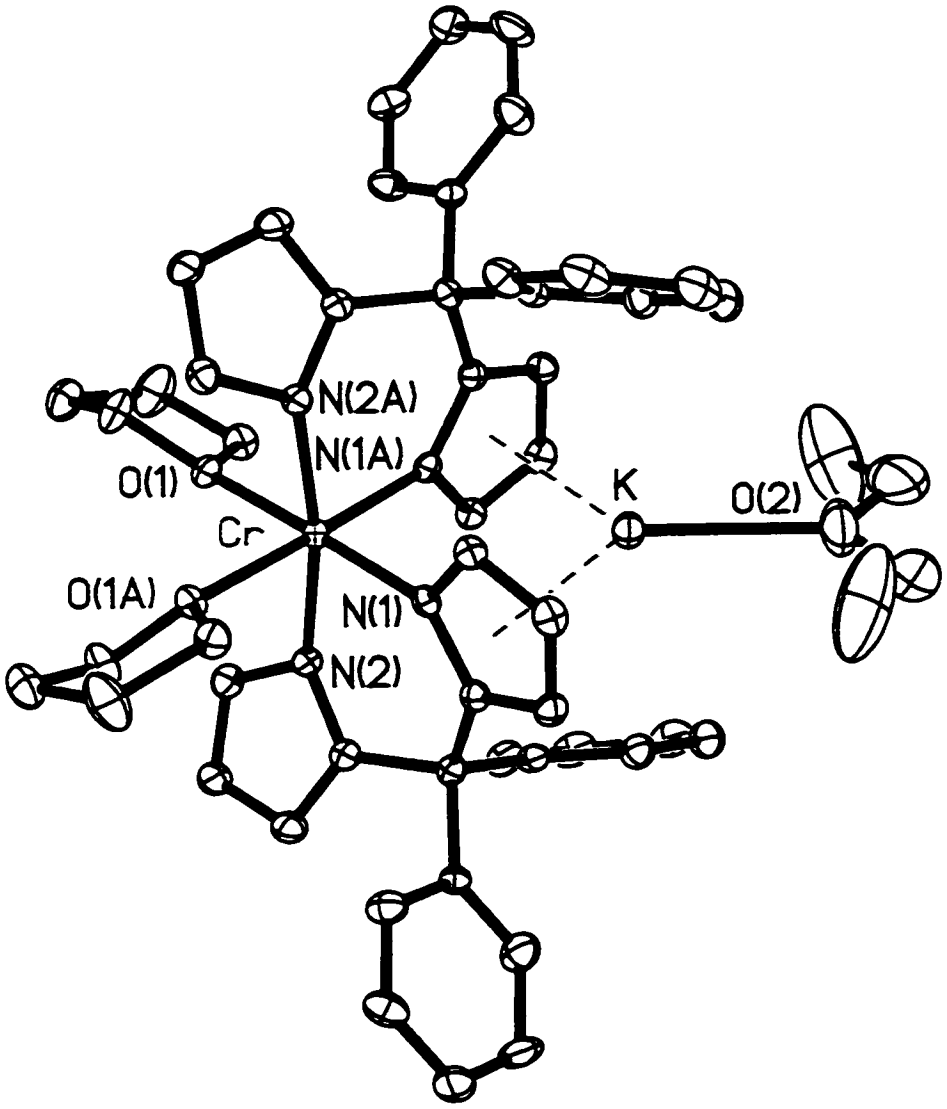

Selected Bond Distances (Å) and Angles (º) for $[Ph_2C(C_4H_3N)_2]_2Cr(THF)_2$ K (ether) (7.9)

Distances	Angles
Cr-N(1) = 2.004(2)	N(1)-Cr-N(2) = 88.56(9)
Cr-N(2) = 2.040(2)	N(1)-Cr-O(1) = 175.80(8)
Cr-O(1) = 2.1526(19)	N(1)-Cr-N(1A) = 90.28(13)
K-O(2) = 2.667(5)	N(1)-Cr-N(2A) = 98.44(9)
	N(1)-Cr-O(1A) = 87.96(9)

7.5 Results and Discussion

The diphenyldipyrrolemethane ligand was prepared by the reaction of pyrrole with benzophenone in the presence of a catalytic amount of methanesulphonic acid (Scheme 5.1). Characterization of the ligand via ^{1}H NMR analysis revealed the typical proton shifts at 7.92 (2H in the *para*-position) and 7.25 (8H protons in the *ortho*- and *meta*-positions) ppm assigned to the phenyl protons and chemical shifts at 7.10 (2H, α-protons), 6.74 (2H, β-protons) and 5.93 (2H, γ-protons) ppm are attributed to the pyrrole moiety of the ligand. The ^{13}C NMR also presented the expected resonances. Peaks at 128.8, 128.5 and 127.4 ppm are attributed to the phenyl rings and those at 117.1, 110.2 and 108.6 ppm are assigned to the pyrrole carbons. Analytical data in agreement with the proposed formulation was also obtained.

Scheme 7.1 Synthesis of diphenyldipyrrolemethane

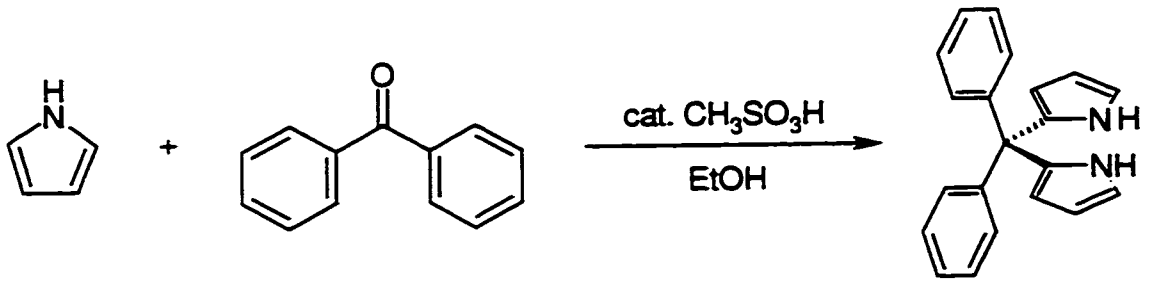

The reaction of the diphenyldipyrrolide salt with $ZrCl_4$ afforded two different products depending on the stoichiometry employed for the reaction. Reactions carried out with a zirconium to ligand ratio of 1:1 afforded a dark brown microcrystalline solid of complex **7.2**, which was dissolved in freshly distilled THF. Upon addition of THF the solid changed colour to light orange and $Ph_2C(C_4H_3N)_2ZrCl_2(THF)_2$ (**7.3**) was crystallized from toluene (Figure 7.1).

Scheme 7.2 Reactivity of $ZrCl_4$ with *meso*-diphenyldipyrrolidemethane

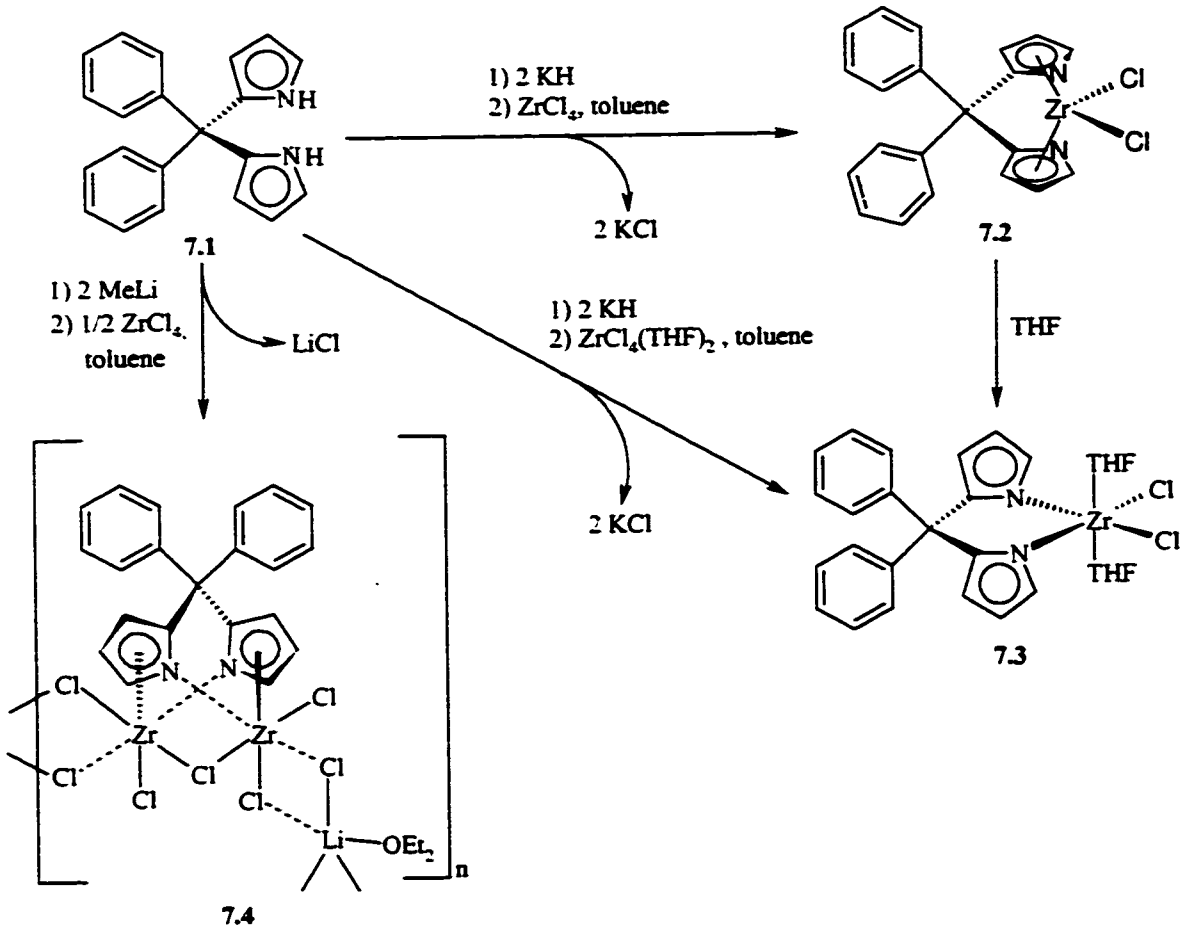

The ^1H NMR spectrum of complex **7.3** reveals the presence of two distinct multiplets at 7.15 and 7.03 ppm that are attributed to the phenyl rings and three broad resonances at 6.70, 5.98 and 5.73 ppm, which are, attributed to the coordinated pyrrolyl rings. The ^{13}C NMR showed sharp peaks at 130.44, 128.01 and 126.91 ppm that are consistent with shifts previously assigned to the phenyl rings while the peaks at 118.36, 110.33 and 107.36 ppm are assigned to the pyrrolyl rings. The quaternary carbons of the pyrrolyl rings are attributed to the signal at 148.22 ppm, the quaternary carbons of the phenyl rings was found at 136.51 ppm while the quaternary carbon of the methane is responsible

for the up-field signal at 56.83 ppm. Complex **7.3** was also synthesized in higher yield through direct synthesis using $ZrCl_4(THF)_2$ with one equivalent of ligand.

In spite of reiterated efforts to grow crystals of suitable quality, complex **7.2** escaped crystallographic characterization a minimum of identification of the species was obtained by IR and NMR. Upon comparison of the ^1H and ^{13}C NMR spectra of **7.2** and **7.3** the chemical shifts present suggest that the pyrrolide rings in complex **7.2** are possibly π-bound to the metal center and may be bridging two metal centres as seen in complex **7.4** whose chemical shifts differ slightly from those of complex **7.3**. Complex **7.2** is particularly attractive since it is the pyrrolyl analogue of the *ansa*-metallocene complexes. Since crystallographic data were not obtained, a conclusive demonstration of the nature of the bonding modes in complex **7.2** was not obtained. Should complex **7.2** possess a polymer-type structure, the ligand would have both the η^1-bonding mode and the η^5-bonding mode to two different Zr (IV) metal centres as observed in complex **7.3**. The synthetic pathways to complexes **7.2** and **7.3** can be found in the general reaction scheme described in Scheme 7.2.

Changing the stoïchiometry of the reaction from 1:1 to a 1:2 ratio of ligand to zirconium drastically changed the nature of the product obtained. Reactions carried out with a ligand/Zr stoïchiometric ratio of 1:2 using the dilithium salt of the ligand led to the formation of dark-red crystals of a complex formulated as $C_{25}H_{26}Cl_7LiN_2OZr_2$ (**7.4**). The ^1H NMR of this species shows characteristic signals of the ligand as two multiplets at 7.18 and 7.06 ppm due to the phenyl protons and three broad resonances at 6.68, 5.96 and 5.71 ppm which are assigned to the coordinated pyrrolide rings. The integration indicates also the presence of a half equivalent of diethyl ether per ligand. The ^{13}C NMR also

showed the characteristic resonances. The peaks at 130.43, 129.99 and 126.90 ppm are attributed to the phenyl protons and the peaks at 118.35, 110.29 and 107.30 ppm are assigned to the pyrrolide protons. The quaternary carbon on the pyrrole ring is attributed to a signal at 148.21 ppm, the quaternary carbon on the phenyl ring is attributed to the signal at 136.49 ppm and the quaternary carbon of the methane is attributed to the signal at 55.66 ppm. The chemical connectivity of **7.4** was demonstrated by an X-ray crystal structure. The structure of **7.4** consists of a monomeric unit of two zirconium atoms, seven chlorine atoms and one diphenyldipyrrole ligand. The NMR features are consistent with the solid-state crystal structure.

The reaction of $VCl_3(THF)_3$ with *meso*-diphenyldipyrrolylmethane afforded dark red crystals (**7.5**). The complex is paramagnetic and shows a magnetic moment in agreement with the d^2 electronic configuration of a V(III) metal centre. The crystal structure (Figure 7.3) shows a bimetallic complex with two distorted octahedral V(III) centres bridged by two chlorides. Unlike the Zr(IV) chemistry, the possibility of the vanadium center to bind in a η^5-fashion was not observed probably due to the presence of coordinated THF molecules. This may also be due to the "hard" character of vanadium enhancing the σ-bonding mode as opposed to the π-bonding mode since vanadium is a first row transition metal and Zr is a second row transition metal having more diffuse valence orbitals.

Preliminary polymerization tests indicated no activity. Therefore, in order to increase the catalytic activity two equivalents of a potassium 2,6-di-*tert*-butyl-4-methylphenoxide salt were added. The reason was two-fold: 1) replacing the chlorides by oxygen donor based ligands might force the interaction with the Al co-catalyst; 2) the

presence of a sterically demanding ligand bearing *tert*-butyl groups in the 2 and 6 positions of the phenyl rings might eliminate the coordinated THF from the coordination sphere of the vanadium centre. Upon abstraction of the aryloxide ligand open coordination sites could be available for the ethylene coordination and insertion steps. Scheme 7.3 presents the reactivity of complex **7.5** with three equivalents of the potassium salt of the aryloxide.

Scheme 7.3 Reactivity of Complex 7.5 with 2,6-di-*tert*-butyl-4-methylphenoxide

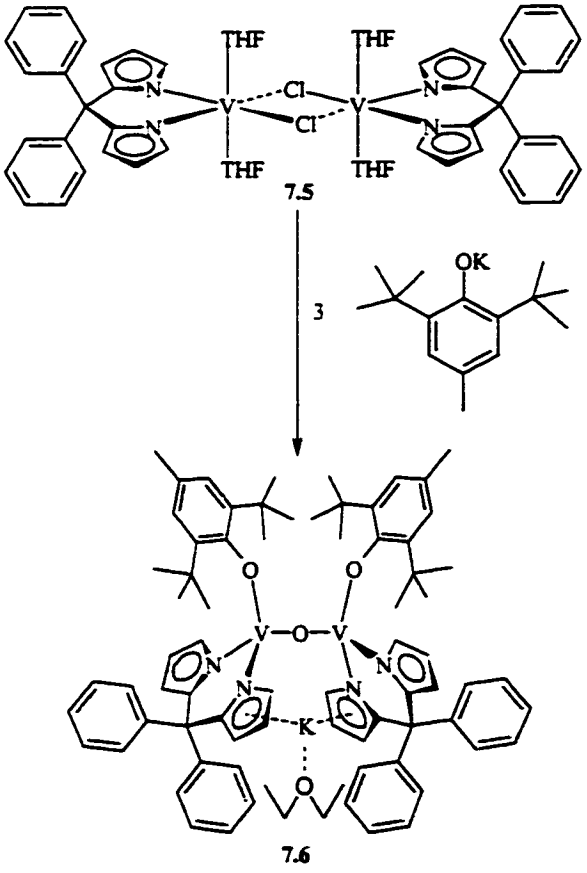

As expected the bulky tertiary butyl groups in the 2 and 6 positions of the phenyl group have eliminated the coordinated THF molecules and have lowered the coordination

number from 6 to 4 thus leaving empty coordination sites for ethylene coordination after alkylation of the vanadium centre. Interestingly, a deoxygenation of the aryloxide also occurred yielding to the formation of a bridging oxygen between both vanadium centres each bearing a 2,6-di-*tert*-butyl-4-methylphenoxy and a diphenyldipyrrole ligand. One potassium cation was also retained in the structure coordinated to two of the four-pyrrolide moieties in a η^5-fashion. Magnetic moment susceptibility measurements indicate a mixed valence dimer with a value of 3.45 μ_{BM} that would formally represent three unpaired electrons delocalised between both vanadiums. The slight decrease in the value of the magnetic moment is probably due to some residual anti-ferromagnetic coupling through the bridging oxygen between the two vanadium centres.

Further reactivity of the *meso*-diphenyldipyrrolide dianion with Cr(III) and Cr(II) lead to the formation of complexes **7.7** and **7.8**. The reaction of $CrCl_3(THF)_3$ with the diphenyldipyrrolide ligand afforded a complex iso-structural with the vanadium (III) complex (**7.5**) with one ligand in the equatorial plane, bridging chlorides between the two octahedral chromium atoms and two THF molecules in the axial positions. The complex is paramagnetic and presents a magnetic moment of 3.68 μ_{BM} per chromium, which is in good agreement with the d^3 electron configuration of trivalent chromium. The Cr(II) complex **7.8** (Figure 7.6) is structurally very similar to complexes **5.7** and **5.6** when ignoring the two THF molecules in the axial positions of the octahedral metal centres. The four coordination sites around each distorted square planar Cr(II) is comprised of one bidentate dianionic *meso*-diphenyldipyrrolide ligand and two bridging chlorides, yielding an overall -2 charge which is counterbalanced by the presence of two THF solvated lithium cations (omitted in Figure 7.6 for clarity). Magnetic susceptibility measurements

of complex **7.8** are in agreement with a d^4 electronic configuration for each Cr(II) centre yielding a value of 9.52 μ_{BM} per dimer.

Scheme 7.4 **Reactivity of the *meso*-diphenyldipyrrolide dianion with $CrCl_2(THF)_2$ and $CrCl_3(THF)_3$**

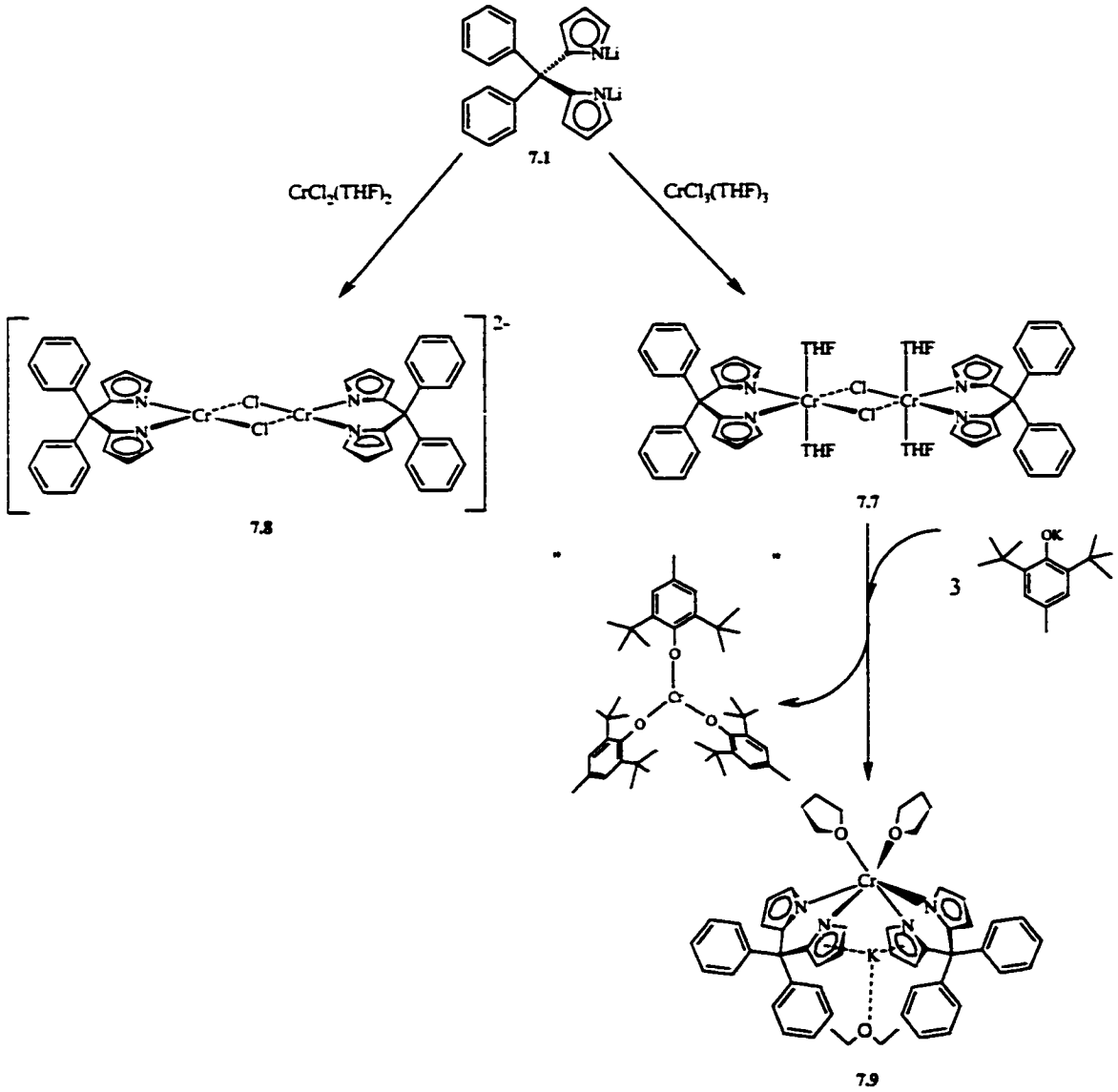

Both complexes **7.7** and **7.8** have been tested for catalytic activity towards α-olefin polymerization and have presented negligible activity. In the light of this negative

result the same approach that was successful in the case of vanadium (i.e. the introduction of an aryloxide group) in the formation of complex **7.6** was attempted. The Cr(III) complex (**7.7**) was treated with three equivalents of 2,6-di-*tert*-butyl-4-methylphenoxide potassium salt affording dark-brown crystals of complex **7.9** which were suitable for single crystal x-ray structure determination. The result of the reaction was unexpected since ligand shuffling was observed. Complex **7.9** as presented in Figure 7.7 bears two diphenyldipyrrolide ligands around the Cr(III) metal centre as well as two THF molecules and one potassium cation coordinated in an η^5-fashion to two pyrrolide moieties. The fact that complex **7.9** is mononuclear and contains not one but two dipyrrolide ligands implies the formation of tris(2,6-di-*tert*-butyl-4-methylphenoxide)Cr as a by-product.

All the compounds described in this chapter were tested for catalytic activity towards ethylene polymerization. The two zirconium complexes showed moderately low activity (Table 7.1) which was expected on the basis that both complexes retained THF or ether, which are notoriously known as polymerization retardants. MAS-^{13}C-NMR carried out on the sample of polyethylene produced by complex **7.4** indicates a rather crystalline polyethylene with virtually no branching. The vanadium complex **7.5** did not show any polymerization activity as well as all the chromium complexes synthesized in this chapter. The most potent catalyst synthesized bearing the diphenyldipyrrolide ligand was complex **7.6**, which polymerized ethene gas at room temperature under 1 atm of pressure of ethylene and using dimethylaluminium chloride or diethylaluminium chloride as co-catalysts. Higher activities, in the range of 1305 g mmol^{-1} h^{-1} atm^{-1}, were obtained upon using a dimethylaluminium chloride co-catalyst. Activities were recorded at an all time high for a V(III) complex in the order of 2074 g·mmol^{-1}·h^{-1}·atm^{-1}.Characterization of the

polyethylene polymer was not completed by GPC due to insolubility problems. Complex **7.6** was also active towards co-polymerisation of ethylenene and propene monomers with slightly lower activity than in the polymerization of straight ethene even though the activity is still reasonably high (926 $g \cdot mmol^{-1} \cdot h^{-1} \cdot atm^{-1}$) in comparison to other vanadium catalysts. Characterization of the copolymer yielded a 23:77 C_2:C_3 ratio. GPC have demonstrated that the system is uni-modal with molecular weight fractions of 489 000 with a narrow polydispersity factor of 2.34.

7.6 Conclusion

In this chapter, we have described unprecedented Zr(IV), V(III), Cr(III) and Cr(II) complexes of the dipyrrolide ligand system. The solid state structures of the seven reported compounds indicate that the tendency of the dipyrrole ligand to bind to the metal centre in a π-bonding fashion is coupled with the tendency of the ligand to work as a bi-nucleating agent. Conversely, employment of first row transition metals mainly gave the expected σ-bonding mode with the ligand working as a standard chelating agent. The moderate activity of the Zr(IV) compound as a catalyst was as expected given the presence of coordinated THF to the metal center. The non-activity of complex **7.5.** is instead rather surprising. The inactivity of the complex was surmounted by reacting **7.5** with an aryloxide whose presence liberates coordination sites for ethylene insertion as well as rendering an electron deficient 14 electron complex (**7.6**) upon deoxygenation of the aryloxide.

7.7 References

1.(a) Bochman, M.; *J. Chem. Soc. Dalton Trans.*, **1996**, 255-270

(b) Brintzinger, H. H.; Fischer, D.; Mülhaupt, R.; Rieger, B.; Waymouth, R. M.; *Angew. Chem.*, **1995**, *107*, 1255.

(c) Brintzinger, H. H.; Fischer, D.; Mülhaupt, R.; Rieger, B.; Waymouth, R. M.; *Angew. Chem.*, **1995**, *34*, 1143.

(d) Möhring, P. C.; Coville, N. J.; *J. Organomet. Chem.*, **1994**, *479*, 1.

(e) Gupta, V. K.; Satish, S., Bhardwaj, I. S.; *Rev. Macromol. Chem. Phys. C;* **1994**, *34*, 439.

(f) Kaminsky, W.; *J. Chem. Soc. Dalton Trans.*; **1998**, 1413.

(g) Soga, K.; Shiono, T.; *Prog. Polym. Sci.*; **1997**, *22*, 1503.

(h) Jordan, R. F.; *Adv. Organomet. Chem.*; **1991**, *32*, 325.

2.(a) Shah, S. A. A.; Dorn, H.; Voigt, A.; Roesky, H. W.; Parisini, E.; Schmidt, H. G.; Noltemeyer, M.; *Organometallics*, **1996**, *15*, 3176.

(b) Warren, T. W.; Schrock, R. R.; Davis, W. M.; *Organometallics*, **1996**, *15*, 308.

(c) Tinkler, S.; Deeth, R. J.; Duncalf, D. J.; McCamley, A.; *Chem Comm.*, **1996**, 2623.

(d) Cloke, F. G. N.; Geldbach, T. J.; Hitchcock, P. B.; Love, J. B.; *J. Organomet. Chem.*, **1996**, *506*, 343.

(e) Male, N. A. H.; Thornton-Pet, M.; Bochmann, M.; *J. Chem. Soc. Dalton Trans.*; **1997**, 2487.

(f) Tsuie, B.; Swenson, D. C.; Jordan, R. F.; *Organometallics*, **1997**, *16*, 1392.

(g) Scollard, J. D.; McConville, D. H.; Payne, N. C.; Vittal, J. J.; *Macromol.*; **1996**, *29*, 5241.

(h) Scollard, J. D.; McConville, D. H.; *J. Am. Chem. Soc.*; **1996**, *118*, 10008.

(i) Scollard, J. D.; McConville, D. H.; Rettig, S. J.; *Organometallics*, **1997**, *16*, 1810.

(j) Scollard, J. D.; McConville, D. H.; Vittal, J. J.; *Organometallics*, **1997**, *16*, 4415.

(k) Gibson, V. C.; Kimberley, B. S.; White, A. J. P.; Williams, D. J.; Howard, P., *Chem Comm.*; **1998**, 313.

(l) Mack, H., Eisen, M. S.; *J. Organomet. Chem.*, **1996**, *525*, 81.

(m) Horton, A. D.; de With, J.; *Chem. Comm.*, **1996**, 1375.

3.(a) Younkin, T. R.; Connor, E. F.; Henderson, J. I.; Friedrich S. K.; Grubbs, R. H.; Bansleben, D. A.; *Science*, **2000**, *287*, 460.

(b) Hicks, F. A.; Brookhart, M.; *Organometallics*, **2001**, *20(15)*, 1709.

4.(a) Dubé, T.; Gambarotta, S.; Yap, G. P. A.; *Organometallics*, **2000**, *19*, 115

(b) Dubé, T.; Conoci, S.; Gambarotta, S.; Yap, G. P. A.; *Organometallics*; **2000**, *19*, 1182.

(c) Dubé, T.; Conoci, S.; Gambarotta, S.; Yap, G. P. A.; Vasapollo, G.; *Angew. Chem. Int. Ed.*, **1999**, *38 (24)*, 3657.

(d) Dubé, T.; Ganesan, M.; Conoci, S.; Gambarotta, S.; Yap, G. P. A.; **2000**, *19*, 3716.

5. Gibson, V. C.; Maddox, P. J.; Newton, C.; Redshaw, C.; Solan, G. A.; White, A. J. P.; Williams, D. J.; *Chem. Comm.*, **1998**, 1651.

6. Unpublished results

7. Manzer, L. E. *Inorg. Synth.*, **1982**, *21*, 138.

8. Köhler, F. H.; Prössdorf, W.; *Z. Naturforsch., Teil B*, **1977**, *32*, 1026.

9. Mabbs, M. B.; Machin, D. *Magnetism and Transition Metal Complexes*; Chapman and Hall; London, 1973.

10. Foese, G.; Gorter, C. J.; Smits, L. J., *Constantes Selectionnées Diamagnétisme, Paramagnétisme, Relaxation Paramagnétique*; Masson: Paris, 1957.

11. Modification of the existing procedure of: *Dolphin, D.; Liu, B.Y.; Brükner, Chem. Commun., 1996, 2141 and references therein)*

Conclusion

8.1 Conclusion

This thesis deals with the synthesis, characterization and reactivity of novel vanadium complexes. During the course of this work, a series of vanadium(III) complexes bearing nitrogen and oxygen-donor based supporting ligands systems were prepared, characterized and tested for their activity towards α-olefin polymerization. In the case where activity was relatively high, further reactivity with the co-catalyst was investigated to attempt to obtain a better understanding of the alkylation, initiation, propagation and termination steps.

In chapter two, the V(*acac*)$_3$, fourteen electron complex was studied in greater detail to unveil the "true" active species which is suspected to be a vanadium-aluminium cluster. Unfortunately, the conclusive elucidation of the structure of the catalytic species was not possible. Isolation of the catalytic active species since the vanadium/aluminium interaction leads to a short-lived intermediate, which is quickly deactivated through reduction of the vanadium metal centre to an inactive oxidation state. Therefore insight into the activation and the nature of vanadium/aluminium interactions were investigated as well as a better understanding of the catalyst deactivation through reductive pathways to low oxidation states. We have demonstrated that the reduction of V(R-acac)$_3$ (vanadium in the +3 oxidation state) pro-catalysts to V(II) is responsible for the inactivity of the system. Polymerization studies of complexes **2.1, 2.2, 2.3, 2.4.** indicated that the nature of the ligand, whether the modification was of steric nature or had a greater nucleophilic character, had little effect on the activity or the structure of the polymer. These observations lead to the conclusion that the *acac* ligand migrates to the co-catalyst regardless of the nature of the ligand due to the fact that the aluminium co-catalyst has

greater oxophilic character. The low-valent vanadium complexes and aluminium residues isolated from the direct catalyst/co-catalyst reaction have proved this point.

The fourteen-electron complex synthesized and described in chapter three addressed the problem of ligand migration but revealed direct involvement of the ligand during the process. In this case, the nitrogen-donor ligand rather than migrating to the aluminium co-catalyst, was directly involved in the in the alkylation of the vanadium(III) metal centre. Alkylation of complex **3.2** occurred at the *ortho* position of the pyridine ring of the ligand. In the process, formation of a V-N amido bond was observed as well as liberation of a coordination site suitable for the coordination of ethylene. The steric hindrance of the ligand imposed by the isopropyl groups in the 2 and 6-positions of the phenyl groups have shown to have an effect on the insertion and, in spite of high activity, other monomers such as propylene could not be incorporated into the polymer. Deactivation pathways of the catalyst were established to occur through a two-electron reduction of the vanadium metal centre to V(I). Two V(I) complexes were isolated and characterized as the first two non-Cp supported V(I) alkyl complexes reported in the literature. In both cases, the reduction involved the ligand either through a second alkylation occurring at the *meta* position of the pyridine ring or in alkyl abstraction via radical coupling mechanism. The ligand system described in chapter three plays an important role in the catalytic process controlling ethylene insertion into the polymeric chain and reducing branching of the polymer. As a result of this the obtained polymer is of high molecular weight and highly linear with relatively little branching. Another interesting feature of this system is the tendency of vanadium to chain transfer the growing polymeric chain to the aluminium co-catalyst at high Al:V ratios creating a

second molecular weight fraction, which is literally absent at lower Al:V ratios. The ligand also played an important role in stabilizing the active and reduced alkylated species.

In contrast to the high activity of the V(III) complex, the Ti(III), Cr(III), Mn(II) and Mn(I) congeners did not exhibit nearly the same polymerization activity in spite of the fact that the Ti(III) (**4.3**) and Cr(III) (**4.4**) complexes are iso-structural with the vanadium analog (**3.2**). The main difference between complexes **3.2**, **4.3**, **4.4**, is the electron count. The Ti(III) is a thirteen-electron species, the V(III) complex is a fourteen-electron species and the Cr(III) is a fifteen-electron species. This property raises the question about the higher activity of the fourteen-electron species. As seen in the present thesis work and extended to group IV catalytic systems, cationic complexes having a low electron count (14 electrons or less) are better candidates towards high polymerization activity and yielding high molecular weight polymers as opposed to electron rich complexes which have a greater tendency to yield lower molecular weight polymers which are characteristic of catalysts of the Shell Higher Olefin Process (SHOP) that have greater tendency to follow rapid β-hydrogen elimination termination steps. The Fe(II) and Co(II) complexes prepared and investigated by Brookhart and Gibson[1] are sixteen and seventeen-electron species respectively and have both higher electron counts and exuberant activities. These examples are exceptions to this trend and rely on the unique steric and electronic properties of the bis(imino)pyridyl ligand.

The bis(imino)pyridyl ligand was also complexed to Mn(II) (**4.1**) to form a fifteen-electron compound which did not display any catalytic activity. Reactivity of **4.1** towards alkylation yielded the reduced Mn(I) alkyl species (**4.2**) which is the first isolated

Mn(I) alkyl characterized by X-ray diffraction without CO or Cp as supporting ligand systems. Unlike the alkylation of **3.2**, the Mn(II) complex was not reduced through a two-electron reduction like the V(III) complex. The chlorides were simply substituted by alkyls upon which two methyls from two alkylated complexes, coupled radically eliminating one molecule of ethane. Once more the bisiminopyridyl ligand has demonstrated to be an ideal ligand to support rare low-valent early transition metal alkyls.

Chapter 5 describes the preparation of two novel vanadium catalysts of extremely high activities. Aside the polymerization activity, both complexes also demonstrate the versatility of vanadium(III) to mediate synthetic organic coupling reactions involving carbonyl moieties. The ligand used to synthesize **5.1** bears both the oxygen and nitrogen moieties to create a combination of the electronic properties of *acac* and those of the bis(imino)pyridyl systems. Upon reacting the potassium salt of acetylpyrrole with V(III) the aldolic condensation of the ligand occurred yielding a trianionic tetradentate ligand bridging two V(III) metal centres (**5.1**). In order to understand the catalyst deactivation process a V(II) complex of the same ligand system was prepared and characterized. In the process, complex **5.2** was synthesized where the acetylpyrrole ligand has undergone a pinacolic coupling reaction to form a tetradentate, tetraanionic ligand. The pinacolic coupling of two acetylpyrrole is mediated by two vanadium(III) centres as in the case of the aldolic coupling reaction involving two vanadium centres. Both complexes presented high activities surpassing those of the industrially used V(*acac*)$_3$ system.

The bulky N,N,N, *tris*-trimethylsilyldiethylenediamidoamino ligand has allowed us to isolate V(III) catalysts and to study the aggregation with the aluminium co-catalyst

to form Al-V clusters. The reduction of the vanadium centre also observed in this case is also related to the strength of to the Lewis acid properties of the aluminium co-catalyst triggering either disproportionation or destabilizing the V-C bond.

Exploratory work on the reactivity of diphenyldipyrrolide ligand, iso-structural with the *ansa*-metallocenes, with Zr(IV), V(III), Cr(III) and Cr(II) have given us insight into the possible bonding modes of the ligand. The hard/soft character of the metal is basically determining the type of bonding (η^1 versus η^5). Preliminary polymerization tests with a wide variety of co-catalysts indicated poor activity for all the synthesized complexes (**7.3, 7.4, 7.5, 7.7, 7.8**). Activity was increased tremendously upon reacting complex **7.5** with potassium 2,6-di-tert-butyl-4-methylphenoxide, which yielded **7.6**. Complex **7.6** does not bear coordinated THF, which is thought to be detrimental to the catalytic process. In the reaction of **7.5** with the aryloxide, one oxygen was abstracted and used to bridge two vanadium centres thus liberating two coordination sites ready for olefin insertion. The electron deficient species polymerizes and co-polymerizes α-olefins with high catalytic activity, yielding polymers having random insertion of the co-monomers. Similar reactions with **7.7** and potassium 2,6-di-tert-butyl-4-methylphenoxide lead to ligand scrambling where **7.9** was obtained and further determined to be completely inactive towards polymerization.

8.2 Epilogue

I hope this work on vanadium(III) catalysts will inspire the following graduate student working on α-olefin polymerization catalyst design and give him some insight

into the complexity and the beauty of the activation and deactivation processes of vanadium based catalysts.

Future endeavours in the design of vanadium catalyst should focus on novel nitrogen-donor based ligand systems since they have proven to withstand the "leaching powers" of the aluminium co-catalyst. Tuning the electronic properties of the ligand to synthesize an electron deficient organometallic complexes (a 14 electron species) and tuning the ligand to induce a stereoselective transition state by adding bulky groups to the ligand, would be the first step towards designing a novel vanadium based catalyst that would induce tacticity into the polymer. A greater achievement would be to isolate the intermediate catalytic species to understand the role of the aluminium co-catalyst and furthermore the vanadium/aluminium interaction. The results obtained in the present thesis indicate possible pathways of activation (alkylation) of the pre-catalyst, deactivation (reduction of vanadium) of the catalytic species and in some cases the reactivation of the catalytic species with ethyl-1,1,1-trichloroacetate. An understanding of the vanadium/aluminium interaction could lead towards the elimination of the co-catalyst thus lowering the industrial cost of production of the catalyst. Following the trend observed in the synthesis of Group IV polymerization catalysts and the effect of the metal on polymerization activities upon moving from Ti(IV) to Zr(IV), understanding the activation and deactivation of niobium and tantalum analogues of vanadium could be of great interest.

8.3 References

1.(a) Small, B. L.; Brookhart, M.; Bennett, A. M. A.; *J. Am. Chem Soc.;* **1998**, *120*, 4049.

(b) Small, B. L.; Brookhart, M.; *Polymer Prep. (Am. Chem. Soc., Div. Polym. Chem.)*, **1998**, *39*, 213.

(c) Britovsek, G. J. P.; Gibson, V. C.; Kimberley, B. S., Maddox, P. J.; McTavish, S. J.; Solan, G. A.; White, A. J. P.; Williams, D.; *Chem.Comm.*, **1998**, *120*, 849.

(d) Britovsek, G. J. P.; Bruce, M.; Gibson, V. C.; Kimberley, B. S.; Maddox, P. J.; Mastroianni, S.; McTavish, S. J.; Redshaw, C.; Solan, G. A.; Strömberg, S.; White, A. J. P.; Williams, D. J.; *J. Am. Chem. Soc.*, **1999**, *121*, 8728.

(e) Britovsek, G. J. P.; Dorer, B. A.; Gibson, V. C.; Kimberley, B. S.; Solan, G. A., (BP Chemicals Limited), WO 99/12981, **1999** [*Chem Abstr.* **1999**, *130*, 252793].

(f) Bennett, A. M. A. (DuPont), WO 98/27124, **1998**, [*Chem Abstr.* **1998**, *129*, 122973x]

(g) Bennett, A. M. A., *CHEMTECH*, **1999**, *July*, 24-28

Appendix

Appendix 1 Crystal Data and Structure Analysis Results for Complexes 2.4, 2.6a, 2.7 and 2.8

Complex	2.4	2.6a	2.7	2.8
	$Al_2C_{18}H_{30}O_6Cl_4$	$VC_{16}H_{30}N_2O_4$	$C_{56}H_{108}N_4O_8V_2ZnCl_4$	$VC_{28}H_{54}N_2O_4CuCl_2$
	538.18	365.36	1274.51	668.11
	triclinic, $P\bar{1}$	triclinic, $P\bar{1}$	orthorhombic, Pbcn	monoclinic, C 2/c
	8.916(3)	7.896(1)	18.723(7)	13.676(5)
	9.802(3)	10.032(2)	19.675(7)	19.521(3)
	15.390(5)	13.134(2)	18.836(7)	13.206(3)
	88.156(4)	75.265(2)		
	86.041(4)	88.520(2)		98.47(3)
	82.710(4)	71.445(2)		
	1330.7(7)	952.1(3)	6939(4)	3487.2(9)
	2	2	4	4
	0.71073	0.71073	0.71073	0.71073
	213(2)	173(2)	213(2)	213(2)
	1.343	1.274	1.220	1.273
	5.40	5.40	8.08	10.62
	560	390	2720	1416
	0.1288, 0.2114, 1.114	0.0786, 0.1921, 1.089	0.0636, 0.1722, 1.010	0.0345, 0.0918, 1.096

[a] $R = \Sigma F_o - F_c / \Sigma F_o R_w = [(\Sigma(F_o - F_c)^2/\Sigma w F_o^2)]^{1/2}$

Appendix 2 Crystal Data and Structure Analysis Results for Complexes 3.1, 3.2and 3.3

	3.1	3.2	3.3
	$C_{33}H_{43}N_3$	$C_{33}H_{43}Cl_3N_3V(CH_2Cl_2)_{1.3}$	$C_{34}H_{46}Cl_2N_3V(C_6H_{12})_{0.5}$
	481.70	752.23	661.66
	monoclinic	Monoclinic	monoclinic
	$P2_1/c$	$P2_1/n$	$P2_1/c$
	15.215(3)	18.267(5)	15.741(2)
	21.572(4)	16.643(4)	16.565(2)
	9.051(2)	38.195(9)	15.849(2)
	94.662(3)	96.061(5)	100.316(3)
	2960.8(8)	11547(5)	4066.0(9)
	4	12	4
	0.71073 Å	0.71073 Å	0.71073 Å
	203	226	203
	1.081	1.298	1.081
	0.630	0.678	0.401
	1048	4704	1412
	0.0587, 0.1157	0.0548, 0.1573	0.074, 0.1954
	1.045	1.110	1.069

[a] $R = \Sigma(F_o - F_c)/\Sigma F_o$. $R_w = [(\Sigma (F_o - F_c)^2/\Sigma wF_o2)]^{1/2}$.

Appendix 3 Crystal Data and Structure Analysis Results of Complexes 3.3 and 3.4

	3.3	3.4
[redacted]	$C_{47}H_{79}LiN_3O_3V$	$C_{51}H_{87}LiN_5O_2V(Et_2O)_{0.5}$
[redacted]	792.01	897.20
[redacted]	orthorhombic	monoclinic
[redacted]	Pnma	$P2_1/n$
[redacted]	19.724(6)	11.932(3)
[redacted]	22.001(7)	25.362(6)
[redacted]	11.035(3)	18.957(4)
[redacted]		96.587(4)
[redacted]	4789(3)	5699(2)
[redacted]	4	4
[redacted]	0.71073 Å	0.71073 Å
[redacted]	204	213
[redacted]	1.099	1.046
[redacted]	0.246	0.214
[redacted]	1728	1964
[redacted]	0.0863, 0.2279	0.1148, 0.2280
[redacted]	1.002	1.019

[a] $R = \Sigma(F_o - F_c)/\Sigma F_o$. $R_w = [(\Sigma (F_o - F_c)^2/\Sigma wF_o2)]^{1/2}$.

Appendix 4 Crystal Data and Structure Analysis Results for Complexes 4.1 and 4.2

Complex	4.1	4.2
	$MnCl_2C_{33}H_{43}N_3$	$MnC_{34}H_{46}N_3$
	607.54	551.68
	Triclinic, P-1	Monoclinic, P2(1)/n
	8.741(2)	14.159(3)
	9.793(2)	8.7749(17)
	20.843(5)	25.300(5)
	82.333(4)	90
	88.424(5)	94.784(4)
	65.987(4)	90
	1614.5(7)	3132.40(10)
	2	4
	0.71073	0.71073
	203(2)	203(2)
	1.250	1.170
	6.00	4.47
	642	1184
	0.0564, 0.1463, 1.039	0.0618, 0.1582, 1.043

a$R = \Sigma F_o - F_c / \Sigma F_o R_w = [(\Sigma(F_o - F_c)2/\Sigma wF_o2)]1/2$

Appendix 5 Crystal Data and Structure Analysis Results for Complexes 4.3 and 4.4

Complex	4.3	4.4
	$TiCl_3C_{33}H_{43}N_3$	$CrCl_{5.67}C_{34.33}H_{45.67}N_3$
	749.19	753.29
	Monoclinic, P2(1)/n	Monoclinic, P2(1)/n
	18.237(4)	18.124(2)
	16.555(2)	16.440(1)
	37.894(7)	37.861(3)
	90	90
	95.90(1)	95.932(2)
	90	90
	11380(3)	11220(2)
	12	12
	0.71073	0.71073
	203(2)	203(2)
	1.312	1.338
	6.52	7.38
	4692	4716
	0.0729, 0.2211, 1.018	0.0702, 0.2064, 1.022

a$R = \Sigma F_o - F_c / \Sigma F_o R_w = [(\Sigma(F_o - F_c)2/\Sigma wF_o2)]1/2$

Appendix 6 Crystal Data and Structure Analysis Results for Complexes 5.1, 5.2 and 5.3

Complex	5.1	5.2	5.3
	$K_2V_2C_{44}H_{50}N_6O_8$	$K_2V_2C_{47}H_{52}N_6O_8$	$VC_{18}H_{28}N_4O_2$
	970.98	1005.96	383.38
	monoclinic	orthorhombic	monoclinic
	11.348(1)	16.267(4)	10.485(3)
	15.675(2)	16.905(4)	14.218(4)
	12.780(1)	21.523(5)	14.129(4)
	103.618(2)		105.679(5)
	2209.4(4)	5919(2)	2027.8(9)
	2	4	4
	0.71073	0.71073	0.71073
	203(2)	203(2)	203(2)
	1.460	1.129	1.256
	6.71	5.03	5.07
	1008	2090	812
	0.0400, 0.0868	0.0839, 0.2280	0.0524. 0.1126
	1.023	1.056	1.065

[a] $R = \Sigma_o - F_c/\Sigma F_o R_w = [(\Sigma (F_o - F_c)^2 / \Sigma_w F_o^2)]^{1/2}$.

Appendix 7 Crystal Data and Structure Analysis Results for Complexes 6.3, 6.4 and 6.5

Complex	6.3	6.4	6.5
	$C_{26}H_{70}N_6Cl_2Si_6V_2$	$C_{19}H_{43}N_4Si_3V$	$C_{30}H_{82}Al_2C_{12}N_6Si_6V_2$
	808.20	462.78	922.30
	Monoclinic, P2(1)/c	Monoclinic, P2(1)/n	Triclinic, P-1
	10.534(1)	10.7952(5)	10.433(2)
	37.931(4)	16.6050(8)	11.260(2)
	11.707(1)	14.7725(8)	12.639(3)
	90	90	97.09(2)
	109.701(1)	93.228(1)	105.52(1)
	90	90	115.10(1)
	4403.5(8)	2643.8(2)	1246.8(4)
	4	4	1
	0.71073	0.71073	0.71073
	223(2)	203(2)	203(2)
	1.219	1.163	1.228
	7.34	5.23	6.89
	1728	1000	494
	0.0807, 0.1597, 1.167	0.0609, 0.1250, 1.052	0.0639, 0.1962, 1.071

[a] $R = \Sigma F_o - F_c / \Sigma F_o R_w = [(\Sigma(F_o - F_c)^2 / \Sigma w F_o^2)]^{1/2}$

Appendix 8 Crystal Data and Structure Analysis Results for complexes 6.6, 6.7 and 6.9

Complex	(6.6)	(6.7)	(6.9)
	$C_{13}H_{35}AlCl_5N_3Si_3V$	$C_{40}H_{86}Al_2Cl_{10}N_6Si_6V_3$	$C_{10}H_{26}Cl_2N_3Si_2V$
	572.88	1380.97	366.36
	Monoclinic, P2(1)/c	Triclinic, P-1	Monoclinic, C2/c
	9.373(5)	10.476(5)	20.385(3)
	20.215(9)	11.647(7)	10.2967(12)
	14.794(7)	15.177(6)	20.698(3)
		69.75(3)	
	97.950(5)	87.53(5)	117.222(2)
		73.54(5)	
	2776(2)	1663(1)	3865.1(8)
	4	1	8
	0.71073	0.71073	0.71073
	203(2)	203(2)	203 (2)
	1.371	1.379	1.259
	10.06	9.82	9.04
	1188	717	1536
	0.0509, 0.1094, 1.065	0.0638, 0.1049, 1.055	0.0453, 0.1069, 1.001

[a] $R = \Sigma F_o - F_c / \Sigma F_o R_w = [(\Sigma(F_o - F_c)^2 / \Sigma w F_o^2)]^{1/2}$

Appendix 9 **Crystal Data and Structure Analysis Results for Complexes 7.3, 7.4 and 7.5**

Complex	7.3	7.4	7.5
	$ZrCl_2C_{29}H_{32}N_2O_2$	$Zr_2Cl_7C_{25}H_{26}N_2Li$	$VClC_{36}H_{40}N_2O_2$
	602.69	808.01	619.09
	Monoclinic, P2(1)/c	Monoclinic, P2(1)/n	Monoclinic, P2(1)/n
	14.584(5)	14.1601(15)	14.483(2)
	9.730(2)	10.2143(11)	12.026(2)
	19.338(8)	22.889(2)	18.859(4)
	90	90	90
	102.37(3)	106.578(2)	103.06(1)
	90	90	90
	2680(2)	3172.9(6)	3199.7(9)
	4	4	4
	0.71073	0.71073	0.71073
	203(2)	203(2)	203(2)
	1.493	1.691	1.285
	6.39	12.69	4.28
	1240	1600	1304
	0.0664, 0.1167, 1.058	0.0545, 0.0723, 1.022	0.0537, 0.1361, 1.016

[a] $R = \Sigma F_o - F_c / \Sigma F_o R_w = [(\Sigma(F_o - F_c)^2/\Sigma w F_o^2)]^{1/2}$

Appendix 10 Crystal Data and Structure Analysis Results for Complexes 7.6, 7.7, 7.8 and 7.9

Complex	7.6	7.7	7.8	7.9
[redacted]	$V_2C_{76}H_{90}N_4O_4K$	$Cr_2Cl_2C_{72}H_{80}N_4O_4$	$CrClC_{37}H_{47}N_2O_4Li$	$CrC_{54}H_{58}N_4O_3K$
	1264.50	1240.30	678.16	902.14
	Monoclinic, C2/c	Monoclinic, P2(1)/n	Triclinic, P-1	Monoclinic, C2/c
	26.418(5)	12.3219(15)	9.6099(9)	17.491(4)
	14.332(2)	13.1685(16)	12.873(1)	15.736(5)
	17.896(3)	19.528(2)	14.371(2)	16.824(3)
	90	90	88.650(2)	90
	103.161(3)	97.208(2)	88.539(2)	90.96(3)
	90	90	88.022(2)	90
[redacted]	6598.1(19)	3143.5(7)	1775.7(3)	4630(2)
Z	4	2	2	4
[redacted]	0.71073	0.71073	0.71073	0.71073
	223(2)	203(2)	208(2)	203(2)
	1.273	1.310	1.268	1.294
	3.99	4.84	4.37	3.86
	2684	1308	718	1908
[redacted]	0.0622, 0.1294, 1.001	0.0423, 0.1227, 1.028	0.0532, 0.1430, 1.013	0.0537, 0.1524, 1.079

[a] $R = \Sigma F_o - F_c / \Sigma F_o R_w = [(\Sigma(F_o - F_c)^2 / \Sigma w F_o^2)]^{1/2}$